Behavior and Testing of Fastenings to Concrete for use in Seismic Applications

Von der Fakultät Bau- und Umweltingenieurwissenschaften
der Universität Stuttgart zur Erlangung der Würde
eines Doktor-Ingenieurs (Dr.-Ing.)
genehmigte Abhandlung

Vorgelegt von

Matthew Stanton Hoehler

aus Kalifornien, USA

Hauptberichter:	Prof. Dr.-Ing. Rolf Eligehausen
Mitberichter:	Prof. Dr.-Ing. Lothar Stempniewski

Tag der mündlichen Prüfung: 2. August 2006

Institut für Werkstoffe im Bauwesen der Universität Stuttgart
2006

Acknowledgements

First and foremost I would like to thank my PhD advisor Prof. Dr.-Ing. Rolf Eligehausen. Thank you for your commitment to a research environment that allows students the freedom to take chances and learn how research is conducted from beginning to end. Moreover, thank you for your support and encouragement to pursue activities beyond research, such as teaching, code development activities and publication. You have been both a mentor and friend during my time in Stuttgart and for that I am forever grateful.

I would like to thank my second evaluator Prof. Dr.-Ing. Lothar Stempniewski for his technical insight during the course of my work.

I owe a great debt to Dr.-Ing. Werner Fuchs for hours of technical discussions and for support on all things administrative. Thank you for keeping my German readable.

I thank Prof. Dr.-Ing. Joško Ožbolt for sharing with me his deep understanding of computational mechanics. I also thank Prof. Dr.-Ing. Hans-Wolf Reinhardt, Prof. Dr.-Ing. Pieter Vermeer and Prof. Dr.-Ing. Siegfreid Schmauder for allowing me to participate in the development and administration of their COMMAS courses.

Thanks to all my current and former colleagues at the IWB for making the years in Stuttgart so enjoyable. A special thanks to the following “Dipl.’s”: Jörg Appl, Lubor Bezecny, Jens Borrmann, Stefan Fichtner, Giovacchino Genesio, Thorsten Hüer, Sven Mönnig, Anita Negele, Goran Periskic, Kerstin and Michael Rößle, Isabelle Simons and “Dr.’s”: Florian Finck, Jan Hofmann, Christian Große, Markus Krüger, Steffen Lettow, Thilo Pregartner, Marcus Schreyer and Georg Weiß for your support and friendship. Thank you Monika Werner for finding nearly every publication I ever requested.

The research in this dissertation would not have been possible without the support of our laboratory technicians. In particular, I thank Mike Langenfeld, Eugen Lindenmeier and Peter Scherf for lending me their experience and their hands.

A big thanks to all of the secretarial staff at the institute. A special thanks to Silvia Choynacki and Hella Schmidt for their help and friendship.

I am grateful to the firm Würth for their financial support of the research presented in this dissertation. I would particularly like to thank Götz Bauer, Edwin Dereser and Gregor Kerl from the firm Würth and Dr.-Ing. Longfei Li from the firm MKT for their interest in the work. Additionally, I thank Johannes Lißner from Robusta-Gaukel and Rainer Trillmich from Köster & Co. for their generous support and donations.

Finally, I would like to thank my wonderful wife Anja for her unbounded support and patience during the past few years. I love you dearly.

Matthew S. Hoehler
Stuttgart, August 2006

Abstract

This dissertation investigates the behavior in concrete of cast-in and post-installed fastenings under earthquake conditions and provides background for the development of seismic qualification methods and performance assessment criteria for fasteners.

Chapters 1 and 2 define the problem and provide the context for the research.

Chapter 3 puts existing literature related to the behavior and testing of fasteners under earthquake conditions into a cohesive framework. This chapter also reviews and summarizes normative standards for the design and testing of fasteners for seismic applications.

Chapter 4 investigates the conditions to which fasteners may be subjected during an earthquake so that realistic boundary conditions for testing can be established. It is shown that fasteners used to connect structural and nonstructural elements to a reinforced concrete structure experience both crack cycling and load cycling at dynamic rates during an earthquake. Based on theoretical considerations and numerical studies, this chapter establishes typical values for crack widths and the number of crack opening and closing cycles during an earthquake for use in fastener qualification tests. Cumulative damage based cycle counting methods are used to develop tension and shear load cycling time-histories for fasteners.

Chapters 5, 6 and 7 present and discuss the results of experimental investigations of fastener behavior under seismic conditions. Chapter 5 deals with fastener performance in wide cycled cracks when full crack closure occurs, i.e. when the cracks are pressed closed as could occur during a moment reversal in a member. This chapter describes in detail the load-displacement response of various fastener failure modes during extreme crack cycling. Chapter 6 presents results from tests with pulsating tension loads. Tests with cast-in headed bolts are used to develop an equation to predict head slip during tension load cycling. Tests with post-installed fasteners investigate the performance of various load-transfer mechanisms during tension cycling at near-ultimate load. Chapter 7 focuses on the behavior of fasteners under high (earthquake relevant) loading rates. Under certain conditions some fasteners can exhibit a lower ultimate capacity at high loading rate than at quasi-static loading rate or may undergo a change in failure mode.

Chapter 8 demonstrates that some existing design guidelines have an insufficient margin of safety to avoid brittle fastener failure. This chapter also shows that the deformation capacity of anchors designed for ductile steel failure can be controlled using the margin of safety between steel failure and brittle failure.

Finally, Chapter 9 makes recommendations to improve qualification testing methods and assessment criteria for fasteners used for earthquake applications.

Kurzfassung

In der vorliegenden Dissertation wird das Verhalten von einbetonierten und nachträglich in Beton verankerten Befestigungssystemen unter Erdbebenbeanspruchung untersucht. Die Grundlagen für die Entwicklung von Zulassungsverfahren für Dübelsysteme unter seismischen Beanspruchungen werden beschrieben und Beurteilungskriterien für Befestigungselemente entwickelt.

Kapitel 1 und 2 erläutern die Aufgabenstellung und den Kontext der Forschungsarbeiten.

Kapitel 3 fasst die vorhandene Literatur zum Tragverhalten von Befestigungssystemen unter Erdbebenbeanspruchung zusammen. Zusätzlich werden Bemessungsnormen und Zulassungsverfahren für Befestigungselemente für seismische Anwendungen aus verschiedenen Ländern dargestellt und vergleichend ausgewertet.

In Kapitel 4 werden die Bedingungen, denen Befestigungssysteme während eines Erdbebens ausgesetzt sind untersucht, um die Rahmenbedingungen für die Versuchsdurchführung festzulegen. Es zeigt sich, dass Verankerungen von tragenden und nichttragenden Bauteilen zyklischen Last- und Rissbreitenänderungen unterworfen sind. Die Größe der Rissbreiten und die Anzahl der Rissbreitenänderungen werden auf Basis von theoretischen und numerischen Untersuchungen angegeben. Basierend auf einer kumulativen Schädigungsmethode werden zyklische Zug- und Schubbelastungsgeschichten für die Prüfung von Dübelsystemen entwickelt.

In den Kapiteln 5, 6 und 7 werden die Ergebnisse von im Rahmen der vorliegenden Dissertation durchgeführten experimentellen Untersuchungen vorgestellt und diskutiert. Kapitel 5 behandelt das Tragverhalten von Befestigungselementen bei großen Rissbreitenänderungen wobei die Risse überdrückt werden. Das Last-Verschiebungsverhalten in Abhängigkeit der unterschiedlichen Versagensarten während extremer Rissbreitenänderungen wird beschrieben. In Kapitel 6 werden die Ergebnisse verschiedener Untersuchungen mit Befestigungselementen unter zyklischer Zuglast vorgestellt. Ergebnisse der Untersuchungen mit einbetonierten Kopfbolzen wurden verwendet, um eine Gleichung für die Zunahme des Kopfschlupfs unter zyklischer Zuglast zu entwickeln. Untersuchungen mit nachträglich montierten Befestigungen zeigen das Tragverhalten bei unterschiedlichen Lasteinleitungsmechanismen unter versagensnaher zyklischer Zuglast. Kapitel 7 beschreibt das Ankerverhalten unter schneller (erdbebenrelevanter) Belastung.

Kapitel 8 zeigt auf, dass der Sicherheitsspielraum zwischen duktilem und sprödem Versagen in einigen Bemessungsnormen für Befestigungselemente nicht ausreicht, um den gewünschten Versagensmodus zu gewährleisten. Weiterhin wird gezeigt, dass das Verformungsvermögen von Ankern über den Sicherheitsspielraum zwischen duktilem und sprödem Versagen kontrolliert werden kann.

Die Untersuchungen münden in Empfehlungen für neue Zulassungsmethoden und Beurteilungskriterien für Befestigungen in seismischen Anwendungen.

Table of Contents

Notation

COMMON SUBSCRIPTS

ave	Average
c	Concrete
cb	Concrete breakout (anchor)
cyc	Cyclic or cycle
cyl	Cylinder
d	Design
eff	Effective
eq	Earthquake (seismic) or equivalent
m	Mean
max	Maximum
min	Minimum
n, nom	Nominal
pt	Pull-through (anchor)
r	Residual
s	Steel
sa	Steel (anchor)
test	Value obtained from test
u	Ultimate
y	Yield

LATIN UPPERCASE LETTERS

A_a	Response amplification factor
A_{eff}	Effective cross sectional area
A_{gross}	Gross cross sectional area
A_h	Bearing area of anchor head
A_s	Area of steel
$A_{s,total}$	Cross sectional area of total longitudinal reinforcement
D	Damage variable
E	Modulus of elasticity
E_{cm}	Secant modulus of elasticity of concrete
E_s	Modulus of elasticity of steel
F	Load or force
F_2	Desired compression load on the anchorage component
F_{ha}	Horizontal seismic force acting on a nonstructural element
F_m	Load applied to the anchorage component (member)
$F_{m,1}$	Member load required to attain the desired crack opening width w_1
$F_{m,2}$	Member load required to attain the desired crack closing width w_2 or the desired compression load level F_2
F_{va}	Vertical seismic force acting on a nonstructural element
H	Building height measured from foundation or from the top of a rigid basement
I	Moment of inertia of a cross-section
L	Length
L_{CF}	Length to point of contraflexure of a member
M	Moment
N	Axial load or force
$NA(x)$	Depth of neutral axis at location x

NA_{LE}	Depth of neutral axis in linear elastic range
N_f	Number of uniform cycles to failure
$N_{u,30}$	Ultimate axial load normalized to a concrete strength of 30 N/mm^2
N_w	Sustained axial load
P_{bd}	Ultimate dynamic bond resistance
P_{cd}	Ultimate dynamic concrete cone resistance
P_{ud}	Ultimate dynamic (total) resistance
R	Resistance
S	Soil factor
S_a	Horizontal seismic coefficient applicable to nonstructural elements
S_{va}	Vertical seismic coefficient applicable to nonstructural elements
T	Period
T_1	Fundamental vibration period of a building
T_a	Fundamental vibration period of a nonstructural element
T_g	'Central' period of the ground motion
V	Shear load or force
V_i	Shear load in load cycle 'i'
W_a	Weight of a nonstructural element

LATIN LOWERCASE LETTERS

a	Anchor head undercut length
a_g	Design ground acceleration
a_{vg}	Vertical component of the design ground acceleration
b	Overall width of a cross-section
c_x	Depth of compression zone in concrete section
d, d_{nom}	Diameter of fastener or threaded rod
d_0	Diameter of drilled hole
d_h	Diameter of anchor head
d_x	Effective depth of a cross-section
f	Frequency
f_c	Compressive cylinder strength of concrete
f_{cb}	Bending (tensile) strength of concrete
f_{cc} (β_w)	Compressive cube strength of concrete
f_{cm}	Mean value of concrete cylinder compressive strength
f_{ct}	Tensile strength of concrete
$f_{NA}(x)$	Function describing variation of the neutral axis depth along a member
f_u	Ultimate strength of steel
$f_{wCr}(x)$	Function describing variation of the crack width along a member
f_y	Yield strength of steel
$f_{y,conn}$	Yield strength of steel attachment (connection)
g	Gravity
h	Overall depth of a cross-section
$h_{1,2,\ or\ 3}$	Various cross-section depths
h_b	Bond length of an anchor
h_c	Concrete cone depth
h_{ef}	Effective embedment depth
h_{nom}	Nominal embedment depth
i, j, m, n	Counting variables
$k_{1,2,3,4,5,6,t,a,A}$	Coefficients
l_p, l_{cr}	Plastic hinge (critical region) length
n_{eq}, N_{cy}	Number of equivalent damage cycles
p	Bearing pressure
p_d	Dynamic load
p_f	Probability of failure

q_a	Behavior factor of a nonstructural element
s	Spacing
s_0	Head slip at maximum bearing stress
s_{ave}	Average crack spacing
s_{cyc}	Head slip during load cycling
s_{max}	Maximum crack spacing
t	Time
t_b	Distance from concrete surface to center of outermost reinforcement
u	Plastic deformation of an element
w	Crack width
w_1, w_o	Crack opening width
w_2, w_u	Crack closing width
w_{ave}	Average crack width
w_k	Characteristic crack width
w_{max}	Maximum crack width
$w_{max,ave}$	Maximum average crack width inside of the plastic hinge
$w_{y,ave}$	Average crack width 'near' yield strain
z	Height of a nonstructural element above the level of application of the seismic action

GREEK UPPERCASE LETTERS

Δ_{CF}	Transverse displacement at point of contraflexure
Δw	Change in crack width
$\Phi(n,f)$	Cyclic anchor head slip coefficient

GREEK LOWERCASE LETTERS

α	Exponent | Ratio of the design ground acceleration on type A ground, a_g, to the acceleration of gravity g
β	Safety index
γ_a	Importance factor of a nonstructural element
γ_{inst}	Installation partial safety factor
γ_M	Material partial safety factor
γ_{Mc}	Material partial safety factor for concrete failure
α_b	Dynamic strength increase factor for bond failure
α_c	Dynamic strength increase factor for concrete cone failure
δ	Displacement
δ_{10}	Displacement after 10 crack cycles
δ_{1000}	Displacement after 1000 crack cycles
δ_{add}	Additional displacement during pullout test after crack cycling
δ_{co}	Displacement contribution from concrete deformation
δ_{cr}	Displacement contribution from crack opening
$\delta_{f,c}$	Displacement at concrete cone failure during crack cycling
$\delta_{f,pt}$	Displacement at pull-through failure during crack cycling
δ_{st}	Displacement contribution from steel deformation
δ_θ	Rotational ductility
δ_{80a}	Displacement at 80% N_u on ascending branch of load-displacement curve
δ_{80d}	Displacement at 80% N_u on descending branch of load-displacement curve
ε	Strain
ε_c	Strain in the zone of compressed concrete around anchor head
ε_{cc}	Concrete creep strain
ε_{cm}	Mean strain in concrete between cracks

ε_{ct}	Strain in concrete at crack tip
ε_{el}	Elastic strain
ε_s	Steel strain
ε_{sm}	Mean steel strain
θ	Rotation
θ_{IN}	Prescribed rotation
θ_p	Plastic hinge rotation
θ_{pz}	Rotation in plastic hinge zone
θ_t	Total relative member rotation
$\theta^{TR}{}_i$	Trial rotation
θ_y	Yield rotation
κ	Curvature
μ	Mean value
μ_m	Mean margin of safety
ρ	Reinforcement ratio of longitudinal tension reinforcement
ρ'	Reinforcement ratio of longitudinal compression reinforcement
ρ_t	Reinforcement ratio of total longitudinal reinforcement
σ	Stress | Standard deviation
σ_B	Fastener bearing stress
σ_m	Standard deviation of margin of safety
σ_s	Steel stress
$\tau_{b,m}$	Mean bond stress
ϕ	Diameter of reinforcement bars | Load reduction factor (ACI 318)
$\phi(t,t_0)$	Creep coefficient

1 Problem Statement

Fasteners, such as cast-in headed studs and post-installed mechanical and chemical anchors, are a versatile means of forming connections in concrete structures. They find widespread application for the fastening of nonstructural elements to structures and are frequently used to connect new structural elements to existing structures in earthquake retrofit schemes. Although the majority of fasteners on the market today are designed and tested for use in non-seismic environments, they are commonly used for applications in structures located in earthquake regions. Inadequately tested or inappropriately used fasteners can lead to unanticipated behavior that can compromise structural performance during an earthquake and endanger human life.

Both the fastening industry and practicing engineers have recognized the advantages of standardized (pre-)qualification of fasteners for specific applications. Qualification is the process by which products are tested using standardized methods and granted an approval based on prescribed acceptance criteria. While our understanding of the behavior of fasteners, as well as the methods used for their qualification, have advanced significantly over the past 30 years, relatively little information exists about the behavior of fasteners under earthquake conditions.

The primary goals of this dissertation are:

(1) To present a comprehensive overview of research related to the seismic behavior of fastenings and existing seismic qualification methods for fasteners.
(2) To provide background to establish improved guidelines for the qualification of fastenings to be used in seismic areas. Specifically, representative load cycling histories for fastenings and for the cycling of cracks in the anchorage material are studied. This is done by means of transfer of knowledge from other branches of earthquake engineering and new theoretical and numerical investigations.
(3) To investigate experimentally some key aspects of fastener behavior under earthquake conditions. The investigations fill gaps in our understanding in this area, explore the feasibility of potential seismic testing methods and establish performance characteristics that should be sought when developing assessment criteria for fastener approval. In particular, the behavior of fasteners in wide opening and closing cracks, the performance of various failure mechanisms during near-ultimate tension load cycling and the effect of loading rate on failure are addressed.

Based on the results of the investigations, recommendations for the development of testing methods and assessment criteria for the qualification of fastenings for seismic applications are proposed.

2 Context for the Research

In 2007, the European structural design codes (Eurocodes) will begin replacing national codes for civil engineering projects in both the public and private sectors. The adoption of the Eurocodes, specifically *Eurocode 8 (2003)*, will increase the need for standardized qualification of fastening products for seismic applications. The Guideline for European Technical Approval of Metal Anchors for Use in Concrete (*ETAG 001 1997*), which regulates the qualification of such products in Europe, does not currently include testing guidelines or assessment criteria for seismic applications. Therefore, an extension to this guideline will likely be developed in the next few years. This new qualification guideline should have test methods and performance assessment criteria that reflect the actual demands placed on fastenings during earthquakes.

2.1 Applications for fasteners in earthquake regions

When discussing fastenings for seismic applications it is useful to distinguish between structural and nonstructural applications (Figure 2.1). This distinction is important since different loadings exist for the two types of applications and different factors of safety may need to be considered in the design of the fastening. For seismic applications *Eurocode 8 (2003)* provides the following definitions:

Nonstructural elements	-	Architectural, mechanical or electrical elements, systems and components which, whether due to lack of strength or to the way they are connected to the structure, are not considered in the seismic design as load carrying elements.
Primary seismic members (Structural elements)	-	Members considered as part of the structural system that resists the seismic action, modeled in the analysis for the seismic design situation and fully designed and detailed for earthquake resistance according to the rules of Eurocode 8.

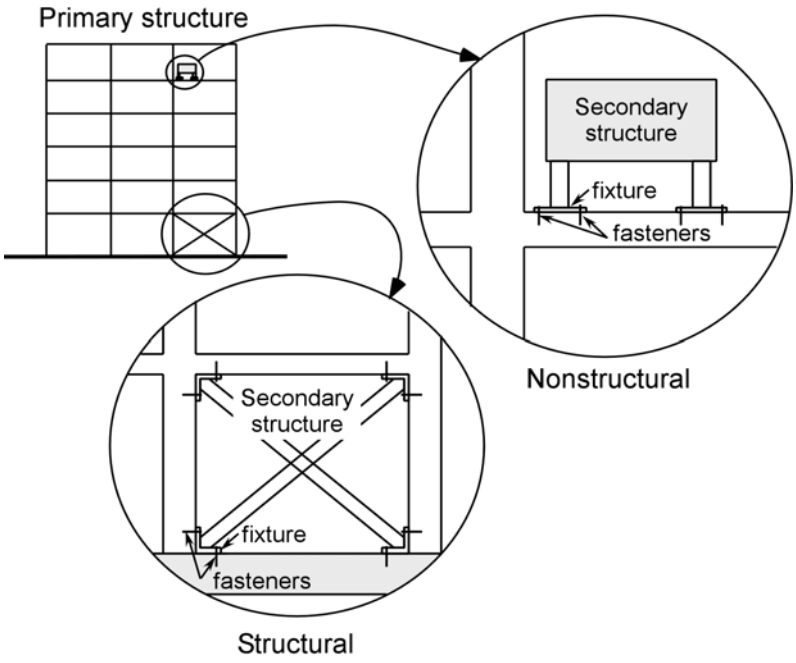

Figure 2.1 Structural and nonstructural applications for fastenings

Some typical uses for fasteners in standard and seismic applications are listed in Table 2.1 and pictured in Figure 2.2. It is worth noting that the primary purpose of the fasteners in the applications in the left-hand column in Table 2.1 is anchorage against non-seismic loads, e.g. gravity load. If the structure in which these anchorages are located is subjected to an earthquake, however, they become seismic relevant applications and should be designed as such.

Table 2.1 Applications for fastenings

Standard fastening applications in both seismic and non-seismic regions	Strengthening and rehabilitation
• Facades • Suspended ceilings • Heating, ventilation, air conditioning • Pipelines • Mechanical equipment • Structural connections	• Structural connections between new and existing structures • Restraint of wire and fiber reinforced polymer meshes

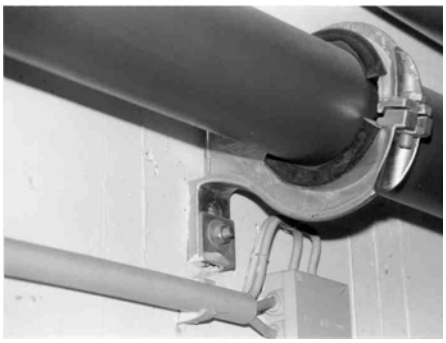

(a)

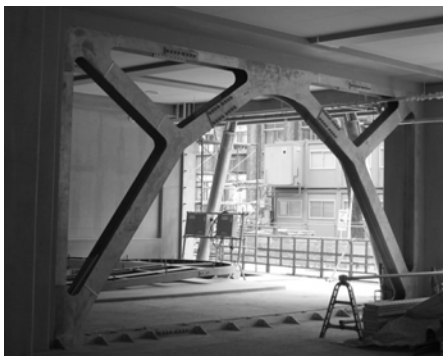

(b)

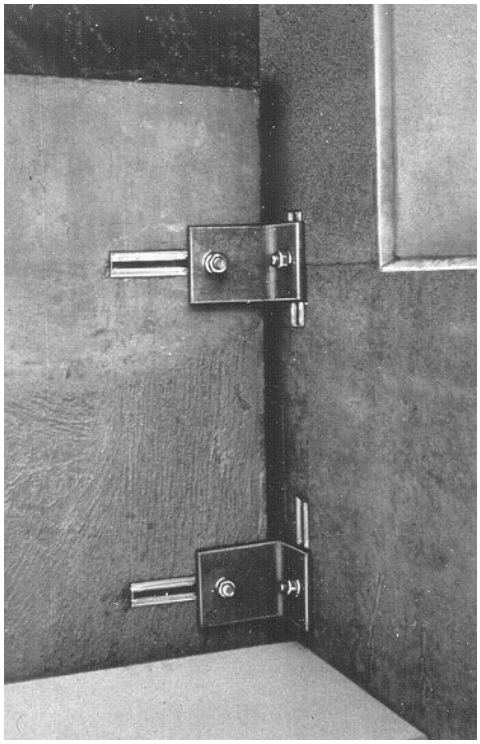

(c)

Figure 2.2 Fastening applications: (a) nonstructural (pipe hanger); (b) structural (steel brace); (c) structural or nonstructural (precast elements)

2.2 Post-earthquake reconnaissance

The goal of qualification testing of fasteners is to reduce the chance of unanticipated anchorage failure. At the present, it is difficult to estimate the extent of damage caused by failure of fastenings during historic earthquakes due to the limited number of publicly available investigations (*Ohkubo 1996, 1997*). Furthermore, distinction is seldom made in post-earthquake reconnaissance reports as to the cause of damage to nonstructural systems, which represent a large percentage of the applications that use fasteners. A step to improve this situation was made within the scope of this dissertation by

developing a reconnaissance form targeted at fastener performance for the Earthquake Engineering Research Institute (EERI) Learning from Earthquakes Program (*EERI 1996)* (Appendix A). To date, no reconnaissance has been conducted using the form and it is therefore not further discussed in this dissertation.

The photographs in Figure 2.3 and Figure 2.4 suggest that deficient fastener performance is not always the cause of failure during an earthquake, but rather that inadequate seismic design measures and improper selection of fasteners frequently lead to failure of a component or system. The failure of the anchor bolt in Figure 2.3 was likely the result of using a simple elastic design approach together with an unconservative assumption for the design ground acceleration. The failure in Figure 2.4 occurred because the short, deformation-controlled ('drop-in') expansion anchors were installed in the nonstructural surfacing of the building. Such an anchorage is inappropriate even for non-seismic applications.

(a) ***(b)***

Figure 2.3 Overturned tank at the Olive View Hospital, 1994 Northridge earthquake: (a) oxygen tank; (b) detail of fastener failure (Degenkolb Engineers)

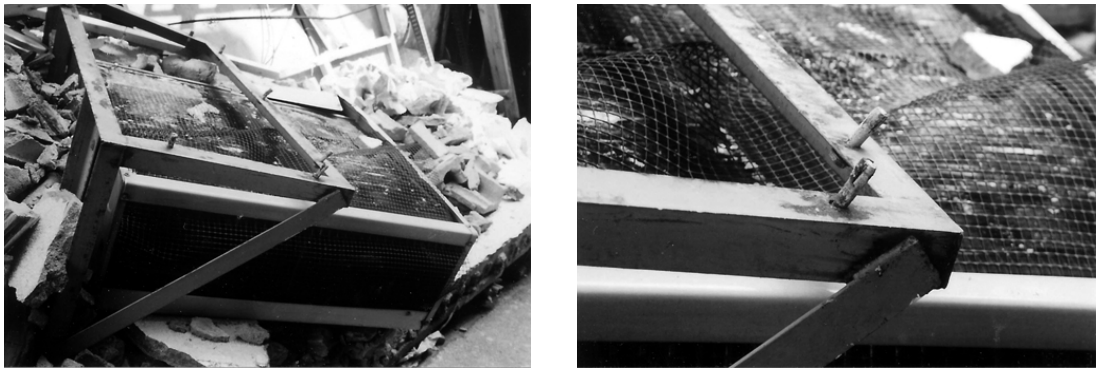

(a) ***(b)***

Figure 2.4 Collapsed air conditioning unit, 1995 Kobe earthquake: (a) air conditioning unit; (b) detail of fastener failure (courtesy of M. Ohkubo)

2.3 Seismic design and qualification

As indicated in Section 2.2, the risk of failure can only be minimized if suitably qualified products are sensibly applied together with appropriate design provisions. Design guidelines that represent the current state of knowledge for seismic applications using fasteners are given in *ACI 318 (2005)* and in the *CEN TS (in preparation)*. Practical fastening solutions for the seismic restraint of mechanical equipment are provided in

FEMA 412 (2002). In addition to design measures, qualification tests for fasteners under representative seismic conditions are required to establish whether a given fastener is suitable for the intended application.

Although this dissertation focuses on the behavior of fasteners and the development of seismic testing methods, it indirectly relates to the development of design guidelines because there is an interrelation between design guidelines and qualification testing. Design guidelines establish the boundary conditions that must be represented in qualification tests. Furthermore, most modern design methods for fasteners explicitly require characteristic loads obtained from product qualification approvals. This interrelation is evident in the determination of maximum crack widths for testing (Chapter 4) and the definition of fastener ductility (Chapter 6).

3 State of the Art

3.1 Types of fasteners

Eligehausen et al. (2006) show that fasteners can be differentiated according to the way they transfer tension loads to the anchorage material. Load-transfer mechanisms are typically identified as mechanical interlock, friction or bond (Figure 3.1).

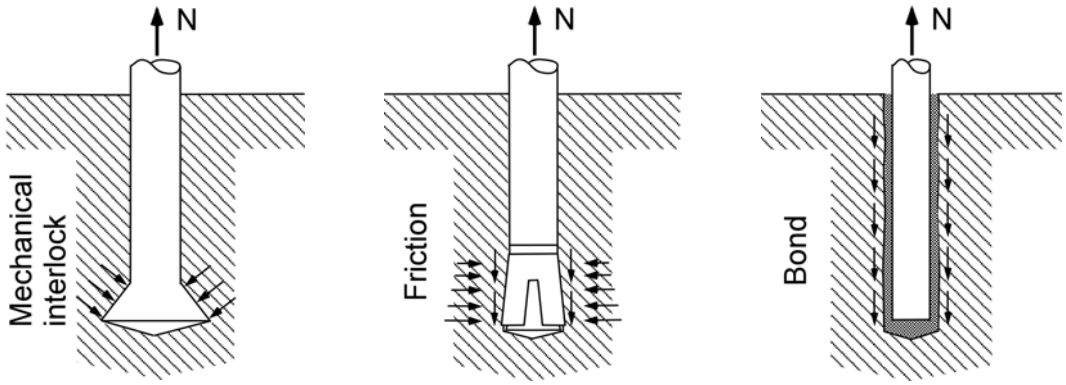

Figure 3.1 Tension load-transfer mechanisms for fasteners

Mechanical interlock involves transfer of load by bearing of the fastener on the anchorage material. Fasteners that transfer load by friction have a geometry that generates an expansion force, which in turn gives rise to a friction force between the anchor and the sides of the drilled hole. This friction force resists the applied tensile force. In the case of bond, the tension load is transferred to the anchorage material by means of chemical interlock, i.e. some combination of adhesion and micro-keying. Most commercially available fasteners resist tension loads via one or more of the above described mechanisms.

Fastening systems can be further differentiated by the way they are installed. A distinction is made here between cast-in and post-installed systems. Cast-in fasteners are secured in the formwork prior to concrete casting. Post-installed fasteners are installed into the hardened anchorage material.

3.1.1 Cast-in fasteners

Typical cast-in fasteners are headed bolts or studs, anchor channels, lifting inserts and bent reinforcement bars with internally threaded couplers (Figure 3.2). These fasteners transfer load by mechanical interlock. The advantages of cast-in fasteners are that they provide reliable performance in both cracked and uncracked concrete and are typically economical. Furthermore, since they are placed before casting, supplementary reinforcement can be provided around the anchor to increase the ultimate strength after cracking occurs. The disadvantage is that the anchorage locations must be known during the design phase of a project and erroneous placement can be costly to correct.

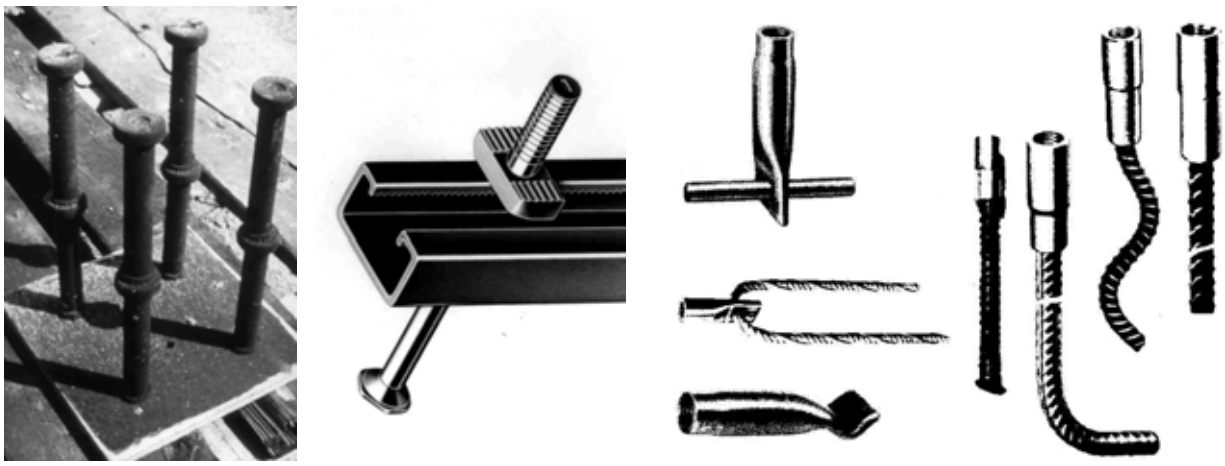

Headed studs *Anchor channel* *Lifting inserts* *Bent rebar*

Figure 3.2 Typical cast-in fasteners (Eligehausen et al. 2006)

3.1.2 Post-installed fasteners

Post-installed fasteners are installed into the hardened anchorage material either by direct installation or insertion into a pre-drilled hole. Direct installation refers to installation where studs or nails are driven into the anchorage material using powder cartridges or pneumatic action. For relatively soft anchorage materials, e.g. aerated concrete or pumice masonry units, specially designed fasteners can be set directly without pre-drilling. The majority of post-installed fasteners, however, require drilling. The increasing use of post-installed fasteners can largely be attributed to advances in drilling technology over the past few decades.

The main advantage of post-installed fasteners over cast-in fasteners is the flexibility they provide for planning and execution of a connection. Furthermore, in seismic strengthening and rehabilitation they are frequently the only option available to form a connection to an existing structure.

Three installation configurations may be distinguished for post-installed fasteners (Figure 3.3):

- Pre-positioned
- In-place
- Stand-off

In a pre-positioned installation, the fastener is installed in the anchorage material before the element to be fastened is attached. In an in-place installation, the fastener is installed through the element to be fastened, i.e. the fixture is used as a drilling template. In a stand-off installation, the item to be fastened is mounted at a distance from the surface of the anchorage material.

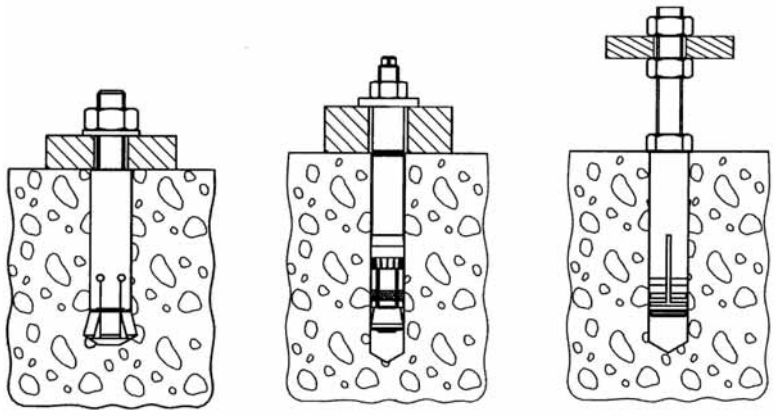

Figure 3.3 Installation configurations (Eligehausen et al. 2006)

Post-installed fasteners for use in concrete, which are inserted into a pre-drilled hole, may be classified as mechanical expansion anchors, undercut anchors, screw anchors, bonded anchors, ceiling hangers and plastic anchors (Figure 3.4 to Figure 3.9). Mechanical expansion anchors, ceiling hangers and plastic anchors transfer applied tension load into the anchorage material mainly by friction, undercut and screw anchors by mechanical interlock and bonded anchors by bond.

Mechanical expansion anchors can be divided into two groups:

- torque-controlled, which generate friction resistance by drawing one or more expansion cones into an expansion sleeve (or expansion segments), thereby expanding the expansion element(s) against the sides of the drilled hole when a torque or axial tension load is applied to the anchor,
- displacement-controlled, where friction resistance is generated by driving an expansion plug into a sleeve with a setting tool and a hammer (cone-down) or, alternatively, by driving the sleeve over the cone (cone-up).

Torque-controlled expansion anchors may be further classified as either sleeve-type or bolt-type. Sleeve-type anchors generally consist of a bolt or threaded rod with nut, washer, spacer and expansion sleeve and one or more expansion cones. Bolt-type anchors typically consist of a bolt, the end of which has been swaged or machined into a conical shape, expansion segments nested in the recessed conical end of the bolt and a nut and washer.

Combination anchors such as bonded-expansion anchors and bonded-undercut anchors also exist.

Detailed descriptions of the various fastener types and their load transfer mechanisms are provided in *Eligehausen et al. (2006)*.

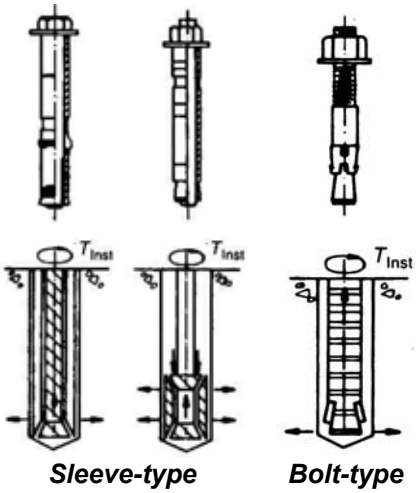

Sleeve-type *Bolt-type*

Torque-controlled

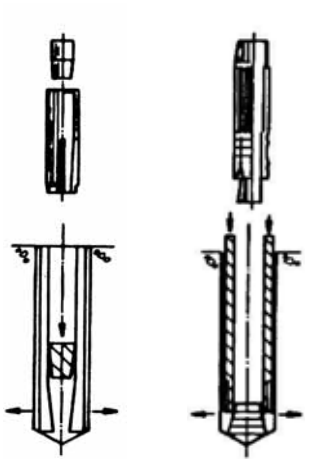

Cone-down *Cone-up*

Displacement-controlled

Figure 3.4 Typical mechanical expansion anchors

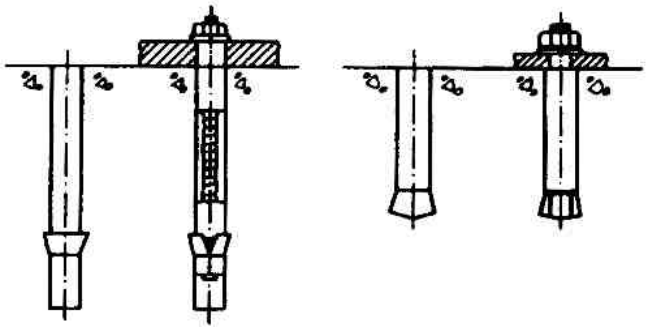

Figure 3.5 Typical undercut anchors

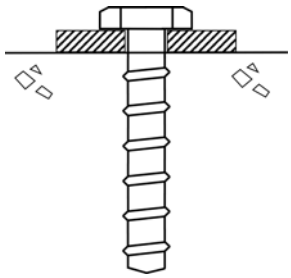

Figure 3.6 Typical screw anchor

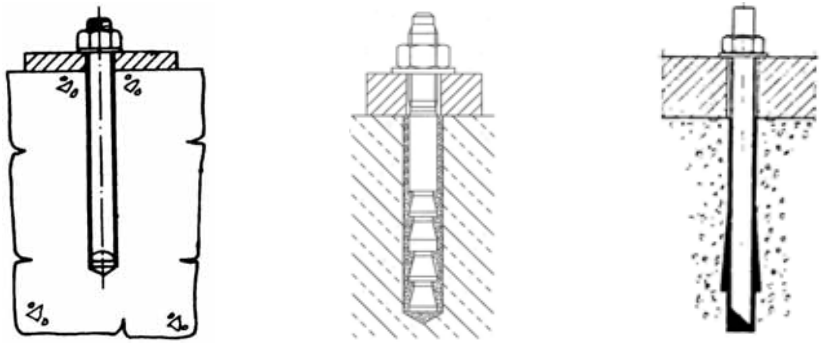

Standard *Bonded-expansion* *Bonded-undercut*

Figure 3.7 Typical bonded anchors

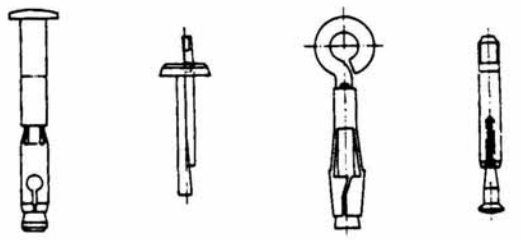

Figure 3.8 Typical ceiling hangers

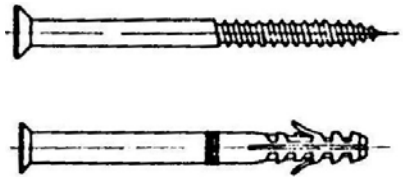

Figure 3.9 Typical plastic anchor

3.2 Fastener load-bearing behavior

Load-bearing behavior encompasses both the load-displacement behavior and the failure mode of a fastening. It is product dependent and is a function of numerous geometrical, material and environmental parameters. A comprehensive discussion of fastener load-bearing behavior can be found for example in *CEB (1994)* or *Eligehausen et al. (2006)*. A brief overview of behavior relevant for this dissertation is presented below.

3.2.1 Failure modes

Fastenings may be loaded in tension, shear, combined tension and shear, or by bending moments (Figure 3.10).

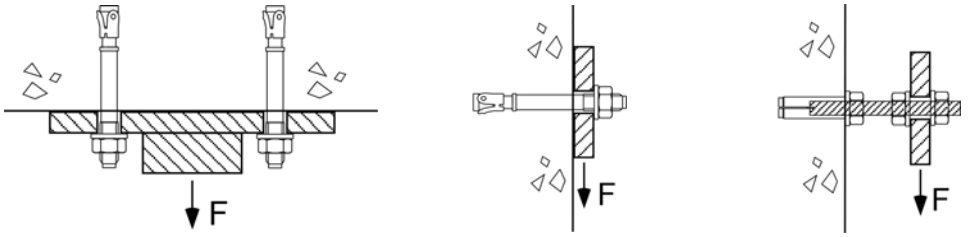

Figure 3.10 Loadings on fastenings

For loading in tension, four general failure modes can be distinguished: pull-out or pull-through, concrete cone failure, splitting and steel failure (Figure 3.11).

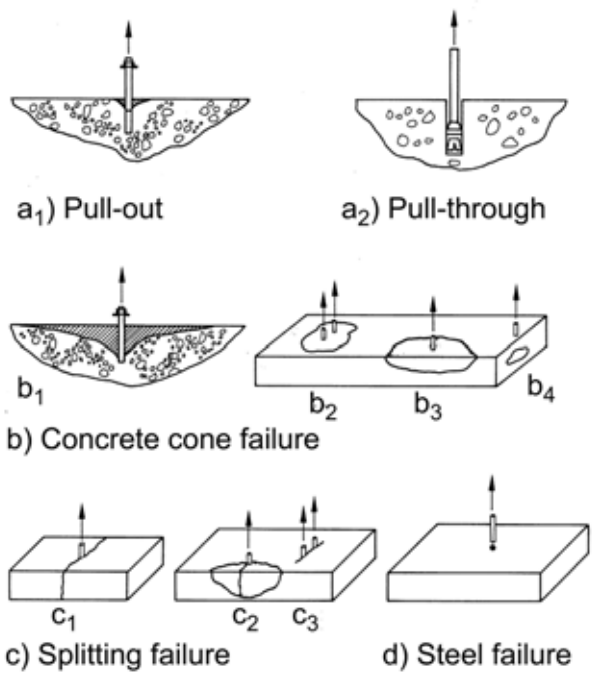

Figure 3.11 Tension failure modes (Eligehausen et al. 2006)

Pull-out failure is characterized by the anchor being pulled out of the drilled hole, whereby the concrete in the immediate vicinity of the anchor may or may not be damaged (Figure 3.11a_1). This failure mode can occur with expansion anchors, plastic anchors and ceiling hangers if the expansion force is not sufficient, with headed, screw and undercut anchors if the bearing area is not sufficient and with bonded anchors. *Pull-through* failure is unique to torque-controlled expansion anchors and is characterized by the expansion cone being pulled through the expansion elements, i.e. the expansion elements remain in the drilled hole (Figure 3.11a_2).

Concrete cone failure is characterized by a cone-shaped concrete breakout (Figure 3.11b). The individual concrete cones for a group of anchors may overlap

(Figure 3.11b_2) or the cone may be truncated if it is located close to an edge (Figure 3.11b_3). Fastenings located very close to an edge that generate a high bearing pressure can cause local concrete breakout near the head ('*blow-out*') (Figure 3.11b_4).

Failure due to *splitting* of the concrete typically occurs when the dimensions of the concrete component are limited (Figure 3.11c_1), the anchor is installed too close to an edge (Figure 3.11c_2) or a line of anchors are installed in close proximity to each other (Figure 3.11c_3).

Steel failure of the anchor bolt or sleeve represents the upper limit of the load carrying capacity of a fastener.

Fastenings with large edge distances and embedment depths loaded in shear will fail by local concrete spalling in front of the anchor followed by *steel failure* (Figure 3.12a). If the fastening is located close to an edge (Figure 3.12b_1,b_2) or in a corner (Figure 3.12b_3) and loaded in shear towards the edge, *concrete edge breakout* will occur. This failure mode is similar to concrete cone failure in tension. For thin (Figure 3.12b_4) or narrow (Figure 3.12b_5) members, the concrete breakout body will be truncated. Stiff fastenings with relatively shallow embedment depths may fail by *pry-out* of the concrete on the side of the anchor opposite to the direction of the applied shear load (Figure 3.12c_1,c_2). Mechanical expansion anchors loaded in shear can fail by *pull-out* if the expansion force provide by the anchor is not sufficient to resist the tension forces induced by the shearing (Figure 3.12d).

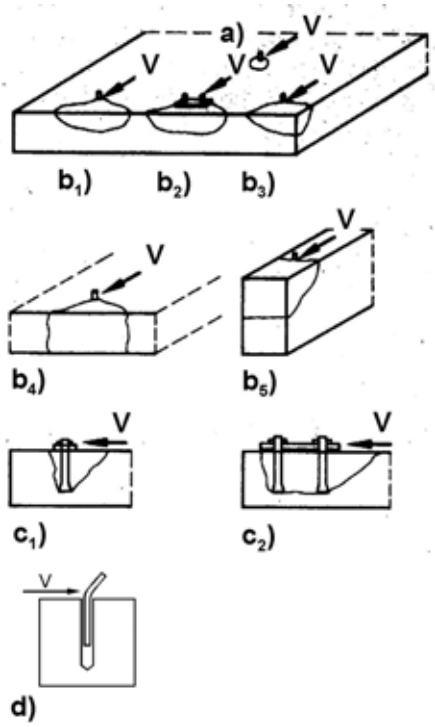

Figure 3.12 Shear failure modes (Eligehausen et al. 2006)

In addition to the above-described failure modes in tension and shear the following distinctions are made for bonded anchors failing by *pull-out*: failure between *the threaded rod and the mortar* (Figure 3.13a), failure between *the mortar and the concrete* (Figure 3.13b) and *mixed failure* (Figure 3.13c). In all three cases a concrete cone with a depth of 2·*d* to 3·*d* (*d* = threaded rod diameter) forms near the surface of the anchorage material and bond failure occurs along the rest of the embedment depth.

Screw anchors may also exhibit *mixed failure,* where a concrete cone forms near the surface and the lower portion of the screw is pulled out (*Küenzlen & Sipple 2001*).

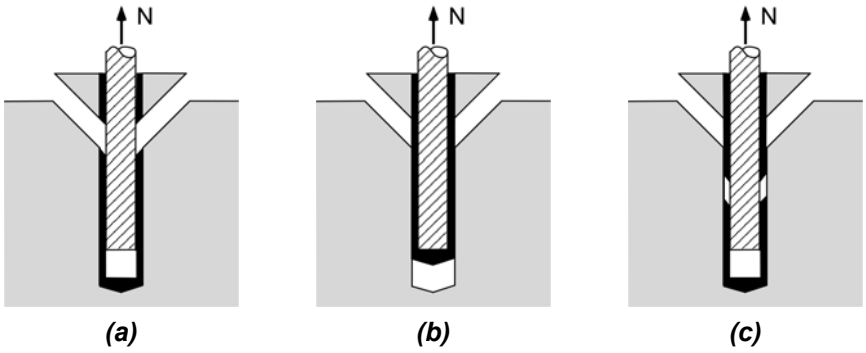

Figure 3.13 Pull-out failure modes of bonded anchors: (a) threaded rod / mortar; (b) mortar / concrete: (c) mixed failure (after Cook et al. 1998)

3.2.2 Load-displacement behavior under monotonic loading

Figure 3.14 depicts idealized load-displacement curves for various tension failure modes for fasteners suggested by *Fuchs et al. (1995)*.

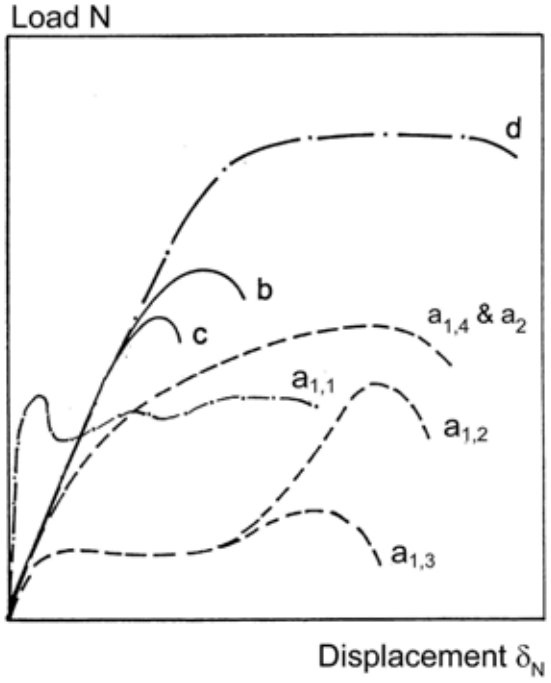

Figure 3.14 Idealized load-displacement curves for various tension failure modes for fasteners (after Fuchs et al. 1995)

Curve $a_{1,1}$ is typical for a displacement-controlled expansion anchor failing by *pull-out*. *Pull-out* failure can also occur with torque-controlled expansion anchors when the 'follow-up' expansion, i.e. the expansion generated by loading of the fastener, as opposed to by the installation torque, does not develop properly. In this case, the anchors will undergo a large amount of displacement at a relatively low load level as illustrated by curves $a_{1,2}$ and $a_{1,3}$. Headed or undercut anchors undergoing *pull-out* are represented by curve $a_{1,4}$. Torque-controlled expansion anchors that fail by *pull-through* exhibit load-displacement behavior similar to that for *pull-out* of headed bolts and undercut anchors (curve a_2).

Load-displacement curves for anchors failing by *concrete cone failure* and by concrete *splitting* are illustrated by curves b and c, respectively.

The load-displacement behavior for an anchor loaded in tension failing by *steel failure* is indicated by curve d. Ductile behavior, as indicated by curve d, will occur only if sufficient bolt length is available for elongation.

It is important to note that the *concrete cone* and concrete *splitting* failure modes, as well as many *pull-out* and *pull-through* failure modes are characterized by significant strain-softening behavior on the post-peak portion of the load-displacement curve.

Figure 3.15 Illustrates typical load-displacement behavior of a (preloaded) fastening located far from any edges loaded in shear. The corresponding curve associated with tension loading for the same anchor is provided for comparison. Initially, shear force is transferred between the concrete and the fixture (baseplate) via friction generated by the preload in the anchor. When the externally applied shear load exceeds the available friction resistance, the fixture slips until the gap between the anchor and the edge of the clearance hole in the fixture has been eliminated. With sufficient embedment depth, the anchor may be capable of resisting additional load until steel failure of the anchor bolt occurs. Owing to the locally high bearing stresses, the spalling of the concrete and the associated bending deformation of the anchor, displacements associated with shear loading at ultimate are markedly greater than for axial loading.

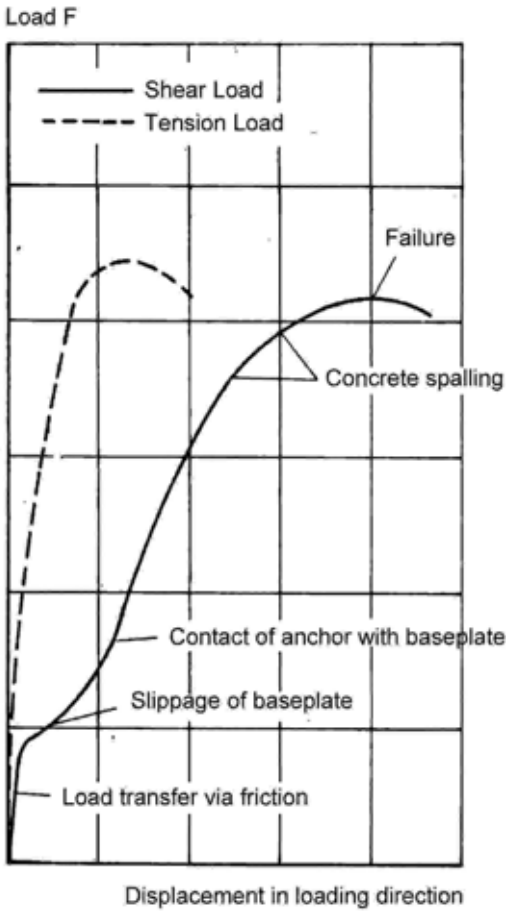

Figure 3.15 Typical load-displacement curves for anchors failing in tension and shear (after Rehm et al. 1988)

Fastenings located close to an edge of a component and loaded toward the edge in shear will exhibit a similar behavior to that shown in Figure 3.15, however, the ultimate load will depend on the resistance provided by the concrete breakout body.

Product specific load-displacement behavior for anchor channels (*Kraus 2003*), bonded anchors (*Meszaros 1999*), plastic anchors (*Pregartner 2003*) and screw anchors (*Küenzlen 2005*), are available in the literature.

Analytic methods to determine the ultimate loads of fasteners failing in the various failure modes discussed above under monotonic loading can be found in several documents, e.g. *CEB (1994)* or *Eligehausen et al. (2006*).

3.2.3 Behavior in static cracks

Numerous investigations have shown that the load-bearing behavior of fasteners in cracked concrete can differ significantly from that in uncracked concrete, e.g. *Cannon (1981)* or *Eligehausen & Balogh (1995*). The difference in behavior is expressed as a change in stiffness, ultimate load capacity, and possibly, in the failure mode of the fastener (Figure 3.16).

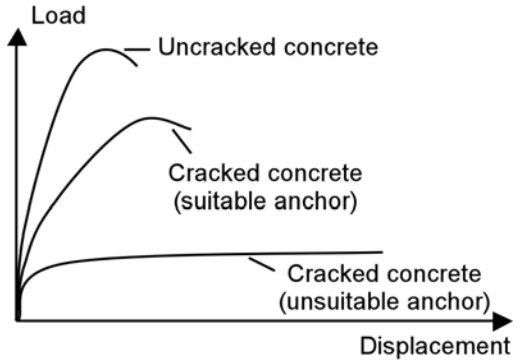

Figure 3.16 Effect of cracking on the tension load-displacement curves for a torque-controlled expansion anchor

Many fasteners designed for use in uncracked concrete are not suitable for use in cracked concrete. Critical factors in determining the extent of the influence due to cracking are: the fastener type and design, the location of the crack relative to the fastener, the load applied to the fastener and the crack width.

Tests on a variety of anchors loaded in tension in static cracks, i.e. not cycled, show reductions of the load-bearing capacity of 30% and more even at relatively small crack widths (Δw = 0.3 mm). Figure 3.17 shows experimentally obtained ratios of the ultimate load capacity in cracked and uncracked concrete and the trends for reduction of capacity due to cracking for some typical fastener types.

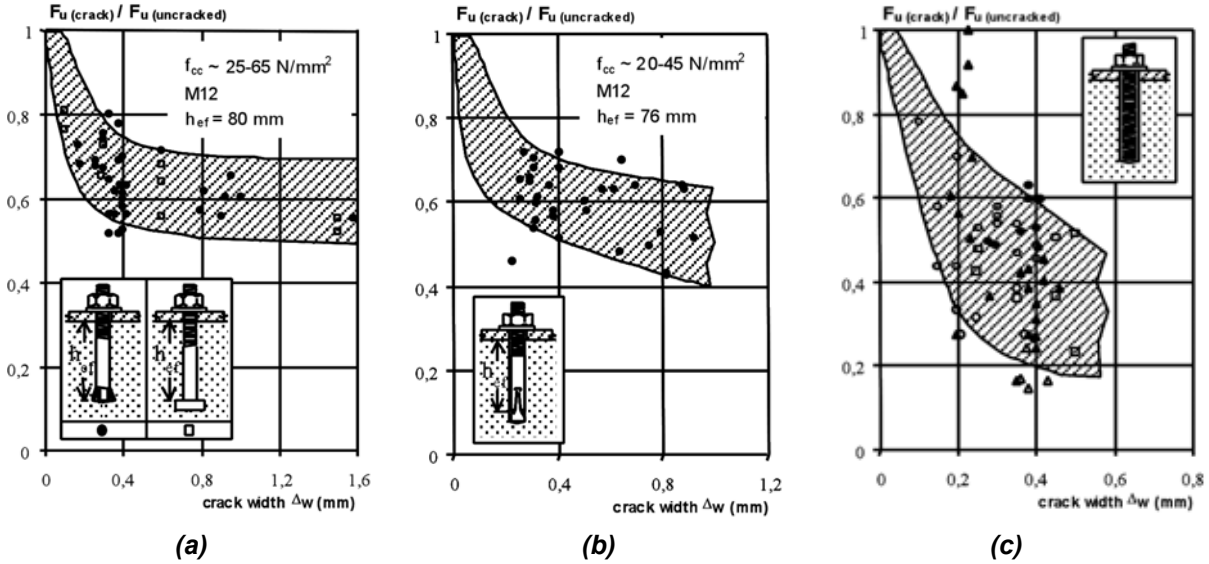

(a) *(b)* *(c)*

Figure 3.17 Ultimate bearing capacity of fasteners in cracks under tension loading: (a) undercut anchors and headed studs; (b) torque-controlled expansion anchors designed for use in cracked concrete; (c) bonded anchors (after Eligehausen & Balogh 1995)

3.3 Fastener behavior under seismic conditions

As will be discussed in Chapter 4, during an earthquake a fastener may be subjected to a combination of cyclic tension and shear forces. Furthermore, the fastener may be located in a crack that either forms during the earthquake or has traversed the fastener location at some prior time. This crack width will typically vary over the duration of the

earthquake, e.g. the crack will open and close several times, as a result of deformation of the structure in which the fastening is located. Consequently, the seismic behavior of anchorages depends on numerous parameters, including:

- the amplitude, rate, sequence and number of cycles of the imposed actions,
- the direction of application of the actions (axial, shear, combined),
- the state of the surrounding concrete (uncracked or cracked, crack orientation relative to the anchor axis, crack behavior during the strong ground motion),
- quantity and orientation of reinforcement in the vicinity of the anchorage, and
- the characteristics of the anchor, including load transfer mechanism, material properties, diameter and embedment.

A chronological review of investigations of cast-in and post-installed fastenings to concrete under seismic relevant conditions is presented in this section. The reviews have been grouped according to those dealing with load cycling, loading rate and behavior in cycled cracks. Investigations that have dealt with multiple aspects of fastener behavior may appear in more than one section, however, the aspects are reviewed separately.

3.3.1 Influence of load cycling

For earthquake applications, large amplitude ($F \geq 0.5 \cdot F_{u,m}$), low cycle ($n < 1000$) loadings are of interest. Several of the investigations reported below have been adopted from *CEB (1994)*.

3.3.1.1 Tension cycling

Cannon (1981)

Reinforced concrete beams (f_c = 40 N/mm^2) were loaded cyclically in bending, whereby the load was transmitted to the beams by a pin-connected fixture fastened to the beam with post-installed anchors. The fastener type and number, the reinforcement steel ratio, the loading magnitude and frequency, as well as the rigidity of the fixture were varied. Cannon concludes that under cyclic loading the performance of expansion anchors depends on: (a) the magnitude of the applied load, (b) the coincidence of flexural cracking with the anchor location, and (c) the rigidity or flexibility of the attachment. He further notes that when the load producing flexural cracking is transferred to a beam by anchors, cracks will almost always coincide with the anchor locations.

Lindquist (1982)

Lindquist (1982) performed an extensive literature study of test data on the performance of post-installed fastenings to concrete (6000 tests) to identify research needs. He then conducted 36 exploratory tests to study the effect of various anchor preload levels on the ultimate strength of torque-controlled and displacement-controlled expansion anchors M20 (¾ inch) in uncracked concrete (f_c = 41 N/mm^2). The majority of the tests used low-cycle dynamic loading in tension, shear and inclined tension (load angle 30° to anchor axis). A stepwise increasing cyclic load was used, whereby 40 cycles were applied at each load level. The upper load cycling levels were 0.2, 0.4, 0.6, 0.8 and 1.0 times the mean ultimate reference load and the lower load level was constant at negative 2 kN (500 lbs). The negative load caused impacting to occur as the load was

cycled through the zero point. Although the cyclic load alternated between positive and negative values, the large asymmetry toward the upper load level made it similar to a pulsating tension load.

The key results for tension load cycling can be summarized as follows:

- Failure occurred due to anchor steel failure, pull-out or local breakout of concrete.
- The ultimate tension strengths obtained from the cyclic tests were not significantly lower than the corresponding monotonic reference strengths.
- The ultimate tension capacities were not affected by the preloading level.
- The majority of the anchor displacement occurred during the first few cycles at a given load level.

Copley & Burdette (1985)
Similar to the tests by *Cannon (1981)*, a reinforced concrete slab (f_c = 41 N/mm^2) was loaded cyclically in bending, whereby the load was transmitted by a pin-connected fixture fastened to the slab with fasteners. Groups of four anchors were connected through a plate that was stiffened to eliminate the influence of the fixture stiffness. The anchors tested were deformation-controlled (self-drilling) expansion anchors, torque-controlled (bolt type) expansion anchors and grouted bolts. The authors conclude that that there is a direct relation between the slab curvature and the fastener displacement during tension load cycling, i.e. there is a direct relation between the crack widths and the fastener displacement. The fact that the load was cycled was of secondary importance in the study and the influence was not discussed in detail.

Eibl & Keintzel (1989a)
Tension load cycling tests were performed using undercut anchors M12 installed in normal strength (f_{cc} = 30 N/mm^2) cracked concrete (w = 0.7 mm and 1.1 mm). Single anchors were tested with large anchor spacing and edge distance. The setup was such that an unrestricted concrete cone could form. Sinusoidal load cycles at 1 Hz, 5 Hz or 10 Hz were applied to the fastener for a duration of 10 seconds, i.e. 10, 50 or 100 load cycles. The load was cycled between 2 kN and 0.8 times the average failure load from monotonic reference tests. A pullout test was performed subsequent to the cycling to determine the residual capacity. Concrete cone failure was achieved in most cases.

Eibl and Keintzel (1989a) reached the following conclusions:

- Hysteresis was nearly non-existent during tension load cycling.
- The fastener displacement during cycling stopped increasing (converged) after about 50 load cycles (Figure 3.18). If failure occurred during load cycling, however, displacement began to diverge shortly before failure.
- The applied tension load cycling to 80 percent of the reference failure load did not significantly reduce the load-bearing capacity (concrete cone failure) of the fastener (Figure 3.19). This was independent of the cycling rate.
- The secant stiffness (to ultimate load) of the fastener increased after load cycling.
- The combined mechanical work that occurred during cycling and subsequent loading was approximately the same as that under the monotonic loading curve.

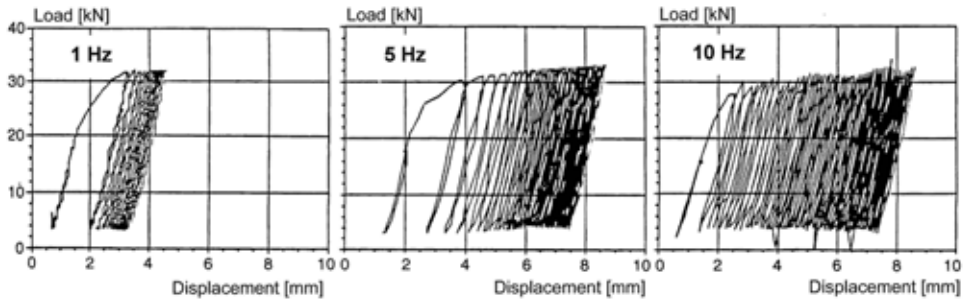

Figure 3.18 Load-displacement curves for undercut anchors M12 in cracked concrete (w = 0.7 mm) under tension load cycling at 1 Hz, 5 Hz and 10 Hz (after Eibl & Keintzel 1989a)

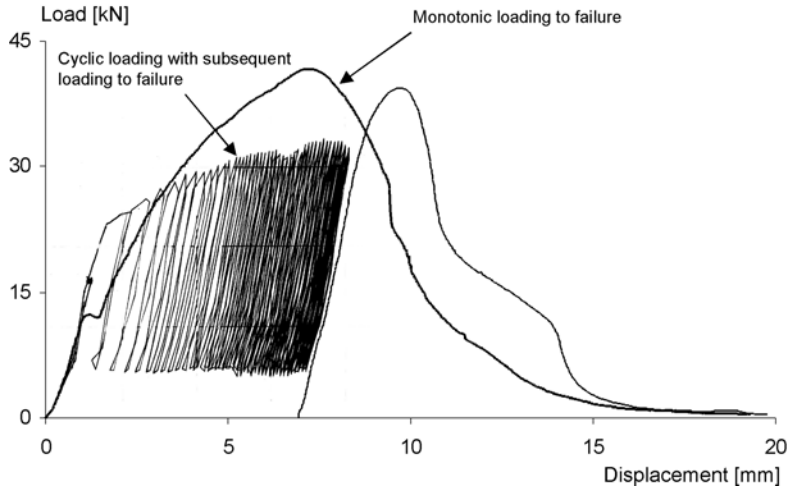

Figure 3.19 Load-displacement curves for undercut anchors M12 failing by concrete breakout in cracked concrete (w = 0.7 mm) under monotonic and cyclic tension load (after Eibl & Keintzel 1989a)

Eibl & Keintzel (1989b)

The tests performed in *Eibl and Keintzel (1989a)* were extended to include torque-controlled expansion anchors M12 and alternating axial loading, i.e. tension/compression cycling. All tests were performed in normal strength (f_{cc} = 30 N/mm^2) cracked concrete (w = 0.7 mm). The alternating sinusoidal load cycles were applied to the fastener at 0.1 Hz for a duration of 100 seconds, i.e. 10 load cycles. The load was cycled between ±0.8 times the average failure load determined from monotonic reference tests. A pullout test was performed subsequent to the cycling to determine the residual capacity. Concrete cone failure was achieved in most cases.

Eibl and Keintzel (1989b) reached the following conclusions:

- The investigated torque-controlled expansion anchor performed comparably to the undercut anchors under tension and alternating load cycling.
- The alternating axial load cycling to 80 percent of the reference failure load did not significantly reduce the load-bearing capacity (concrete cone failure) of the fasteners, however, the displacements that occurred during alternating cycling were much larger than during tension load cycling (Figure 3.20).
- Hysteresis was more pronounced during alternating axial load cycling than during tension cycling.

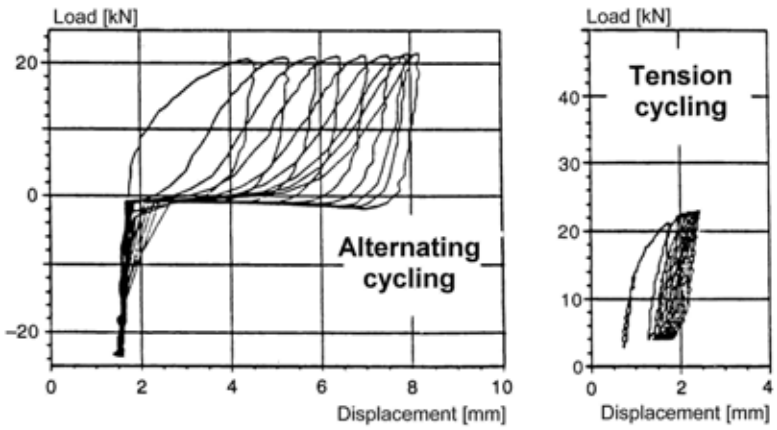

Figure 3.20 Load-displacement curves for torque-controlled expansion anchors M12 in cracked concrete (w = 0.7 mm) under alternating and tension load cycling (after Eibl & Keintzel 1989b)

3.3.1.2 Shear cycling

Usami et al. (1980)

Cyclic shear tests were performed on groups of headed studs (d = 19 mm; f_u = 480 MPa) cast in uncracked concrete (f_c = 22.5 N/mm^2) with large edge distances. The embedment depth (h_{ef} = 5.3·d and 8.4·d), the number of anchors (n = 2 and 4) and the anchor spacing (150 and 200 mm) were varied, as was the type of loading (pulsating and alternating shear loading). Specimens with both one and two shear planes were tested. The results can be summarized as follows:

- Failure was generally caused by fracture of the anchor steel during cycling (low-cycle fatigue).
- The failure load obtained with the two-plane specimen was significantly higher than that obtained with the one-plane specimen under the same conditions. The conditions in practice are better represented by the one-plane specimen,
- The displacement under pulsating shear loading at failure (~ 45 mm) was much larger than under alternating shear (~15 mm) (Figure 3.21).
- With alternating shear loading the shear strength was only about 70% to 80% of the value for pulsating loading (Figure 3.21). In two of the three tests used to determine these values, a change of failure mode from concrete breakout (pulsating shear) to steel failure (alternate shear) occurred. Monotonic reference tests to determine the influence of the pulsating shear loads were not reported.
- During alternating shear loading, considerable pinching and degradation of the force response was observed.

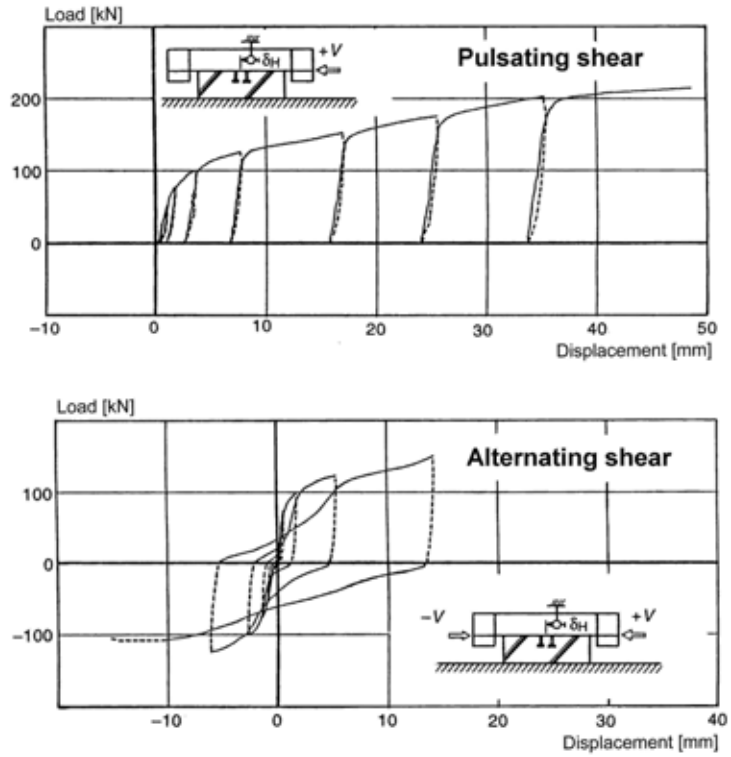

Figure 3.21 Load-displacement curves for a group of two headed anchors (d = 19 mm; one shear plane) subjected to pulsating and alternating shear loads (Usami et al. 1980)

Usami et al. (1981)

Injection-type bonded anchors (epoxy mortar) were subjected to alternating shear displacements. The bar diameter was d = 20 mm, the drilled hole diameter was d_0 = 40 mm and the embedment depth was h_{ef} = 10·d. The test specimens and set-up were the same as for the tests described above (*Usami et al. 1980*). All bolts failed by rupture of the anchor steel. Similar tests were performed with capsule-type bonded anchors M20 (polyester mortar). In the tests with one shear plane, anchors with h_{ef} = 5·d were pulled out, while anchors with h_{ef} = 10·d failed by rupture of the steel.

Klingner et al. (1982)

Klingner et al. (1982) tested single anchor bolts (d = 19 mm) with an embedment depth of h_{ef} = 10.7·d, embedded in unreinforced concrete with varying edge distances and embedded in reinforced concrete with edge distances of 50.8 mm and 101.6 mm under monotonic and alternating shear loads. For the investigated anchors embedded in unreinforced concrete an edge distance of 254 mm was sufficient to avoid concrete failure. Although the anchors in reinforced concrete had edge distances well below this value, the anchor bolts were able to develop their full shear strength, i.e. steel failure, due to the presence of appropriately designed and detailed tieback reinforcement. The displacement at ultimate load for the anchors with tieback reinforcement was large since the concrete had to crack before the reinforcement could be activated.

Anchors in unreinforced concrete with large edge distances (254 mm) and with tieback reinforcement and small edge distances (50.8 mm and 101.6 mm) were also subjected to stepwise-increasing alternating shear loads (Figure 3.22). The results can be summarized as follows:

- Substantial decrease of the shear stiffness with cycling occurred.
- Pinching of the hysteresis loops near the origin was pronounced.
- The shear deformation corresponding to the maximum shear load increased with increasing number of cycles. The deformation was attributed to crushing of the concrete around the anchor near the surface of the anchorage component.
- Under alternating cyclic loading, bolts placed both with and without tieback reinforcement typically failed at loads approximately 50% lower than those resisted by monotonically loaded bolts owing to the effects of low-cycle fatigue.

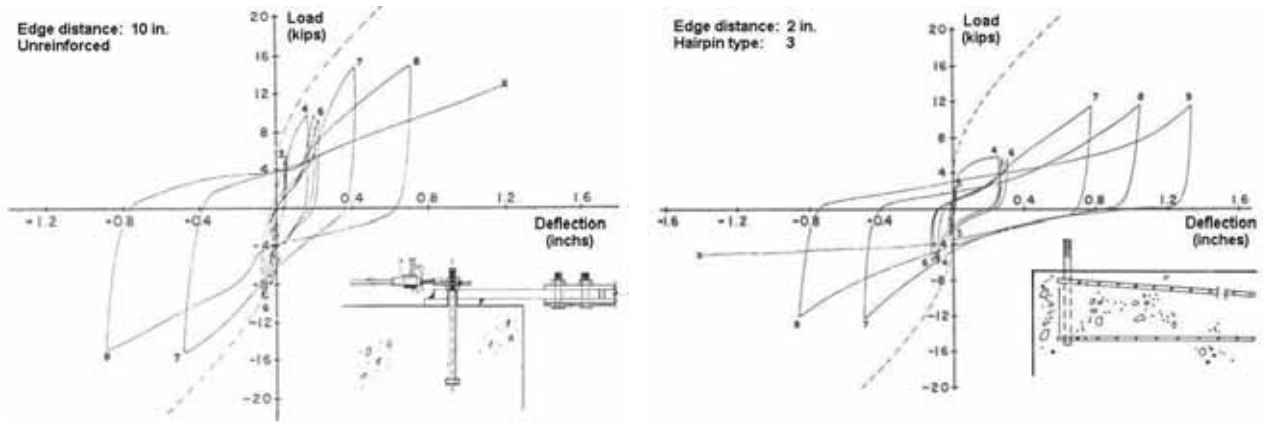

Figure 3.22 Load-displacement curves for headed anchors under alternating shear loads: (a) without tieback at large edge distances; (b) with tieback at small edge distances (Klingner et al. 1982)

Lindquist (1982)

Shear load cycling tests were performed using the test setup and procedure described in Section 3.3.1.1. The anchors failed by steel failure.

The results showed that the ultimate shear strengths were not affected by the anchor tension preload level. Furthermore, the ultimate shear strengths were not affected by the applied 'nearly pulsating' load cycling. Failure of the anchors typically occurred, however, within 20 cycles when the upper load was 100 percent of the mean ultimate reference load.

Endo & Shimizu (1985)

Endo and Shimizu (1985) report on cyclic shear tests on various types of mechanical expansion anchors and bonded anchors used to connect shear walls. The influence of roughening the interface between the new and existing structures, as well as the effect of spiral reinforcement placed close to the interface, was investigated. Displacement-controlled alternating shear tests exhibited force-displacement behavior with features typical for force-controlled tests (Figure 3.22a), i.e. pinched hysteresis loops. The primary difference in the displacement-controlled tests was that degradation of the force occurred for repeated cycles to a given displacement. This degradation was most pronounced during the early cycles and reduced during subsequent cycles.

Giuriani & Grisanti (1986)

Giuriani and Grisanti (1986) subjected dowels and headed studs used as connectors in steel-concrete composite structures to repeated shear loads. One of the main parameters investigated was the embedment length of the connectors, which varied between $3 \cdot d$ and $8 \cdot d$. The anchors were located far from any edges so that steel failure of the anchors could occur. The results showed that the hysteresis loops were much narrower for short anchors ($h_{ef} = 3 \cdot d$) than for longer anchors. Furthermore, the degradation due to repeated loading was more significant for short anchors.

Henzel & Stork (1990)

Henzel and Stork (1990) report on alternating shear tests with mechanical expansion anchors and bonded anchors M12 located far from edges in uncracked concrete (f_{cc} = 25 N/mm^2). Although the tests were not representative of seismic conditions, i.e. since a large number of low amplitude shear cycles were applied, the authors concluded that the length of the bending arm in shear, such as exists for a stand-off mounting or which can develop as concrete spalls around the anchor during cycling, has a significant influence on the shear cycling capacity of the fastener. This conclusion is likely applicable for seismic applications.

Vintzeleou & Eligehausen (1991)

Alternating shear tests (displacement-controlled) were performed on torque-controlled expansion anchors, undercut anchors and bonded anchors M12 installed in normal strength (f_c = 25 N/mm^2) cracked concrete (w = 0.1 to 0.8 mm). The crack was parallel to the direction of loading. The embedment depths were h_{ef} = 80 mm (expansion and undercut anchors) and h_{ef} = 100 mm (bonded anchors).

The fasteners were installed without tieback reinforcement at a distance of 80 to 150 mm from the edge of the anchorage component. Depending on the edge distance and steel strength, two failure modes were observed: concrete edge breakout and steel failure accompanied by a shell-shaped local spalling of concrete in front of the anchor.

Figure 3.23 shows typical hysteresis loops obtained for the investigated anchors. The curves are characterized by their pronounced pinching near the origin and the force degradation during repeated cycles to a constant displacement level.

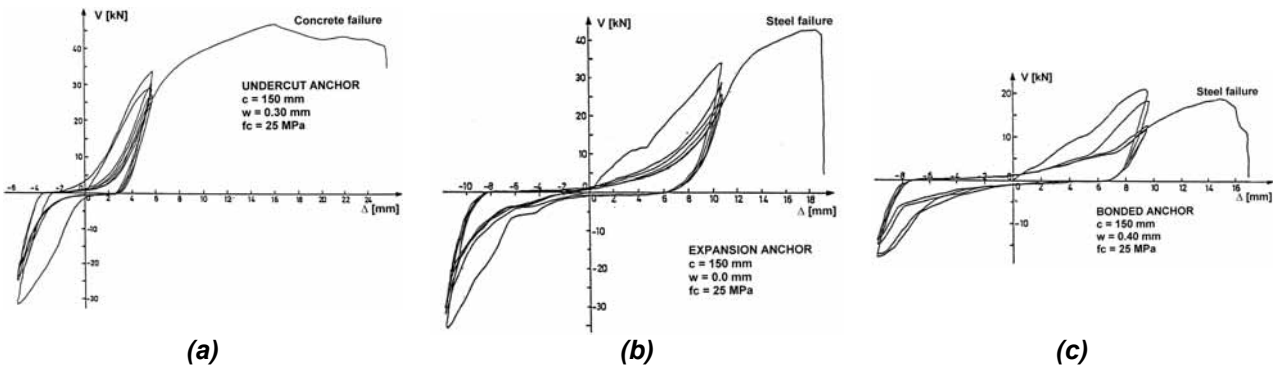

Figure 3.23 Load-displacement curves under shear cycling: (a) undercut anchor; (b) expansion anchor; (c) bonded anchor (after Vintzeleou & Eligehausen 1991)

Figure 3.24 shows the force degradation (V_n/V_1) in the n^{th} cycle as a function of the number of cycles. The results of all cyclic tests in Figure 3.24 are plotted independently of the crack width and edge distance since no clear influence of these parameters on the hysteretic behavior was observed. Since no failure occurred during the load cycling, the authors concluded that the strength and stiffness degradation was due to the local deterioration of the concrete on the loaded side of the anchor.

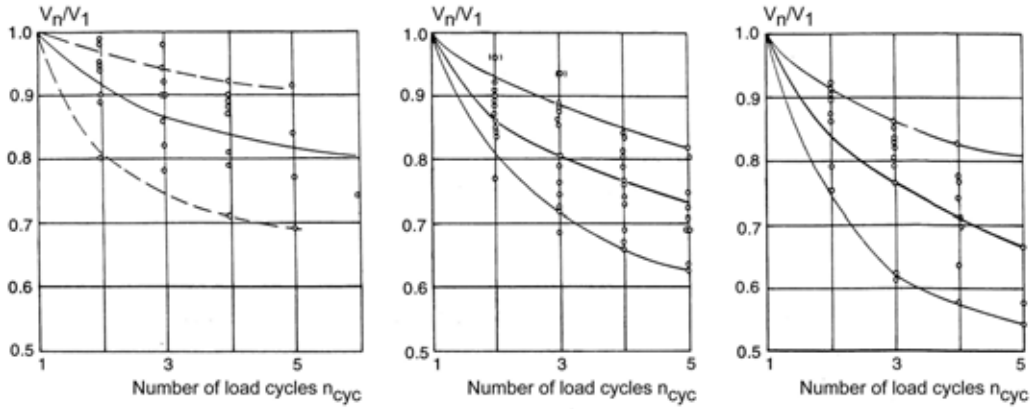

Figure 3.24 Force degradation due to shear cycling: (a) undercut anchor; (b) expansion anchor; (c) bonded anchor (Vintzeleou & Eligehausen 1991)

Vintzeleou and Eligehausen (1991) reached the following conclusions:

- All of the investigated anchors behaved similarly under monotonic and cyclic shear loading in spite of the fact that their behavior under tension loading is rather different, especially in cracked concrete.
- For both failure modes (concrete and steel) the load-displacement curve after ultimate load was almost vertical. Therefore, reliable cycling behavior can only be obtained for imposed displacements smaller than the value corresponding to ultimate load under monotonic loading δ_u.
- Force degradation was pronounced for all investigated anchor types during symmetric alternating shear cycling between displacement values $\delta_{max} \leq 0.75 \cdot \delta_u$ independent of the failure mode. Torque-controlled expansion anchors and especially bonded anchors seemed to be more sensitive to the cyclic actions than the undercut anchors.
- For displacement values larger than the maximum value during cycling, the monotonic envelope was reached and then followed. Alternating cyclic displacement to $\delta_{max} \leq 0.75 \cdot \delta_u$ therefore has no significant influence on the shear capacity and the displacement at peak load. This is valid for concrete failure and steel failure when low-cycle fatigue does not occur.
- In cracked concrete ($w \geq 0.3$ mm) the concrete edge failure load is approximately 70% of the value in uncracked concrete. In the case of steel failure, the failure load is not significantly influenced by the cracks.
- The displacement at failure increased with increasing edge distance and reached a maximum for steel failure.

Akiyama et al. (1997)

Monotonic and cyclic shear tests were performed on 76 single or grouped mechanical expansion anchors (d = 19, 22, and 25 mm; $h_{ef} = 5 \cdot d$) and bonded reinforcement bars (d = 22 and 25 mm; $h_{ef} = 5 \cdot d$ and $7.5 \cdot d$; epoxy mortar) in uncracked concrete (f_c = 35 N/mm^2). The anchors were located 175 mm away from the edge of the specimen and loaded parallel to the edge. Five alternating shear cycles to approximately 50 percent of the design steel yield strength were performed before loading the fasteners to failure in shear. The observed failure modes were splitting of the concrete, pull-out, pull-through and shear failure of the anchor steel. The results can be summarized as follows:

- For the bonded anchors with diameter d = 22 mm and embedment depth $h_{ef} = 5 \cdot d$, the ultimate load after cycling was reduced by about 25 percent relative to the monotonic tests. For all other anchors, no effect of the cycling on the subsequent ultimate load was observed.
- The mechanical expansion anchors ($h_{ef} = 5 \cdot d$) typically failed by pull-through before shear failure of the anchor steel could occur. The bonded anchors with embedment depth $h_{ef} = 7.5 \cdot d$ typically failed by shear failure of the anchor steel. The bonded anchors with embedment depth $h_{ef} = 5 \cdot d$ typically failed by pull-out. Consequently, the bonded anchors with an embedment depth of $h_{ef} = 7.5 \cdot d$ had a higher ultimate load than those with $h_{ef} = 5 \cdot d$ (2.1 times larger).
- A limit state shear displacement of 7.5 mm for fasteners used in seismic strengthening applications is defined. This value was calculated assuming that the anchor was used to connect a reinforced concrete strengthening wall in a building with 3 meter story height and that the story drift was about 1/200 when the wall reached its maximum shear strength.

Rieder (2002, 2004)

Rieder (2002) reports on tests with undercut anchors (M6 to M16) and bolt-type expansion anchors (M8 to M24) in cracked (Δw = 0.3 mm) C20/25 and C50/60 concrete loaded monotonically to failure in shear. Rieder concludes that cold formed anchors failing by steel failure exhibit more deformation ductility than machined anchors and that the influence of the steel strength ratio f_{yk} / f_{uk} on the deformation capacity is negligible. Furthermore, the bolt-type expansion anchors exhibited more deformation capacity than the undercut anchors under monotonic shear loading.

Rieder (2004) extended his investigations to shear load cycling. Size M12 (steel grade 8.8) expansion and undercut anchors were tested in cracked C20/25 concrete using stepwise-increasing reversed shear load. The load cycles began at 57% of the characteristic resistance for steel failure taken from the anchor approval and increased in steps of 10% after 5 cycles until failure occurred. Rieder shows that the investigated undercut anchors could dissipate more energy during shear load cycling than the expansion anchors. Furthermore, the undercut anchors reached 80% of the static capacity before steel rupture, whereas the expansion anchors reached only 55% of the static capacity. From the presented data it appears that the undercut anchors were subjected to about 35 reversed load cycles before failing. Rieder attributes the poorer performance of the expansion anchors to increased spalling of concrete at the point of shear load transfer and the consequent induced bending moments.

3.3.1.3 Combined tension and shear cycling

Usami et al. (1980, 1981)

Usami and his coworkers tested the response of a rigid frame anchored by groups of headed anchors (d = 19 mm; f_u = 480 MPa) and bonded anchors M20 (epoxy-based injection system and polyester-based capsule system) in uncracked concrete (f_c = 20 N/mm^2). An alternating horizontal force was applied along the vertical axis of the frame, thereby loading the anchors simultaneously in tension and shear.

In the tests with headed anchors the embedment depth was $h_{ef} = 8.4 \cdot d$. The vertical distance between the anchors and the applied horizontal force (y) and the horizontal distance between the anchors (x) was varied (y/x = 0.25 to 4.0) to investigate both tension and shear dominated behavior. The number of anchors was also varied (2 or 8 anchors). For anchorage with 2 anchors, i.e. one in tension and one in compression, steel failure occurred for ratios of $y/x \leq 1.0$, otherwise concrete cone failure occurred. For anchorage with 8 anchors, i.e. four in tension and four in compression, concrete cone failure occurred in all cases ($y/x \geq 0.5$). Similar results were obtained with bonded anchors.

Okada & Seki (1984)

Okada and Seki (1984) anchored cantilever columns in uncracked concrete using groups of four or six headed bolts (d = 22 mm; $h_{ef} = 5.8 \cdot d$ and $9.5 \cdot d$). The extent of the interaction between tension and shear behavior of the fastening assembly cannot be evaluated, since the program did not include tests on identical specimens with separated action for the two types of loading. It was observed, however, that in the case of the small embedment depth concrete cone failure of the group occurred, whereas with large embedment depth steel failure occurred. The test results demonstrate that the behavior of fastenings under combined tension and shear cycling is sensitive to the failure mode.

Meszaros & Eligehausen (1994)

Displacement-controlled expansion anchors M12 and bonded anchors M12 located in cracked concrete (f_{cc} = 28 N/mm^2; w ~ 0.3 mm) were subjected to constant tension load (N) and simultaneously to alternating cyclic shear load (V). Approximately 1000 shear load cycles were performed at service load levels. The ratio between N and V was varied to obtain resultant load inclination angles of 15°, 45° and 75° to the anchor axis. If no failure occurred during load cycling, the fasteners were tested monotonically to failure with the respective load inclination angle.

The ultimate strengths obtained from the subsequent anchor pullout tests are shown in tension-shear interaction diagrams in Figure 3.25 along with the results for the same anchors tested monotonically (without prior cycling) with combined tension and shear load (*Dieterle & Optiz 1988*). The curves (1) and (2) in the figures are simplified interaction curves given by equations (3.1) and (3.2), respectively.

$$\frac{N}{N_{u,m}} \leq 1; \quad \frac{V}{V_{u,m}} \leq 1; \quad \frac{N}{N_{u,m}} + \frac{V}{V_{u,m}} \leq 1.2 \tag{3.1}$$

$$\left(\frac{N}{N_{u,m}}\right)^{5/3} + \left(\frac{V}{V_{u,m}}\right)^{5/3} = 1 \qquad (3.2)$$

The displacement-controlled expansion anchors with resultant load inclination angles of 45° and 75° failed by pull-out during the load cycling and are not plotted.

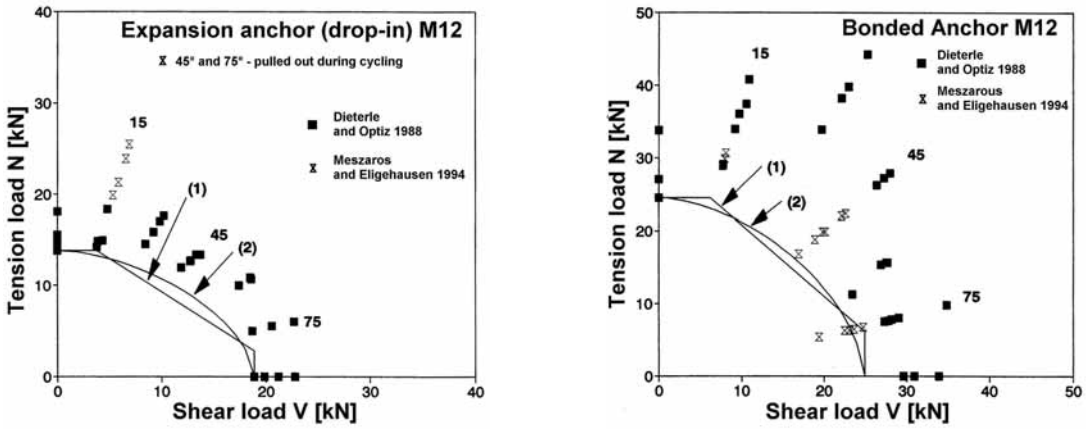

Figure 3.25 Interaction diagrams for anchors tested with an inclined load after being subjected to a constant axial tension load and simultaneous alternating shear cycling in cracked concrete (w ~ 0.3 mm): (a) expansion anchors; (b) bonded anchors (Meszaros & Eligehausen 1994)

Meszaros and Eligehausen (1994) conclude that:

- A constant load in combination with an alternating shear load may negatively influence fastener behavior.
- The ultimate strength of the displacement-controlled expansion anchors that did not fail during the load cycling was not affected by the inclined load cycling.
- The bonded anchors did not fail during load cycling. During the subsequent tests to failure, rupture of the steel was observed. The ultimate load was slightly lower than that for comparable anchors without previous load cycling.

Zhang (1997)

Multiple-anchor connections (4 anchors) with torque-controlled expansion anchors M20 and undercut anchors M10, M16 and M20 were subjected to alternating horizontal displacement applied by means of a steel profile welded to a stiffened baseplate. By varying the point of loading on the steel profile the ratio between the tension and shear forces on the anchors was varied. Tests were performed in both cracked (w = 0.3 mm) and uncracked concrete (f_c = 32.4 N/mm^2). The embedment depth of the anchors was sufficient to result in steel failure of the anchors in uncracked concrete under quasi-static loading. The alternating horizontal displacement was determined from the first 6 seconds of the El Centro 1940 earthquake (north-south component) run through a single degree of freedom system with a stiffness and mass determined using the experimentally obtained response of the attachment. Each specimen was loaded repeatedly by the generated displacement input. As each test progressed, the input was scaled by larger and larger factors until failure occurred. Monotonic tests were also conducted for comparison.

Zhang (1997) reached the following conclusions for combined tension and shear cycling:

- Multiple-anchor connections designed for ductile behavior in uncracked concrete under static loading will probably still behave in a ductile manner in cracked concrete under dynamic loading.
- Anchors that show relatively good performance when tested individually in cracked concrete will probably also show relatively good performance in multiple-anchor connections subjected to seismic loading.
- Cyclic load-displacement behavior of multiple-anchors connections is accurately bounded by the corresponding static load-displacement envelope. Dynamic cycling does not significantly influence the fundamental load-displacement behavior of multiple-anchor connections. The horizontal displacement at ultimate load, however, may be greater during cycling than in equivalent static tests due to spalling of the concrete in front of the anchors.
- The investigated torque-controlled expansion anchors (bolt-type) experienced pull-through failure when loaded cyclically with a large eccentricity to the point of load application (tension dominated) in cracked concrete.

CSTB (2003)

Torque-controlled expansion anchors, undercut anchors and bonded anchors located far from edges in cracked concrete (w = 0.5 mm) were subjected to a constant tension or shear load and simultaneously to cycled load in the orthogonal direction, i.e. in shear or tension, respectively, to investigate cyclic interaction up to failure. The load cycles were applied using a stepwise-increasing pattern with around 10 cycles per step (approximately 140 cycles to failure). The ratio of the magnitude of the tension and shear loads was kept constant throughout the test, i.e. as the cyclic load increased, the constant load in the orthogonal direction increased proportionally. The test results indicate that in many cases a quadratic interaction (Static) might be unconservative (Figure 3.26). A linear interaction is recommended for seismic applications.

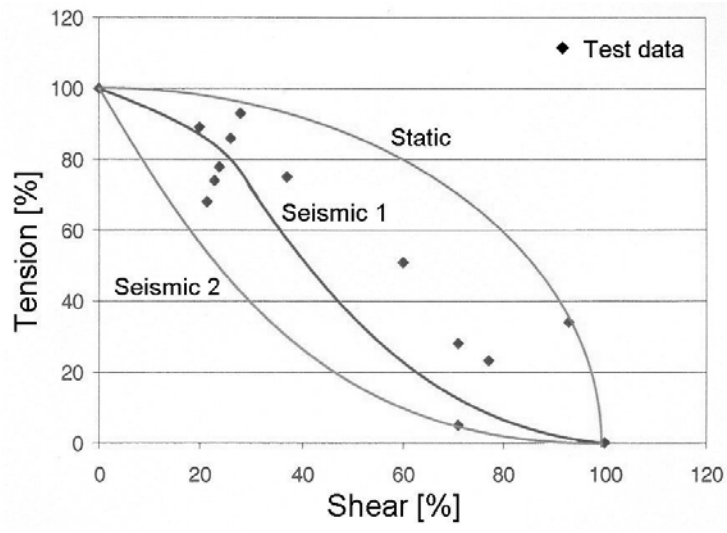

Figure 3.26 Tension-shear interation for various post-installed anchor types under conbined cyclic load (CSTB 2003)

Rieder (2005)
Triaxial shake table tests were performed with steel masses connected to cracked C20/25 concrete blocks using single undercut, expansion and bonded anchors. Artificially generated earthquake ground motion time-histories of varying magnitudes were applied. The tests indicated that anchors with large axial deformation capacity can experience increased pounding between the baseplate and the concrete, which can in turn negatively affect the anchorage performance. Additionally, the author suggests that a maximum force reduction factor of q_a = 3.0 (as opposed to 2.0) is more appropriate for use in the *CEN Technical Specification (in preparation)* guidelines to determine seismic forces acting on nonstructural components.

3.3.1.4 Load cycling pattern

Lieberum & Weigler (1984)
Torque-controlled expansion anchors M16 (h_{ef} = 190 mm) anchored in intersecting cracks (w = 2.0 mm; f_{cc} = 25 N/mm^2) were subjected to pulsating tension loads. Stepwise increasing and decreasing loading patterns were investigated. Each pattern had a total of 700 cycles (pulses). The maximum pulse amplitude did not exceed 30% of the ultimate fastener strength.

Figure 3.27 shows the attachment (fastener) displacement as a function of the number of cycles for a stepwise-increasing and a stepwise-decreasing load collective. Figure 3.27b indicates that for cycling at loads levels below the previous maximum, anchor displacements tend to stabilize.

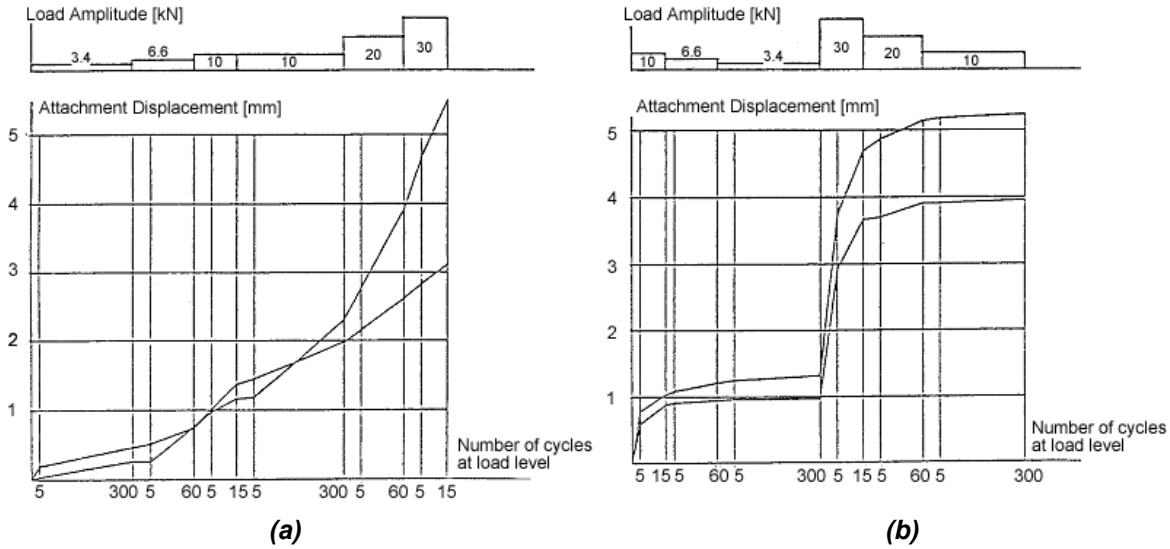

Figure 3.27 Tension load-displacement behavior of expansion anchors M16 with cycled load: (a) increasing load amplitude; (b) decreasing load amplitude (Lieberum & Weigler 1984)

3.3.2 Influence of loading rate

Hunziker (1983, 1984, 1987)
Early experimental investigations of the behavior of post-installed fasteners at high tension loading rates were performed by *Hunziker (1983, 1984, 1987)*. The tests were performed to qualify fasteners for structures in the case of a nuclear explosion. Several types of fasteners (expansion anchors, bonded anchors and ceiling hangers) were

installed in cracked concrete (w = 1.0 mm) and subjected to two successive shock loadings generated by a falling mass. Acceptance was based on achieving a displacement of no more than 5 mm measured subsequent to the shocks. Hunziker concludes that sufficient follow-up expansion is necessary to achieve acceptable performance at high load rates. Due to the simple pass/fail nature of the experiments no conclusions could be drawn for seismic relevant loading rates.

Collins (1988)

Collins (1988) performed impact tests on cast-in headed bolts, grouted bolts, bonded anchors, mechanical expansion anchors and undercut anchors in uncracked concrete (f_c = 35 N/mm^2). Loads were applied to the anchors using a triangular impulse approximately 0.25 seconds long. Three pulses were applied to the anchor at a load of $0.60 \cdot f_y A_s$. If the anchor did not fail, three pulses at $0.80 \cdot f_y A_s$ and three pulses at $1.00 \cdot f_y A_s$ were conducted. In a static test, all of the anchors failed by steel failure. *Collins (1988)* reached the following conclusions:

- The applied impact loading had no effect on the anchor strength when the anchors were embedded sufficiently to develop the full tension capacity of the anchor steel under static loads.
- Fully embedded cast-in anchors, bonded anchors and grouted anchors showed no reduction in the secant stiffness up to yield-level ($f_y A_s$) impact loads,
- Fully embedded expansion and undercut anchors show a slight reduction in secant stiffness between impact loads of increasing magnitude due to an increase in slip. However, this slip was no greater during impact loads than during static loads to the same load level. The slight reduction in secant stiffness had no effect on the anchor strength for properly designed undercut anchors.

Eibl & Keintzel (1989a)

Quasi-static and dynamic tension tests were performed using single undercut anchors M12 installed in normal strength (f_{cc} = 30 N/mm^2) cracked concrete (w = 0.7 mm and 1.1 mm). The setup was such that an unrestricted concrete cone could form. In the quasi-static tests the ultimate load N_u was reached in 3 to 5 minutes. For dynamic loading, a jump of the fastener displacement of about 20 mm was specified. The resulting rise time to ultimate load was about 0.04 seconds. *C*oncrete cone failure was achieved in most cases.

Eibl and Keintzel (1989a) reached the following conclusions:

- The ultimate load and the displacement at ultimate load for a fastener failing by concrete breakout increase with increasing loading rate (Figure 3.28). The observed mean increase in ultimate load was 26% independent of the crack width. The increase in the mean displacement at ultimate load was 56% and 12% for 0.7 mm and 1.1 mm crack widths, respectively.
- The secant stiffness measured to about 30% of the mean ultimate strength, as well at the secant stiffness measured to the ultimate load, was unaffected or increased only slightly for the rise time to ultimate load of 0.04 seconds.
- Greater mechanical work was performed by the fasteners loaded at high rates.

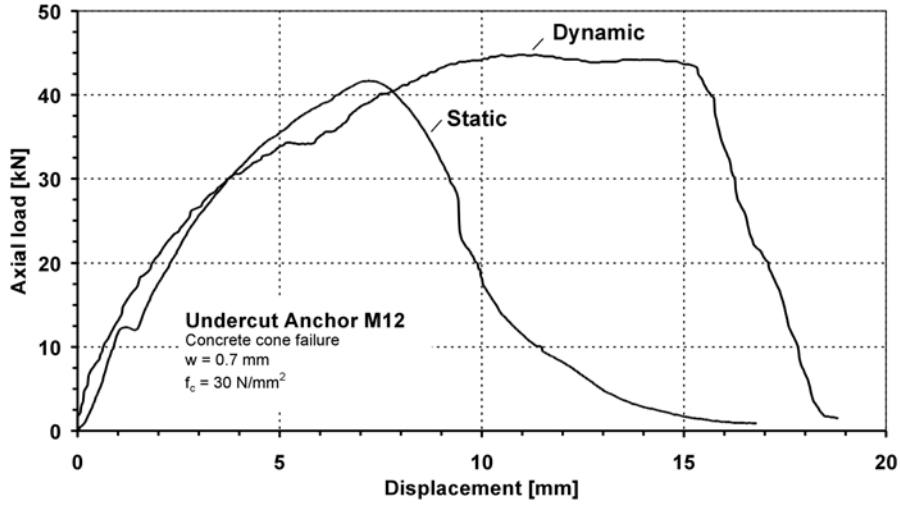

Figure 3.28 Load-displacement curves for undercut anchor M12 in cracked concrete (w = 0.7 mm) under static and dynamic (rise time = 0.04 sec.) tension load (after Eibl & Keintzel 1989a)

Eibl & Keintzel (1989b)

The investigations performed by *Eibl and Keintzel (1989a)* were extended to higher loading rate in *Eibl and Keintzel (1989b)*. Quasi-static and dynamic tension tests were performed using single undercut and torque-controlled expansion anchors M12 installed in normal strength (f_{cc} = 30 N/mm^2) cracked concrete (w = 0.7 mm). For dynamic loading, a jump of the fastener displacement of about 20 mm was specified, whereby the resulting rise time to ultimate load was about 0.01 seconds. Concrete cone failure was achieved in most cases.

Eibl and Keintzel (1989b) confirmed the conclusions reached in *Eibl and Keintzel (1989a)* pertaining to shock loading. Additionally, they:

- attribute the increase in the concrete cone failure load to the increase in concrete tensile strength with loading rate;
- show that the conclusions are valid for the investigated expansion anchors, which generated a concrete cone failure, as well as for undercut anchors.

Klingner et al. (1998)

Klingner et al. (1998) summarize the experimental work on the behavior of fasteners under seismic conditions performed by *Rodriguiz (1995)*, *Hallowell (1996)*, *Lotze and Klingner (1997)* and *Zhang (1997)* for the U.S. Nuclear Regulatory Commission.

Quasi-static and high load rate tension and shear tests were performed in normal strength (f_c = 20 to 32 N/mm^2) uncracked and cracked concrete (w = 0.3 mm) slabs. The investigated fasteners were cast-in bolts, grouted anchors, undercut anchors and bolt-type and sleeve-type expansion anchors of various sizes and embedment depths. The setup was such that an unrestricted concrete cone could form. For the tests at high (earthquake relevant) loading rate, the rise time to ultimate load was about 0.1 seconds.

Figure 3.29 shows the ratio between the dynamic and static ultimate tensile capacities of the investigated fastener types in uncracked and cracked concrete. Each capacity is based on the average value of at least 5 test replicates. In the case of the bolt-type torque-controlled expansion anchors (expansion bolts) results for various anchor types (type EA and type EAII) and sizes have been combined. In most cases failure both under static and dynamic loading occurred due to concrete cone failure (CC). Pull-through (Pt) failure, however, was observed frequently for the expansion bolts and pull-out (Po) failure for the grouted anchors in cracked concrete under dynamic loading. Ignoring the results for the expansion bolts and grouted anchors for the moment, Figure 3.29 indicates that if concrete failure occurs under both static and under dynamic loading, the ultimate capacity under dynamic loading will be at least as large as under static loading. On average the concrete cone capacity increased 23% for a rise time to ultimate load of 0.1 seconds.

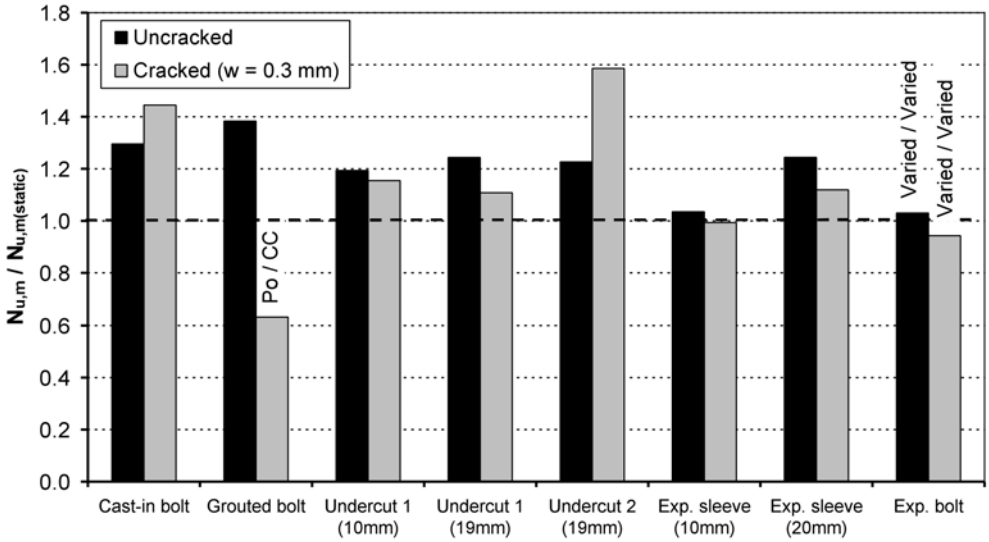

Figure 3.29 Ratio between dynamic and static ultimate tensile capacity (after Klingner et al. 1998)

The effect of dynamic loading rate on the pull-through capacity of fasteners can be observed by separating the test results for the bolt-type expansion anchors. Table 3.1 provides the mean ultimate loads for anchors that failed by pull-through both under static and dynamic loading. The coefficient of variation (COV) is shown for the test data. A decrease in the mean pull-through capacity of 17% occurred for a rise time to ultimate load of 0.1 seconds. *Klingner et al. (1998)* point out that dynamic loading worsens the condition of load transfer at the heads of expansion anchors, probably due to reduction in the coefficient of friction between the expansion cone and expansion elements, and between the expansion elements and the wall of the drilled hole (*Rabinowicz 1995*).

Table 3.1 Tension test results (pull-through failure) (after Klingner et al. 1998)

Fastener Type	**Type of Loading**	**Failure Mode**	**No. of Tests**	**Mean Ultimate Load $N_{u,m}$ [kN]**	**COV [%]**	$\frac{N_{u,m}}{N_{u,m(static)}}$
Expansion bolt (EA)	Static	Pt	5	69.8	10.6	1
h_{ef} = 100mm	Dynamic	Pt	5	57.8	20.2	0.83

A change in failure mode between static and dynamic loading was observed for some bolt-type expansion anchors and for the grouted anchors in cracked concrete. The effect of the change in failure mode on the ultimate load is summarized in Table 3.2. The results indicate that a change of failure mode from concrete cone (CC) under quasi-static loading to pull-out (Po) or pull-through (Pt) at dynamic loading rate may result in a decrease in the ultimate load capacity. The reduction in capacity was particularly large for the grouted bolts that underwent bond failure between the grout and the concrete at the high loading rate.

Table 3.2 Tension test results (failure mode varied) (after Klingner et al. 1998)

Fastener Type	Concrete Condition	Type of Loading	Failure Mode	No. of Tests	Mean Ultimate Load $N_{u,m}$ [kN]	COV [%]	$\frac{N_{u,m}}{N_{u,m(static)}}$
Expansion bolt (EA)	Uncracked	Static	CC	5	44.4	9.9	1
h_{ef} = 62 mm		Dynamic	Pt + CC	5	44.6	7.0	1.00
Expansion bolt (EAII)	Uncracked	Static	CC	5	86.8	3.8	1
h_{ef} = 100 mm		Dynamic	Po + Pt	5	78.4	5.7	0.90
Grouted bolt	Cracked	Static	CC	5	59.7	26.1	1
h_{ef} = 102 mm	(w = 0.3 mm)	Dynamic	Po	5	37.9	33.1	0.63

The effect of the dynamic loading rate on the concrete breakout capacity in shear is shown for several fastener types in Table 3.3. Only results without tie-back reinforcement are presented. As in the case of concrete cone failure in tension, the concrete breakout capacity in shear increases with the increased loading rate.

Table 3.3 Shear test results (concrete breakout failure) (after Klingner et al. 1998)

Fastener Type	Concrete Condition	Type of Loading	Failure Mode	No. of Tests	Mean Ultimate Load $V_{u,m}$ [kN]	COV [%]	$\frac{V_{u,m}}{V_{u,m(static)}}$
Cast-in bolt	Uncracked	Static	CC	5	39.1	-	1
		Dynamic	CC	5	49.8	-	1.27
	Cracked	Static	CC	5	32.0	-	1
	(w = 0.3 mm)	Dynamic	CC	5	46.2	-	1.44
Undercut anchor	Uncracked	Static	CC	5	40.9	-	1
(UC1)		Dynamic	CC	5	45.8	-	1.12
Expansion bolt (EAII)	Uncracked	Static	CC	5	35.1	-	1
		Dynamic	CC	5	42.7	-	1.22

- COV not given in *Klingner et al. (1998)*.

UE Anchor Project (2001)

Quasi-static and dynamic tension tests were performed using single M12 and M16 bonded-expansion anchors, undercut anchors and headed studs installed in normal strength (C25/30) and high performance (C100/120) uncracked concrete members. The fasteners were loaded using a stress pulse generated by a prestressing/sudden release device and propagated through an incident bar to the fastener. This method allowed very high loading rates to be achieved (rise time < 0.001 seconds). The setup was such that an unrestricted concrete cone could form.

The results in the *UE Anchor Project (2001)* report are provided as a function of strain rate rather than load rate. As will be discussed in Chapter 4 it is necessary to assume an effective strain length in order to compare the results with the loading rates used in other investigations. By assuming that the effective strain length is equal to the anchor embedment depth h_{ef} and determining the approximate displacement at ultimate load, the approximate rise time to ultimate load can be determined. These rise times are given along with the experimentally obtained ultimate loads in Table 3.4.

Table 3.4 Ultimate loads for tension tests in C20/25 uncracked concrete (UE Anchor Project 2001)

Anchor Type	Size	h_{ef} [mm]	Strain Rate [1/s]	Approx. Disp. to $N_{u,m}$ [mm]	Rise Time to $N_{u,m}$ [sec]	No. of Tests	Mean Ultimate Load $N_{u,m}$ [kN]	COV [%]	$\frac{N_{u,m}}{N_{u,m(static)}}$
Bond-Exp.	M12	65	Quasi-static	2.0	200	2	35.6	22.5	1
			$10^{-3} \le \dot{\varepsilon} \le 10^{0}$		$30 \le t \le 0.03$	2	52.0	8.2	1.46
			$10^{0} \le \dot{\varepsilon} \le 10^{2}$		$0.03 \le t \le 0.0003$	2	52.5	4.0	1.48
	M16	90	Quasi-static	3.0	200	3	104.4	2.0	1.00
			$10^{-3} \le \dot{\varepsilon} \le 10^{0}$		$30 \le t \le 0.03$	4	122.3[a]	4.3	1.17[a]
			$10^{0} \le \dot{\varepsilon} \le 10^{2}$		$0.03 \le t \le 0.0003$	2	114.5	0.6	1.10
Undercut	M12	65	Quasi-static	3.0	200	2	56.2	0.9	1.00
			$10^{-3} \le \dot{\varepsilon} \le 10^{0}$		$50 \le t \le 0.05$	2	60.0	7.1	1.07
			$10^{0} \le \dot{\varepsilon} \le 10^{2}$		$0.05 \le t \le 0.0005$	2	72.0	7.9	1.28
	M16	90	Quasi-static	6.0	200	3	105.0	3.8	1.00
			$10^{-3} \le \dot{\varepsilon} \le 10^{0}$		$70 \le t \le 0.07$	3	115.0	7.7	1.09
			$10^{0} \le \dot{\varepsilon} \le 10^{2}$		$0.07 \le t \le 0.0007$	2	131.5	7.0	1.25
Headed bolt	M12	65	Quasi-static	2.0	200	2	44.8	3.2	1.00
			$10^{-3} \le \dot{\varepsilon} \le 10^{0}$		$30 \le t \le 0.03$	2	66.5	3.2	1.48
			$10^{0} \le \dot{\varepsilon} \le 10^{2}$		$0.03 \le t \le 0.0003$	2	81.5	14.7	1.82
	M16	90	Quasi-static	4.0	200	3	78.1	6.2	1.00
			$10^{-3} \le \dot{\varepsilon} \le 10^{0}$		$40 \le t \le 0.04$	3	122.7	3.4	1.57
			$10^{0} \le \dot{\varepsilon} \le 10^{2}$		$0.04 \le t \le 0.0004$	2	131.0	1.1	1.68

[a] Steel failure.

Because the strain ranges cover several orders of magnitude, the rise times to ultimate load also vary greatly. The intermediate strain range ($10^{-3} \le \dot{\varepsilon} \le 10^{0}$) is comparable with that used in other tests discussed in this section. The results indicate an increase in the ultimate capacity with increasing tensile loading rate. It is mentioned in the report that failure usually occurred due to concrete cone failure. The results also suggest that the capacity increase due to dynamic loading is not as large for the bonded expansion anchors and undercut anchors as for the headed bolts. One must keep in mind, however, that a very limited number of tests were conducted in each case.

Fujikake et al. (2003)

Fujikake et al. (2003) investigated headed anchors and bonded anchors subjected to rapid tension loading. They differentiated between anchors failing by concrete cone failure, bond failure and mixed bond and concrete cone failure.

The tests were performed in three phases. In Phase I, the test specimen consisted of a concrete block (W300 x L300 x H200 mm) in which a headed anchor with a nominal diameter of 12 mm and a head size of 20 mm was installed with a 40 mm embedment depth. In Phase II, the test specimen consisted of a concrete cylinder surrounded by a steel tube (D216 x H200 mm) in which a bonded anchor M12 was installed at an embedment depth of 40, 65 or 90 mm. In Phase III, the test specimen consisted of a concrete block (W300 x L300 x H300 mm) in which a bonded anchor M12 was installed at an embedment depth of 70 or 120 mm.

All tests were performed in concrete with a concrete cylinder (D100 mm x H200 mm) compressive strength at the time of testing of 32.0 N/mm^2. The investigated loading rates were: 1.0 x 10^{-1}, 4.0 x 10^2, 4.0 x 10^3, 4.0 x 10^4 kN/s. These rates correspond to rise times to ultimate load on the order of 10^2, 10^{-1}, 10^{-2}, 10^{-3} seconds, respectively.

Figure 3.30 shows the relationship between the ultimate concrete cone resistance and the loading rate for the headed bolts tested using a wide support (Phase I). Fujikake and his coauthors attribute the increase in ultimate resistance to the increase in the concrete tension strength at dynamic loading rates. The following dynamic strength increase factor for concrete cone failure α_c is suggested:

$$\alpha_c = \exp\left[0.00126\left(\log_{10}\frac{\dot{\sigma}}{\dot{\sigma}_s}\right)^{3.373}\right] \qquad (3.3)$$

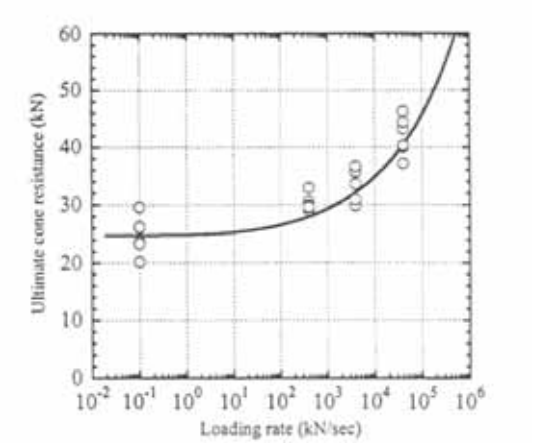

Figure 3.30 Relationship between the ultimate concrete cone resistance (headed bolts) and loading rate (Fujikake et al. 2003)

where $\dot{\sigma}$ is the stress rate calculated based on loading rate and the projected area of the failure cone (*MPa/s*) and $\dot{\sigma}_s = 2.8 \times 10^{-3}$ *MPa / s* . This function is plotted with the test data from Phase I in Figure 3.30.

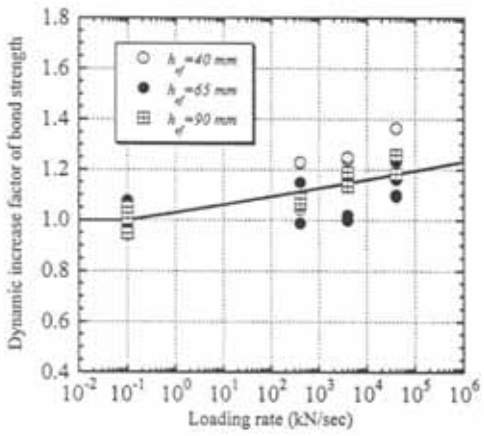

Figure 3.31 Relationship between the dynamic and static bond strength (Fujikake et al. 2003)

Figure 3.31 shows the relationship between the ultimate bond resistance and the loading rate for the bonded anchors tested using a close support (Phase II). The values have been normalized by the mean resistance under quasi-static loading. In all cases bond failure occurred at the interface between the adhesive and the concrete. Based on the results, Fujikake and his coauthors suggest the following dynamic strength increase factor for bond failure α_b:

$$\alpha_b = \left(\frac{\dot{p}_d}{\dot{p}_{sd}}\right)^{0.013} \qquad (3.4)$$

where $\dot{p}_d$ = dynamic loading rate (kN/s) and $\dot{p}_{sd} = 1.0 \times 10^{-1}\ kN/s$. This function is plotted with the test data from Phase II in Figure 3.31.

In Phase III, failure occurred due to a combination of concrete cone and pull-out failure (Figure 3.13c). To determine the effect of each failure mode on the ultimate dynamic resistance P_{ud} the following three resistances were calculated for the investigated embedment depths (h_{ef} = 70 and 120 mm): 1) dynamic ultimate cone resistance P_{cd} calculated using an early version of the CC-Method (cone depth h_c = 35 mm) together with Equation (3.3); 2) dynamic ultimate bond resistance P_{bd} calculated assuming uniform bond (bond length $h_b = h_{ef} - h_c$) and using the increase factor in Equation (3.4); 3) the summation $P_{cd} + P_{bd}$. The calculated resistances together with the experimental data are shown in Figure 3.32. The authors concluded that the concrete cone failure preceded the bond failure. Furthermore, when the ultimate bond resistance P_{bd} is greater than the ultimate cone resistance P_{cd}, after the cone failure occurs, the ultimate dynamic resistance P_{ud} increases to the ultimate bond resistance. On the other hand, when the bond failure length is rather short, $P_{cd} < P_{bd}$ and the ultimate dynamic resistance P_{ud} is likely to correspond to P_{cd}.

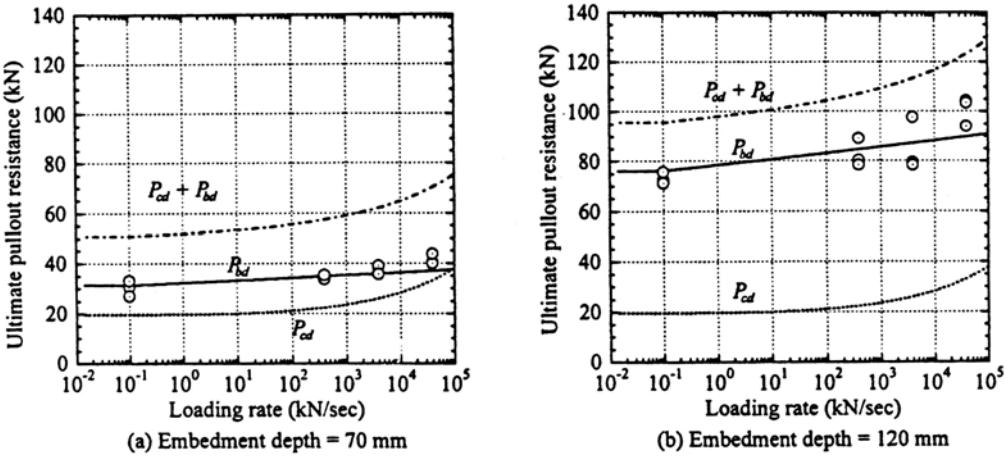

Figure 3.32 Relationship between ultimate mixed mode resistance and load rate for bonded anchors M12 in uncracked concrete (Fujikake et al. 2003)

<u>*Ožbolt et al. (2006)*</u>

Ožbolt et al. (2006) investigated the behavior of headed bolts with large embedment depths (h_{ef} = 150, 890 and 1500 mm) under high loading rate using a 3D finite element model that couples rate process theory (*Krausz & Krausz 1988*) with the M2-O microplane model for concrete (*Ožbolt et al. 2001*). After demonstrating that the model realistically predicts the influence of loading rate on the uniaxial compressive behavior of concrete, the authors verify the increase in concrete cone capacity with increased loading rate that has been observed experimentally. Moreover, the study shows that for moderately high loading rates the size effect for concrete cone failure, i.e. the decrease in the nominal strength with increased cone size, becomes stronger. For very high loading rates, however, inertial effects will become so pronounced that the contribution of the size effect vanishes and the nominal strength increases with the loading rate. The authors conclude that a problem dependent critical loading rate for which the size effect is minimum must exist.

3.3.3 Influence of opening and closing cracks

All known investigations of fastener behavior in opening and closing cracks performed to date have been aimed at determining performance under service conditions, i.e. 1000 crack cycles between about 0.1 and 0.3 mm with service level axial loads applied to the fastener, and not for representative seismic conditions.

Rehm & Lehmann (1982)

Torque-controlled and displacement-controlled expansion anchors situated in cracks and loaded with a constant axial load were subjected to repeated crack opening and closing cycles. Reinforced concrete slabs loaded in bending served as the anchorage material. The crack cycling was performed primarily to damage the anchorages prior to performing an axial pull-out test, i.e. no systematic study of the effect of the number of crack cycles or the amplitude of the crack opening and closing widths on the fastener performance was conducted. The authors demonstrate that fastener displacement increases as a result of crack opening and closing and that this increase depends on the type of fastener as well as on the crack width. Furthermore, a progressive increase of the fastener displacement as a function of the number of crack cycles (logarithmic scale) during crack cycling indicates the start of failure.

Seghezzi (1985)

Seghezzi (1985) showed that the crack closing width can have a significant influence on the displacement behavior of axially loaded fasteners subjected to crack cycling. Figure 3.33 plots the displacement increase of two fastener types as a function of the number of crack cycles for two different crack cycling patterns. In both test series the crack opening width was w_o = 0.3 mm. In series A the crack closing width was maintained at w_u = 0.0 mm. In series B the crack closing width during the first cycle was w_u = 0.0 mm, but grew to w_u = 0.15 mm after 1000 cycles. For the crack cycling pattern in series A the fastening displacement increased progressively for both types of fasteners. In series B the displacement increased degressively after about 200 cycles.

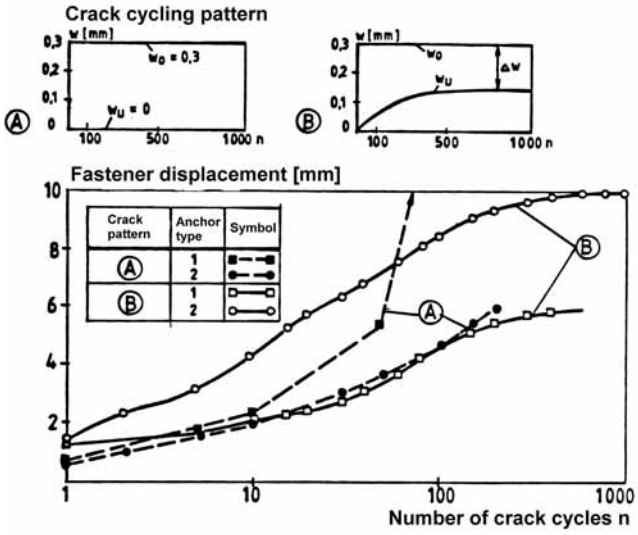

Figure 3.33 Influence of crack closing width on fastener displacement during crack cycling (Seghezzi 1985)

Furche (1987)

Exploratory tests in cycled cracks were performed with M12 torque-controlled expansion anchors (h_{ef} = 80 mm), undercut anchors (h_{ef} = 80 mm) and bonded anchors (h_{ef} = 110 mm) in unreinforced concrete blocks (f_{cc} = 38.3 N/mm^2) in which two anchors were tested simultaneously (Figure 3.34). Some of the anchors tested were not qualified for use in cracked concrete. Crack opening (~0.3 mm) was achieved by the splitting forces generated by the loaded anchors and crack closing (~0.1 mm) by an externally applied compression force on the concrete block. A mean compressive stress on the crack surface of 9.3 N/mm^2 (~25% of f_c) could be achieved during crack closure. It was shown that the different fastener types require different levels of externally applied compression load to achieve a crack closure w < 0.1 mm. The bonded anchor required the least load (~75 kN). *Furche (1987)* concludes that the load required for crack closure depends on the splitting force generated by the fasteners. Furthermore, a compressive stress on the crack surface of about f_c/4 was sufficient to achieve w < 0.1 mm for all of the investigated fasteners.

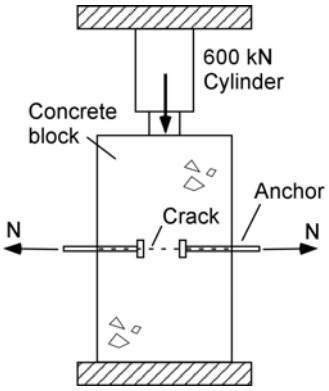

Figure 3.34 Test setup

Between 50 and 1000 crack cycles were performed between crack widths of about 0.3 mm and 0.1 mm. During the crack cycling a constant axial load N = 7.8 kN (~0.2·$N_{u,m}$) applied to the fasteners. It proved difficult to control the crack opening and closing widths with the test setup. If the anchors survived the crack cycling, a subsequent monotonic test to failure in a static crack (w = 0.3 mm) was performed. The displacement increase as a function of the logarithm of the number of crack cycles, as well as the mean load-displacement curves in the subsequent pull-out tests are plotted in Figure 3.35. Figure 3.35b shows that if the anchors withstood the crack cycling without failing, a significant residual strength was present.

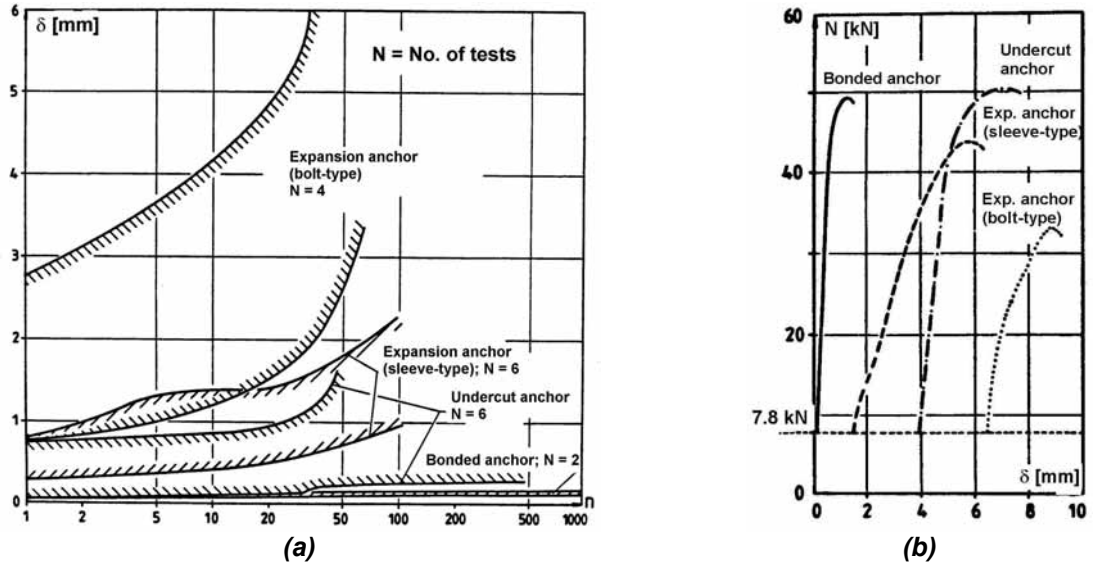

Figure 3.35 Fastener behavior during crack cycling: (a) scatter bands for fastener displacement as a function of the number of crack cycles; (b) load-displacement in subsequent pullout test (Furche 1987)

Furche (1987) concludes that:

- The anchors not suitable for use in cracked concrete showed large initial displacement and a large displacement increase during crack cycling.
- Expansion anchors suitable for use in cracked concrete and undercut anchors showed significantly smaller displacements.
- The investigated bonded anchors showed almost no displacement during crack cycling. The anchor remained bonded to one side of the crack interface since the applied axial load was not sufficient to overcome the available bond resistance.

Lotze & Faoro (1988)

The mechanisms for the displacement of fasteners that function by mechanical interlock or friction during service level crack cycling are developed. These mechanisms are presented with slight modifications for seismic applications in Chapter 5. *Lotze and Faoro (1988)* conclude that displacement increase during crack opening is primarily influenced by the type of fastener, its diameter, the minimum and maximum crack opening width and the number of crack cycles. Secondary influencing parameters include the concrete strength, the reinforcement ratio in the anchorage component and the magnitude of the applied load. The authors also show that the fastener influences the crack width in the anchorage component by the splitting forces that it generates.

Exploratory test are performed with expansion anchors M12 and undercut anchors M18 in cycled bending cracks (1000 crack cycles between 0.1 mm and 0.3 mm with service level axial fastener loads). *Lotze and Faoro (1988)* conclude that when the crack opening width is held constant during crack cycling, the fastener displacement increases linearly as a function of the logarithm of the number of crack cycles. When load applied to the anchorage component to open the crack is held constant during crack cycling, i.e. the crack opening width grows as bond between the reinforcement and the concrete is destroyed, the fastener displacement increases progressively.

Furche (1988, 1990)

Extensive tests were performed on headed bolts (d = 12 and 20 mm) loaded with an axial tension load and subjected to 1000 crack opening and closing cycles. The head undercut length (a = 1, 2, 3 and 5 mm), the undercut angle (α = 90°, 30° and 5°), as well as the applied axial load (N = 7.8 kN and 12.5 kN) were varied. Reinforced concrete (f_{cc} = 35 N/mm^2) tension members were used as the anchorage material. The crack opening width (0.3 mm) was held approximately constant throughout the test while the crack closing width (0.1 mm; initial) was free to grow during the crack cycling.

The key results of the tests can be summarized as follows:

- Crack opening widths change rapidly during the first 10 ten crack cycles and then become more stabile.
- The effect of the applied axial load and the undercut length can be summarized together by the bearing stress ($\sigma_B = N / ((d^2 - a^2)\cdot\pi/4)$).
- Bearing stress requirements for fasteners for stable displacement behavior during service level crack cycling are suggested (Table 3.5 and Figure 3.36).

Table 3.5 Bearing stress to achieve displacement criteria during crack cycling (Furche 1990)

Undercut angle	Criteria	
	(1) δ (n) → linear	**(2) δ (n=20) ≤ 3 mm**
$\alpha \geq 25°$	Max. $\sigma_B \approx 2$ to $2.5 \cdot f_{cc,200}$	Max. $\sigma_B \approx 3$ to $4 \cdot f_{cc,200}$
$\alpha = 5°$	Max. $\sigma_B \approx 2.7 \cdot f_{cc,200}$	Max. $\sigma_B \approx 2.5 \cdot f_{cc,200}$

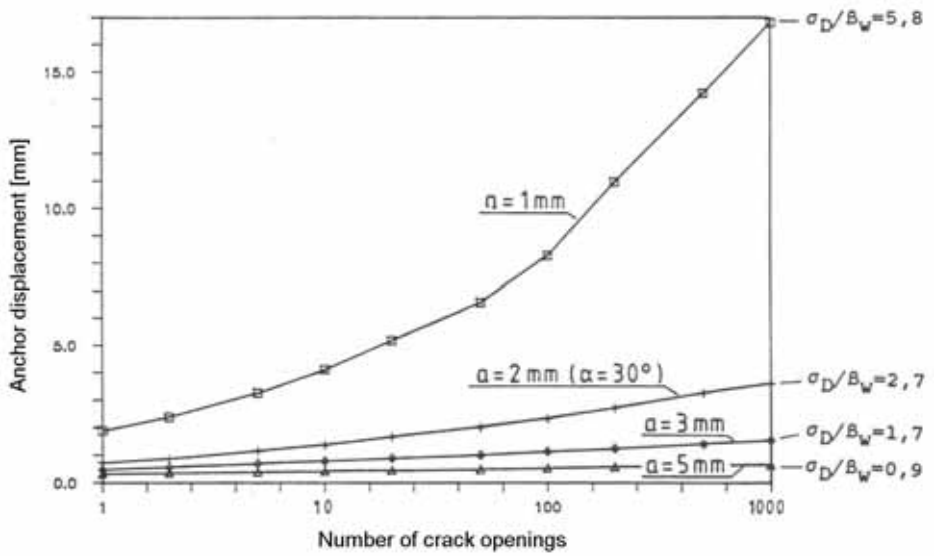

Figure 3.36 Displacement of headed bolts in cycled line cracks; d = 12 mm, α = 90°, N = 7.8 kN (Furche 1990)

Eligehausen & Asmus (1991)

Numerous experimental data for qualified undercut (M6 to M16) and mechanical expansion anchors (M8 to M16) loaded with a constant load (1.3 times the allowable design load) and subjected to 1000 crack cycles between 0.1 mm and 0.3 mm were evaluated to determine acceptable displacement limits for fasteners during crack cycling. Two acceptance criteria are proposed:

(1) An approximately linear or degressive increase of the fastener displacement as a function of the logarithm of the number of crack cycles.
(2) A maximum allowable fastener displacement in any single test of 2 mm after 20 crack cycles and 3 mm after 1000 crack cycles.

A variation of criterion 2 is also proposed in which mean displacements of 1.4 mm and 2.0 mm after 20 and 1000 cracks cycles, respectively, are acceptable as long as the standard deviation of the individual test values is less than 50%.

3.4 Normative standards for fasteners

Modern design of fastenings to concrete is typically performed using standardized design procedures coupled with fastener performance data provided by qualification tests of proprietary products.

The development of seismic design and testing standards for fastenings to concrete has been addressed by several authors over the years including *Senkiw (1984)*, *Czarnecki and Sliter (1988)* and *Ammann (1992)*. A comprehensive overview of these developments is presented by *Silva (2001, 2003)* with emphasis on the United States. Recently, *Bursi (2005)* investigated seismic qualification methods for cast-in anchor channels and shear connector devices.

3.4.1 A brief history

3.4.1.1 Seismic design codes and standards

In the United States and Canada the nuclear industry was a driving force for the early development of design codes and standards for fastening products.

The U.S. nuclear industry began encouraging ductile steel failure of anchorages for seismic applications in the 1970s (*Silva 2001*). Anchor bolt design provisions were included in the Code Requirements for Nuclear Safety Related Structures issued by the American Concrete Institute (ACI) in 1985 (*ACI 349 1985*). Outside of the nuclear industry, fastening design for seismic applications in the United States has been treated in several documents including the Uniform Building Code (UBC), the Recommended Provisions for Seismic Regulations for New Buildings and Other Structures prepared by the Building Seismic Safety Council (BSSC) prepared as part of the National Earthquake Hazard Reduction Program (NEHRP) for the Federal Emergency Management Agency (FEMA), the Building Code Requirements for Structures (ACI 318) and in the design provisions of several local agencies in the State of California. The most recent and widely accepted provisions for the seismic design of fastenings in the United States are in ACI 318 Appendix D (*ACI 318 2005*). The provisions in ACI 349 were reassessed for their applicability to post-installed anchors in the early 1990s and have since been harmonized with the provisions of ACI 318 Appendix D. Furthermore, the International Building Code (IBC), which is phasing out the UBC for structural design in the seismic regions of the U.S., defers to ACI 318 Appendix D for the seismic design of anchorages.

Design Requirements for Concrete Containment Structures for CANDU Nuclear Power Plants issued by the Canadian Standards Association (CSA) have included seismic design provisions for anchorages since 1978 (*Tang & Deans 1983*).

In Europe, seismic design requirements for general fastening applications are provided in the European Committee for Standardization (CEN) Technical Specification Design of Fastenings for Use in Concrete that is due to appear in 2006.

Additionally, some fastener manufactures have published literature on fastener design for earthquake applications (*Hilti 2003*).

Table 3.6 provides an overview of design codes and standards with provisions for seismic fastening applications. Details are provided in Section 3.4.2 and Appendix B.

Table 3.6 Design codes and standards with provisions for seismic fastening applications

Reference	Title	Comments
	United States	
ACI 318 (2005)	Building code requirements for structural concrete (ACI 318-05) and commentary (ACI 318R-05)	Appendix D contains design provisions for post-installed mechanical anchors in cracked and uncracked concrete.
ACI 349 (2001)	Code requirements for nuclear safety related concrete structures (ACI 349-01) and commentary (ACI 349R-01)	Contains seismic design concepts similar to ACI 318 adapted for nuclear applications.
FEMA 368 (2001)	NEHRP recommended provisions for seismic regulations for new buildings and other structures	Provides seismic provisions for model codes in the United States, including the UBC and IBC.
UBC (1997)	Uniform Building Code	Extensively used in the earthquake prone regions of the United States prior to the introduction of the IBC.
IBC (2003)	International Building Code	Defers to ACI 318 for seismic design of fastenings.
	Europe	
CEN TS (in prep.)	Design of fastenings for use in concrete	Seismic design concepts similar to ACI 318, however, in general slightly more conservative. Allows for brittle failure of nonstructural attachments.
	Canada	
CSA-N287.3 (1999)	Design requirements for concrete containment structures for CANDU nuclear power plants	Concrete design based on 45° failure pyramid method.

3.4.1.2 Seismic qualification testing and assessment criteria

In the United States, prior to 1997, testing of post-installed anchors for seismic performance was not common practice outside of the nuclear and telecommunications industries (*Silva 2001*). Based on long-standing tradition, post-installed anchors were routinely listed by the International Code Council Evaluation Service Inc. (ICC-ES; formerly ICBO-ES) as suitable for wind and seismic loading based on static tests in uncracked concrete. Connection failures during the 1994 Northridge earthquake prompted a review of this practice and for the period 1995 to 1997, mechanical post-installed anchors were not permitted for seismic applications. Test criteria based loosely on the CSA Standard N287.2 were adopted by the ICC-ES in 1997 and listing of mechanical anchors for seismic loading resumed in 1998 (*Silva 2001*). As an alternate means of qualification for seismic loading, the ICC-ES adopted load cycling tests developed by the Structural Engineers Association of Southern California (SEAOSC). Both the ICC-ES and SEAOSC tests were performed in uncracked concrete.

Test programs and evaluation requirements for post-installed mechanical anchors in cracked concrete were introduced in the United States in 2001 in ACI 355.2. Shortly thereafter, the ICC-ES developed new acceptance criteria (AC193) for mechanical anchors based on ACI 355.2. Recently, ICC-ES extended these criteria to cover bonded anchors in cracked concrete (AC308). The acceptance criteria in these documents serve as the basis for issuing fastener approvals in the United States.

In 1998, the *Deutsches Institut für Bautechnik* (DIBt) issued guidelines for the use and testing of fastenings in German nuclear facilities. The guidelines are applicable for anchors used to fasten safety relevant components in the case of extreme loading conditions such an earthquake, an explosion or an aircraft impact. This is the only known guideline that is intended to qualify fasteners for use inside of plastic hinges.

Table 3.7 provides an overview of test programs and acceptance criteria for approval of fastenings for seismic applications. Details are provided in Section 3.4.3 and Appendix B.

Table 3.7 Seismic qualification test programs and acceptance criteria for fastenings

Reference	Title	Comments
	United States	
ACI 355.2 (2004)	Qualification of post-installed mechanical anchors in concrete	Test programs and evaluation requirements for post-installed mechanical anchors in cracked and uncracked concrete. Verifies the performance of fasteners for design according ACI 318.
AC01, AC58, AC60, AC106, AC193, AC308 (2005)	(Various titles)	Acceptance criteria for ICC-ES evaluation reports. Evaluation reports verify fastener performance for design according to the UBC and IBC. Only AC193 and AC308 are valid for cracked concrete.
SEAOSC (1997)	Standard method of cyclic load test for anchors in concrete or grouted masonry	Provides an alternate test method for cyclic loading in uncracked concrete based on comparison with cast-in bolts.
	Germany	
DIBt (1998)	Use of anchors in nuclear power plants and nuclear technology installations, guideline for evaluating fastenings for granting permission in individual cases according to the state structure regulations of the federal states of Germany	Prescribes supplementary monotonic and cyclic load tests, as well as crack movement tests for fastenings to be used in German nuclear facilities.
	Canada	
CSA-N287.2 (2003)	Material requirements for concrete containment structures for CANDU nuclear power plants	Prescribes monotonic and load cycling tests in uncracked concrete.

3.4.2 Current seismic design guidelines

Existing design guidelines for seismic fastening applications generally consist of one or more of the following components:

(1) General restrictions on the use of fasteners for seismic applications, e.g. the guidelines are limited to fasteners located outside plastic hinge zones or restrictions are placed on the use of specific fastener types.

(2) Modification of the design resistance for seismic applications. It is generally assumed that design of a fastening for seismic applications can be performed using the methods developed for non-seismic design situations when the characteristic fastener resistances are obtained from appropriate seismic qualification tests. In some guidelines, e.g. *ACI 318 (2005)* and *CEN TS*

(in preparation), static design values for concrete failure modes are reduced by 25% to provide additional conservatism.

(3) Seismic design options:
   a. design for ductile steel failure of the fasteners (Figure 3.37a);
   b. design for ductile failure of the attached element or fixture at a load level that ensures that the ultimate resistance of the fastening will not be reached, i.e. fastener overload protection (Figure 3.37b);
   c. design for brittle failure of the fastening using an increased design load (Figure 3.37c).

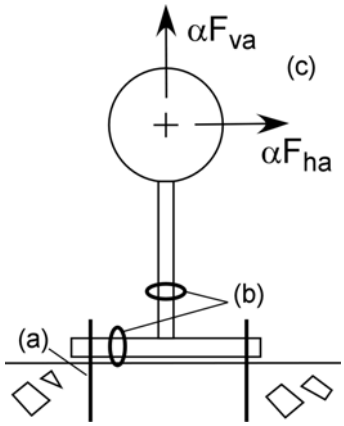

Figure 3.37 Seismic design options: (a) ductile steel failure of the fastener; (b) ductile failure of the attached element or fixture; (c) brittle failure with factored loads

Detailed summaries of the seismic design criteria in the references in Table 3.6 are provided in Appendix B.

3.4.3 Current seismic qualification tests and assessment criteria

Existing seismic qualification tests for fasteners generally consist of one of more of the following components:

(1) Tests to verify the tension and shear capacity of the fastener in cracked concrete.
(2) Simulated seismic load cycling tests with pulsating tension and alternating shear.
(3) Tests in which a sustained axial load is applied to the fastener while it is subjected to crack opening and closing cycles (crack movement test).

Test components contained in the references in Table 3.7 (AC60 excepted) are summarized in Table 3.8.

Table 3.8 Fastener qualification test components related to seismic loading

Reference	(1) Cracked Concrete	(2) Simulated Seismic Load	(3) Crack Movement
ACI 355.2 (2004)	✓	✓	✓
AC01, AC58, AC106 (2005)		✓	
AC193, AC308 (2005)	✓	✓	✓
SEAOSC (1997)		✓	
DIBt (1998)	✓	✓	✓
CSA-N287.2 (2003)		✓	

In *ACI 355.2 (2004)*, as well as in *AC193 (2005)* and *AC308 (2005)*, fastener performance is verified in Δw = 0.3 mm and Δw = 0.5 mm wide cracks. These crack widths are also used to verify fastener performance for non-seismic use, i.e. the crack widths represent those under service, rather than seismic, conditions. In addition to

requiring that fastener performance be verified in these crack widths, *DIBt (1998)* also verifies performance in Δw = 1.0 mm and Δw = 1.5 mm wide cracks. These large crack widths assume that fasteners could be located in plastic hinges where the reinforcement in the anchorage component has undergone a strain of 0.005.

Three loading patterns are currently used for simulated seismic load cycling tests. These are illustrated for the case of tension in Figure 3.38. The shear load cycling patterns are similar, however, the load alternates symmetrically around zero. Key simulated seismic load cycling test parameters and assessment criteria contained in the references in Table 3.7 are summarized in Table 3.9.

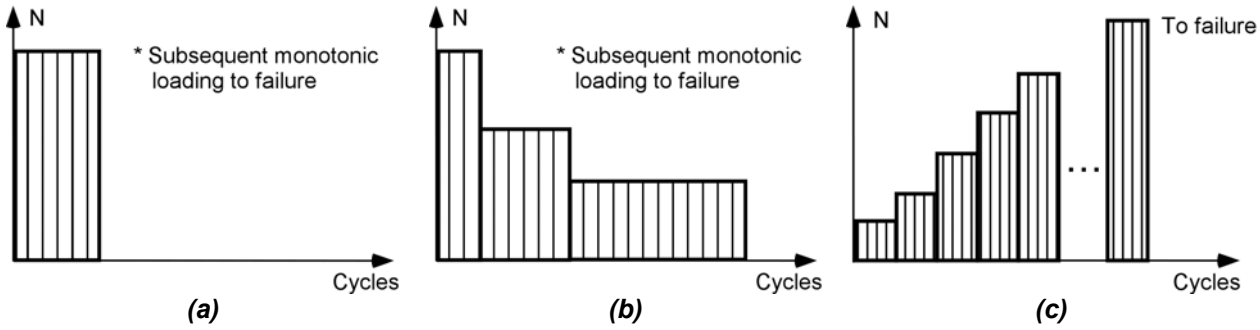

Figure 3.38 Simulated seismic load cycling tests (tension): (a) constant; (b) stepwise decreasing; (c) stepwise increasing

Table 3.9 Simulated seismic load cycling test parameters and assessment criteria

Reference	Load Cycling Amplitude	Load Type[a]	Crack Width [mm]	No. of Load Cycles	Load Level Factors	Assessment Criteria
ACI 355.2	Decreasing	PT	0.5	10/30/100	0.50/0.375/0.25[c]	$N_u \geq 0.8 \cdot N_{u,m}$[c,h]
(2004)		AS	0.5	10/30/100	±0.50/0.375/0.25[c]	$V_u \geq 0.8 \cdot V_{u,m}$[c,h]
AC01, AC58,	Decreasing	PT	-	10/30/100	~ 0.50/0.375/0.25[d]	$N_u \geq 0.8 \cdot N_{u,m}$[d,h,i]
AC106 (2005)		AS	-	10/30/100	~ ±0.50/0.375/0.25[d]	$V_u \geq 0.8 \cdot V_{u,m}$[d,h,i]
AC193, AC308	Decreasing	PT	0.5	10/30/100	0.50/0.375/0.25[c]	$N_u \geq 0.8 \cdot N_{u,m}$[c,h]
(2005)		AS	0.5	10/30/100	±0.50/0.375/0.25[c]	$V_u \geq 0.8 \cdot V_{u,m}$[c,h]
SEAOSC	Increasing	PT	-	5/5/5/5 …	0.25/0.50/0.75/1.0 …[e]	$N_u \geq N_{u,m(bolt)}$[j]
(1997)		AS	-	5/5/5/5 …	±0.25/0.50/0.75/1.0 …[e]	$V_u \geq V_{u,m(bolt)}$[j]
DIBt	Constant	PT[b]	1.5	15	~ 0.45[f]	$N_u \geq 0.7 \cdot N_{u,m}$[f,h]
(1998)		AS	1.0	15	~ 0.45[f]	$V_u \geq 0.9 \cdot V_{u,m}$[f,h]
CSA-N287.2	Decreasing	PT	-	30/30/80/200	0.53/0.45/0.30/0.15[g]	$N_u \geq N_{s,y}$[g,h]
(2003)		AS	-	30/30/80/200	±0.16/0.12/0.08/0.04[g]	$V_u \geq V_{s,y}$[g,h]

[a] PT = Pulsating tension; AS = Alternating shear.
[b] Fastener pushed back to initial position during each unloading cycle.
[c] Factor(s) based on mean ultimate load ($N_{u,m}$, $V_{u,m}$) in reference tests in cracked concrete (Δw = 0.3 mm).
[d] Factor(s) based on mean ultimate load ($N_{u,m}$, $V_{u,m}$) in reference tests in uncracked concrete.
[e] Factor(s) based on First Major Event, e.g. stiffness change, during reference tests in uncracked concrete.
[f] Factor(s) based on mean ultimate load ($N_{u,m}$, $V_{u,m}$) in reference tests in cracked concrete (Δw = 1.0 mm).
[g] Factor(s) based on specified steel yield strengths ($N_{s,y}$, $V_{s,y}$).
[h] No failure allowed during load cycling.
[i] Fastener displacement limits during load cycling are imposed.
[j] $N_{u,m(bolt)}$ and $V_{u,m(bolt)}$ are obtained from tests with comparable cast-in bolts.

In crack movement tests, a fastener is installed in a closed hairline crack and loaded by a sustained tension load (N_w) that is a fraction of the ultimate value. Crack opening (w_1) and closing (w_2) is typically achieved by applying an external load to the anchorage component. In existing crack movement tests, a pulsating tension load is applied to the anchorage component and the initial crack closing width w_2 is allowed to increase as cycling progresses (due to the splitting force developed by the anchor and degradation of the reinforcement bond) as long as a minimum difference $w_1 - w_2$ is maintained (Figure 3.39). After completion of the crack cycles, the fastener is loaded in tension to failure in an open crack to determine the residual strength.

Key crack movement test parameters and assessment criteria contained in the references in Table 3.7 are summarized in Table 3.10.

Detailed summaries of the seismic qualification tests and acceptance criteria in the references in Table 3.7 are provided in Appendix B.

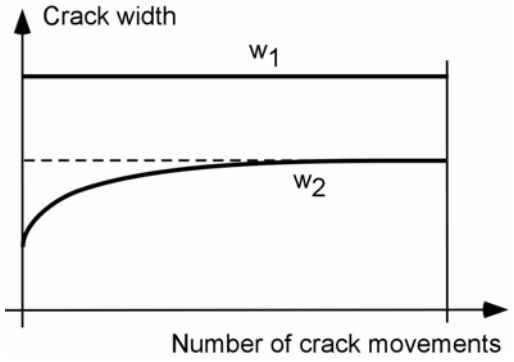

Figure 3.39 Typical crack width progression during a crack movement test

Table 3.10 Crack movement test parameters and assessment criteria

Reference	Crack Width w_1 [mm]	Crack Width w_2 [mm]	No. of Crack Cycles	Sustained Tension Load Level N_w	Assessment Criteria
ACI 355.2 (2004)	0.3	0.1	1000	$0.30 \cdot N_{u,m}$[a]	$N_u \geq 0.9 \cdot N_{u,m}$[a,c,d]
AC193, AC308 (2005)	0.3	0.1	1000	$0.30 \cdot N_{u,m}$[a]	$N_u \geq 0.9 \cdot N_{u,m}$[a,c,d]
DIBt (1998)	1.5	1.0	10	~$0.45 \cdot N_{u,m}$[b]	$N_u \geq 0.7 \cdot N_{u,m}$[b,c]

[a] Mean ultimate tension load ($N_{u,m}$) based on reference tests in cracked concrete (Δw = 0.3 mm).
[b] Mean ultimate tension load ($N_{u,m}$) based on reference tests in cracked concrete (Δw = 1.0 mm).
[c] No failure allowed during crack cycling.
[d] Fastener displacement limits of 2.0 mm after 20 cycles and 3.0 mm after 1000 crack cycles are imposed.

4 Theoretical Background for the Development of Test Parameters

4.1 Characteristics of seismic actions

Earthquakes generate actions (forces and displacements) on a structure in a variety of ways. These include acceleration of the ground (strong ground motion), differential settlement of the foundations resulting from liquefaction or other ground phenomena and lateral and vertical displacement across a fault trace (for structures unlucky enough to be located directly on a fault rupture). From a design perspective, induced structure acceleration represents the most obvious and prevalent loading case to be considered. However, imposed deformations, not inertial forces, are frequently the cause of connection failures in earthquakes, particularly when those connections have not been designed to accommodate large deformations.

Typically, ground accelerations are translated through a structure via the foundations, which interact with the surrounding and supporting soil and rock via a complex interplay of frictional and bearing forces. The input motions from the ground generate varying responses in the structure depending on the magnitude, frequency content and duration of the ground motion, the efficiency of the soil-structure interface and the dynamic characteristics of the structure. As the structure responds to the ground motion, degradation of the primary structure, which serves as the anchorage material, can occur. In reinforced concrete structures this degradation is in large part expressed through cracking in the structural elements. Additionally, the motion of the primary structure will generate actions on secondary structures. If the secondary structure is connected to the primary structure by fasteners, the motion of the primary structure generates tension and shear forces on the fasteners (Figure 4.1).

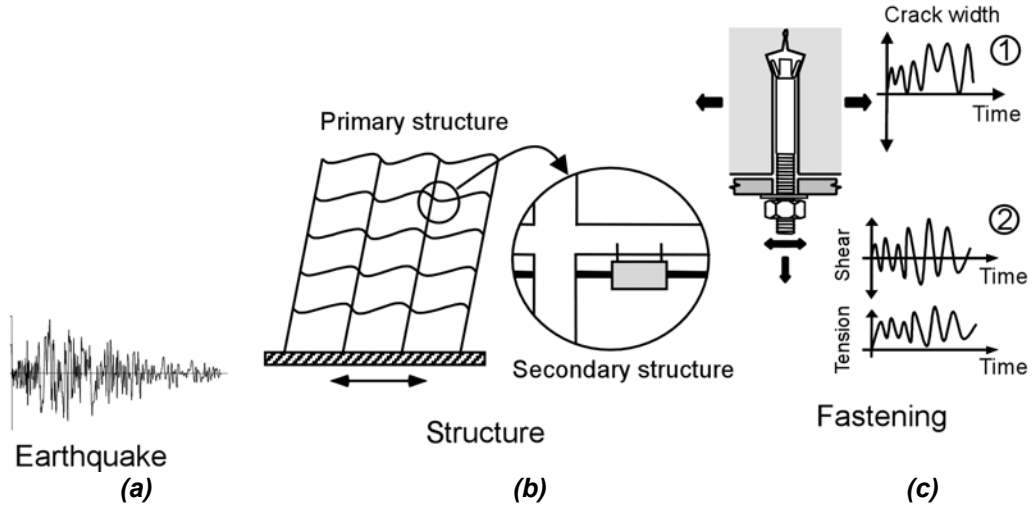

Figure 4.1 Actions acting on a nonstructural anchorage under earthquake loading

Earthquake induced forces vary with time and are designated as dynamic forces. Although many forces encountered in civil engineering practice vary with time, slowly varying forces can be treated as quasi-static (Figure 4.2a) since the inertial and damping components of the forces are negligible. The presence of inertial and damping forces, which arise as a result of strong ground motion, is the critical distinction between dynamic and static loading.

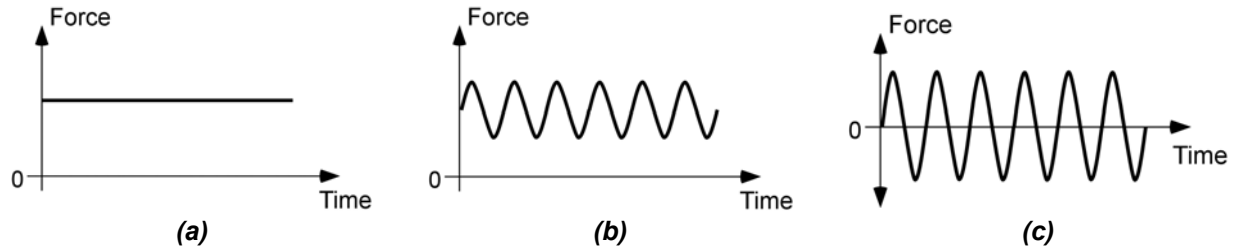

Figure 4.2 Types of force: (a) quasi-static; (b) pulsating; (c) alternating (after Ammenn 1991)

If the axial forces acting on a fastener (Figure 4.1c_2) lead to load cycles only in tension or compression, they are referred to as 'pulsating' axial forces (Figure 4.2b). If changes from tension to compression and vice versa occur, the forces are referred to as 'alternating' axial forces (Figure 4.2c). Axial forces on pre-positioned and in-place mounted anchorages are typically pulsating tensile forces because compression forces are transferred to the anchorage material via the fixture (Figure 4.3a,b). Axial loads on stand-off mounted anchorages can be either pulsating or alternating (Figure 4.3c). Shear forces can similarly be designated as 'pulsating' or 'alternating' depending on whether the sign of the force changes. Shear loads on anchorages during earthquakes can be pulsating or alternating, however, are in general alternating.

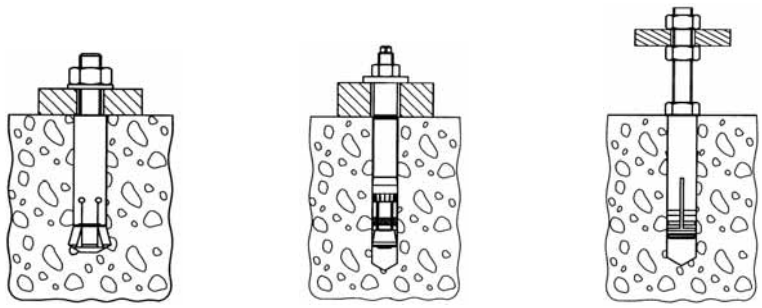

Axial	Pulsating	Pulsating	Pulsating / Alternating
Shear	Pulsating / Alternating	Pulsating / Alternating	Pulsating / Alternating
	(a)	***(b)***	***(c)***

Figure 4.3 Typical axial and shear loadings on fasteners for various mountings: (a) pre-positioned; (b) in-place; (c) stand-off

Important time-dependent features of actions are:

- the number of cycles,
- the peak values of the dynamic action and their sequence in time,
- the strain rate or rate of loading on the anchor and base material, and
- the probability of occurrence of the earthquake induced action during the life of the anchor.

In the following sections, several of these features are quantified for cracking in the anchorage material and loading on the fastener.

4.2 Cracking in the anchorage material

As a structure responds to earthquake ground motion it experiences displacements and consequently deformation of its individual members. These deformations lead to the formation and opening of cracks in members. Furthermore, distinct regions of inelastic deformation can often be distinguished. This is illustrated in Figure 4.4 for a typical moment-resisting reinforced concrete frame building.

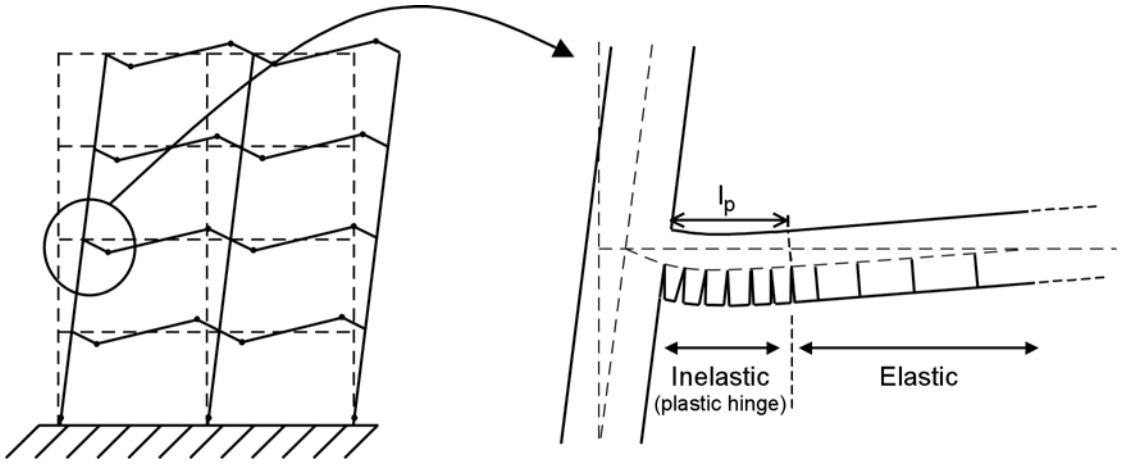

Figure 4.4 Mechanism for accommodating transverse motion of a building through beam deformation (l_p = plastic hinge length)

When the direction of the displacement of the structure changes, e.g. from right to left in Figure 4.4, moment reversal will occur in some members and cracks that had been opened during a previous displacement cycle will be pressed closed.

The crack opening and closing widths as well as the number of crack cycles during an earthquake significantly influence the behavior of fasteners (Chapter 3). It is therefore important to realistically quantify these parameters.

4.2.1 Maximum crack opening width

The large variability in earthquake ground motion and the wide variety of structural configurations complicate general predictions of member deformation, and thus crack opening widths, during an earthquake. To develop fastener qualification tests, one would ideally like to know crack widths independent of a specific earthquake time-history and independent of the specific global structure.

A solution to this problem is provided by limiting the placement of fasteners to locations outside of plastic hinge zones (refer to Figure 4.4). This is done in the *ACI 318 (2005)* and *CEN TS (in preparation)* guidelines for the design of fastenings and is sensible for several reasons including:

(1) spalling of concrete inside of the plastic hinge will reduce the fastener embedment depth and negatively effect fastener response under shear loads;
(2) the crack widths inside of the plastic hinge are so large, as will be shown in this section, as to make fastening there impractical.

Outside of the plastic hinge, the maximum crack opening width that can occur is that when the reinforcement steel in the anchorage component just reaches yield strain. This is the maximum crack opening width for which fasteners should be qualified.

In this section, an investigation using empirical equations for the prediction of crack width in reinforced concrete members is first conducted to determine the influence of various material and geometric parameters on crack widths. The trends observed in this initial investigation are used to develop member cross-sections that are designable within the *Eurocode 2 (2002)* provisions, however, produced large crack widths when the reinforcing steel is at yield strain. This set of cross-sections is then analyzed using the empirical equations to determine the maximum crack opening widths predicted for reinforced concrete members at steel yield strain.

An alternate method to determine crack widths based on the distribution of rotational deformation in reinforced concrete members is then presented. The method differs from empirical equations in that it:

- is applicable for determining crack widths in the inelastic, as well as in the elastic, steel strain range,
- provides a visual representation of the spatial distribution of cracking in a member, and
- gives information about the size of the region of inelastic deformation.

The set of cross-sections developed using the empirical equations for the prediction of crack width is then analyzed using the alternative method. The results discussed are the crack widths inside and just outside of the region of inelastic deformation.

4.2.1.1 Crack width based on empirical equations

The empirical equations for the prediction of crack width suggested by *Gergely and Lutz (1968)*, *Martin, Schießl and Schwarzkopf (1980)*, *Oh and Kang (1987)* and *Eurocode 2 (2002)* were investigated. The equations are provided in Appendix C.

For fastener testing under extreme conditions, i.e. earthquakes, the maximum crack width w_{max} or the characteristic crack width w_k is more relevant than the average crack width w_{ave}. The characteristic crack width can be considered to be roughly equivalent to the maximum crack width. Furthermore, in general, bending induced cracks are of more interest than cracks caused by pure tension loads for seismic applications. Therefore, in this study empirical equations developed to calculate maximum (characteristic) crack widths caused by bending are applied.

4.2.1.1.1 Influence of key parameters on crack width

Figure 4.5 shows the cross-section geometry used to study the influence of key parameters on the crack width. In this idealized section the longitudinal steel is assumed to be lumped along a line and the confinement steel is neglected. The investigated parameters are listed in Table 4.1.

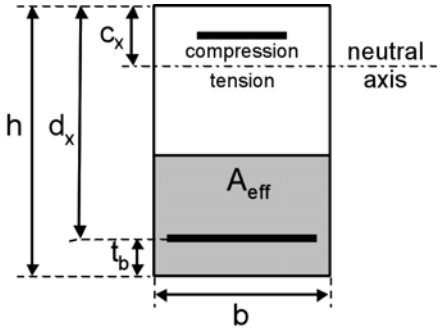

Figure 4.5 Idealized cross-section for study of trends of the empirical equations

Table 4.1 Parameters varied in the study of the empirical equations

Parameter	Range
Concrete cover (t_b) [mm]	10 to 80
Steel yield strength (f_y) [MPa]	100 to 700
Compression reinforcement ratio (ρ') [x ρ]	0 to 1
Tension reinforcement ratio (ρ) [%]	0.25 to 3.75
Reinforcement bar diameter (ϕ) [mm]	10 to 32
Cross-section dimensions (bxh or bxd_x) [mm]	1 - 150x150 2 - 150x450 3 - 300x300 4 - 300x500 5 - 300x900 6 - 600x600 7 - 600x1800 8 - 1000x1000

The parameters in Table 4.1 were determined to be significant for crack width based on a survey of the investigated empirical equations. The parameters were varied over a wide range to encompass typical member designs. Not all parameter combinations, however, lead to sensible member designs or meet requirements of the Eurocode. In the following figures, results that are not sensible or do not meet Eurocode requirements are designated by a dashed line. The dashed line means that at some point between the line segment endpoints the combination of parameters should no longer be considered valid. The results are nevertheless shown as they are sometimes illustrative of behavior.

Although the influence of individual parameters in Table 4.1 on crack width is known, it was desired to compare the various empirical equations and, more importantly, to better understand the effect of simultaneous variation of multiple parameters on the predicted crack widths in order to develop a set of cross-sections for the subsequent studies.

The results of the initial study are illustrated in Figure 4.6 to Figure 4.8. In these figures, it is the trends of the crack width as a function of the varied parameter(s) that are of interest rather than the absolute crack widths. In the figures, the reinforcement steel is at the yield strain.

The following conclusions are reached from Figure 4.6:

(1) Larger concrete cover leads to larger crack width (Figure 4.6a). In practice, however, the minimum allowable concrete cover is typically used for economic reasons. Consequently, the minimum allowable cover for a given member according to the *Eurocode 2 (2002)* is used to determine maximum crack widths.

(2) There is no direct influence of the reinforcing steel strength on the crack width. However, since crack widths at steel yield strain are of interest for fastener tests and because the steel yield strain generally increases with the steel strength, higher strength steels produce larger crack widths at steel yield. The increase in crack width with steel strength is approximately linear (Figure 4.6b). Due to the predominant use of reinforcement steel with a yield strength of 500 MPa in Europe, this steel strength is used to determine maximum crack widths.

(3) The compressive reinforcement ratio indirectly affects crack width by changing the neutral axis depth (Figure 4.5). This effect appears, however, to be negligible (Figure 4.6c). Since compressive reinforcement is required to achieve adequate curvature ductility capacity in reinforced concrete members in which plastic hinges form, a compressive reinforcement ratio equal to one-half of the tension reinforcement ratio ($\rho' = 0.5\rho$) is used to determine the maximum crack widths.

(4) Lower reinforcement ratios lead to larger crack widths (Figure 4.6d). This effect is particularly strong for reinforcement ratios below 1%. For reinforced concrete beams, practical limits for the tensile reinforcement ratio range from $0.0035 \le (\rho = A_s / bd_x) \le 0.015$ (*Paulay & Priestley 1992*). For columns, total reinforcement should be limited to about $0.01 \le (\rho_t = A_{s,total} / A_{gross}) \le 0.04$ (*Eurocode 8 2003*). In the subsequent studies, although a range of reinforcement ratios is investigated, the maximum crack width for 'otherwise comparable sections' (see discussion below) is produced by the section with the lowest tension reinforcement ratio.

(5) Larger reinforcement bar diameters lead to larger crack widths (Figure 4.6e). In the subsequent studies, although a range of reinforcement bar diameters is investigated, the maximum crack width for 'otherwise comparable sections' (see discussion below) is produced by the section with the largest bar diameter that can produce the required reinforcement ratio.

The jump in crack widths in Figure 4.6d,e for the Eurocode 2 equations is due a switch to the limit equation for crack spacing (refer to Appendix C).

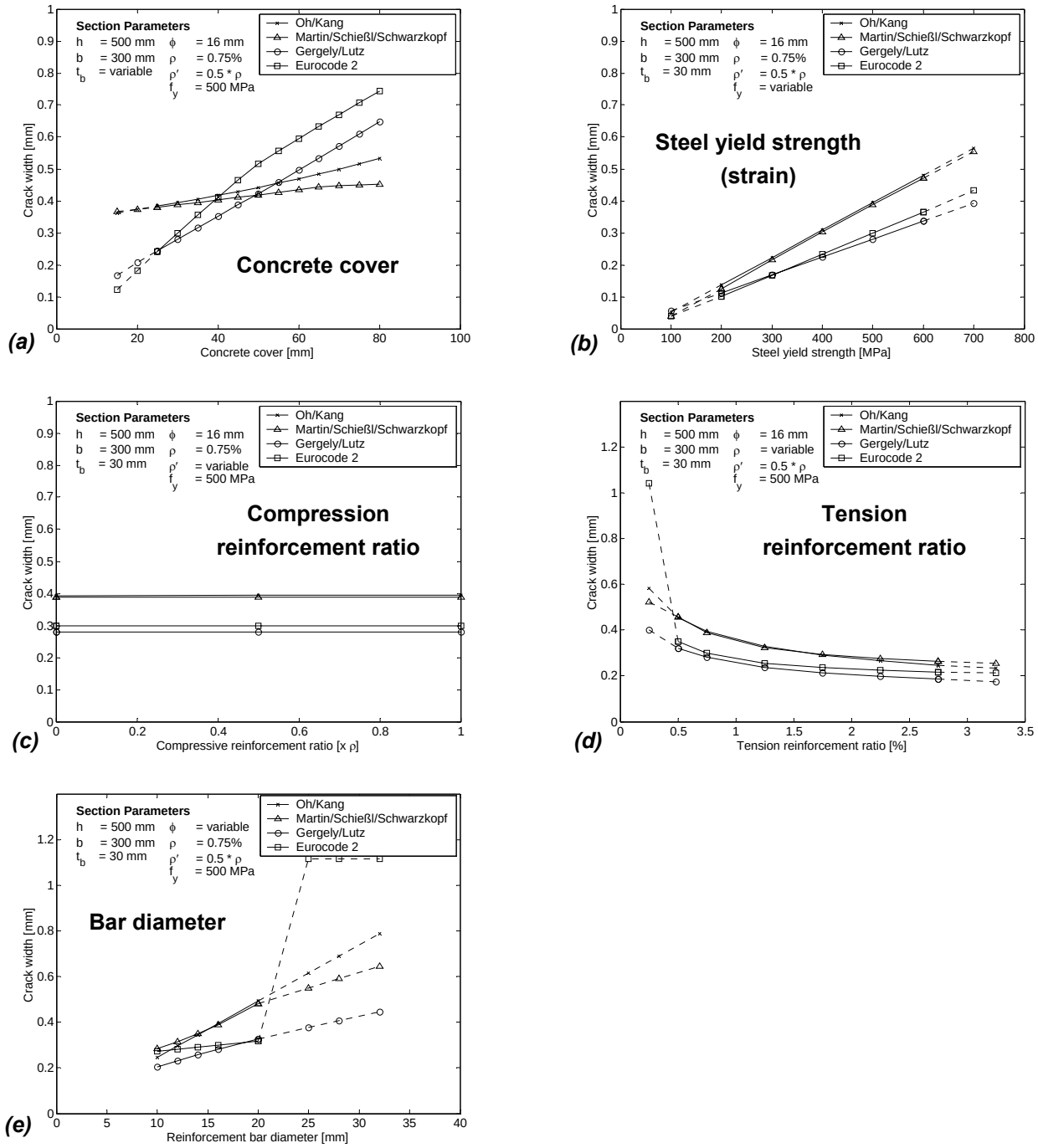

Figure 4.6 Crack widths at steel yield as a function of the investigated parameters

The counter-working effects of the tension reinforcement ratio and the bar diameter on crack width raises the question of which parameter dominates. Figure 4.7 shows crack widths predicted by the empirical equations for the case where the number of tension reinforcement bars is held constant and the tensile reinforcement ratio increases as the reinforcement bar diameter increases. For a given number of reinforcement bars in a section, the Oh/Kang equations suggest that the maximum crack width is achieved by selecting the largest allowable bar diameter regardless of how this affects the reinforcement ratio. The Eurocode 2 equations on the other hand suggest that minimizing the reinforcement ratio maximizes crack width. The other investigated equations predict behavior that lies in between.

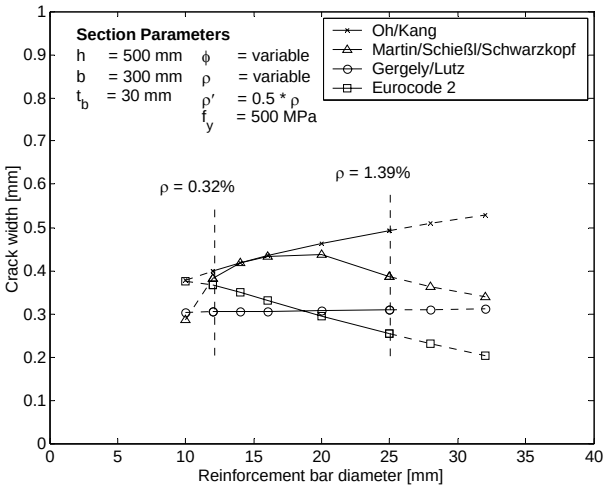

Figure 4.7 Effect of simultaneous change of reinforcement bar diameter and tension reinforcement ratio on crack width as predicted by the investigated empirical equations

The effect of cross-section dimensions on crack width can be difficult to interpret because changing section dimensions affects several parameters simultaneously. The influence of cross-section dimensions on crack width can be summarized as follows:

- If the number of reinforcement bars is allowed to vary and the bar diameter is held constant, for a given reinforcement ratio a proportional increase in the section dimensions or an increase in the section aspect ratio leads to a decrease in crack width (Figure 4.8a).
- If the reinforcement bar diameter is allowed to vary and the number of bars is held constant, for a given reinforcement ratio a proportional increase in the section dimensions typically leads to an increase in crack width. An increase in the section aspect ratio can lead to an increase or a decrease in crack widths depending on which empirical equation is used and on the increase of the reinforcement bar diameter relative to the increase of the effective area surrounding the tension reinforcement (Figure 4.8b).

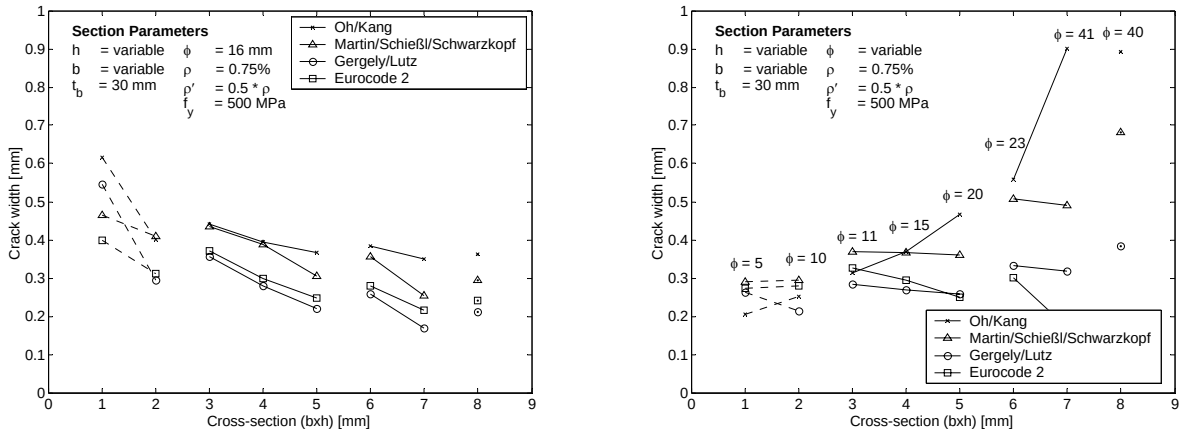

Figure 4.8 Effect of cross-section dimensions (Table 4.1) on crack width as predicted by selected empirical equations: (a) number of bars allowed to vary; (b) diameter of bars allowed to vary

In the subsequent studies the aspect ratio of the sections was selected to vary between $1/3 \leq b / h \leq 1$ to determine maximum crack widths. The values for the section width b varied between 150 and 1000 mm.

A detailed discussion of the above conclusions is provided in *Hoehler (2004a)*.

4.2.1.1.2 Maximum crack widths at steel yield for selected RC sections

The observations in the previous section were used to develop a set of reinforced concrete member cross-sections that are designable within the Eurocode provisions, however, produced large crack widths when the reinforcing steel is at yield strain. In the subsequent studies in this section, the true cross-section dimensions and reinforcement locations (including multiple longitudinal steel layers and confinement steel) are used.

A total of five rectangular 'column' sections and eighteen 'beam' sections were investigated. Column sections are defined as having equal width b and height h and the longitudinal reinforcement is taken to be symmetric, i.e. $\rho' = \rho$. For all column members the total reinforcement ratio is reported $\rho_t = A_{s,total} / A_{gross}$. Columns only up to maximum dimensions of bxh = 300x300 mm were investigated because one can achieve the desired reinforcement ratio using only four corner bars and still meet the restrictions on longitudinal bar spacing in the Eurocode. Larger section dimensions require intermediate bars along the section perimeter to maintain crack width limitation requirements at service load levels (see *Eurocode 2 2002*). These intermediate bars yield at various levels of bending load and require an iterative solution, which makes analysis much more tedious. While column sections with dimensions of 1000x1000 mm and greater are not uncommon in practice, the investigations in Section 4.2.1.1.1 indicate that the key factors for the increase of crack width for larger sections are the larger reinforcing bar diameters and the tendency for more widely spaced longitudinal bars. However, since the Eurocode allows a maximum longitudinal bar spacing of 300 mm and a maximum bar diameter of 32 mm to control crack widths at service load levels (w = 0.3 mm) and because these conditions are covered by the investigated 300x300 mm sections, significantly larger crack widths would not be expected for column sections with dimensions larger than 300x300 mm.

The following parameters were fixed for the study:

(1) mean concrete compressive strength f_{cm} = 38 N/mm^2 and secant modulus E_{cm} = 29180 N/mm^2;
(2) reinforcement steel yield strength f_y = 517 N/mm^2 and elastic modulus E_s = 199900 N/mm^2;
(3) the minimum concrete cover allowed by the Eurocode for a given section was assumed in all cases except one, where double the minimum cover was used;
(4) the presence of confinement steel was taken into account;
(5) pure bending was assumed;
(6) all crack widths were determined at steel yield strain;
(7) short-term loading was assumed;
(8) the effects of cycling on the crack width were neglected.

Table 4.2 shows the crack widths at steel yield predicted by the empirical equations. The maximum values predicted by a given equation when the minimum allowable concrete cover according to Eurocode 2 is maintained is designated by a heavy frame.

The following conclusions can be drawn from the data in Table 4.2:

(1) the selected empirical equations predicted maximum (characteristic) crack widths at steel yield strain between 0.64 mm to 1.04 mm for the investigated sections when the minimum concrete cover according to Eurocode 2 is used;
(2) values for typical beams with dimensions bxd_x equal to 300x500 mm ranged from about 0.3 mm to 0.8 mm;
(3) doubling the minimum cover increased the crack width for the selected section by approximately 10% to 60% depending on the equation selected.

The above conclusions most likely hold for all reinforced concrete sections designed according to the Eurocode 2 with dimensions *bxh* (or d_x) up to 600x1750 mm, however, the case of symmetric 600x600 mm sections was not explicitly investigated.

Table 4.2 Maximum (characteristic) crack width at steel yield for the selected members designed according to the Eurocode

						Crack Width at Steel Yield [mm]			
	b **[mm]**	***h*** **[mm]**	d_x **[mm]**	**Bar Diameter [mm]**	**Reinforcement Ratio (ρ)[a] [%]**	**Oh/Kang**	**Martin/ Schießl/ Schwarzkopf**	**Gergely/Lutz**	**Eurocode 2**
Columns	150	150	-	8	0.89%	0.39	0.38	0.46	0.38
	150	150	-	10	1.40%	0.45	0.35	0.48	0.37
	300	300	-	16	0.89%	0.57	0.56	0.52	0.63
	300	300	-	25	2.18%	0.71	0.44	0.61	0.48
	300	300	-	32	3.57%	0.93	0.38	0.79	0.51
Beams	150	-	400	10	0.39%	0.34	0.35	0.33	0.43
	150	-	400	12	0.38%	0.42	0.41	0.39	0.48
	150	-	400	14	0.51%	0.45	0.44	0.40	0.48
	300	-	500	10	0.31%	0.36	0.32	0.33	0.43
	300	-	500	10	0.73%	0.29	0.31	0.29	0.39
	300	-	500	10	1.26%	0.26	0.28	0.28	0.35
	300	-	500	16	0.40%	0.53	0.49	0.44	0.52
	300	-	500	16	0.80%	0.42	0.38	0.35	0.42
	300	-	500	16	1.21%	0.38	0.34	0.34	0.40
	300	-	501	25	0.65%	0.72	0.63	0.54	0.58
	300	-	501	25	1.31%	0.56	0.41	0.44	0.44
	300	-	500	32	1.07%	0.81	0.54	0.65	0.63
	300	-	850	16	0.32%	0.54	0.38	0.38	0.47
	300	-	851	25	0.38%	0.79	0.60	0.52	0.58
	300	-	850	32	0.63%	0.87	0.66	0.61	0.64
	300	-	850	32	0.63%	0.96	0.71	0.86	1.02[b]
	600	-	1750	16	0.31%	0.52	0.30	0.32	0.41
	600	-	1750	32	0.31%	1.04	0.56	0.58	0.64

[a] Total reinforcement ratio for columns and tension reinforcement ratio for beams.

[b] Double the minimum allowable concrete cover according to Eurocode used.

4.2.1.2 Crack width based on distribution of rotational deformation

In this section an alternate method for approximating crack widths in reinforced concrete flexural members subjected to prescribed deformations is presented. The intent of the method is to provide an efficient and visual way to assess the overall crack state of beam, column and slab members for earthquake loading.

The method offers the following advantages over empirical equations:

- it is applicable for approximating crack widths in both elastic and inelastic regions of members;
- it is formulated in terms of member deformations (rotations) and can be directly linked to member deformation limits in performance based design codes;
- it provides a representation of the spatial distribution of cracking in a member;
- it provides information about the plastic hinge length.

The method has the following limitations:

- in its current form it is only applicable for members with approximately linear moment distributions, i.e. without significant distributed loads;
- it is only applicable for members that have an approximately unique moment-curvature (M-κ) relation up to the maximum required moment;
- in its current form it is only applicable for bending, i.e. no shear effects;
- reinforcement bar slip at beam-column connections is neglected.

At the end of this section a comparison of the method with crack widths determined by empirical equations is conducted using the cross-sections developed in Section 4.2.1.1.

4.2.1.2.1 Description of method to determine crack widths

Bachmann (1967) proposed a method to determine plastic rotations in reinforced concrete members using a summation of crack measurements. Due to the difficulty of obtaining the necessary parameters, e.g. every crack width in a member, and the development of efficient numerical methods to determine plastic member rotations in the 1970s, the approach did not see widespread application. However, by reversing the idea of describing rotations through discrete cracking and taking rotational deformation as a starting point, one can develop a method to predict crack widths.

The idea is as follows: the total rotational deformation in a reinforced concrete member is assumed to be accounted for solely by crack opening. One can envision this as representing a reinforced concrete member by a series of appropriately sized rigid blocks, which are allowed to rotate about the points of contact along the block edges through which the neutral axis passes (Figure 4.9). The size of the rigid blocks is determined by the crack spacing. The relative widths of the cracks are determined by a weighting function derived from the steel strain distribution in the longitudinal tension reinforcement.

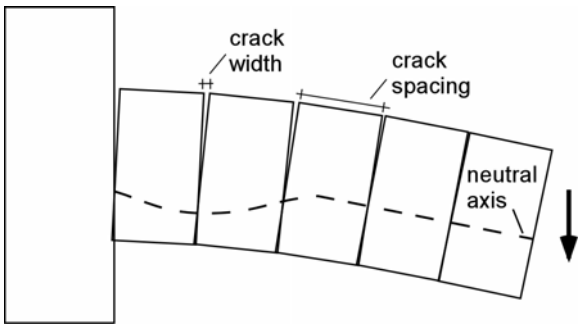

Figure 4.9 Concept to determine crack widths from member rotation (beam-column joint)

The method assumes that all elastic deformation in a member is accounted for by cracking. While this is not physically correct, for the load levels relevant for earthquakes, the contribution of the elastic deformation to the member rotation can be conservatively neglected for the present purposes. Solution for the crack widths is thus reduced to a geometric problem. The constitutive relations, including bond relations, are taken into account when determining the moment required to achieve the desired rotation and in determining the crack spacing and crack width distribution.

Figure 4.10 provides a flowchart of the suggested method. The critical steps in this method are discussed below.

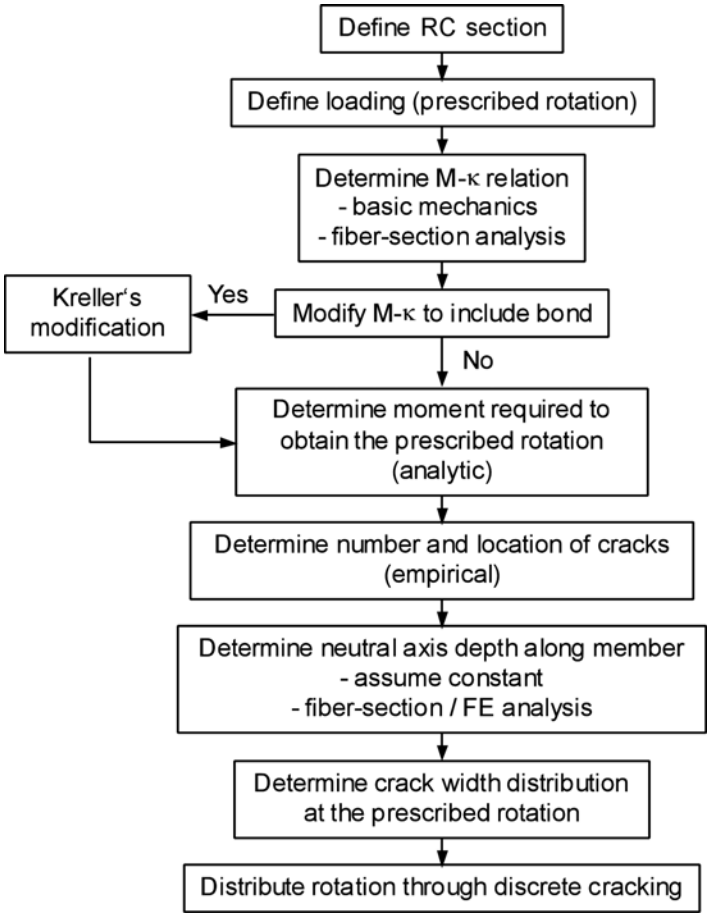

Figure 4.10 Flowchart of method for determining crack widths and locations

Define reinforced concrete section

The geometric and material parameters of the section must be defined.

Define loading (prescribed rotations)

The member loading is defined in terms of a prescribed rotation. Rotation limits are set in some seismic design guidelines (e.g. *ATC-40 1996*). Two definitions of member rotation are relevant for the present method: the total relative member rotation θ_t (Figure 4.11a) and the rotation in the plastic hinge θ_{pz} (Figure 4.11b).

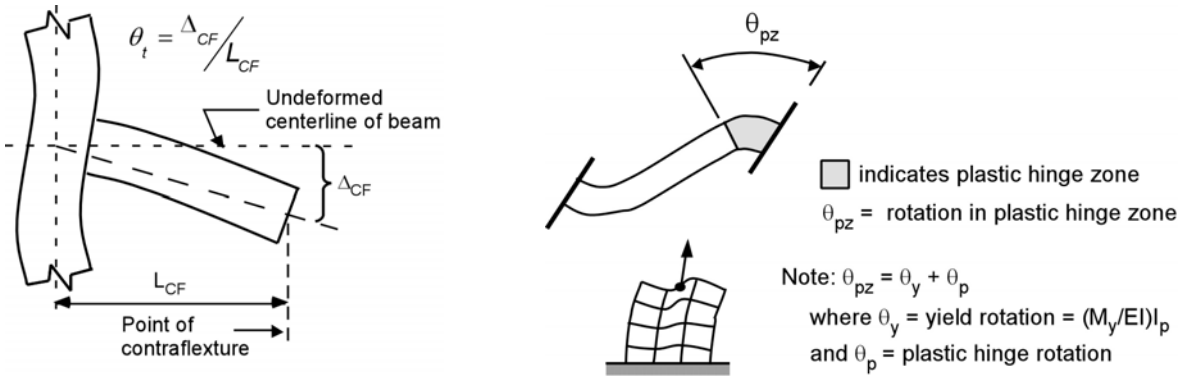

Figure 4.11 Definitions of member rotation: (a) total rotation; (b) plastic hinge rotation (ATC-40 1996)

Determine *M-κ* relation and tension stiffening (bond)

The force-deformation behavior of a reinforced concrete section is provided by its moment-curvature (*M-κ*) relation. For the present method, four descriptions of *M-κ* were investigated:

(1) a bilinear relation obtained from simplified cracked section analysis (BL_{CSA}),
(2) a nonlinear relation obtained from fiber section analysis (NL_{FIB}),
(3) a bilinear approximation of the nonlinear relation obtained from fiber section analysis (BL_{FIB}),
(4) and a multi-linear relation obtained from BL_{FIB} including tension stiffening (ML_{FIB}).

Descriptions 3 and 4 proved to be the most appropriate.

The nonlinear *M-κ* relation based on fiber section analysis was obtained using the commercially available program *XTRACT (2001)*. XTRACT allows for a realistic definition of the section geometry and includes realistic material models (Figure 4.12). The multi-linear (four segments) *M-κ* relation, which accounts for the effects of tension stiffening and the consequent reduction of rotation capacity of a member due to bond, was obtained using the recommendations of *Kreller (1989)*.

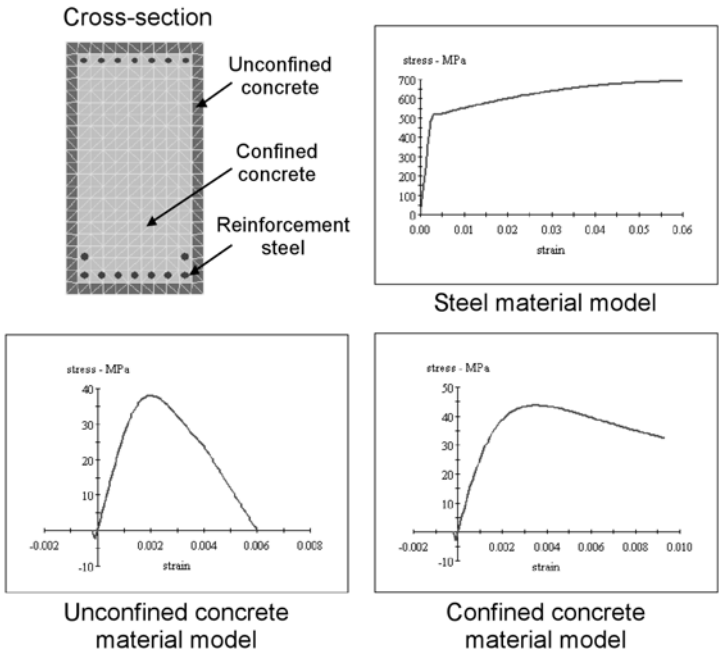

Figure 4.12 Example of input geometry and material models for fiber section analysis

Figure 4.13 schematically shows the modification of a bilinear (in-crack) *M-κ* relation to obtain the average (ave) multi-linear, i.e. stiffened, *M-κ* relation. The subscript 'r1' designates the formation of the first crack in a member, 'rn' designates the end of crack formation, 'y' designates reinforcement steel yield and 'u' designates the ultimate capacity. The equations used to calculate the multi-linear curve and additional information about tension stiffening can be found in *Kreller (1989)* or *CEB (1993)*.

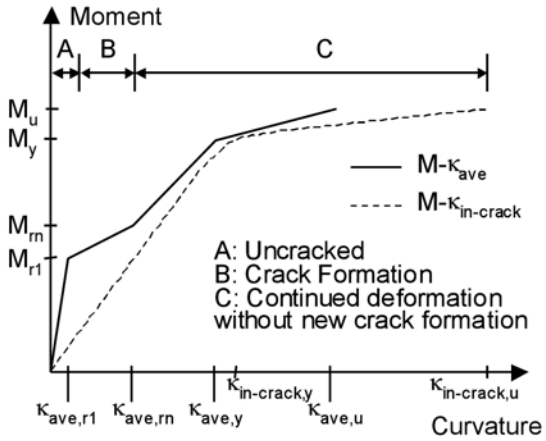

Figure 4.13 Modified bilinear M-κ with tension stiffening (after Kreller 1989)

<u>Determine moments required to achieve the prescribed rotations</u>

A general solution for the rotation of a member with a given moment distribution, or alternatively for the moment distribution for a prescribed rotation, can be obtained using the finite element method. A simple analytical solution to this problem, however, can be found if the following two assumptions are made:

(1) the *M-κ* relation is 'approximately' unique, in terms of curvature at a given moment, up to the required moment, and

(2) that a linear moment distribution is a sufficient approximation of the actual moment distribution.

In most well-designed reinforced concrete members the assumption of unique curvature κ for a given moment M is valid up to peak load. The term 'approximately' is used because small decreases in moment can be neglected (Figure 4.14). The assumption of linear moment distribution is more restrictive than the first assumption, however, it holds for all members where the gravity load induced moments are relatively small compared to the earthquake induced moments. This is often the case for members that serve as part of the lateral load resisting system in structures located in regions of high seismicity.

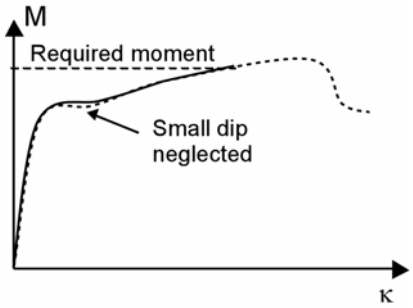

Figure 4.14 M-κ relation where the curvatures are unique up to the required moment (solid line)

If the two above-mentioned assumptions are made, the moment distribution required to achieve a prescribed rotation can be found in the manner described below.

Figure 4.15 shows a section of a reinforced concrete flexural member. Point A is the connection between a beam and column and point B is the point of contraflexure in the beam. The moment distribution is assumed to be linear. The curvature variation along the member represents the actual curvature distribution and is highly nonlinear. The curvature values at the cracks can be determined from the 'in-crack' moment-curvature relations as shown in the figure.

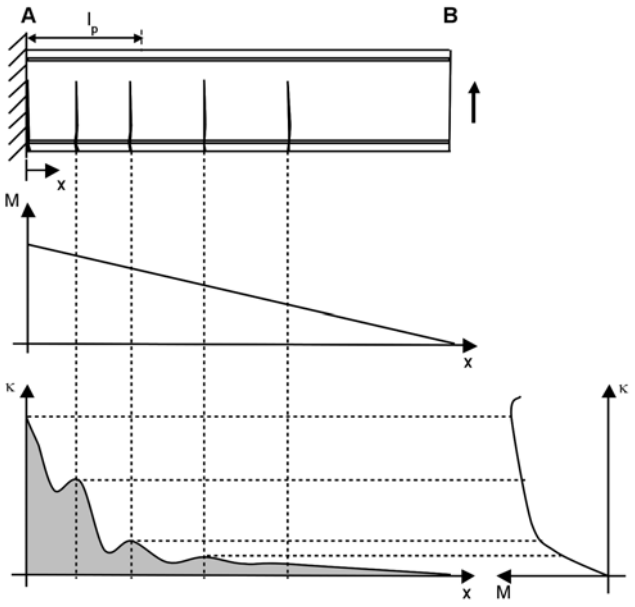

Figure 4.15 Relation between moment, curvature, and cracking along a flexural member

Rotation can be described as the integration of curvatures along a given length in a member (A - B), which is designated by the shaded area in Figure 4.15 and calculated as follows:

$$\theta = \int_{A}^{B} \kappa \cdot dx \tag{4.1}$$

We are interested in formulations for both the total relative rotation θ_t (Figure 4.11a) and the rotation in the plastic hinge zone θ_{pz} (Figure 4.11b). These rotations are described in terms of integrated curvatures by the shaded regions in Figure 4.16.

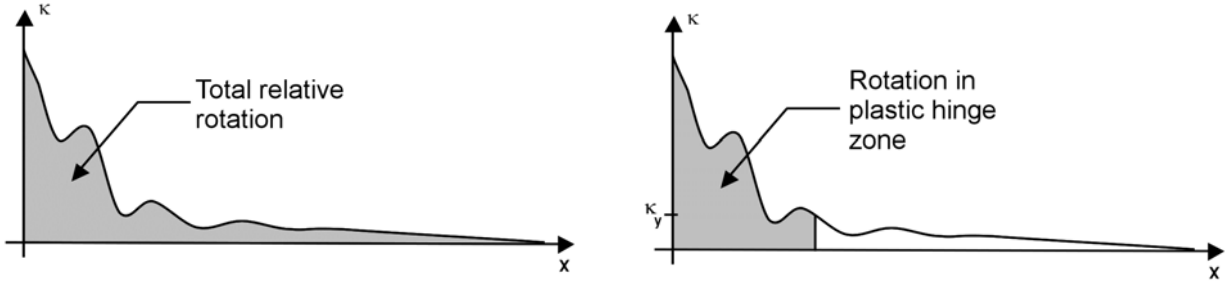

(a) ***(b)***

Figure 4.16 Definitions of rotation in terms of integrated curvatures: (a) total relative rotation θ_t; (b) rotation in plastic hinge zone θ_{pz}

Under the assumptions of a linear moment distribution and a segmentally linear M-κ relation where the curvature always increases with moment, an analytic solution for the peak moment, and thus also the moment distribution, for a prescribed input rotation θ_{IN} can be obtained using the solution yielded by the following quadratic equation where the positive sign before the discriminant is chosen:

$$M_{\max} = \frac{-b + \sqrt{b^2 - 4ac}}{2a} \tag{4.2}$$

where,

$$\begin{aligned} a &= \frac{1}{2} \cdot \frac{\kappa_i - \kappa_{i-1}}{M_i - M_{i-1}} \cdot L_{CF} \\ b &= \left[\kappa_{i-1} - \frac{\kappa_i - \kappa_{i-1}}{M_i - M_{i-1}} \cdot M_{i-1} \right] \cdot L_{CF} - \theta_{IN} \\ c &= \left[\frac{1}{2} \sum_{j=start}^{i} \left(\kappa_{j-1} + \kappa_j \right) \cdot \left(M_j - M_{j-1} \right) - \frac{1}{2} \cdot \left(2 \cdot \kappa_{i-1} - \frac{\kappa_i - \kappa_{i-1}}{M_i - M_{i-1}} \cdot M_{i-1} \right) \cdot M_{i-1} \right] \cdot L_{CF} \end{aligned} \tag{4.3}$$

The algebraic coefficients a, b, and c are obtained from the M-κ relation, the prescribed input rotation θ_{IN} and the member length to the point of contraflexure L_{CF}.

Figure 4.17 shows an arbitrary, segmentally linear M-κ relation with N segments. The curvature at a location between any two M-κ points, e.g. i and i-1, can be determined using the following equation:

$$\kappa_i^m = \kappa_{i-1} + \frac{\kappa_i - \kappa_{i-1}}{M_i - M_{i-1}} \cdot \left(M - M_{i-1}\right) \qquad (4.4)$$

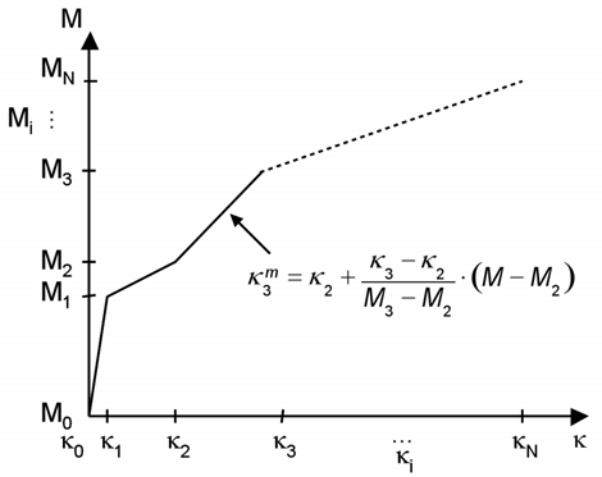

Figure 4.17 Arbitrary, segmentally linear M-κ relation in which the curvature always increases with the moment

To determine the coefficients in Equation (4.3), one has to project the M-κ relation on the member using a chosen moment distribution. This is shown for the case of a linear moment distribution in Figure 4.18. The origin represents the point of maximum moment, which in this case is at the beam-column connection. This methodology could also be formulated for higher-order moment distributions, i.e. quadratic moment distributions that include distributed loads, however, one would have to solve third-order or higher equations to determine M_{max}, which cannot in general be done in closed form.

By looping through the segments of the M-κ relation, i.e. $i = 1$ to N, one can determine on which segment of the M-κ curve the required moment lies or if a linear extrapolation from the ultimate curvature is required to achieve the prescribed rotation θ_{IN}.

The rotation yielded when the point i is selected as the maximum, i.e. the trial rotation, can be determined as:

$$\theta_i^{Tr} = \frac{1}{2} \sum_{j=start}^{i} \left(\kappa_{j-1} + \kappa_j\right) \cdot \left[\left(1 - \frac{M_{j-1}}{M_i}\right) - \left(1 - \frac{M_j}{M_i}\right)\right] \cdot L_{CF} \qquad (4.5)$$

The following algorithm summarizes the looping procedure:

```
for i = 1 to N
    calculate θ_i^Tr
    if (θ_i^Tr ≥ θ_IN  or  i == N)
        calculate a, b, c and M_max
    else
        go to next i
    end
end
```

Using the value 'start' in Equations (4.3) and (4.5), which defines the point where the summation of curvatures should begin, one can designate whether $\theta_{IN} = \theta_t$ or $\theta_{IN} = \theta_{pz}$. For $\theta_{IN} = \theta_t$, 'start' should be set to 1 and for $\theta_{IN} = \theta_{pz}$ 'start' should be set to the index '*i*' corresponding to the first point greater than the yield moment.

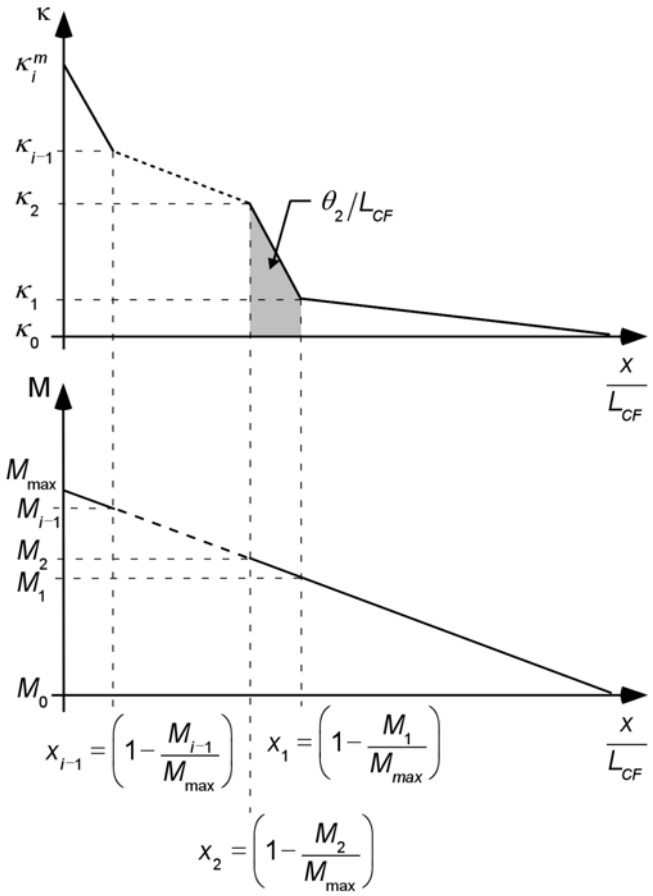

Figure 4.18 Projection of M-κ relation using a linear moment distribution

Determine number and location of cracks

The crack spacing, which determines the size of the rigid blocks in the model (see Figure 4.9), can be determined using empirical equations. In the present implementation the equation for crack spacing by *Oh and Kang (1987)* was used (see Appendix C). In the case of bending, the moment distribution, and thus the steel strain, varies along a member. Since the Oh/Kang equation was developed to predict the average crack spacing in regions of constant moment, it must be applied appropriately for bending. This is done by approximating the moment distribution as a sequence of stepwise constant regions.

The first crack is assumed to occur at the point of maximum moment. The average crack spacing is determined at this location based on the strain in the reinforcement. The average crack spacing is then determined at a distance equal to this spacing away from the first crack in the direction of decreasing moment. This spacing will be equal to or greater than the first spacing because of the decrease in moment.

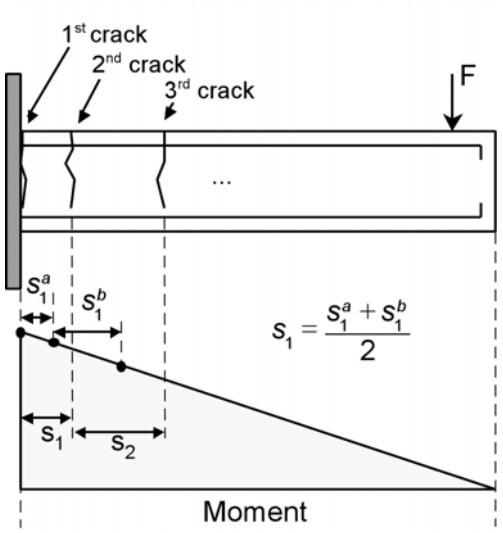

Figure 4.19 Calculation of crack spacing in a member with linearly varying moment

The two values for spacing are averaged to determine the location of the second crack. This process is repeated until no further crack formation is possible or the end of the member, i.e. the point of contraflexure, is reached. This procedure is shown schematically for a linear moment distribution in Figure 4.19.

For a given crack n, the spacing can be determined as:

$$s_n = \frac{s_n^a + s_n^b}{2} \tag{4.6}$$

Determine neutral axis depth

It is assumed that bending cracks extend from the extreme tension fiber of the member to the neutral axis. Therefore, it is necessary to determine the neutral axis depth in the section as it deforms. Two options for defining the neutral axis depth were investigated: (1) constant neutral axis depth along the entire length of the member and (2) variable neutral axis depth obtained from nonlinear fiber-section analysis (Figure 4.20).

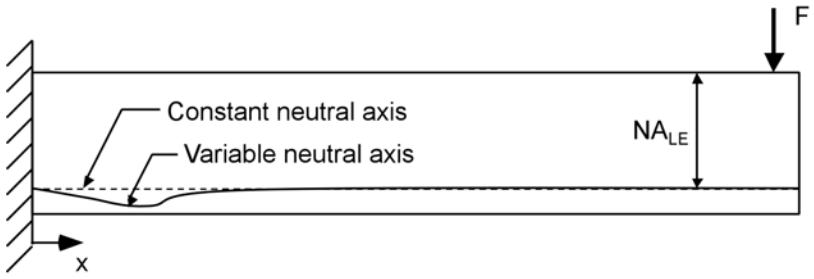

Figure 4.20 Neutral axis depth at ultimate member capacity

A normalized function of the variation of the neutral axis depth can be expressed as:

$$f_{NA}(x) = \frac{NA(x)}{NA_{LE}} \tag{4.7}$$

where $NA(x)$ is the neutral axis depth at a given location and NA_{LE} is the depth within the linear elastic range of deformation.

Investigations using nonlinear fiber-section analysis showed that the depth of the neutral axis increased by a maximum of 21% at the peak load compared to the depth in the elastic range. A constant neutral axis depth $f_{NA}(x) = 1$ was assumed to be sufficiently accurate for the present study.

Determine crack width distribution

The distribution of crack width along the member is determined assuming that the relative crack width varies proportionally with the steel strain in the tensile reinforcement. The steel strain is, in turn, a function of the location along the member *x*. If the neutral axis is assumed to be constant along the member at all levels of deformation, the weighting factors can be determined directly from the curvature distribution as:

$$f_{wCr}(x) = \frac{\kappa(x)}{\kappa_{max}} \qquad (4.8)$$

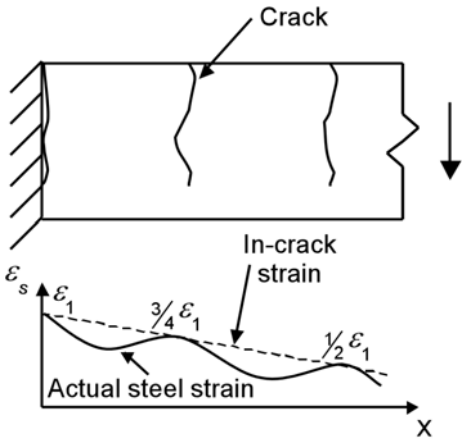

Figure 4.21 Idealized reinforcement steel strain distributions in a bending member

This is illustrated in Figure 4.21 for a reinforced concrete beam loaded above the point where new crack formation has stopped, but below steel yield.

Determine crack widths

The total rotation of the member can be found by summing the rotations in the individual cracks (Figure 4.22).

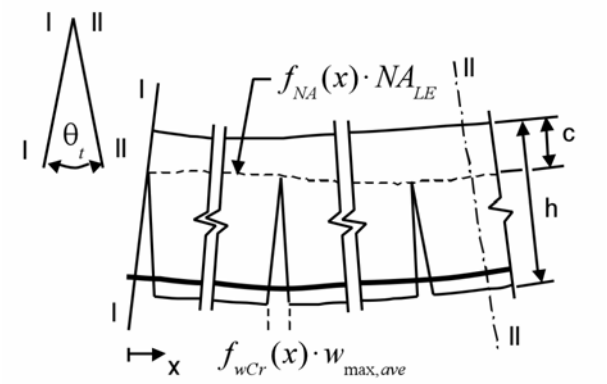

Figure 4.22 Sketch of bending through discrete cracking

Equation (4.9) is an adaptation of the equation used by *Bachmann (1967)*, however, it allows for variation of the neutral axis and assumes a function for the distribution of crack width along the member based on a maximum value.

$$\theta_t = \sum_{i=1}^{\#\text{ of cracks}} \frac{\left(f_{wCr}(x_i) \cdot w_{max,ave}\right)}{h - \left(h/2 - \left\|f_{NA}(x_i) \cdot NA_{LE}\right\|\right)} \qquad (4.9)$$

where θ_t is the total relative member rotation, h is the member height, $f_{wCr}(x)$ is the crack width distribution function, $f_{NA}(x)$ is a neutral axis depth distribution function, NA_{LE} is the neutral axis depth in the linear elastic range measured from the member's geometric center and $w_{max,ave}$ is the 'maximum average' crack width.

Equation (4.9) can be solved for $w_{max,ave}$ and simplified:

$$w_{\max,ave} = \theta_t \cdot \left[\sum_{i=1}^{\#\text{ of cracks}} \frac{\left(f_{wCr}\right)_i}{h - c_i} \right]^{-1} \tag{4.10}$$

where $c_i = h/2 - \left\| f_{NA}\left(x_i\right) \cdot NA_{LE} \right\|$.

The term 'maximum average' crack width is used because the value is not the absolute maximum value for crack width that can be predicted with some degree statistical certainty, but rather the maximum value obtained by distributing the rotations, which yields a mean (average) value for all crack widths. To allow for comparison with maximum (characteristic) values predicted by empirical equations, the crack widths obtained using this method must be multiplied by a factor 1.7. The value 1.7 is based on numerous observations of crack width and is discussed by several authors including *Broms (1965)* and *Rehm and Martin (1968)*.

It is important to note that the rotation used in Equation (4.10) is the total member rotation, regardless of whether the prescribed member rotation is the total rotation θ_t or the rotation in the plastic hinge zone θ_{pz}.

4.2.1.2.2 Maximum crack widths for selected RC sections

The method described in the Section 4.2.1.2.1 was implemented in the Matlab® programming language and a parameter study was conducted using the set of reinforced concrete sections analyzed in Section 4.2.1.1.2.

Two levels of plastic hinge rotation were applied, θ_{pz} = 0.005 and 0.02, which correspond to the Immediate Occupancy (IO) and Life Safety (LS) seismic performance states of *ATC-40 (1996)*, respectively, for members under predominantly flexural loads.

For all beam members a length to depth ratio L_{CF} / d_x = 5 was used.

Figure 4.23 shows an example of the graphical results yielded by the program for a cross-section analyzed at the two rotation levels under the assumption of a nonlinear M-κ relation obtained from fiber-section analysis (NL_{FIB}). A summary of the critical cross-section parameters, the M-κ relation, as well as graphical depictions of the crack widths and locations along the member are provided.

The moments required to achieve the prescribed rotation (lower left corner of Figure 4.23) provide an idea of how much of the member capacity is used.

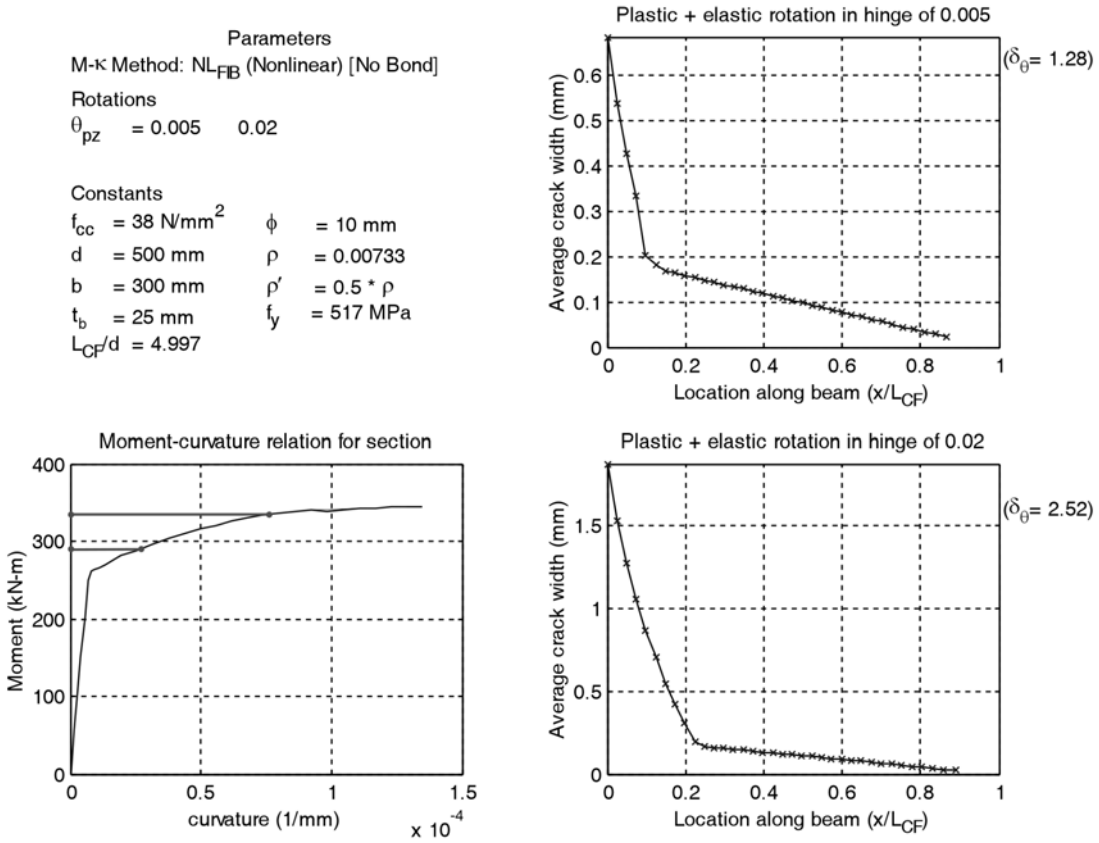

Figure 4.23 Example of graphical results from crack width analysis program

The important information for the study at hand is shown in Figure 4.24. The crack locations are marked by an 'x' and a trend line is provided. The following information shown in this figure is automatically written to a spreadsheet: required rotational ductility δ_θ, plastic hinge length l_p, maximum crack width within l_p and the crack width nearest to the yield point on the elastic side.

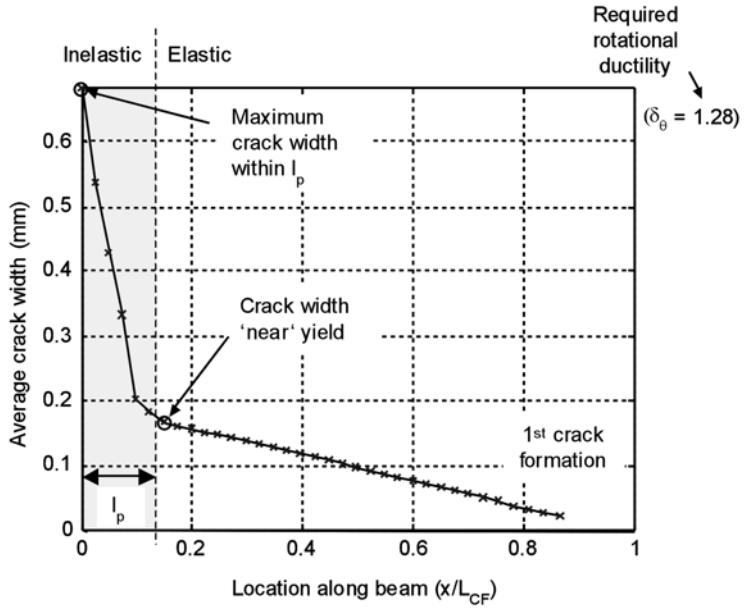

Figure 4.24 Details of graphical results from crack width analysis

It is important to note that the crack width 'near' yield will always be less than or equal to the crack width at yield strain. As is the case in an actual member, it is highly unlikely that a crack will be located exactly at the point where steel is yielding. This should be kept in mind for the subsequent comparisons of crack widths.

The results of the study using a distribution of rotational deformation for predicting crack widths can be summarized as follows:

- A distribution of rotational deformation can be used to determine crack widths in a reinforced concrete member. This approach is applicable to determine crack widths in both elastic and inelastic regions of members and provides a representation of the spatial distribution of cracking in a member.
- The allowable rotations for members in structures during an earthquake suggested in *ATC-40 (1996)* assume that some plastic deformation can occur at all predefined performance objectives.
- Accurate modeling of the size of the region of inelastic deformation was more critical than detailed modeling of tension stiffening (bond) for predicting crack widths in the selected sections.
- The plastic hinge lengths l_p in the sections investigated were in relatively good agreement (maximum difference 27%) with the critical region lengths l_{cr} given in the Eurocode for members designed for medium ductility.
- The maximum 'characteristic' crack widths within the plastic hinge length l_p at the Immediately Occupancy and Life Safety performance states obtained for the investigated sections ranged from 0.89 mm to 4.92 mm and 1.88 mm to 11.84 mm, respectively (Table 4.3). In general these crack widths are much larger than could be tolerated by fastenings. Furthermore, these widths represent a lower value of what could be expected in a real structure, because the additional contribution to crack width from longitudinal elongation of the member and cycling has been neglected. An increase in crack width due to cycling of up to 40% of the initial crack width was suggested by *Leonhardt (1976)*.
- The maximum crack widths near yield at the Immediately Occupancy and Life Safety performance states obtained for the investigated sections were 1.07 mm and 1.01 mm, respectively (Table 4.4). These crack widths are not dependent on the performance state since the reinforcement steel strain is near yield in both cases. Values for typical beams with dimensions bxd_x equal to 300x500 mm ranged from about 0.3 mm to 0.7 mm. The scatter in the values is due to slight differences in the crack location near yield. The agreement with the Oh/Kang equations is very good in most cases. The maximum discrepancy between the values predicted by the suggested method and by the Oh/Kang equations is 34.7% and the average discrepancy is 9.2%. The agreement with the Eurocode 2 equations is good in many cases, however, some significant differences were observed. The maximum discrepancy between the values predicted by the suggested method and by the Eurocode 2 equations is 67.7% and the average discrepancy is 19.7%.

Additional information and detailed discussion of these conclusions are provided in *Hoehler (2004a)*.

Table 4.3 Maximum crack width ($1.7 \cdot w_{max,ave}$) within l_p of the investigated sections at Immediate Occupancy and Life Safety rotation levels

						Maximum 'Characteristic' Crack Width within l_p ($1.7 \cdot w_{max,ave}$) [mm]	
	b **[mm]**	***h*** **[mm]**	d_x **[mm]**	**Bar Diameter [mm]**	**Reinforcement Ratio (ρ)[a] [%]**	θ_{pz} = 0.005 Immediate Occupancy	θ_{pz} = 0.02 Life Safety
Columns	150	150	-	8	0.89%	1.02	1.88
	150	150	-	10	1.40%	0.93	2.73
	300	300	-	16	0.89%	1.74	4.26
	300	300	-	25	2.18%	2.10	6.08
	300	300	-	32	3.57%	1.49	6.20
Beams	150	438	400	10	0.39%	1.57	3.75
	150	439	400	12	0.38%	1.96	4.39
	150	440	400	14	0.51%	1.76	6.54
	300	538	500	10	0.31%	1.64	4.00
	300	556	500	10	0.73%	1.16	3.18
	300	573	500	10	1.26%	0.89	2.97
	300	541	500	16	0.40%	2.29	5.62
	300	541	500	16	0.80%	1.70	4.59
	300	550	500	16	1.21%	1.44	4.36
	300	546	501	25	0.65%	2.77	7.22
	300	546	501	25	1.31%	2.16	5.27
	300	556	500	32	1.07%	2.96	10.66
	300	891	850	16	0.32%	2.61	6.05
	300	896	851	25	0.38%	3.41	8.44
	300	906	850	32	0.63%	3.55	8.99
	300	938	850	32	0.63%	3.85	10.93[b]
	600	1801	1750	16	0.31%	2.53	6.11
	600	1806	1750	32	0.31%	4.92	11.84

[a] Total reinforcement ratio for columns and tension reinforcement ratio for beams.

[b] Double the minimum allowable concrete cover according to Eurocode used.

Table 4.4 Crack width near yield ($1.7 \cdot w_{y,ave}$) of the investigated sections at Immediate Occupancy and Life Safety rotation levels (values from select empirical crack width equations shown for comparison)

						'Characteristic' Crack Width Near Yield ($1.7 \cdot w_{y,ave}$) [mm]			
	b [mm]	**h [mm]**	**d_x [mm]**	**Bar Diameter [mm]**	**Reinforcement Ratio (ρ)[a] [%]**	θ_{pz} = 0.005 Immediate Occupancy	θ_{pz} = 0.02 Life Safety	**Oh/Kang** characteristic crack width at yield [mm]	**Eurocode 2** characteristic crack width at yield [mm]
Columns	150	150	-	8	0.89%	0.36	0.34	0.39	0.38
	150	150	-	10	1.40%	0.39	0.36	0.45	0.37
	300	300	-	16	0.89%	0.54	0.50	0.57	0.63
	300	300	-	25	2.18%	0.61	0.53	0.71	0.48
	300	300	-	32	3.57%	0.74	0.61	0.93	0.51
Beams	150	438	400	10	0.39%	0.33	0.32	0.34	0.43
	150	439	400	12	0.38%	0.41	0.38	0.42	0.48
	150	440	400	14	0.51%	0.41	0.33	0.45	0.48
	300	538	500	10	0.31%	0.36	0.34	0.36	0.43
	300	556	500	10	0.73%	0.29	0.27	0.29	0.39
	300	573	500	10	1.26%	0.25	0.24	0.26	0.35
	300	541	500	16	0.40%	0.50	0.49	0.53	0.52
	300	541	500	16	0.80%	0.40	0.38	0.42	0.42
	300	550	500	16	1.21%	0.38	0.34	0.38	0.40
	300	546	501	25	0.65%	0.66	0.60	0.72	0.58
	300	546	501	25	1.31%	0.53	0.51	0.56	0.44
	300	556	500	32	1.07%	0.72	0.57	0.81	0.63
	300	891	850	16	0.32%	0.54	0.53	0.54	0.47
	300	896	851	25	0.38%	0.75	0.72	0.79	0.58
	300	906	850	32	0.63%	0.82	0.81	0.87	0.64
	300	938	850	32	0.63%	0.89	0.83	0.96	1.02[b]
	600	1801	1750	16	0.31%	0.55	0.54	0.52	0.41
	600	1806	1750	32	0.31%	1.07	1.01	1.04	0.64

[a] Total reinforcement ratio for columns and tension reinforcement ratio for beams.

[b] Double the minimum allowable concrete cover according to Eurocode used.

4.2.2 Minimum crack closing width

The degree to which a previously opened crack in a reinforced concrete member will close during a moment reversal depends on several factors including:

- the width to which the crack was previously opened, which affects the level of damage to bond between the reinforcement steel and the concrete,
- the amount of reinforcement steel that crosses the crack,
- the presence or absence of plastic deformation in the reinforcement steel across the crack,
- the level of the acting compression force, and
- the possible presence of a fastener in the crack that produces splitting forces which hold the crack open.

The level of compression force that acts to close the crack depends on the degree of (bending) deformation of the member and the external loads acting on the member.

Figure 4.25 illustrates crack closure in an idealized exterior beam-column joint undergoing exaggerated deformations as a result of transverse motion of a structure. The distributed load along the horizontal (beam) member acts to prevent the cracks along the underside from closing. The axial compression load on the vertical (column) member, however, will help to close the cracks in this member.

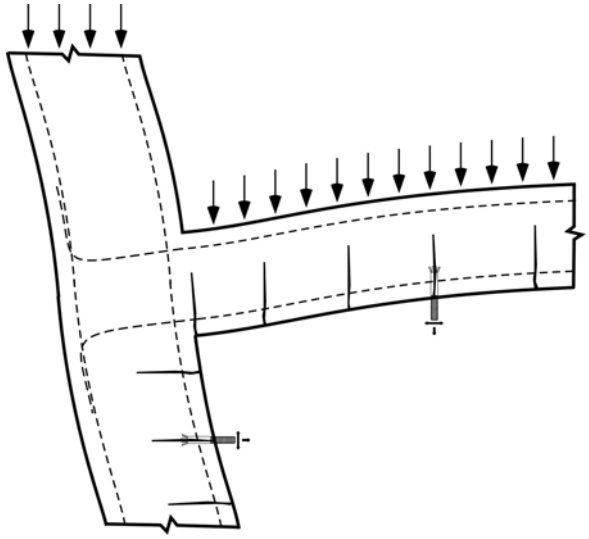

Figure 4.25 Actions influencing crack closure around a fastener

For the purpose of fastener qualification testing it must be assumed that the location of the fastener, e.g. in a beam, column, slab or wall, is not restricted. Therefore, fastener performance under the conditions present in a member with an axial compression load and symmetric moment reversals, e.g. a column or wall, must be verified.

In a well-balanced reinforced concrete member, i.e. one designed such that yielding of the tension reinforcement and crushing of the concrete in compression occur simultaneously, the compression stress in the concrete near the surface of the member at the edge of a plastic hinge will be at ultimate. That is to say, the concrete at this location will be loaded to 100% of the compressive strength. This is the zone in which fasteners are typically anchored. *Furche (1987)*, as well as the test results presented in the next chapter, indicate that compression stress well-below 50% of the ultimate concrete compression strength is usually sufficient to fully close a crack around a fastener (refer to Chapter 3; Section 3.3.3). This holds when no plastic deformation of the reinforcement steel has occurred during crack opening.

Therefore, it can be concluded that seismic crack cycling tests for fasteners should represent the effects of full crack closure, if, as discussed above, it is assumed that fasteners should be qualified for conditions where reinforcement steel strains in the anchorage component up to yield are present.

4.2.3 Number of crack cycles

The number of times that a crack in a reinforced concrete member will open and close during an earthquake depends on the number of cycles of deformation to which the member is subjected. The number of deformation cycles in structural members is, in turn, a function of the earthquake ground motion characteristics (duration, magnitude, frequency) and the dynamic properties of the structure (mass, damping, stiffness).

An extensive review of the problem of cycle counting in earthquake engineering applications is provided by *Hancock and Bommer (2005)*, primarily from a geotechnical perspective. The article includes a comprehensive summary of the relevant literature on the subject. For seismic fastening applications, cycle counting methods based on structural response are most appropriate.

As discussed in Sections 4.2.1 and 4.2.2, the maximum crack opening and closing widths to which a fastener will be subjected during an earthquake occur just outside of the plastic hinge zone when inelastic deformation is occurring. Since earthquake shaking is irregular, some ground motion pulses will result in larger inelastic deformations than others. As shown in Section 4.2.1.2.2, the magnitude of the inelastic deformation inside of the plastic hinge zone is not relevant for the crack opening width outside of this zone. Crack closing widths depend on the level of the resultant compressive force at the crack location. If, for reasons of simplification, it is assumed that only the largest amplitude cycles during an earthquake will lead to complete crack closure, then it would be useful to define an equivalent number of uniform-amplitude inelastic cycles at the maximum amplitude that will cause the same amount of damage as the total number of nonuniform deformations. This has been done by several investigators for various structure types and earthquake ground motions; see for example *Krawinkler et al. (1983)*, *Malhotra (2002)*, *Dutta and Mander (2001)* and *Kunnath and Chai (2004)*.

In the following section, the approach as presented by *Malhotra (2002)* and *Malhotra et al. (2003)* is summarized.

4.2.3.1 Cumulative damage model

Manson (1953) and *Coffin (1954)* independently proposed the following expression for the number of uniform-amplitude cycles to failure:

$$N_f = \frac{1}{C \cdot u^{\alpha}} \tag{4.11}$$

where u = the plastic deformation in an element; and C and α are constants that are determined from experiments. Assuming that each cycle contributes equally to damage in the element, the damage done by a single cycle of amplitude u is:

$$D = \frac{1}{N_f} = C \cdot u^{\alpha} \tag{4.12}$$

Figure 4.26 shows the deformation response of a linear, single degree of freedom system, e.g. an idealized building, with a 2 second period and 10% of the critical damping subjected to the north-south component of the ground motion recorded at Sylmar hospital during the magnitude 6.7M_w 1994 Northridge, California earthquake.

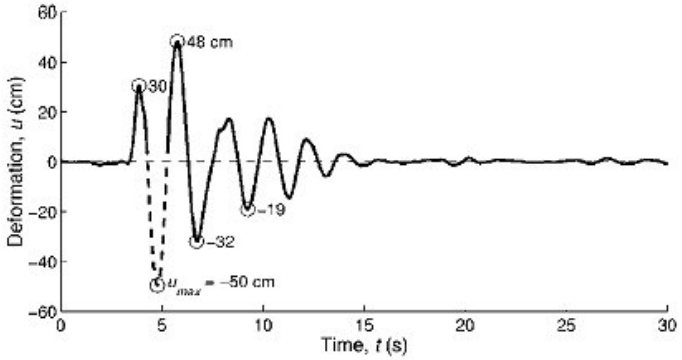

Figure 4.26 Deformation history of a system with 2 second period and 10% damping subjected to the Sylmar ground motion (Malhotra 2002)

The damage caused by a nonuniform deformation history of the type shown in Figure 4.26 can be computed by summing up the damage caused by cycles of different amplitudes, as first proposed by *Miner (1945)*:

$$D = C \cdot \sum_{i=1}^{n} u_i^{\alpha} \tag{4.13}$$

D = 1 implies complete damage (fatigue failure) and n is the total number of cycles.

Because deformation histories are unlikely to contain symmetric cycles (with equal positive and negative amplitudes), *Malhotra (2002)* selected to accumulate damage from each half-cycle instead of each full-cycle. Equation (4.13) is thus rewritten as:

$$D = \frac{C}{2} \cdot \sum_{i=1}^{2n} u_i^{\alpha} \tag{4.14}$$

where u_i = the deformation amplitude of the i^{th} half-cycle and n is now the number of half-cycles.

In the above equation, the load-sequence effects, i.e. the pattern of small and large amplitude cycles, are ignored. No conclusive evidence has been found to suggest that load-sequence is important in low-cycle fatigue (*ATC-24 1992* and *Malhotra et al. 2003*).

There are several uniform-amplitude deformation histories that will cause the same damage as the nonuniform deformation history shown in Figure 4.26. However, if the amplitude of the uniform deformation history is kept the same as the maximum amplitude (u_{max}) of the nonuniform deformation history, then there exists only one uniform-amplitude deformation history that causes the same damage as the nonuniform deformation history shown in Figure 4.26. The only parameter that remains to be

determined is the number of cycles in the uniform-amplitude deformation history. Dividing *D* (Equation (4.14)) by the damage caused by a full-cycle of the largest amplitude u_{max} gives the equivalent number of cycles (of amplitude u_{max}) that cause the same damage as the entire deformation history:

$$n_{eq} = \frac{1}{2} \cdot \sum_{i=1}^{2n} \left(\frac{u_i}{u_{\max}} \right)^{\alpha} \tag{4.15}$$

Values for the experimentally determined damage exponent α = 2 (*Dutta and Mander 2001*), 4 (*Kunnath and Chai 2004*) and 6 (*Jeong and Iwan 1988*) have been suggested for reinforced concrete members. *Malhotra (2002)* used a value of α = 2.

Applying Equation (4.15) to the deformation history shown in Figure 4.26 gives n_{eq} = 2. In other words, the uniform-amplitude deformation history shown in Figure 4.27 causes the same amount of damage as the nonuniform deformation history shown in Figure 4.26. *Malhotra (2002)* further shows that his use of an 'equivalent' linear analysis model and his choice to neglect the contribution of elastic deformations produce a conservative value for the number of uniform-amplitude deformation cycles.

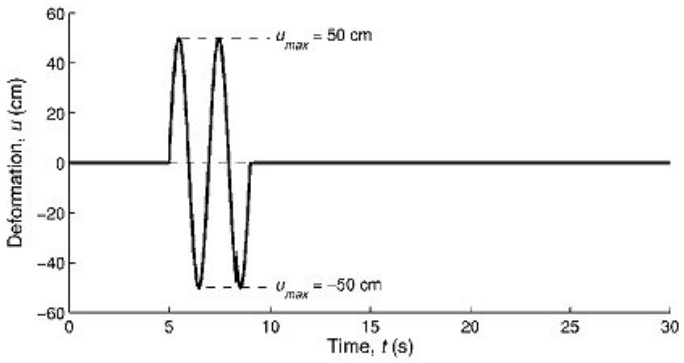

Figure 4.27 Uniform-amplitude deformation history that will cause the same damage as the deformation history shown in Figure 4.26 (Malhotra 2002)

4.2.3.2 Results of numerical studies

Using the method described in Section 4.2.3.1, *Malhotra (2002)* analyzed 71 earthquake ground motions (36 rock + 35 soil sites) to determine the number of uniform-amplitude inelastic deformation cycles to which structures are typically subjected. The results of the study are shown in Figure 4.28.

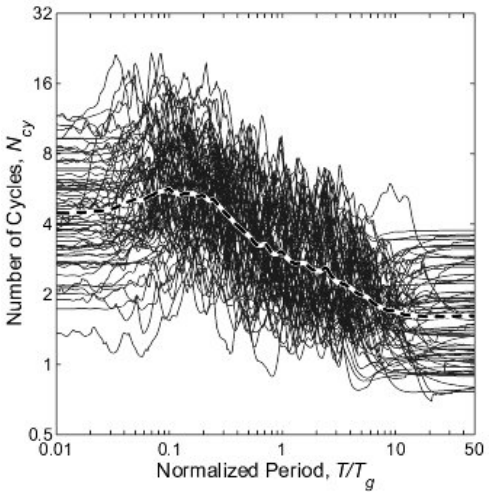

Figure 4.28 Number of cycles (N_{cy} = n_{eq}) as a function of the normalized period T/T_g for 71 ground motions for 10% critical damping and α = 2. The average is shown by the thick dashed line (Malhotra 2002)

The normalizing period T_g is the so-called 'central' period of the ground motion and is defined as:

$$T_g = 2\pi \cdot \sqrt{\frac{PGD}{PGA}} \tag{4.16}$$

where PGD and PGA are the peak ground displacement and acceleration, respectively. A (structural) system with a period $T<T_g$ may be considered stiff and one with a period $T>T_g$ may be considered flexible (*Malhotra 2002*). For the purpose of developing fastener testing criteria it is sufficient to state that this range of periods includes most structures that will be encountered in engineering practice.

Figure 4.28 shows that the number of cycles ranges between about 1 and 20. An average number of cycles for typical buldings is between 2 and 6.

It is noted that reducing damping to 5% of the critical value, which is probably more realistic for reinforced concrete structures, results in a slight increase in the number of cycles. Increasing the damage exponent α decreases the number of cycles (*Malhotra 2002*).

For the design of reinforced concrete columns, *Dutta and Mander (2001)* develop a method to determine numbers of cycles during earthquakes using an approach similar to that described in Section 4.2.3.1, which takes energy considerations into account. *Dutta and Mander (2001)* suggest the following equation for the number of symmetric, uniform-amplitude, inelastic displacement cycles with a hysteretic energy absorption equivalent to that absorbed by the structure over the duration of a typical earthquake:

$$n_{eq} = 7 \cdot T^{-1/3} \tag{4.17a}$$

but

$$4 \leq n_{eq} \leq 20 \qquad (4.17b)$$

where T = period of the structure. For a typical 5-story reinforced concrete moment frame building (T ~ 0.5 seconds) Equation (4.17) yield n_{eq} = 9.

Similar studies on reinforced concrete bridge columns performed by *Kunnath and Chai (2004)* yielded between 1 and 9 cycles for a target displacement demand ductility of 4.

Based on these results, ten (n_{eq} = 10) symmetric, uniform-amplitude inelastic cycles at maximum amplitude are taken to be representative of the number of crack opening and closing cycles during an earthquake for fastener testing purposes. Because the deformation during cycling is inelastic, it is ensured that maximum crack opening, i.e. crack opening at steel yield, and full crack closure will be achieved for each cycle.

4.3 Fastener loading

4.3.1 Load cycling

The amplitude of earthquake actions which act on fasteners used to connect structural elements can be approximated from structural analysis performed using equivalent lateral force, modal response or time-history based methods (Figure 4.29). The amplitude will vary from case to case. The number of equivalent uniform-amplitude load cycles that act on the fastening should be equal to the number of uniform-amplitude crack cycles as presented in Section 4.2.3.2, i.e. around 10 cycles at maximum amplitude response.

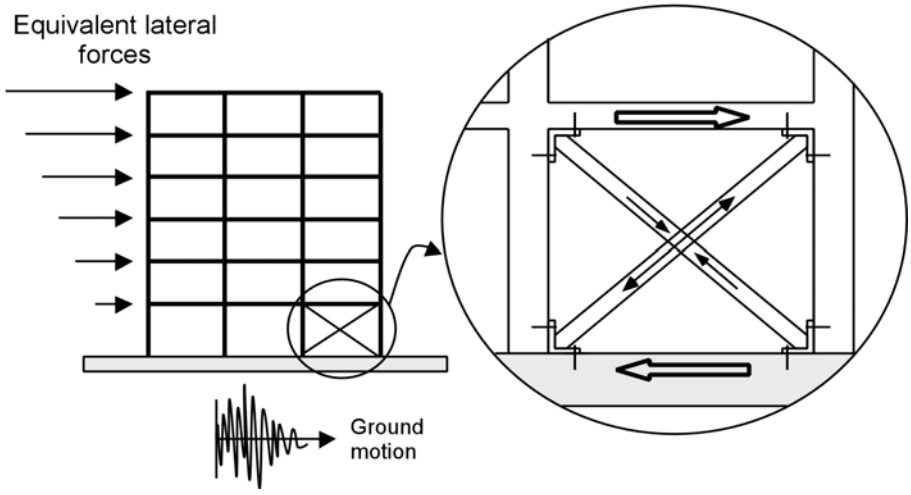

Figure 4.29 Determination of actions on structural anchorages using equivalent lateral forces

In the case of nonstructural elements, ground accelerations are first filtered (modified) by the primary structure and then by the attached nonstructural element before reaching the fasteners (Figure 4.30). This can lead to significant amplification of forces (F_{ha}, F_{va}).

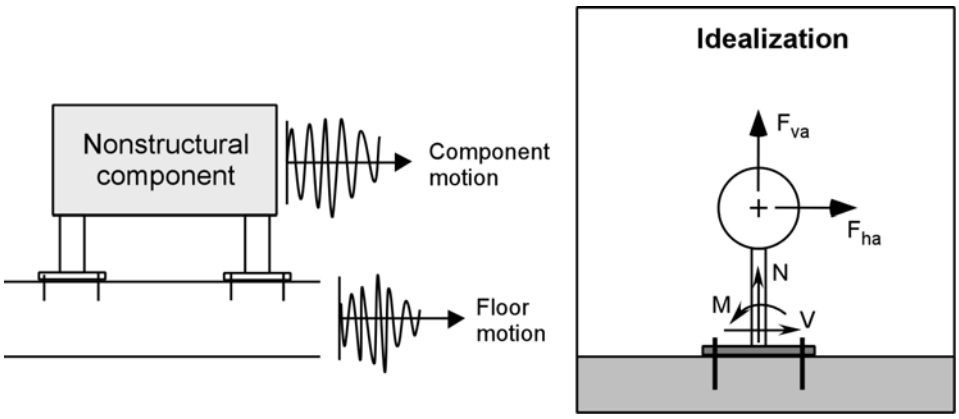

Figure 4.30 Determination of actions on nonstructural anchorages

For example, the building response floor motions can be several times larger than the ground motions. To illustrate this point, Figure 4.31 presents a plot of a 5% damped floor response spectra derived from response motions recorded at the roof of a 6-story hospital building during the 1994 Northridge earthquake. Also shown in the figure is the corresponding ground motion response spectra derived from a field instrument present at the same site (*ATC-58 2004*). Additionally, depending on the period of the attached nonstructural component relative to that of the floor response at the mounting location, the acceleration can be further amplified or decreased.

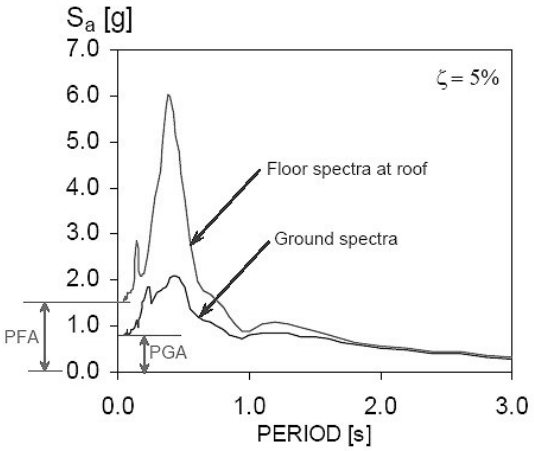

Figure 4.31 Response spectra and floor spectra computed from motions recorded at a 6-story hospital in Sylmar, California during the 1994 Northridge earthquake (ATC-58 2004)

The equations available for estimating the amplitude of nonstructural forces that occur during an earthquake are typically a function of the ground shaking, the weight of the component, the height of the component in the structure, the relative periods of the nonstructural component and the structure, as well as the importance and presumed ductility of the component and its attachment (*IBC 2003* and *CEN TS in preparation*). These equations contain a large degree of uncertainty (*ATC 29 1990* and *ATC 29-1 1998*). Equations for calculating forces on nonstructural elements attached using fasteners according to *CEN TS (in preparation)* are given in Appendix D.

It is noted that for the design of fastenings used to attach nonstructural components, it is frequently important that forces arising from both horizontal and vertical ground accelerations be considered.

To determine the number of load cycles that act on fasteners used to connect nonstructural components, one can look to investigations performed by *Malhotra et al. (2003)*. Using the same approach as described to determine of the number of cycles of structure deformation (Section 4.2.3.1), Malhotra and his co-authors determined the number of equivalent, uniform-amplitude cycles for nonstructural components located in structures. The idealized nonstructural components, with periods ranging from 0.02 to 0.5 seconds (2 to 50 Hz), were subjected to 32 strong-motions recorded at the roof level of 18 buildings (3 to 54 stories) of various types during the 1994 6.7M_w Northridge earthquake. Figure 4.32 shows a histogram of the number of cycles. The median (50-percential) value of the number of cycles is 7 and the 90-percentile value is 11.

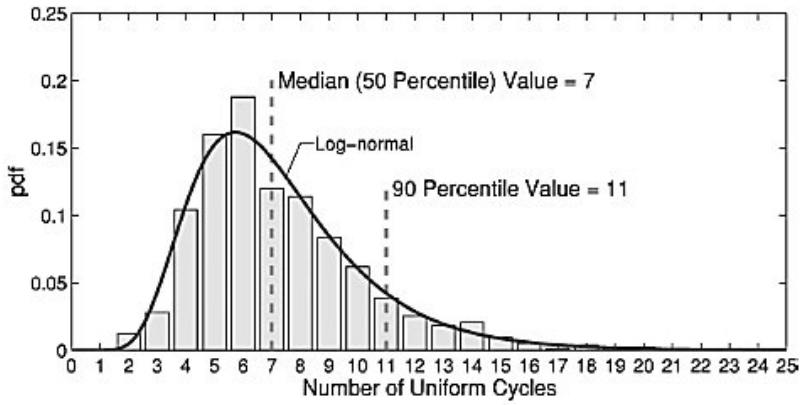

Figure 4.32 Probability density function (pdf) of the equivalent number of uniform-amplitude cycles for nonstructural components (2 to 50 Hz) in response to roof motions recorded during the 6.7M_w 1994 Northridge earthquake (Malhotra et al. 2003)

Under the assumption that the number of cycles is proportional to the duration of the ground motion, which is in turn a function of the earthquake magnitude M_w, the 90-percentile value is increased by 40% (11x1.4=15) to account for earthquake magnitudes up to 7.2M_w. For most sites, the design (475-year return period) earthquake will not be greater than 7.2M_w. Therefore, the number of cycles, which has 10% chance of being exceeded in 50 years, is 15 (*Malhotra et al. 2003*). This value for the number of equivalent, uniform-amplitude cycles has been accepted for the ATC-58 guideline Component Testing for Nonstructural Components that is currently under development (P. K. Malhotra, personal communication, October 18th, 2005).

Therefore, a fastener should be able to sustain at least 15 load cycles at the maximum amplitude to which it will be subjected during an earthquake without failure. Since this maximum amplitude is in general not known, an alternative approach for testing is to determine a stepwise increasing loading pattern that generates the same amount of damage as 15 cycles at the ultimate fastener strength. This can be done using the Miner's rule (*Miner 1945*). The applicability of the Miner's rule for stepwise varying tensile loading of concrete, as is relevant for brittle fastener failure modes, was

demonstrated for the case of high-cycle fatigue of concrete in tension by *Cornelissen and Reinhardt (1984)*. The equivalent number of cycles n_{eq} can be determined as:

$$n_{eq} = \sum_{j=1}^{m} \sum_{i=1}^{n} \left(\frac{j}{m} \right)^{\alpha} \tag{4.18}$$

If the damage exponent is taken as α = 2 and the number of load cycles per step is arbitrarily set to n = 5, seven load levels (m = 7) of increasing amplitudes 1/7, 2/7, ..., 7/7 times the mean ultimate failure load ($N_{u,m}$ or $V_{u,m}$) yields n_{eq} = 14.3. This implies a total of about 35 cycles to failure. It is noted that this is very similar to the loading prescribed by the *SEAOSC (1997)* seismic test method.

A stepwise increasing load function is in general preferable to constant load level cycling for anchor testing because it avoids arbitrary definition of maximum cycling levels and provides anchor stiffness response over the entire anchor loading range.

4.3.2 Loading rate

The rate at which a fastener is loaded during an earthquake depends on the period of the actions acting on the component that it attaches. For the typical application of fastening of a nonstructural component (Figure 4.33), the maximum rate of tension or shear loading may be assumed to be one-quarter of the period of oscillation of the component.

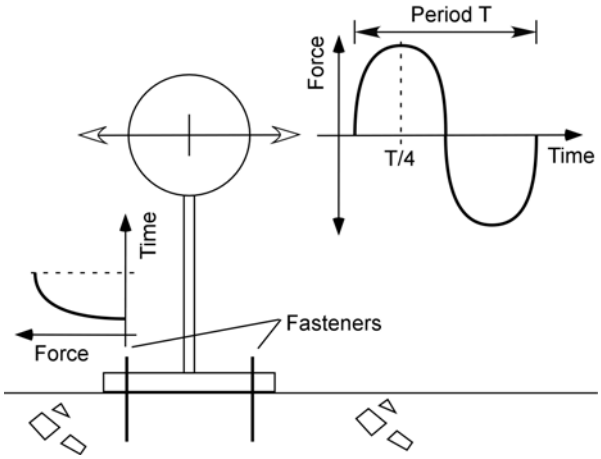

Figure 4.33 Fastener loading during cycling of a nonstructural component

For the testing of fasteners, periods associated with highly energetic oscillations of the component are of interest. The period of oscillation is a function of both the modal periods of the component as well as the frequency content of the input motion. For input motion containing a wide range of frequencies, however, a component idealized as a single degree of freedom system will oscillate with a period close to the natural period of the component (*Chopra 1995*). Components located at ground level are subject directly to the earthquake ground motions and the condition of a broad frequency content of the input motion is likely valid. Components located elsewhere in a structure will be subjected to input motions that are 'filtered' by the primary structure. Since frequency content of the input motion at the location of attachment is not in general known, it is

assumed here that frequencies in resonance with the lower modes of the nonstructural component govern the response.

The periods of vibration of nonstructural components and systems vary depending on the mass and stiffness of the system; including the connection stiffness. Due to the complexity of many nonstructural components and systems, e.g. indeterminate supports, nonlinear connection behavior or the presence of fluid in the system, the actual periods can often only be determined experimentally. According to *AC156 (2004)* Acceptance Criteria for Seismic Qualification by Shake-Table Testing on Nonstructural Components and Systems, the resonant frequency search, which is used to identify the periods of lower modes of vibration, is to be conducted using a sinusoidal sweep from 1.3 to 33.3 Hz ($0.77 \geq T \geq 0.03$ seconds). This range may be assumed to provide limits for the frequencies of interest for nonstructural components and systems. Within this range, however, only frequencies between 1.3 and 8.3 Hz ($0.77 \geq T \geq 0.12$ seconds) are used to generate peak spectral accelerations in the horizontal directions (*AC156 2004*).

Taking frequency limits of 1 and 10 Hz to be representative of the energetic oscillations of typical nonstructural components and systems one obtains a rise time to ultimate load for fasteners between 0.25 and 0.025 seconds.

Klingner et al. (1998) suggest that a rise time to ultimate load of 0.1 seconds for fasteners corresponds to that of typical earthquake response of mounted equipment. This value is based on the assumption of a typical characteristic period of 0.4 seconds (2.5 Hz) for floor response spectra (R. E. Klingner, personal communication, May 22nd, 2005) and fits within the range 0.25 to 0.025 seconds.

4.3.2.1 Definition of loading rate for fastener tests

Although the rise time to ultimate load can be conveniently estimated using structural and nonstructural component periods of vibration and is a quantity that most people can understand intuitively, it is unfortunately not objective for testing fasteners. For example, an M20 anchor with an embedment depth h_{ef} = 125 mm must be loaded much more rapidly than a similar M8 anchor with an embedment depth h_{ef} = 55 mm if both are to reach ultimate load in 0.1 seconds.

Using typical values for the ultimate load and the displacement at ultimate load for a headed bolt with an embedment depth h_{ef} = 80 mm in normal strength (C20/25) cracked concrete (w = 0.3 mm) failing by concrete failure, one obtains approximate load and displacement rates for fasteners during an earthquake (Table 4.5).

Table 4.5 Earthquake relevant loading rates for fasteners based on the response of a headed bolt (h_{ef} = 80 mm) in C20/25 cracked concrete (w = 0.3 mm)

Rise Time to Ultimate Load [sec]	Fastener Loading Rate [kN/s]	Fastener Displacement Rate [mm/s]
0.025	1700	160
0.1	425	40
0.25	170	16

4.3.2.2 Expressing loading rate in terms of strain

Ammann (1992) categorizes fastener loading rates in terms of the strain rate $\dot{\varepsilon}$ (Table 4.6). Quasi-static loads are defined as those with strain rates $\dot{\varepsilon} < 10^{-5}$.

Table 4.6 Characteristics of dynamic forces (Ammann 1992)

	Fatigue	**Earthquake**	**Shock (Impact)**
No. of cycles [-]	$n < 2 \cdot 10^6$	$10 < n < 1000$	$1 < n < 20$
Strain rate [s^{-1}]	$10^{-5} < \dot{\varepsilon} < 10^{-3}$	$0.001 < \dot{\varepsilon} < 1$	$0.01 < \dot{\varepsilon} < 100$
Causes	- traffic - machinery	- earthquakes	- impact - blast wave - collapse of support

Interestingly, in an article published one year earlier, *Ammann (1991)* suggested that strain rates for earthquake loading ranged between $10^{-5} < \dot{\varepsilon} < 10^{-2}$, i.e. two orders of magnitude lower than the values in Table 4.6. The difficultly of expressing (fastener) behavior as a function of strain rate, rather than a displacement or loading rate, is discussed by Ammann himself in his extensive work on the behavior of reinforced and prestressed concrete structures under impact loads (*Ammann 1983*). The problem lays in the definition of the length over which the strains are determined.

For practical applications with fasteners, the definition of the strain rate is problematic for several reasons. First, for different failure modes the location of the relevant strain rate varies. For example, in the case of concrete cone failure of a headed bolt, the important strain rates are those at the crack tip as it propagates through the concrete $\dot{\varepsilon}_{ct}$ and perhaps also in the compressed concrete under the anchor head $\dot{\varepsilon}_c$ (Figure 4.34). These values are likely to be significantly different than the strain rate in the anchor steel $\dot{\varepsilon}_s$. In the case of pull-through failure, the strain rate in the steel at the interface between the expansion cone and the expansion elements is decisive. For bonded anchors, the strain rate along the entire bond failure surface is likely to play a role. Second, in a typical pull-out test the displacement at the point of load application on the fastener and not the strain is measured. Therefore one must assume an effective measurement length to calculate a strain rate even for the steel. The value that should be used as an effective measurement length is not immediately obvious.

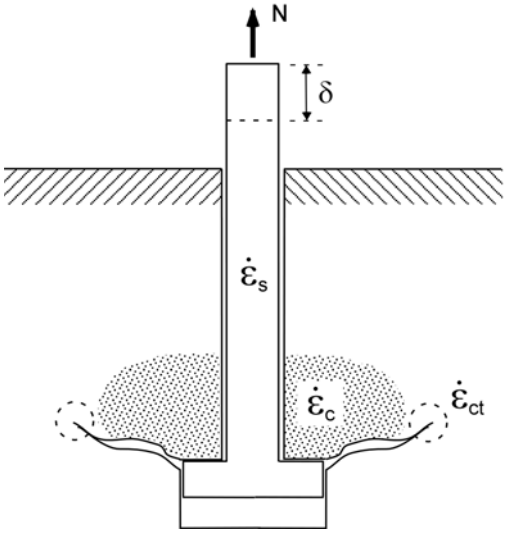

Figure 4.34 Relevant strain rates in a headed bolt under tension loading

Although *Ammann (1992)* does not state an assumed measurement length, based on his studies of material behavior (*Ammann 1983*) it is believed that a reference measurement length of five times the fastener diameter ($5 \cdot d$) is implicit in the strain rates given in Table 4.6. For a fastener of size M12 ($5 \cdot d$ = 60 mm) this would imply a

displacement rate $0.06 < \dot{\delta} < 60$ mm/s for strain rates of $0.001 < \dot{\varepsilon} < 1$, respectively. Depending on the fastener type and failure mode, displacements at ultimate load for an M12 fastener in normal strength (C20/25), cracked concrete (Δw = 0.3 mm) typically range between 10 mm and 1 mm. For the upper boundary for earthquake loading rates suggested by Ammann ($\dot{\delta} = 60$ mm/s), this results in a rise time to ultimate load somewhere between 0.17 and 0.017 seconds. These rise times to ultimate load are similar to those obtained based on the period of oscillation of the structure and nonstructural component (refer to Table 4.5).

Although further study is required, it is suggested that the effective embedment depth of the fastener h_{ef} would be a better first approximation of an effective measurement length for determining strain rates than $5 \cdot d$.

4.4 Testing options

As illustrated in Figure 4.1, during an earthquake fasteners are subjected to dynamic load cycling and simultaneously to opening and closing of cracks in the anchorage material. Such conditions could be recreated in the laboratory using a shake table. Shake table tests, however, are prohibitively expensive for fastener qualification. Therefore, tests are performed using approximations of these conditions (Figure 4.35).

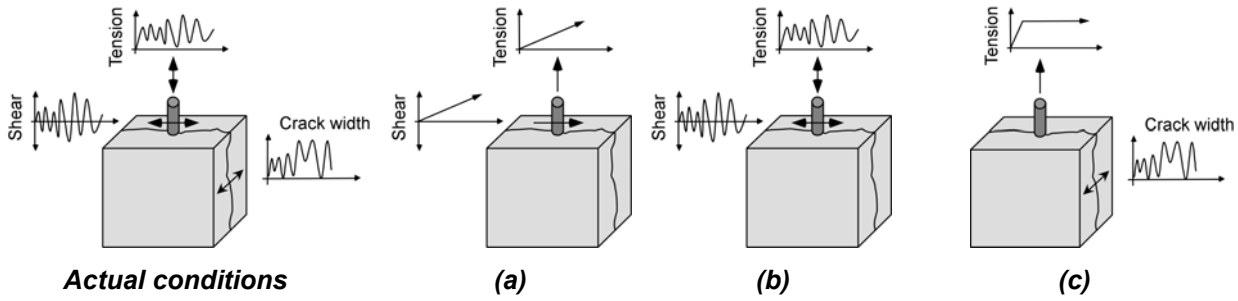

Figure 4.35 Combinations of loading and cracking used to represent the local conditions at a fastening during and earthquake: (a) monotonically increasing load (static or dynamic) and a static crack; (b) cyclic load (static or dynamic) and a static crack; (c) constant load and cycled crack widths

Tests of the three types shown in Figure 4.35 can be found in current seismic qualification protocol for fasteners (*ACI 355.2 2004*, *AC193 2005*, *AC308 2005*). The test parameters used, however, are decisive in determining the fastener performance. Comparison of the existing seismic qualification tests presented at the end of Chapter 3 with the boundary conditions discussed in this chapter indicate that existing tests are in many cases unconservative. This is especially true for crack cycling tests currently used for seismic qualification of fasteners in the United States.

A summary of alternate testing parameters based on the discussion in this chapter is provided in Chapter 9.

5 Experimental Investigations with Cycled Cracks in the Anchorage Material

5.1 Scope

Although it is often presumed that response to cycled cracks will be decisive to determine the suitability of a fastener for seismic applications (*Sippel et al. 2001*), prior experimental evidence is limited and only available for cycling in open cracks, i.e. without full crack closure. Using the seismic relevant crack cycling conditions discussed in Chapter 4, a test setup and procedure was developed to investigate fastener behavior in wide cycled cracks.

Tests with cast-in and post-installed fasteners were performed. The primary objectives of these tests were:

(1) to determine the relative performance of various fastener types and failure modes under representative seismic crack cycling conditions;
(2) to investigate the influence of testing parameters such as the loading sequence and the rate and shape of the crack cycles;
(3) to investigate the influence of fastener head bearing pressure, crack opening width and applied compression load on the anchorage component;
(4) to establish a testing procedure for a seismic crack cycling test.

In this chapter, a summary of the test setups and procedures are presented along with detailed discussions of the key results. The complete test reports are available in *Hoehler (2005b, 2006a)*.

5.2 Experimental setups and testing procedures

5.2.1 Investigated fasteners

The relevant fastener parameters are summarized in Table 5.1. The fasteners were installed according to the manufacturer's recommendations, except where the effective embedment depth h_{ef} was modified (see Table 5.1) to achieve a desired failure mode.

Table 5.1 Fasteners investigated in crack cycling tests

Fastener Type	Size	Drill Hole Diameter d_0 [mm]	Effective Embedment h_{ef} [mm]	Illustration
Headed stud (grade St37)	d_{nom} = 19 mm; d_h = 26.5 mm	19[a]	100	Figure 3.2
Expansion anchor (bolt-type)	M16	16	95[b]	Figure 3.4
Expansion anchor (sleeve-type)	M12	18	80	Figure 3.4
Undercut anchor	M10	20	80[c]	Figure 3.5
Screw anchor	d_{nom} = 20 mm	18	76[d]	Figure 3.6

[a] Nominal shaft diameter.
[b] Actual h_{ef} = recommended h_{ef} + 10 mm.
[c] Actual h_{ef} = recommended h_{ef} - 20 mm.
[d] $h_{ef} = 0.85 \cdot h_{nom}$ (h_{nom} = 90 mm).

5.2.2 Anchorage components

Monotonic (reference) tests were conducted in reinforced concrete slabs made of C20/25 concrete. The slabs were designed to allow for the formation and control of static line cracks using steel splitting wedges driven into sleeves placed in preformed holes in the slab (Figure 5.1).

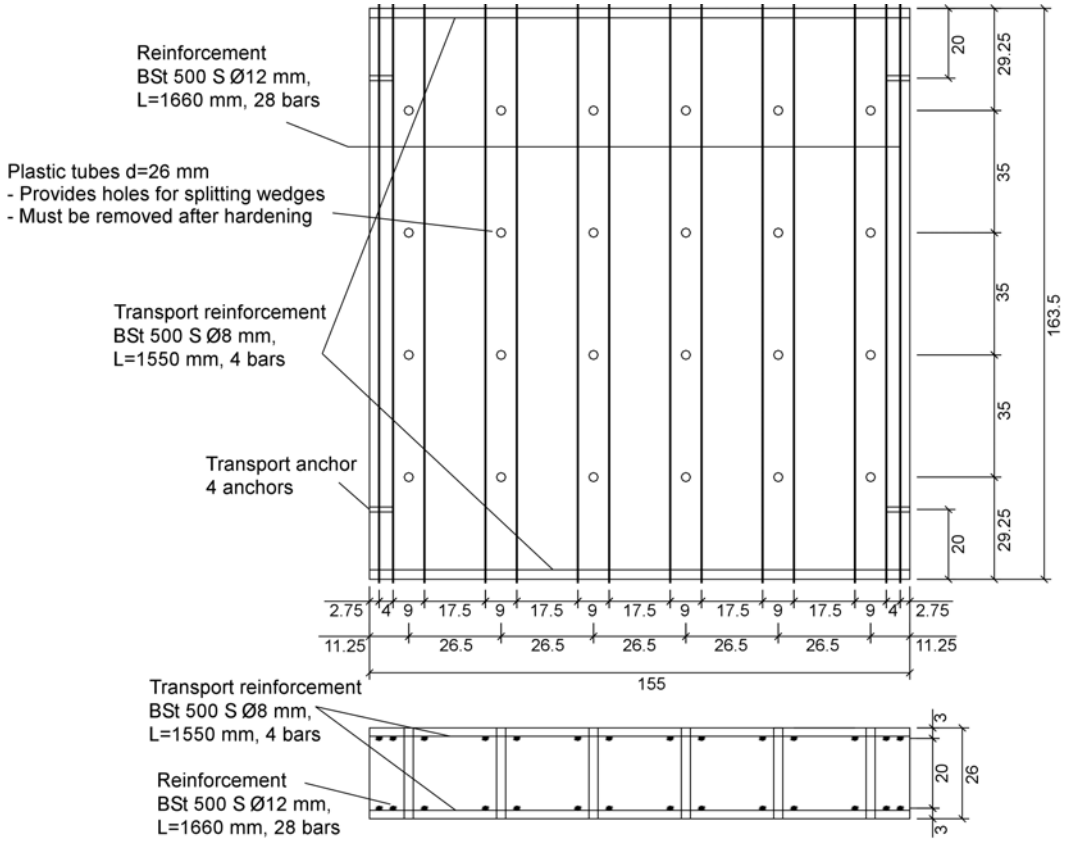

Figure 5.1 Wedge-split slab for tests in static cracks (units in cm unless otherwise noted)

Crack cycling tests were performed in specially designed reinforced concrete members made of C20/25 concrete (Figure 5.2). Special hot-rolled, high-strength steel reinforcement bars (BSt 900/1100), which have a rib pattern that allows for special nuts to be screwed onto the bars, were used for the longitudinal reinforcement. Three stirrups were placed at each of the member ends. Four I-shaped, thin (2 mm) metal plates (crack inducers) were placed along the member at the average calculated crack spacing (s = 350 mm) to aid crack formation. The gross member cross-section area was A_{gross} = 1134 cm^2. The longitudinal reinforcement ratio was ρ = 0.0062. Duct tape was used to destroy the bond between the concrete and the reinforcement bars in a small region ($\pm 25\ mm$) to either side of the crack inducer, which made it easier to generate large crack opening widths.

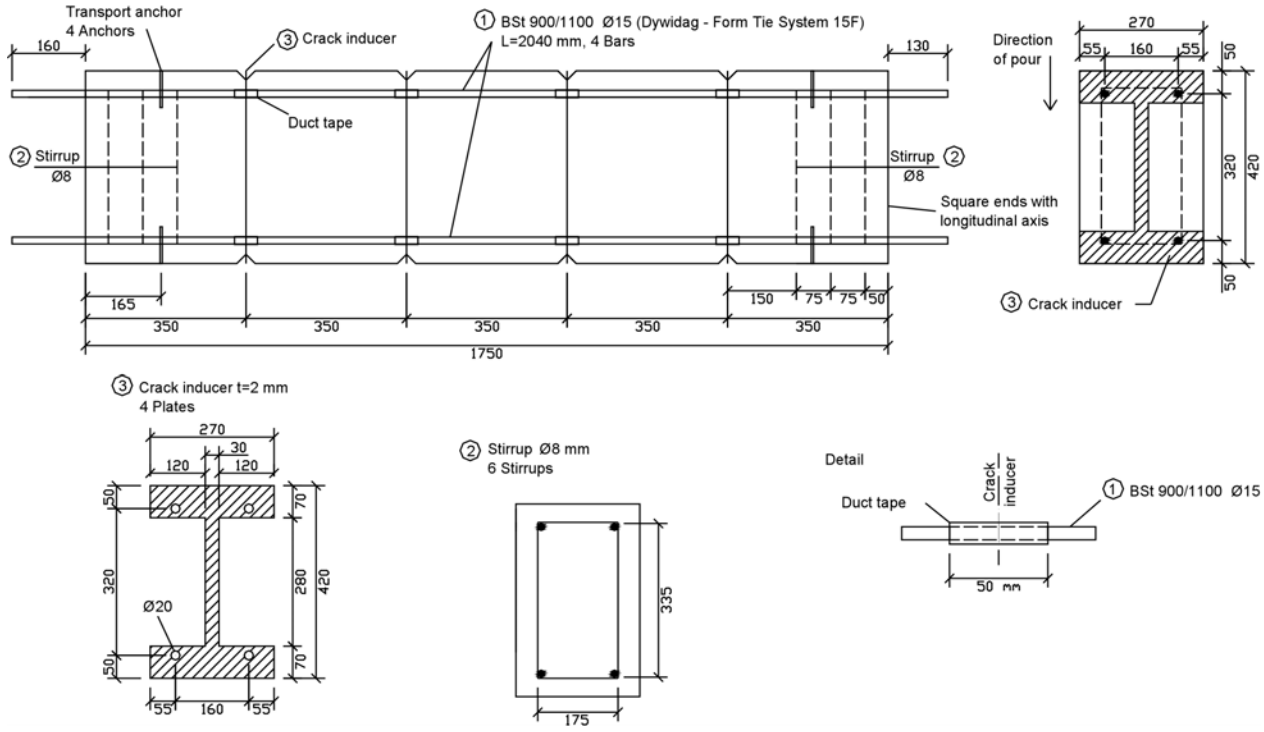

Figure 5.2 Concrete member for seismic crack cycling tests (all units in mm)

The anchorage components were produced according to the state of the art after *DIN 1045 (2001)* and *DIN 1048 (1991)*.

The average concrete cube compressive strength for the members varied from $f_{cc,150}$ = 25.7 N/mm^2 to $f_{cc,150}$ = 31.5 N/mm^2.

5.2.3 Loading setups and testing procedures

5.2.3.1 Reference tension tests

Reference tests in static line cracks were performed in the wedge-split slabs (Figure 5.1). The test setup is shown in Figure 5.3. All tests were performed on single fasteners with large anchor spacing and edge distances. The load cylinder support frame was located at a distance from the fastener so that a complete concrete cone breakout could occur (wide support). The crack was opened by Δw = 0.8 mm after installation of the fasteners, but before loading. Tension load was applied monotonically to the fastener using a 100 kN hydraulic cylinder by slowly increasing the oil pressure (pseudo displacement-controlled). Ultimate load was reached in approximately 1 to 3 minutes. Crack widths were monitored, but not controlled, during loading. The tension load N applied to the fastener, the fastener displacement δ and the crack opening width Δw were measured continually during the test.

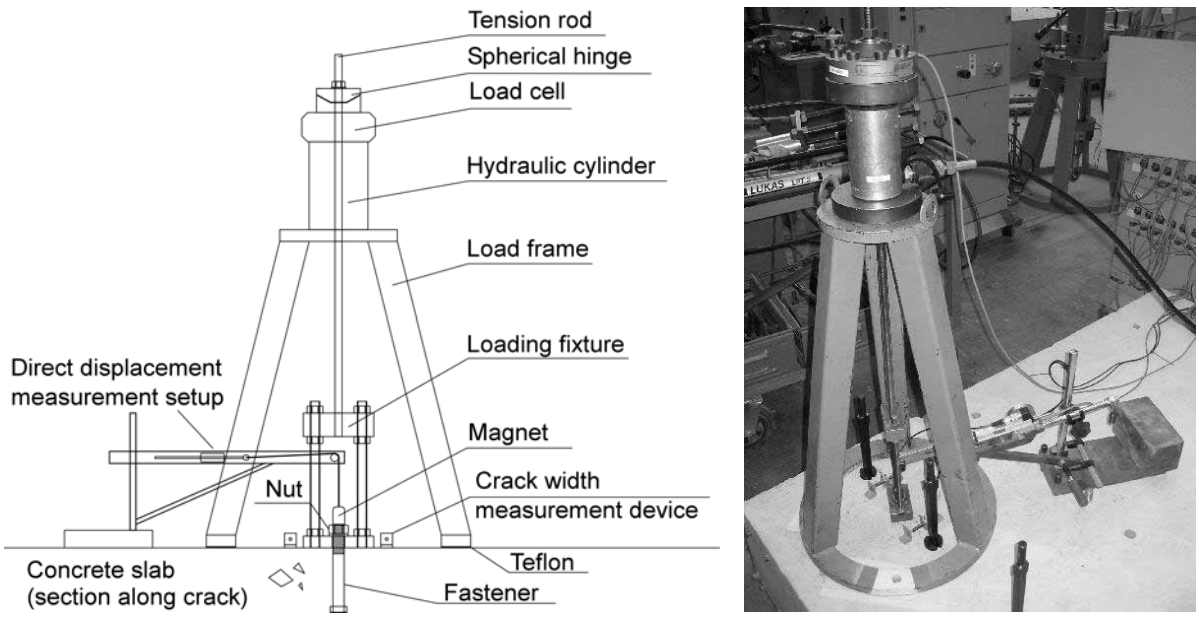

Figure 5.3 Loading setup for reference tension tests in static line cracks: (a) schematic; (b) photograph

5.2.3.2 Seismic crack cycling tests

For the seismic crack cycling tests, four line cracks were generated in the special anchorage components (Figure 5.2) using the loading configuration in Figure 5.4. A servo-hydraulic cylinder with a capacity of 630 kN mounted horizontally in a stiffened L-angle was used to load the member. A similar L-angle was used at the opposite end of the member to provide the necessary reaction.

The anchorage component was attached at the cylinder end of the setup to a stiff plate that was free to rotate horizontally (Figure 5.5a). At the opposite end, the component was connected to a stiff plate that was not free to rotate (Figure 5.5b). Two 1 mm thick Teflon sheets were placed between the component ends and the connection plates to facilitate lateral expansion of the ends during compression.

Track rollers were used to support the anchorage component in the vertical direction.

Additional steel angles were affixed at the sides of the component and a beam was attached above the component as a safety against buckling of the component during compression (not shown in Figure 5.4). A small (~ 5 mm) initial gap was left between the safety supports and the anchorage component.

The cracks were opened via tensile force applied to the four longitudinal reinforcement bars in the anchorage component. The cracks were closed by applying compressive force distributed over the ends of the component.

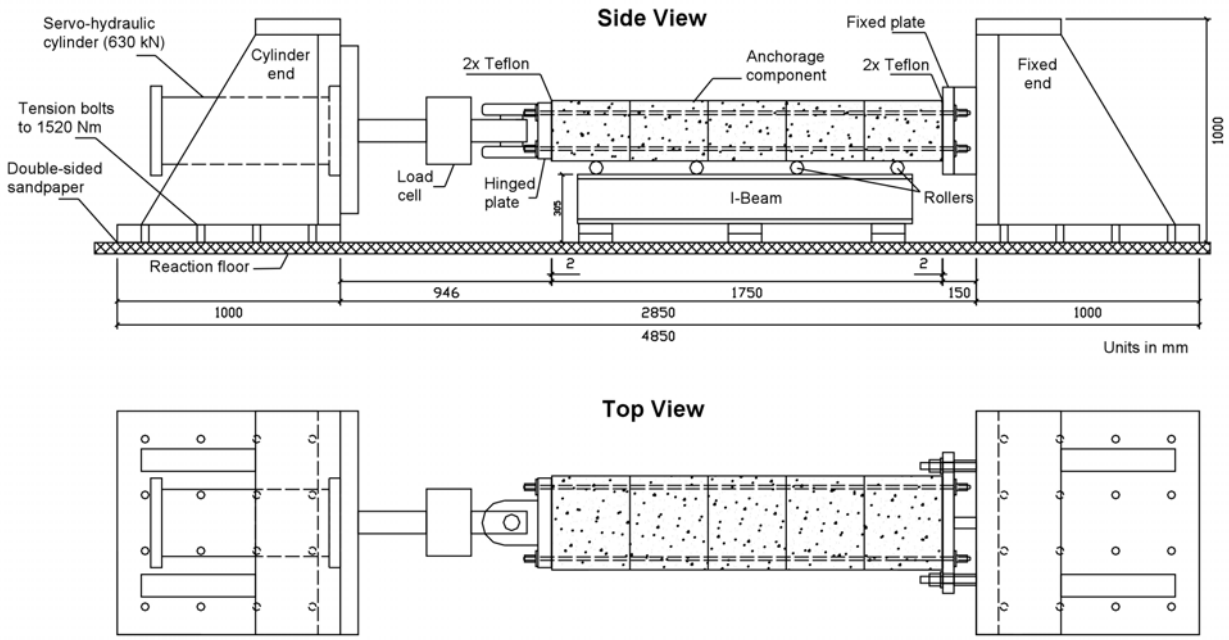

Figure 5.4 Loading configuration for seismic crack member (schematic)

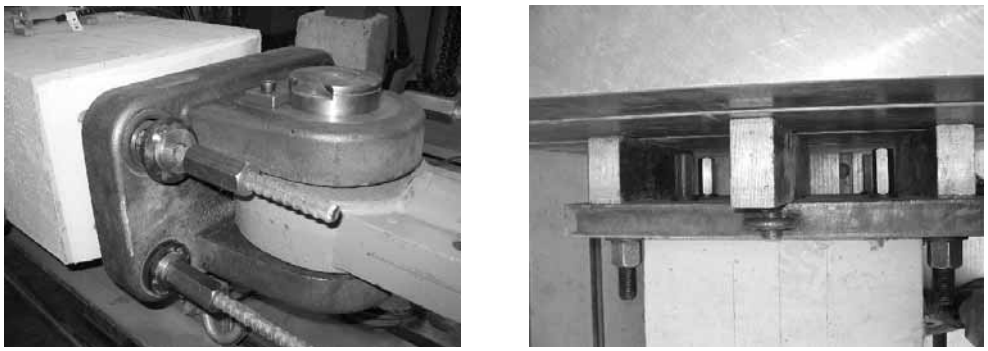

(a) ***(b)***

Figure 5.5 Details of loading configuration for seismic crack member: (a) hinged plate; (b) fixed plate

Fasteners were typically installed in all four cracks in the member and loaded simultaneously with a constant tension load N_w during crack cycling. The loading setup is shown in Figure 5.6. All tests were performed with large anchor spacing and edge distances. Furthermore, the load setups allowed for development of a full concrete cone (wide support). Tension loads were applied to the fasteners by four hydraulic cylinders (38 kN capacity) connected to a single oil pump and automatic pressure regulator that could maintain a constant oil pressure over the duration of the crack cycling.

Pullout tests to determine the residual strengths of the fasteners after crack cycling were performed sequentially along the member with a setup similar to that in Figure 5.3.

The load applied to the anchorage component F_m, the displacement of the servo-hydraulic cylinder attached to the anchorage component δ_{cyl}, the crack widths Δw, the tension loads applied to the fasteners N and the fastener displacements δ were measured continually during the tests.

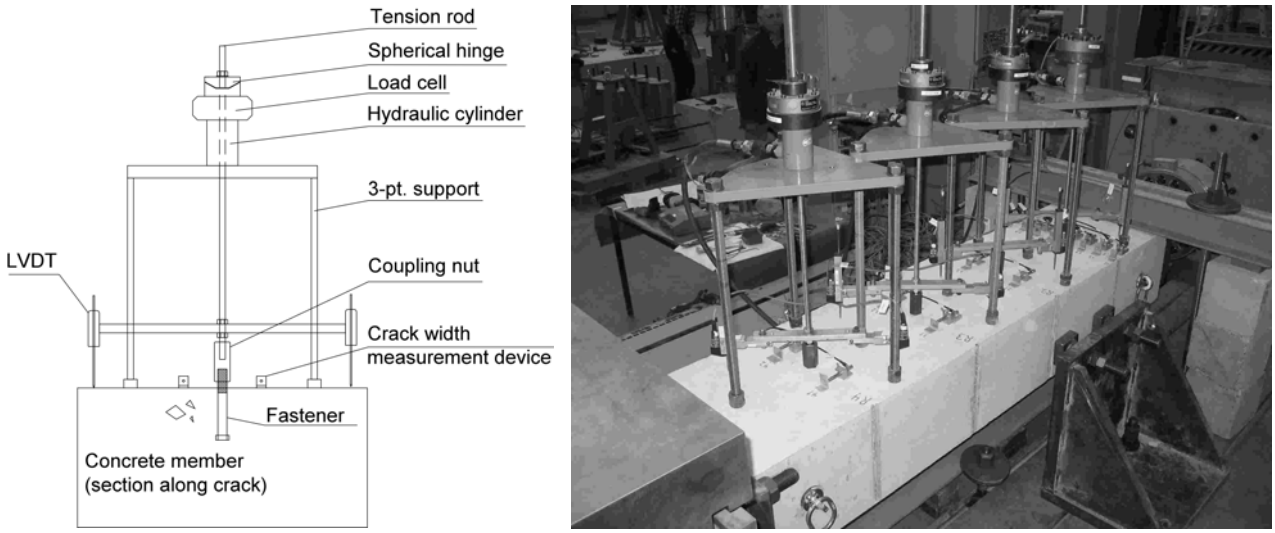

Figure 5.6 Fastener loading setup for seismic crack cycling tests: (a) schematic; (b) photograph

In the following sections, $F_{m,1}$ designates the member load required to attain the desired crack opening width w_1. $F_{m,2}$ is the member load required to attain the desired crack closing width w_2 or the desired compression load level F_2. The variable Δw is used to designate the measured crack opening width beyond the initial hairline crack width.

The seismic crack cycling tests consisted of three phases:

- Phase I: Generate hairline cracks and perform several (approximately 10) opening and closing cycles (without fasteners) to stabilize the crack widths.
- Phase II: Install the fasteners in the closed hairline cracks, open the cracks, apply tension load to the fasteners and then perform crack cycling with a constant tension load on the fasteners.
- Phase III: Perform pullout tests in open cracks subsequent to crack cycling to determine the residual strengths of the fasteners.

Each phase marked a change in the loading and measurement setup.

Loading time-histories for the fasteners and the anchorage component are shown schematically in Figure 5.7. Table 5.2 lists critical events in the time-histories. The load applied to the fasteners N_w, the anchorage component load levels $F_{m,1}$, $F_{m,2}$ and number of crack cycles n varied. The shape and rate of the load cycles on the anchorage component are discussed in Section 5.3.3.4.

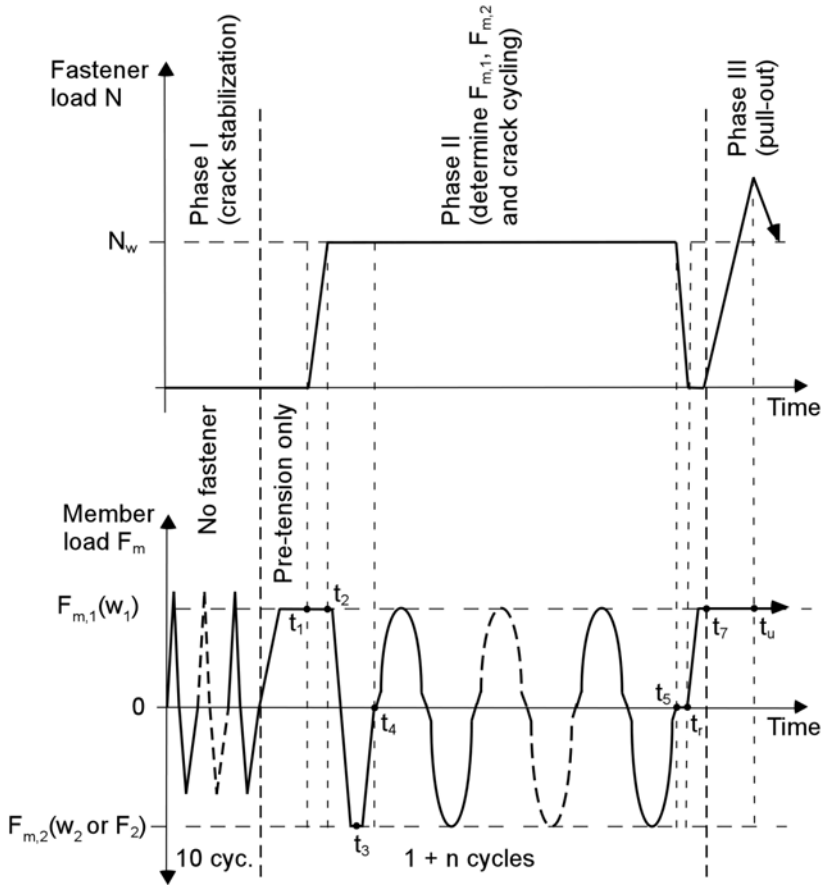

Figure 5.7 Schematic loading time-histories on a fastener and on the anchorage component

Table 5.2 Critical events during the loading time-histories

Time	Critical Event
t_1	Crack opening
t_2	Fastener loading
t_3	1st crack closing
t_4	Start of crack cycling
t_5	End of crack cycling
t_r	Measurement of residuals
t_7	Crack reopening
t_u	Ultimate strength during pullout

At time t_1, the crack was opened to width w_1 with the fastener installed, but unloaded, i.e. fastener pre-tension only. A constant load was then applied to the fastener (t_2) resulting in fastener displacement accompanied by a small additional crack opening. A compression load F_2 was then applied to the anchorage component with the axial load still applied to the fastener (t_3). The anchorage component was then unloaded and the crack cycling was conducted between times t_4 and t_5. After crack cycling the component and the fastener were unloaded and the residual displacements and crack widths were recorded (t_r). Finally, the crack was reopened (t_7) and the fastener was tested to failure in tension (t_u).

5.3 Results and discussion

The results reported for the seismic crack cycling tests presented in this chapter differ significantly in two ways compared to existing crack movement tests (refer to Chapter 3; Section 3.4). These differences are first discussed in Section 5.3.1. Furthermore, new insights into the behavior of cracks in fastener test members were derived from the tests. These insights are presented in Section 5.3.2 and subsequently used in the discussion of fastener behavior in Section 5.3.3.

5.3.1 Reporting results

5.3.1.1 Fastener displacements reported during cycling

Existing crack cycling qualification tests for fasteners in *ACI 355.2 (2004)* and *ETAG 001 (1997)* do not explicitly state at which state of crack opening/closing fastener displacements should be evaluated. In the present investigations, fastener displacements are reported at the point of maximum crack opening (*dw1* in Figure 5.8 and Figure 5.9). This displacement is reported instead of the displacement after completion of the cycle (*d* in Figure 5.8 and Figure 5.9) since it represents the maximum fastener displacement during the cycle and is consistent for all member loading histories. Comparing Figure 5.8 with Figure 5.9 shows that although the displacement after completion of a crack cycle, which was in both cases reported at F_m = 0 kN, always lies between the displacement at maximum crack opening and closing, its position between the boundary curves (*dw1*, *dw2*) varies. This variation depends on the symmetry of the member loading history around the zero load point.

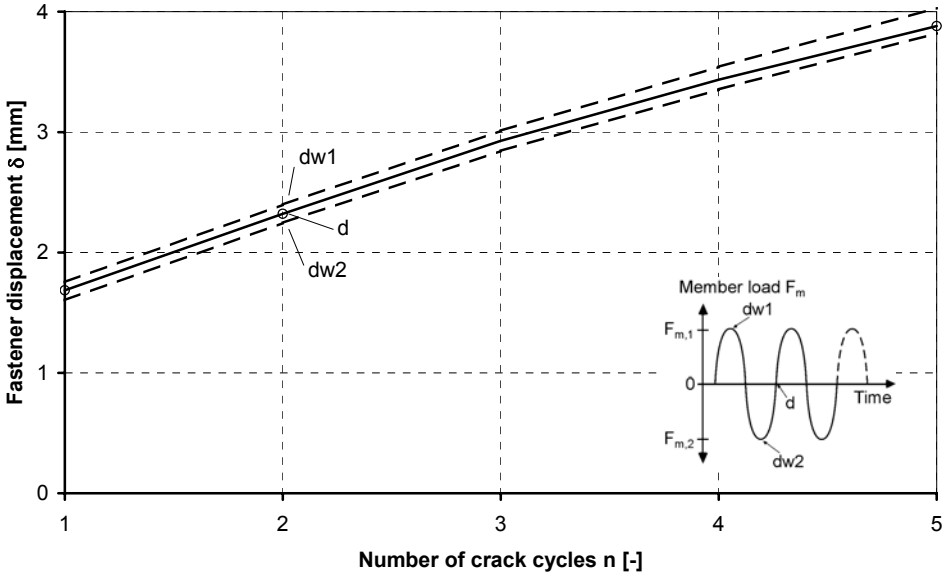

Figure 5.8 Fastener displacement vs. number of crack cycles for a headed stud: nearly symmetric member loading ($N_w = 0.4 \cdot N_{u,m}$, $F_{m,1}$ = 415 kN; $F_{m,2}$ = -500 kN)

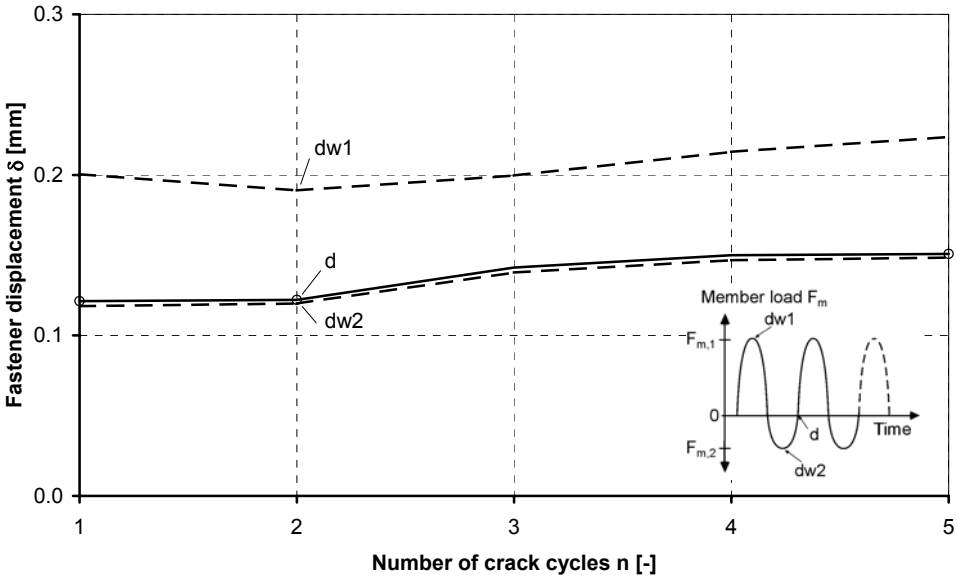

Figure 5.9 Fastener displacement vs. number of crack cycles for a headed stud: asymmetric member loading ($N_w = 0.16 \cdot N_{u,m}$, $F_{m,1} = 550$ kN, $F_{m,2} = -350$ kN)

5.3.1.2 Plotting results as a function of the number of crack cycles

Test procedures for fasteners in cycled cracks in *ACI 355.2 (2004)* and *ETAG 001 (1997)* were developed to represent crack cycling under service conditions. Thus, the fastener is subjected to a large number (1000 cycles) of relatively small amplitude ($w_1 = 0.3$ mm; $w_2 = 0.1$ mm) crack cycles. Fasteners suitable for use under such conditions exhibit stabilization of the fastener displacement with an increasing number of crack cycles. Stabilization typically occurs after about 20 crack cycles. Suitable fastener performance can be verified by showing that after stabilization, displacements increase linearly or degressively as a function of the logarithm of the number of crack cycles (*Lotze and Faoro 1988*). Fasteners that are not suitable, e.g. which exhibit a significant loss of load-bearing capacity, will exhibit progressively increasing displacements and/or failure during crack cycling.

In the present investigations, fasteners were subjected to a small number of crack cycles (10 cycles) of relatively large amplitude ($w_1 = 0.8$ mm; $w_2 = 0.0$ mm). Under these conditions, even suitable fasteners exhibit a progressive increase in displacement when plotted as a function of the logarithm of the number of crack cycles. This is illustrated using the example of headed studs subjected to various bearing pressures ($p = 1.0 \cdot f_{cc,150}$, $2.5 \cdot f_{cc,150}$ and $4.0 \cdot f_{cc,150}$) during crack cycling. Each curve in this example represents the average of three or more test replicates. In Figure 5.10, the fasteners with a bearing pressure of $4.0 \cdot f_{cc,150}$ and $2.5 \cdot f_{cc,150}$ clearly exhibit progressively increasing displacements when plotted as a function of the logarithm of the number of crack cycles. Although it is difficult to see due to the scaling of the figure, even the fasteners with a bearing pressure of $1.0 \cdot f_{cc,150}$ exhibit a progressive increase in displacement. When plotted as a direct function of the number of crack cycles, however, one can see that only the fasteners with a bearing pressure of $4.0 \cdot f_{cc,150}$ exhibit a progressive increase in displacement (Figure 5.11). Pullout tests performed on the fasteners subsequent to the crack cycling showed that the residual strengths of the fasteners with a bearing pressure of $1.0 \cdot f_{cc,150}$ and $2.5 \cdot f_{cc,150}$ during crack cycling was roughly equal to that of reference

tests without prior crack cycling. This is a requirement for suitable performance. The residual strength of the fastener with bearing pressure of $4.0 \cdot f_{cc,150}$ was, however, significantly reduced. Similar results were obtained for the other anchor types and failure modes investigated (see Section 5.3.3.2).

Therefore, in the following sections fastener displacements are plotted as a direct function of the number of crack cycles, as opposed to the logarithm of the number of crack cycles.

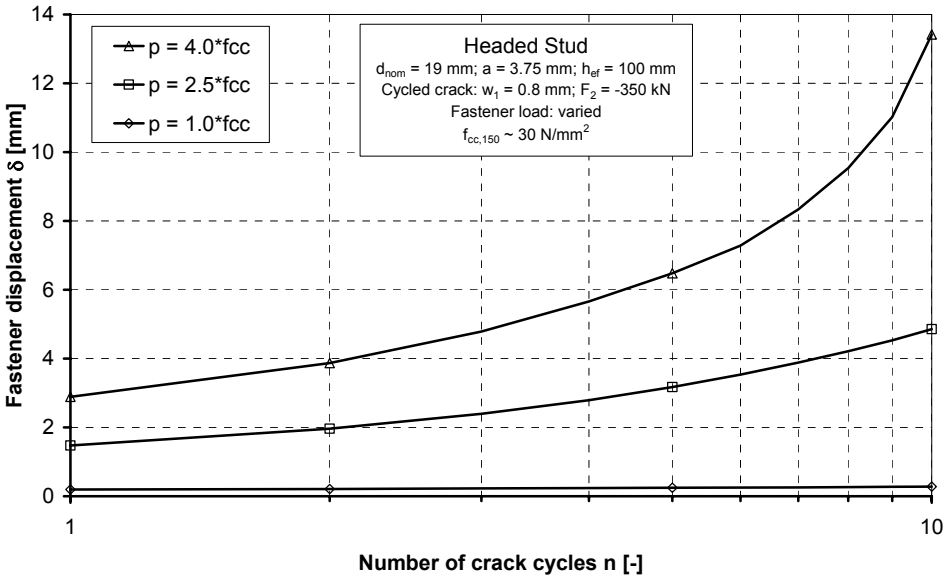

Figure 5.10 Fastener displacement as a function of the number of crack cycles (linear-log scale)

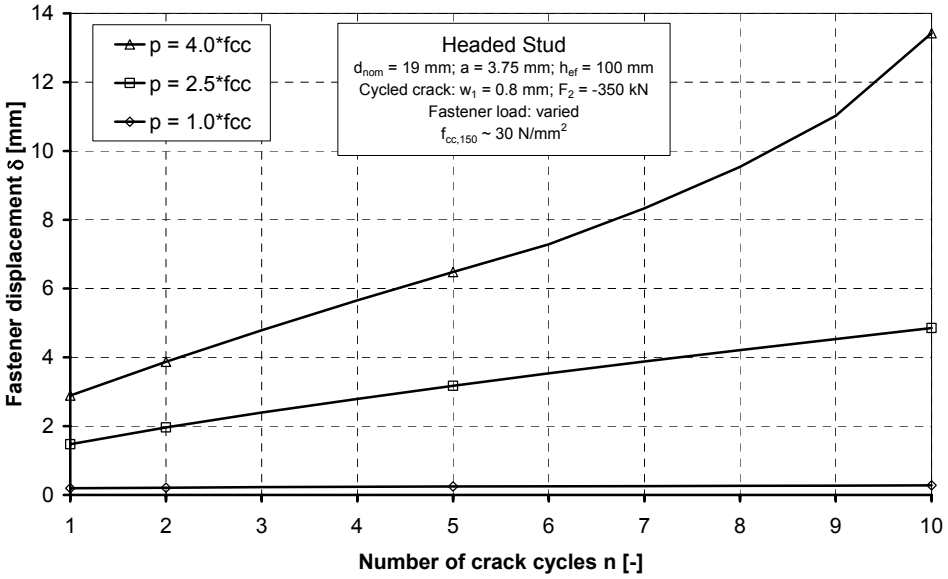

Figure 5.11 Fastener displacement as a function of the number of crack cycles (linear-linear scale)

5.3.2 Crack width measurements

Crack behavior in the seismic crack members was investigated to establish:

(1) the spatial variation of the crack width across the anchorage component and from top to bottom to determine the influence of the measurement location on the reported crack width;
(2) the development of the crack as cycling progressed.

For one test with each investigated fastener type, ten inductive displacement measurement devices (IDTs) were attached across the crack as shown in Figure 5.12 to determine the crack profile.

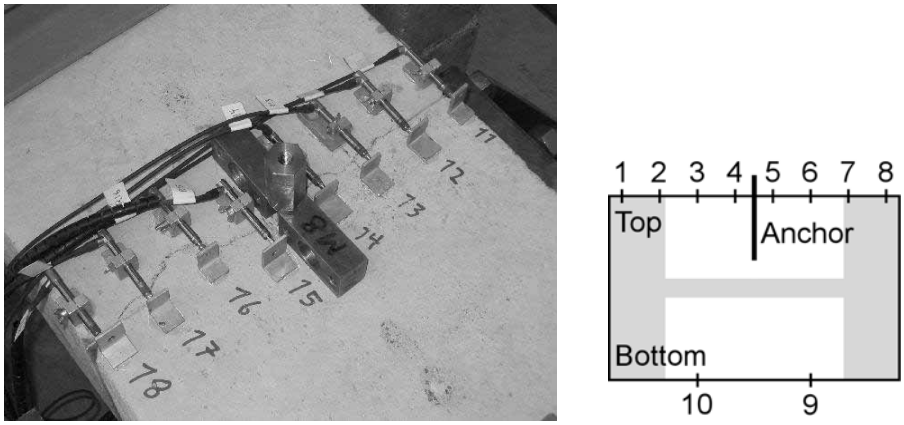

Figure 5.12 Crack width profile setup: (a) photograph; (b) measurement locations

Typical results obtained using the crack profile measurement setup are illustrated using the investigated undercut anchor. The loading time-histories for the fastener and the anchorage component were as shown in Figure 5.7 with $N_w = 0.4 \cdot N_{u,m}$, $w_1 = 0.8$ mm, $F_2 = -350$ kN ($w_2 \sim 0$ mm) and $n = 10$. At time t_1, the crack was opened to the initial width (Δw = 0.91 mm; average of measurement locations 3 and 6 only) with the installed fastener in place, i.e. fastener pre-tension only. A constant load ($N_w = 0.4 \cdot N_{u,m}$) was then applied to the fastener resulting in an additional crack opening of about $\Delta w = 0.03$ mm at t_2. A compression load of $F_m = -350$ kN was then applied to the anchorage component (t_3) with the axial load still applied to the fastener. The affect of these actions on the crack widths measured along the top and bottom surface of the component are shown in Figure 5.13 and Figure 5.14, respectively.

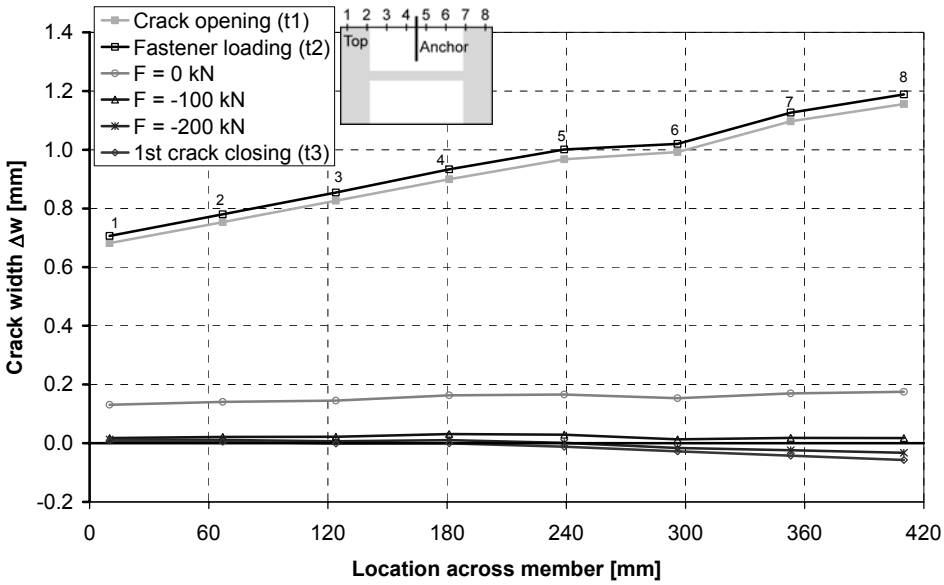

Figure 5.13 Crack width profiles for undercut anchor M10 (top; initial cycle)

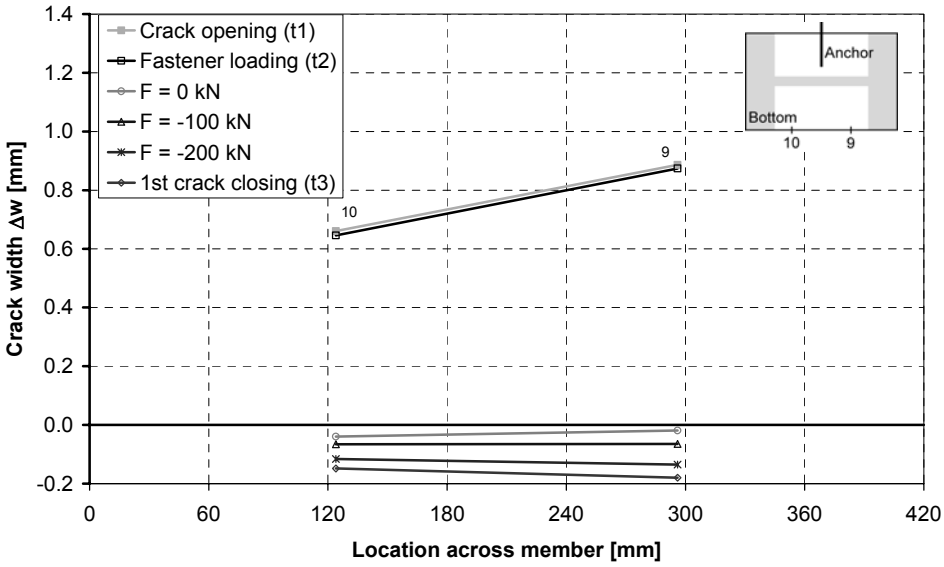

Figure 5.14 Crack width profiles for undercut anchor M10 (bottom; initial cycle)

Figure 5.13 shows that at crack opening (t_1) the crack width across the member varies significantly (Δw ~ 0.7 mm to 1.2 mm; left to right). This variation is approximately linear. Upon applying the tension load to the fastener, the crack width on the top surface increases uniformly across the anchorage component. Simultaneously, the crack width along the bottom of the component decreases slightly. This can be explained by the horizontal component of the forces and bending moment generated by the loaded fastener (Figure 5.15).

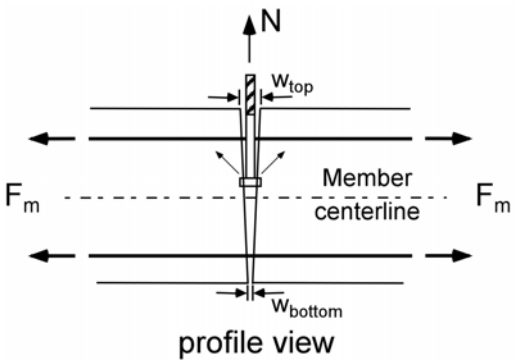

Figure 5.15 Mechanism for crack width decrease from top to bottom of the anchorage component

The anchorage component was then unloaded and loaded in compression. At F_m = 0 kN the crack along the top surface (Figure 5.13) is still open (Δw = 0.15 mm), however, the width is approximately constant across the member. The crack along the top surface completely closed at a compression load of around F_m = -100 kN. The negative crack widths obtained with continued compressive loading were possible because the crack width measurement devices were installed and zeroed across an open hairline crack. After the initial crack cycle, the anchorage component was unloaded and crack cycling commenced.

The crack profiles measured along the top surface of the anchorage component during cycle 10 are shown in Figure 5.16. The crack opening profile (w = 0.8 mm) increased relative to the initial cycle and still varied significantly across the member. The presence of the fastener in the middle of the anchorage component can now be seen in that crack widths bulge around this location (210 mm), particularly during compression. This bulge extends about 70 mm to either side of the fastener. Although during the initial cycle the crack was completely closed at the top surface for a compression load of around F_m = -100 kN (see Figure 5.13), after 10 cycles, the full compression load of F_m = -350 kN was required to close the crack.

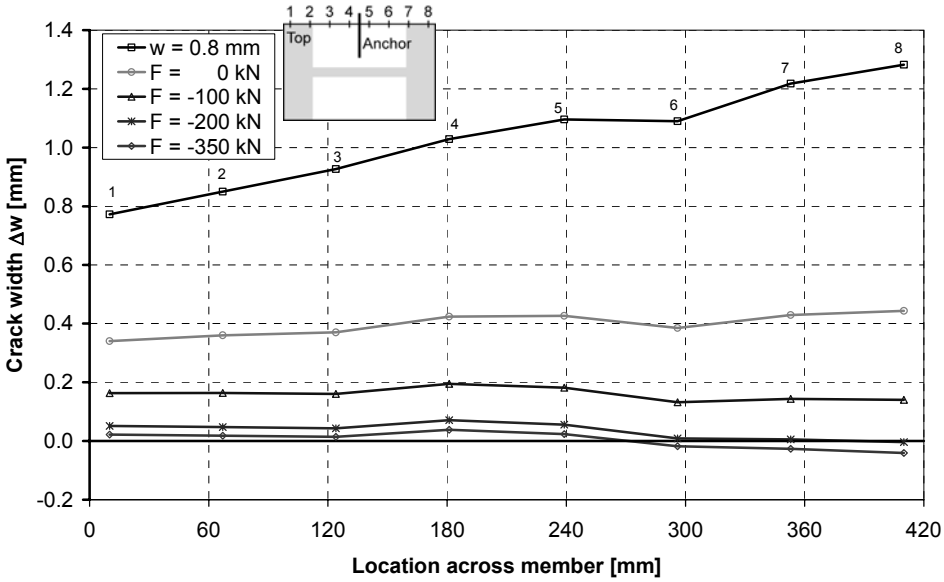

Figure 5.16 Crack width profiles for undercut anchor M10 (top; cycle 10)

By replotting the crack width data, one can observe the variation of the crack width from top to bottom of the anchorage component as crack cycling proceeded (Figure 5.17 and Figure 5.18). For the case of the undercut anchor, the crack widths measured at the top surface of the anchorage component were greater than those measured at the bottom surface. The point of load transfer for the fastener lies in a crack width somewhere in between that measured at the top surface and the bottom surface of the anchorage component. As crack cycling proceeds, the difference in the crack width measured at the top and bottom surface of the anchorage component increases (compare Figure 5.17 and Figure 5.18).

A compilation of the crack width profiles measured along the top surface of the anchorage component for the initial and 10th crack cycle is provided for all of the investigated fastener types in Figure 5.19. A compilation of the crack width profiles measured along the top and bottom surfaces of the anchorage component at maximum crack opening and maximum crack closing for the initial and 10th crack cycle is provided for all of the investigated fastener types in Figure 5.20.

The crack opening widths across the anchorage components shown in Figure 5.19 increase from left to right in some cases and from right to left in others. Furthermore, the relative top and bottom crack widths for the initial cycle in Figure 5.20 appear to vary unpredictably. It is concluded that the variation of the crack width from top to bottom of the anchorage component, as well as across the component, is primarily a result of unequal stress levels in the longitudinal reinforcing bars stemming from the test setup. In all of the tests, however, the crack width at the top surface of the anchorage component increases relative to the crack width at the bottom surface as crack cycling proceeds. This can be explained by the wedging action of the loaded fastener located above the centerline of the axially loaded anchorage components (refer to Figure 5.15).

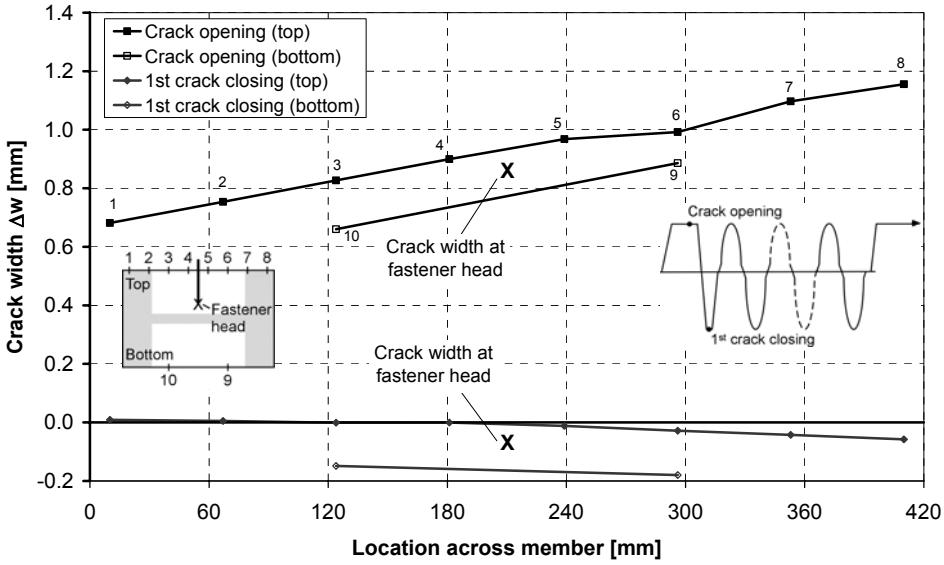

Figure 5.17 Crack width profiles for undercut anchor M10 (top & bottom; initial cycle)

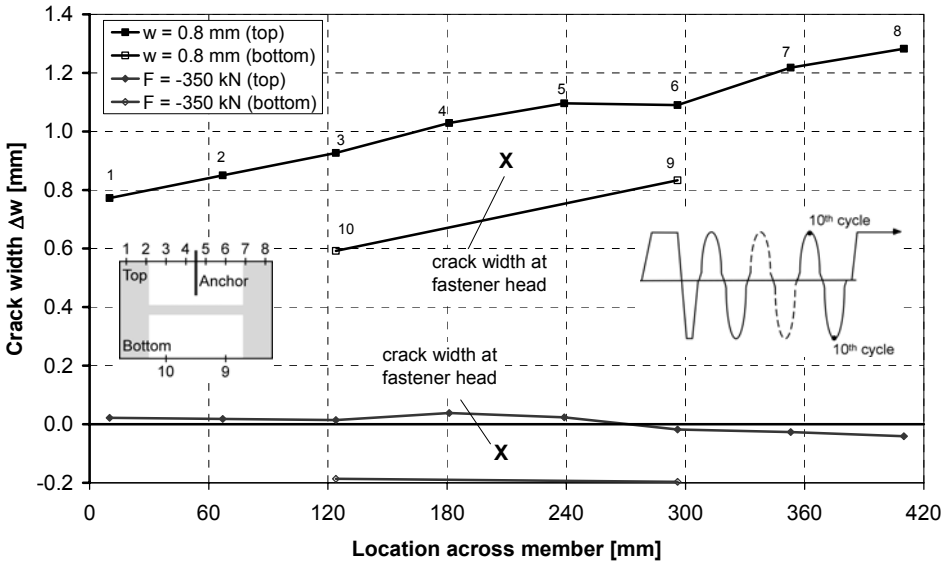

Figure 5.18 Crack width profiles for undercut anchor M10 (top & bottom; cycle 10)

Figure 5.20 shows that a compressive force on the anchorage component of F_2 = -350 kN was sufficient for complete crack closure around the fasteners in all cases under the investigated conditions. This relates to a compressive stress of about $0.10 \cdot f_{cc,150}$ over the gross cross-section area A_{gross} of the anchorage component.

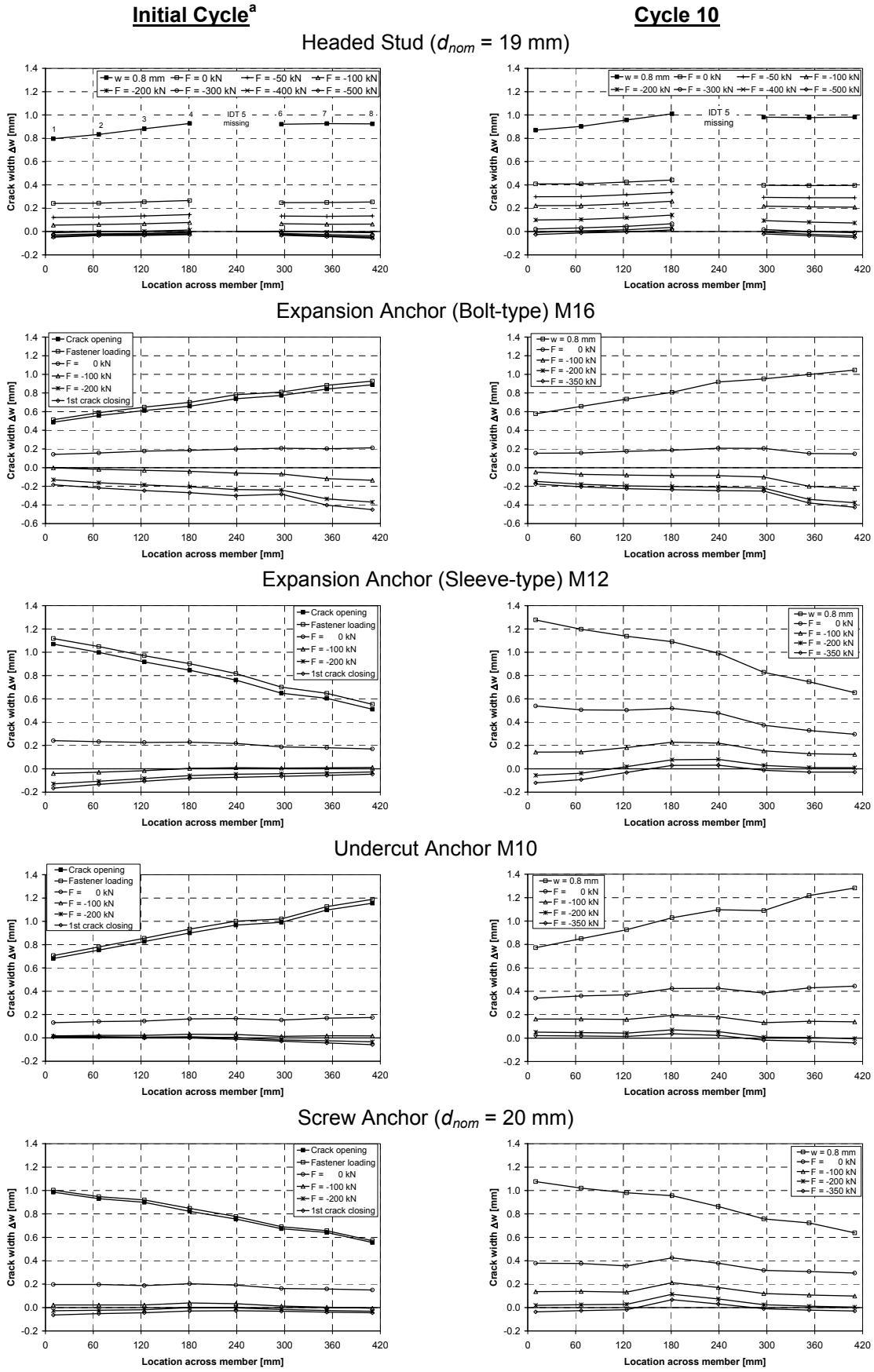

[a] For the headed stud, cycle 1 is shown because a slightly different loading procedure was used.

Figure 5.19 Crack width profiles along the top surface of the member at various stages of loading plotted for all investigated fastener types

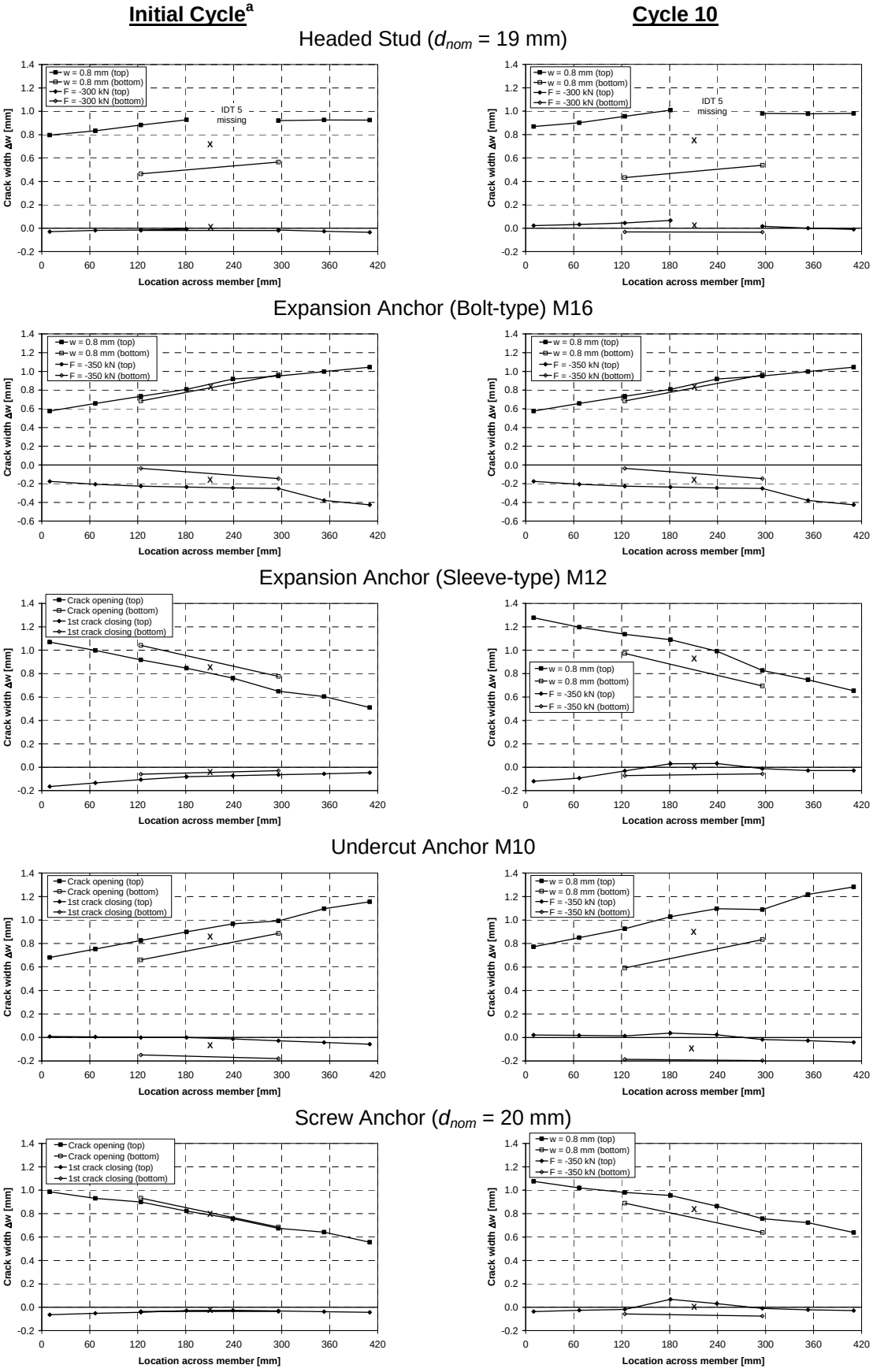

[a] For the headed stud, cycle 1 is shown because a slightly different loading procedure was used.

Figure 5.20 Crack width profiles along the top and bottom surfaces of the member at various stages of loading plotted for all investigated fastener types

5.3.3 Fastener behavior

The load-bearing and displacement mechanisms of fasteners in opening and closing cracks under service conditions were described by *Lotze and Faoro (1988)*. Their work is presented here with a slight modification for the case of seismic conditions.

Figure 5.21 schematically illustrates the behavior of a fastener in an opening and closing crack by example of an undercut anchor.

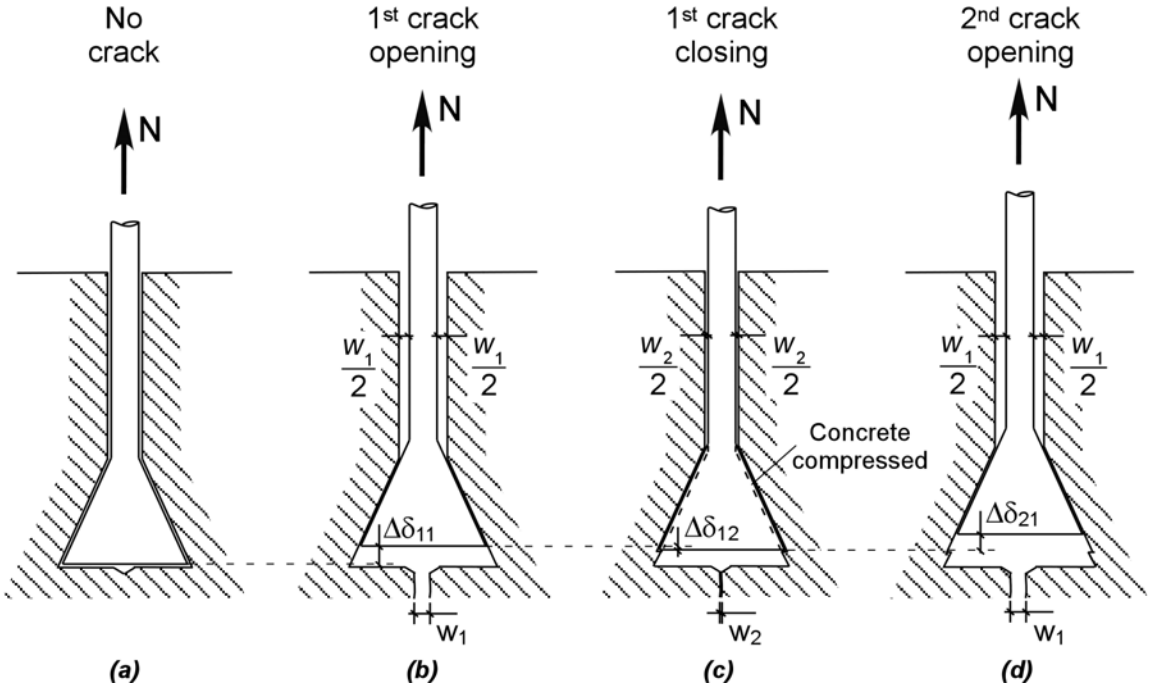

Figure 5.21 Load-bearing and displacement mechanisms for fasteners in opening and closing cracks (after Lotze and Faoro 1988)

Prior to the first crack opening, the fastener bears directly on the surface of the undercut in the concrete (Figure 5.21a). During the first crack opening (Figure 5.21b), the fastener must displace in the direction of the applied load by $\Delta\delta_{11}$ to fulfill equilibrium and compatibility conditions. If the crack is then partially or completely closed, the expansion (undercutting) elements of the fastener will be deformed and pressed into the concrete (Figure 5.21c). For some fastener geometries, if sufficiently large compressive stresses are present, this may result in a small displacement $\Delta\delta_{12}$ opposite to the direction of the applied load. *Lotze and Faoro (1988)* assumed that no displacement opposite to the axial load direction could occur. During the next crack opening, the displacement $\Delta\delta_{12}$ and the elastic portion of the deformation in the expansion elements and the concrete is recovered and the fastener will displace again in the direction of the applied load to reestablish equilibrium (Figure 5.21d). The displacement $\Delta\delta_{21}$ is significantly larger than the displacement $\Delta\delta_{12}$, however, smaller than the displacement during the first crack opening $\Delta\delta_{11}$. This mechanism is valid for the subsequent crack cycles, whereby the amount of increase of the fastener displacement decreases with each cycle.

The load-bearing and displacement mechanisms for torque-controlled expansion anchors in cycled cracks are principally the same as described above. The total

displacement of these fasteners, however, is not caused by sliding of the complete fastener, including the expansion elements, along the wall of the drilled hole, but rather by sliding of the expansion cone inside of the expansion elements. The relative movement of expansion cone and sleeve results in a local increase of the fastener diameter (follow-up expansion) to account for the crack opening. Nevertheless, crack closure results in the deformation of the expansion elements and their compression into the wall of the drilled hole. Therefore, the fastener displacement increases with each subsequent crack cycle.

The failure modes described in Chapter 3 (Figure 3.11) apply to crack cycling.

5.3.3.1 Load-displacement curves

The investigated headed studs, undercut anchors and sleeve-type expansion anchors failed by concrete cone failure in pullout tests performed in an open crack (Δw = 0.8 mm) subsequent to ten large crack opening and closing cycles (w_1 = 0.8 mm; F_2 = -350 kN (w_2 = 0 mm)) with a constant fastener tension load of $N_w = 0.4 \cdot N_{u,m}$. The bolt-type expansion anchors failed by pull-through and the screw anchors failed by pull-out subsequent to the above described crack cycling.

5.3.3.1.1 Concrete cone failure

The current investigations show that the load-displacement behavior of fasteners failing by concrete cone failure in representative seismic crack cycling tests is essentially the same as described by *Furche (1994)* for headed studs under service crack cycling conditions ($N_w = 0.3 \cdot N_{u,m}$, w_1 = 0.3 mm, w_2 = 0.1 mm, n = 1000).

Furche (1994) shows that if the axial fastener displacement during 1000 crack cycles (δ_{1000}) plus the additional displacement up to ultimate load obtained in a subsequent pullout test ($\delta_{u,add}$) is smaller than the displacement at ultimate load in a comparable monotonic test ($\delta_{u,m}$), the ultimate load is not affected by the crack cycling. If the combined fastener displacement ($\delta = \delta_{1000} + \delta_{u,add}$) exceeds $\delta_{u,m}$, the ultimate load decreases as a function of the lost embedment depth (Figure 5.22) according to $C \cdot (h_{ef} - \delta)^{1.5}$. The value C is an empirical constant determined as $C = N_{u,m} / (h_{ef})^{1.5}$, where $N_{u,m}$ is the mean ultimate load of the anchor from reference tests in a static crack and h_{ef} is the initial effective anchorage depth.

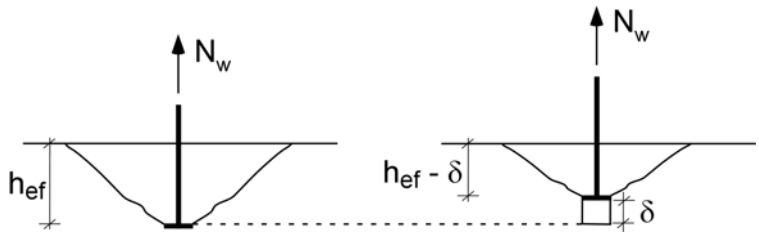

Figure 5.22 Reduction of embedment depth due to fastener head displacement

In *Furche (1994)*, large fastener displacements during crack cycling were achieved by significantly reducing the bearing area of the investigated headed studs. Furche concluded for service crack cycling conditions, that as long as the head bearing area is sufficiently large, the total displacement $\delta_{1000} + \delta_{u,add}$ will be less than the displacement

at ultimate load in monotonic reference tests and design can consequently be performed using equations valid for monotonic loading situations. In crack cycling tests representative of seismic conditions, the large crack cycling widths, high fastener loads and the application of compressive load to the anchorage component to achieve crack closure can result in fastener displacements that exceed those at ultimate load in monotonic reference tests in fewer than ten crack cycles. This is shown for the three fastener types tested that failed by concrete cone failure in Figure 5.23 to Figure 5.25. Because the fastener displacement during crack cycling is a function of the number of crack cycles and the number of cycles was limited to ten, however, the amount of displacement beyond $\delta_{u,m}$ was small and did not reduce the effective anchorage depth enough to result in a significant decrease in the residual strength. In fact, as shown for the case of the headed studs, the residual strength actually increased relative to the ultimate strength in the reference tests. This phenomenon is discussed in Section 5.3.3.3.

The important conclusion that can be drawn is that as long as the effective anchorage depth is not reduced too significantly during crack cycling, the residual strength will be about the same as in monotonic reference tests for the case of concrete failure.

It is noted that the slight increase of the fastener load during crack cycling in Figure 5.23 to Figure 5.25 is a physical phenomenon resulting from closure of the crack. Because the oil volume in the hydraulic cylinders was used to regulate the fastener load, the load increased as the anchor was 'pressed back' into its hole during crack closure (refer to Figure 5.21).

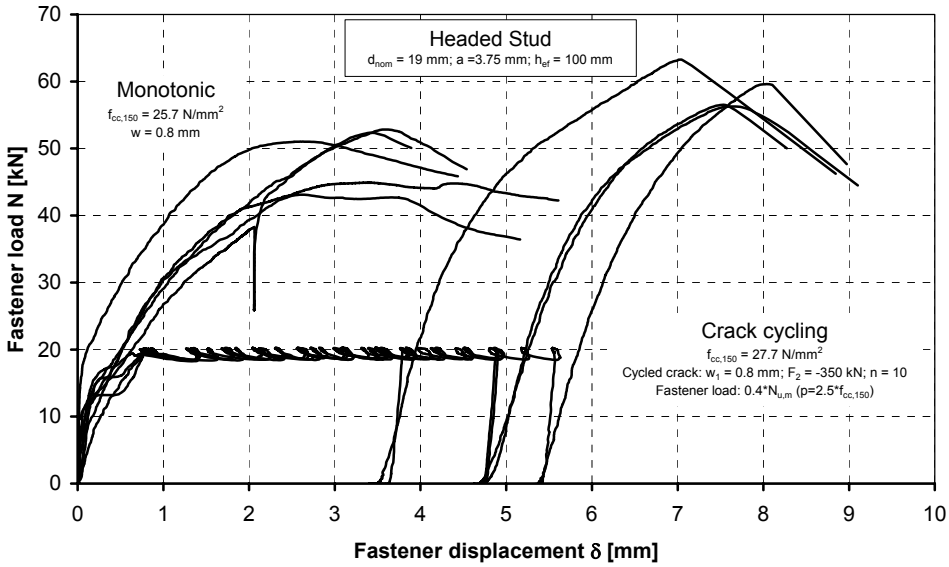

Figure 5.23 Load-displacement curves for monotonic and crack cycling tests with headed studs

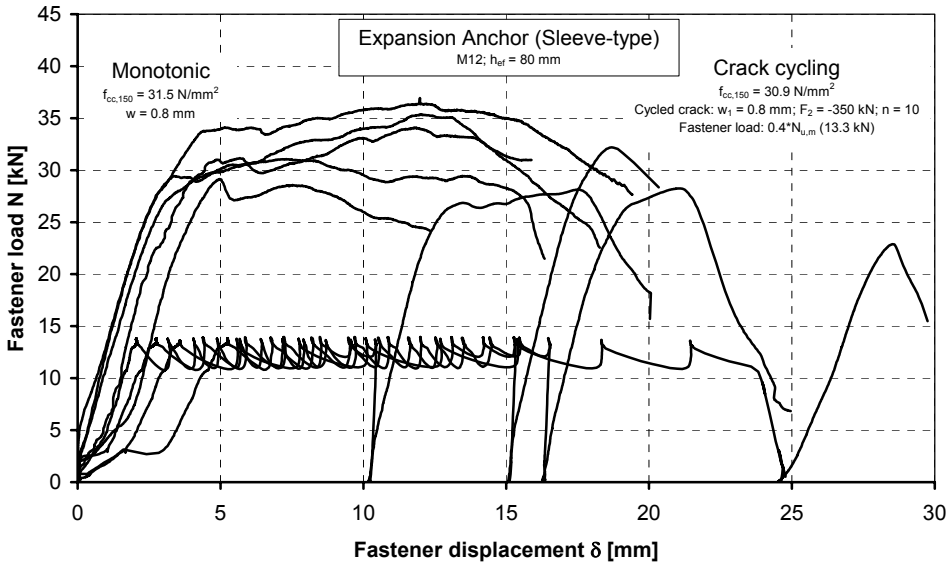

Figure 5.24 Load-displacement curves for monotonic and crack cycling tests with expansion anchors (sleeve-type)

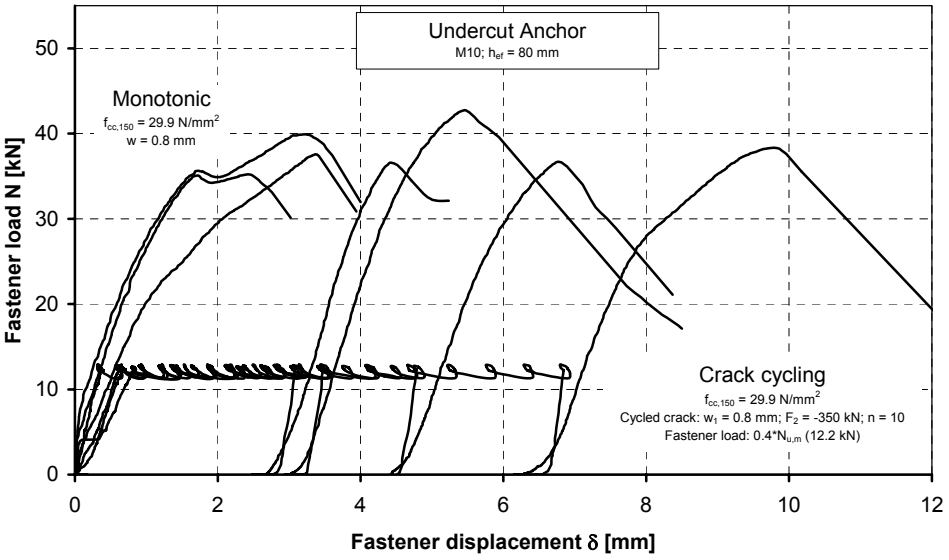

Figure 5.25 Load-displacement curves for monotonic and crack cycling tests with undercut anchors

As illustrated by Figure 5.26, at some point, the reduction of the effective anchorage depth due to crack cycling begins to reduce the residual strength of the fastener; as predicted by *Furche (1994)*. As shown in the figure, however, the head of the tested undercut anchor could theoretically displace over 30 mm before h_{ef} is reduced sufficiently to result in a concrete cone failure at the applied constant load. In practice, however, splitting of the anchorage component may occur before such large displacements are achieved.

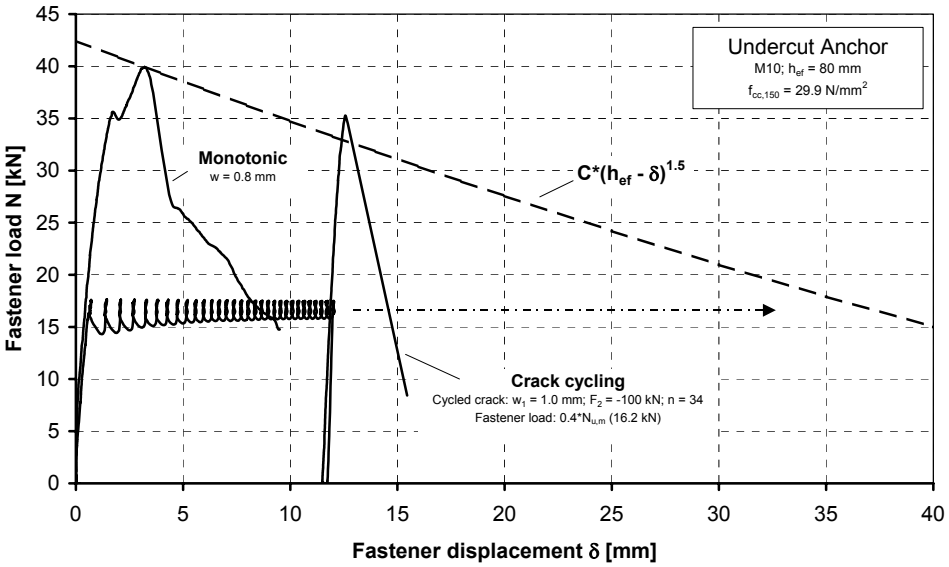

Figure 5.26 Fastener load-displacement behavior in a cycled crack

Four cases can be distinguished based on the amount of displacement that occurs during crack cycling. These are summarized in Table 5.3 and illustrated in Figure 5.27. The fastener displacement that occurs during 10 crack cycles is designated as δ_{10}. The displacement at which the curve $C{\cdot}(h_{ef} - \delta)^{1.5}$ is intersected is designated as $\delta_{f,c}$.

Table 5.3 Displacement conditions during crack cycling and the effect on the total displacement and residual strength in the case of concrete failure

	Condition	Description	Total Displacement	Residual Strength
(1)	$\delta_{10} < \delta_{u,m}$	Displacement during crack cycling is less than that at ultimate load in monotonic reference tests	$\delta_{10} + \delta_{u,add} \le \delta_{u,n}$	$N_{u,c} \ge N_{u,m}$
(2)	$\delta_{u,m} \le \delta_{10} < \delta_{f,c}$	Displacement during crack cycling equals or exceeds that at ultimate load in monotonic reference tests but does not reduce the effective anchorage depth enough to result in concrete cone failure at the applied constant tension load	$\delta_{10} + \delta_{u,add} > \delta_{u,n}$	$N_{u,c} < N_{u,m}$
(3)	$\delta_{10} = \delta_{f,c}$	Displacement during crack cycling reduces the effective anchorage depth enough to result in concrete cone failure at the applied constant tension load	$\delta_{f,c}$	Not applicable
(4)	Splitting	Splitting failure occurs during crack cycling	Unknown	Not applicable

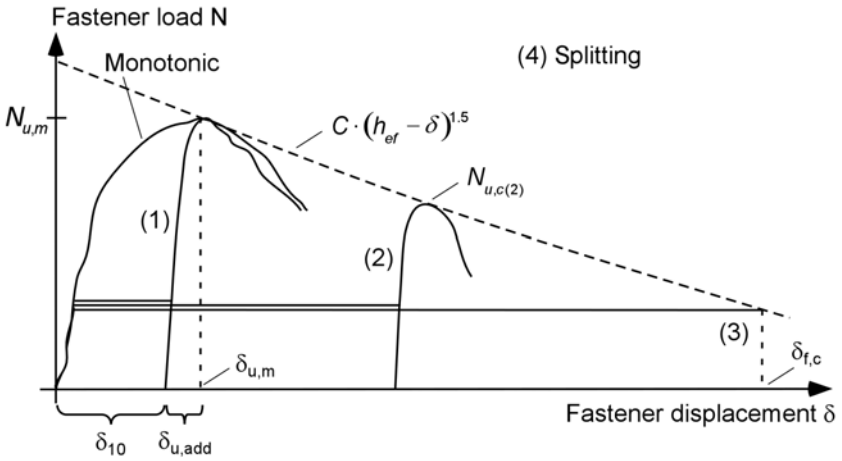

Figure 5.27 Schematic load-displacement curves for crack cycling tests in the case of concrete failure: (1) $\delta_{10} < \delta_{u,m}$; (2) $\delta_{u,m} \leq \delta_{10} < \delta_{f,c}$; (3) $\delta_{10} = \delta_{f,c}$

5.3.3.1.2 Pull-through failure

Unlike the case of concrete cone failure, where the anchor head displaces relative to the wall of the drilled hole during crack cycling, if the friction between the expansion cone and the expansion elements is lower than that between the expansion sleeve and the wall of the drilled hole, the expansion elements will remain fixed while the expansion cone displaces relative to the expansion sleeve. The behavior of a bolt-type expansion anchor failing by pull-through subsequent to repeated large crack opening and closing cycles is shown in Figure 5.28 and Figure 5.29. In the case of pull-through failure where the expansion elements do not slip in the drilled hole, the load-displacement curve is bounded by the descending branch of the monotonic load-displacement curve.

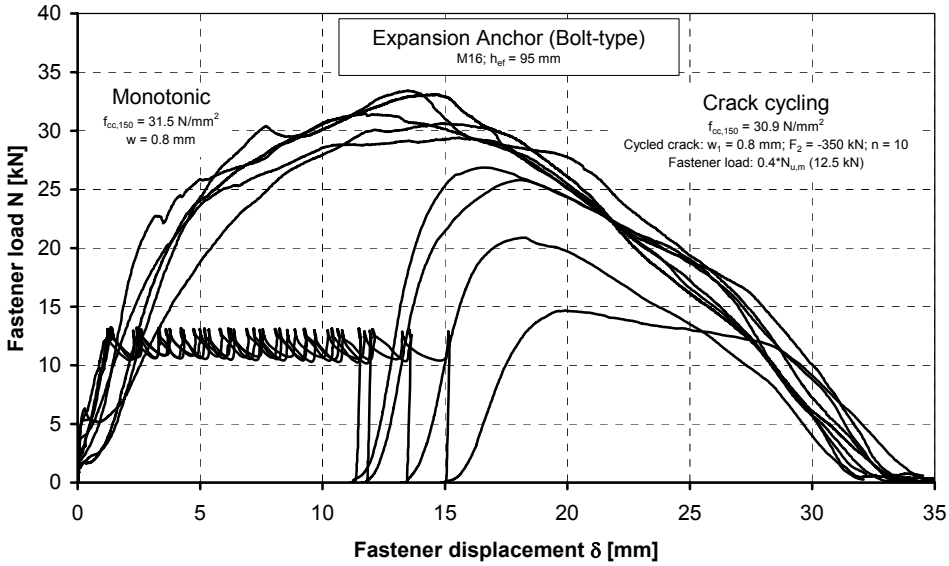

Figure 5.28 Load-displacement curves for monotonic and crack cycling tests in the case of pull-through ($\delta_{10} \approx \delta_{u,m}$)

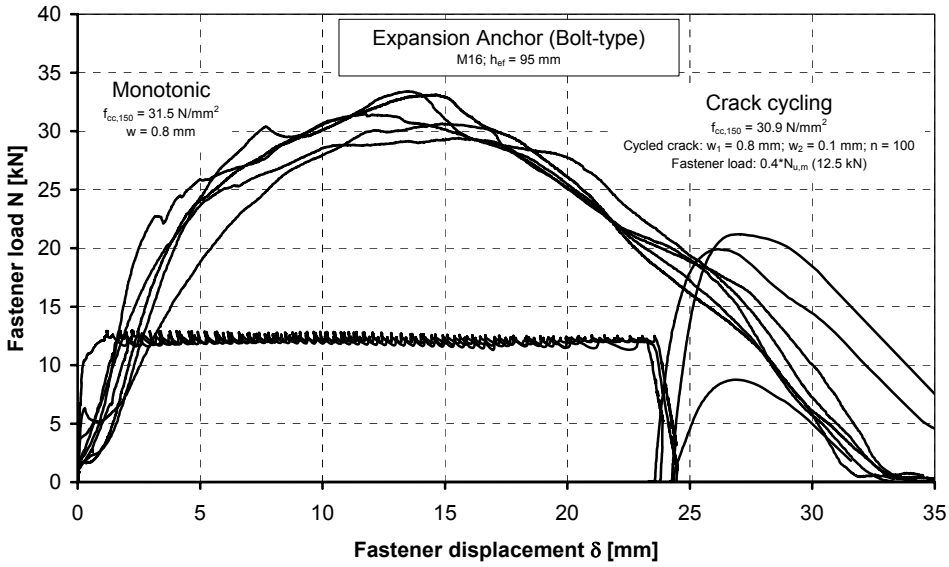

Figure 5.29 Load-displacement curves for monotonic and crack cycling tests in the case of pull-through ($\delta_{10} > \delta_{u,m}$)

Three cases can be distinguished based on the amount of displacement that occurs during crack cycling. These are summarized in Table 5.4 and illustrated in Figure 5.30. Splitting of the concrete was not observed for the investigated fasteners failing by pull-through. The displacement at which the descending branch of the monotonic curve is intersected is designated as $\delta_{f,pt}$.

Table 5.4 Displacement conditions during crack cycling and the effect on the total displacement and residual strength in the case of pull-through failure

	Condition	Description	Total Displacement	Residual Strength
(1)	$\delta_{10} < \delta_{u,m}$	Displacement during crack cycling is less than that at ultimate load in monotonic reference tests	$\delta_{10} + \delta_{u,add} \leq \delta_{u,m}$	$N_{u,pt} \geq N_{u,m}$
(2)	$\delta_{u,m} \leq \delta_{10} < \delta_{f,pt}$	Displacement during crack cycling equals or exceeds that at ultimate load in monotonic reference tests but is less than the displacement at the intersection of the applied constant fastener load with the monotonic envelope	$\delta_{10} + \delta_{u,add} > \delta_{u,m}$	$N_{u,pt} < N_{u,m}$
(3)	$\delta_{10} = \delta_{f,pt}$	Displacement during crack cycling reaches the displacement at the intersection of the applied constant fastener load with the monotonic envelope	$\delta_{f,pt}$	Not applicable

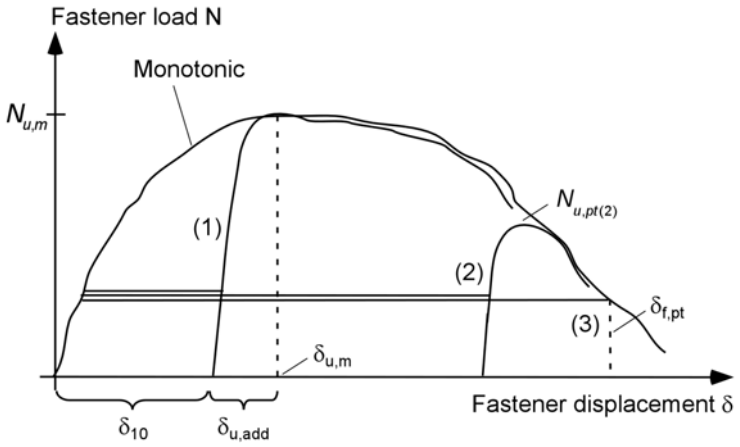

Figure 5.30 Schematic load-displacement curves for crack cycling tests in the case of pull-through: (1) $\delta_{10} < \delta_{u,m}$; (2) $\delta_{u,m} \leq \delta_{10} < \delta_{f,pt}$; (3) $\delta_{10} = \delta_{f,pt}$

5.3.3.1.3 Pull-out failure (screw anchor)

The investigated screw anchor (d_{nom} = 20 mm) failed in mixed pull-out and concrete cone failure in monotonic tests in cracked concrete (Δw = 0.8 mm), i.e. the lower portion of the screw pulled out and a concrete cone formed near the surface of the concrete. In pullout tests performed after the crack cycling, pure pull-out failure occurred. Figure 5.31 compares the monotonic and crack cycling load-displacement behavior. Had the fasteners failed in pure pull-out failure in both the monotonic and crack cycling tests, the load-displacement behavior would be expected to be similar to that described for pull-through failure (Section 5.3.3.1.2), i.e. the load-displacement curve for the crack cycling test is bound by the descending branch of the monotonic load-displacement curve. Figure 5.31 shows the characteristically large scatter for fasteners failing by pull-out. Nevertheless, the average residual strengths after crack cycling are approximately the same as in the monotonic reference tests.

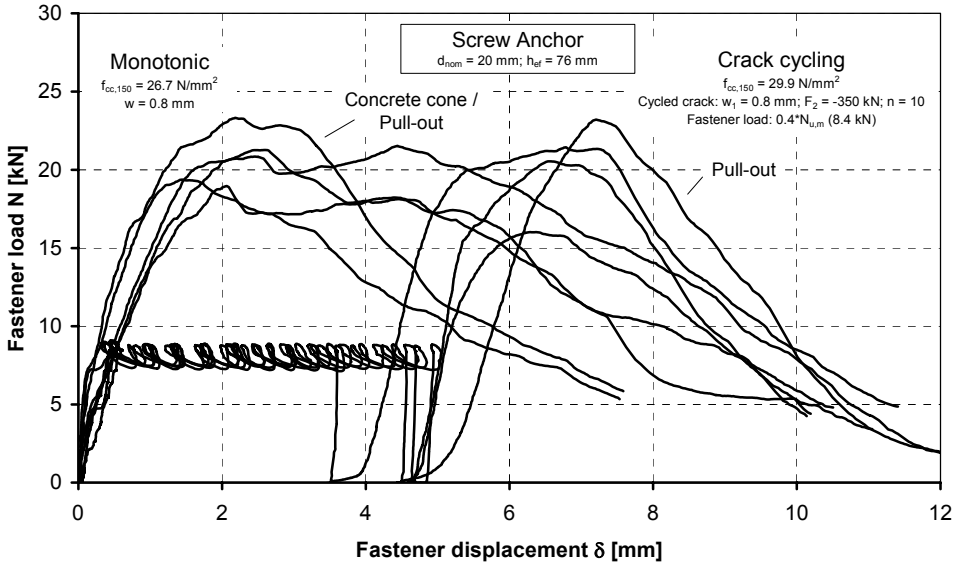

Figure 5.31 Load-displacement curves for monotonic and crack cycling tests in the case of pull-out of screw anchors

The large displacements during crack cycling in Figure 5.31 were made possible by the large thread spacing (~15 mm) of the investigated screw anchors. For screw anchors, the maximum displacement that can occur before pull-out is less than the thread spacing.

5.3.3.2 Fastener displacement

The displacement behavior of the investigated fasteners during crack cycling representative of seismic conditions (w_1 = 0.8 mm; w_2 = 0.0 mm; n = 10) is shown in Figure 5.32. The curves show the total displacement of the fastener recorded at each crack opening cycle. Each curve represents the average of three or more test replicates. In all cases the fasteners were subjected to the same testing conditions. Furthermore, failure did not occur during crack cycling, but rather during a subsequent pull-out test (refer to Figure 5.23). The amount of fastener displacement during crack cycling is a function of several factors. The most important factors are the type of anchor and failure mode, the crack opening and closing widths (w_1, w_2), the number of crack cycles (n) and the applied fastener tension load, i.e. the bearing pressure.

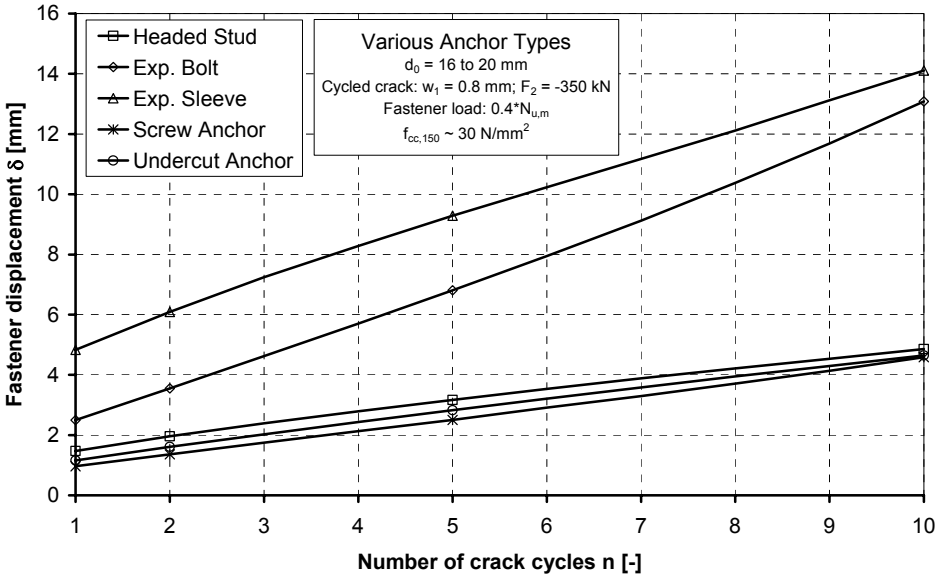

Figure 5.32 Fastener displacement as a function of the number of crack cycles for various fastener types

The following conclusions can be drawn from Figure 5.32:

- For all of the tested fasteners the displacement increase as a function of the number of crack cycles was degressive or nearly linear. A slight progressive increase in displacement was present for the screw anchors and bolt-type expansion anchors.
- The headed stud (concrete cone failure), screw anchor (pull-out failure) and undercut anchor (concrete cone failure) underwent relatively little displacement compared to the bolt-type expansion anchor (pull-through failure) and the sleeve-type expansion anchor (concrete cone failure).

By plotting the displacement in a given cycle relative to the displacement in the first cycle ($\delta_{cyc,1}$) one can observe that the fasteners failing by concrete cone failure (headed studs, sleeve-type expansion anchors, undercut anchors) exhibited a lower relative displacement increase compared to the fasteners failing by pull-out (screw anchors) or pull-through (bolt-type expansion anchors) (Figure 5.33).

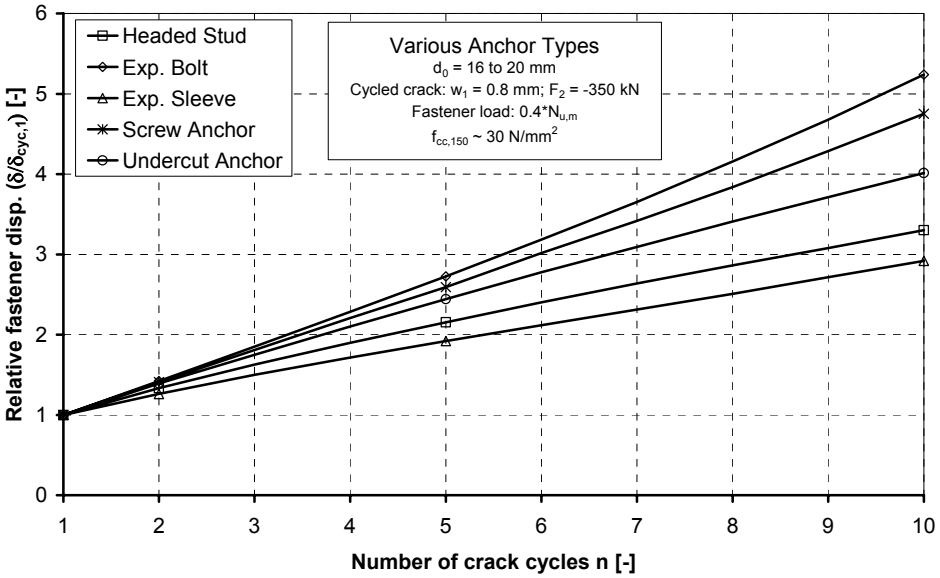

Figure 5.33 Relative fastener displacement plotted as a function of the number of crack cycles for various fastener types

Degressively or linearly increasing displacements plotted as a function of the number of crack cycles (linear-linear scale) appears to be an indicator of acceptable fastener performance (Figure 5.34). This is substantiated by the residual strengths discussed in the following section.

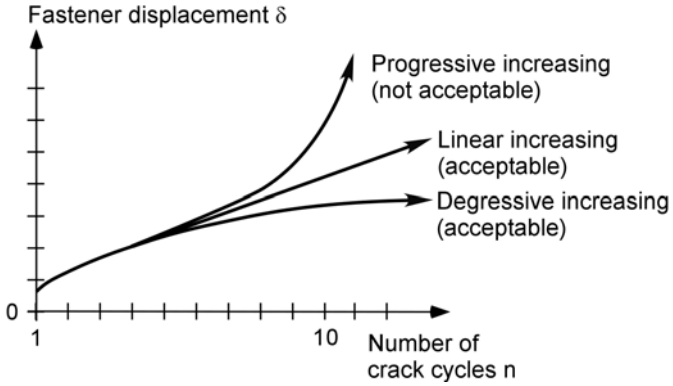

Figure 5.34 Schematic fastener displacement curves for tests with a small number of crack cycles (<100) of relatively large amplitude (w_1-w_2 ≥ 0.5 mm)

Since in many cases it is difficult to determine whether anchor displacement increases linearly or progressively using graphical methods, for seismic prequalification of anchors it might be more suitable to establish absolute allowable displacement limits or limits on the relative anchor displacement. Additionally, the absolute displacement of anchors is important to determine the distribution of loads in an anchor group and can be limited by

the strength and stiffness of the attached system. The problem with prescribing displacements, however, is that acceptable limits vary depending on the failure mode (refer to Section 5.3.1.1). Further research is required.

5.3.3.3 Residual strength

A fastener should maintain a predictable load-bearing capacity subsequent to crack cycling to fulfill its intended purpose. For this reason, existing suitability tests for service load level crack cycling, e.g. in *ACI 355.02 (2004)*, require a fastener to exhibit a residual strength after cycling of at least 90% of the monotonic reference strength.

The residual load-bearing capacities of the investigated fasteners after crack cycling under representative seismic conditions (w_1 = 0.8 mm; F_2 = -350 kN; n = 10) are shown in Figure 5.35 to Figure 5.37. The mean values are designated by solid symbols.

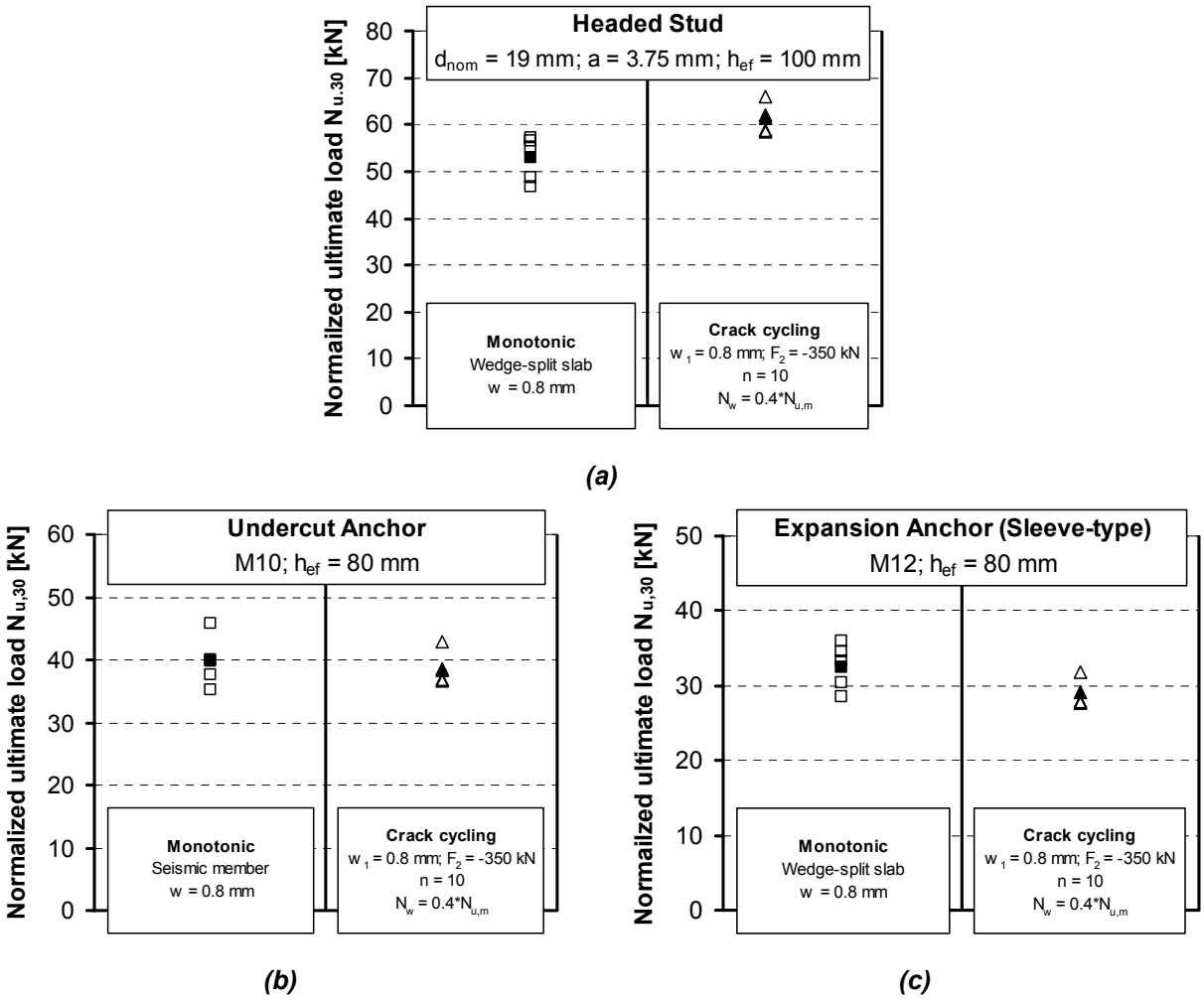

Figure 5.35 Comparison of reference and residual strength after crack cycling for fasteners that failed by concrete breakout: (a) headed stud; (b) undercut anchor; (c) sleeve-type exp. anchor

For the fasteners failing by concrete cone breakout (Figure 5.35), the ultimate loads have been normalized to a concrete strength of 30 N/mm^2 using Equation (5.1).

$$N_{u,30} = N_{u,test} \cdot \sqrt{\frac{30}{f_{cc,150,test}}} \tag{5.1}$$

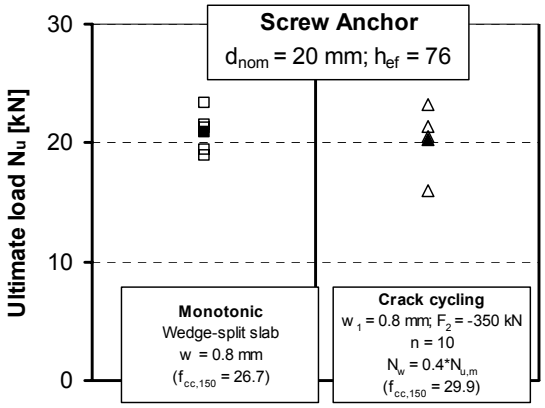

Figure 5.36 Comparison of reference and residual strength after crack cycling for the screw anchor which failed by pull-out

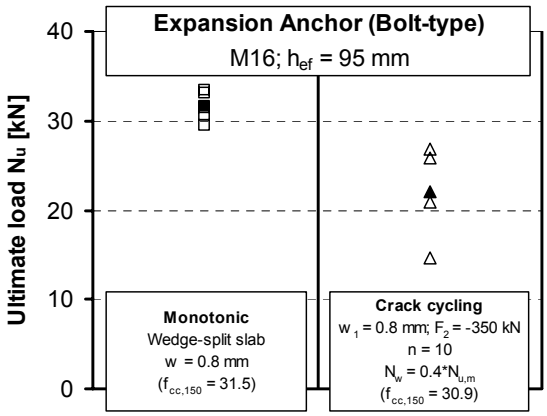

Figure 5.37 Comparison of reference and residual strength after crack cycling for the bolt-type expansion anchor which failed by pull-through

The increase in strength of the headed studs after crack cycling (Figure 5.35a) is believed to be due to the formation of a cone of highly compacted concrete at the head of the stud during crack cycling (Figure 5.38). This alters the load transfer conditions during the subsequent pullout test. Additionally, the use of different test members (wedge-split slab versus seismic member) for the reference and crack cycling tests may have affected the results. For the post-installed anchors failing by concrete cone breakout after crack cycling (Figure 5.35b,c) the residual strength was only marginally reduced by the crack cycling.

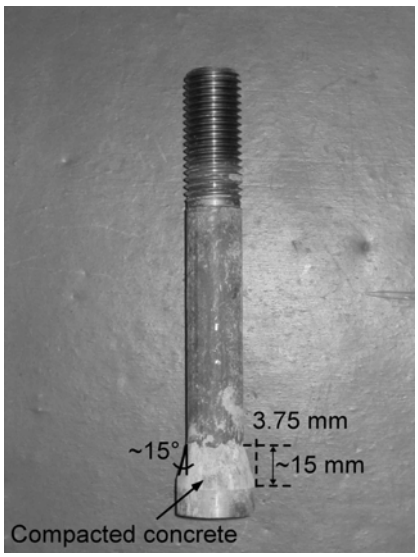

Figure 5.38 Photograph of headed bolt after seismic crack cycling test

The residual strengths of the investigated screw anchors, which failed by pull-out, did not appear to be significantly affected by the crack cycling (Figure 5.36). Only the bolt-type expansion anchors, which failed by pull-through, experienced a significant reduction (~30%) of the residual strength after crack cycling (Figure 5.37).

5.3.3.4 Influence of the shape and rate of crack cycling

Cyclic loading of the anchorage component under control of the applied force where the cycling alternates between tension and compression can be problematic due to the loss of the load path at the 'zero crossing'. Two cyclic loading options which avoid this problem were investigated. The first option was a combination of half-sine functions where the applied force was controlled with transition to ramp loading under control of the cylinder displacement for the zero crossing (Figure 5.39a). The second option was a sequence of positive and negative sloping ramp functions where the cylinder displacement rate was controlled and the peaks of the ramps were the desired load levels (Figure 5.39b).

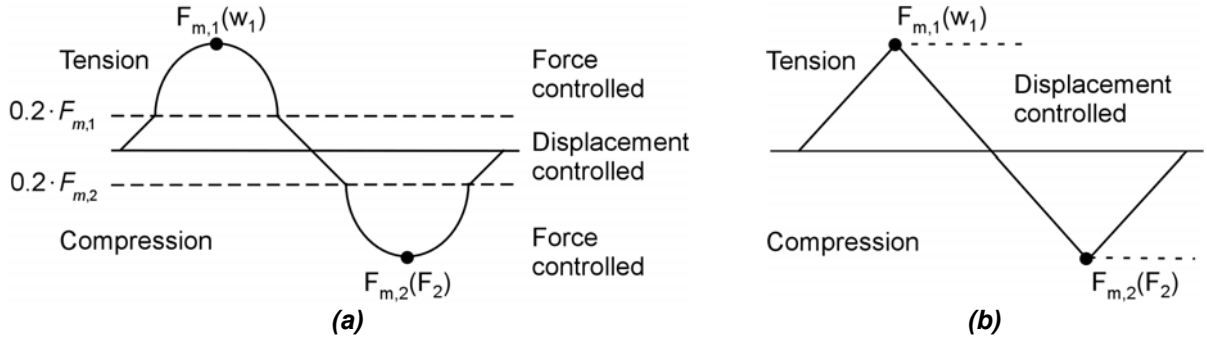

Figure 5.39 Anchorage component loading functions: (a) combined half-sine and ramp functions; (b) cycled ramp functions

Figure 5.40 shows typical crack time-histories for the load functions in Figure 5.39. The sine function resulted in a smoother crack opening curve (Figure 5.40a) compared to the cycled ramp loading (Figure 5.40b). The shape of the load function had no apparent effect on crack closing.

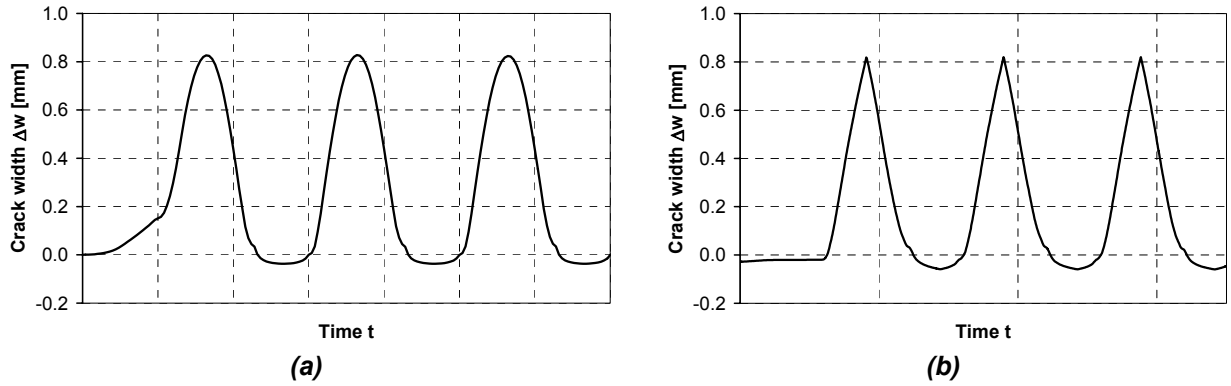

Figure 5.40 Crack cycling curves obtained with the loading functions in Figure 5.39: (a) combined half-sine and ramp functions; (b) cycled ramp functions

Tests were conducted using undercut anchors to investigate how the shape and rate of crack cycling affected fastener behavior. Figure 5.41 shows the anchorage component loading time-history, which was composed of the load functions in Figure 5.39.

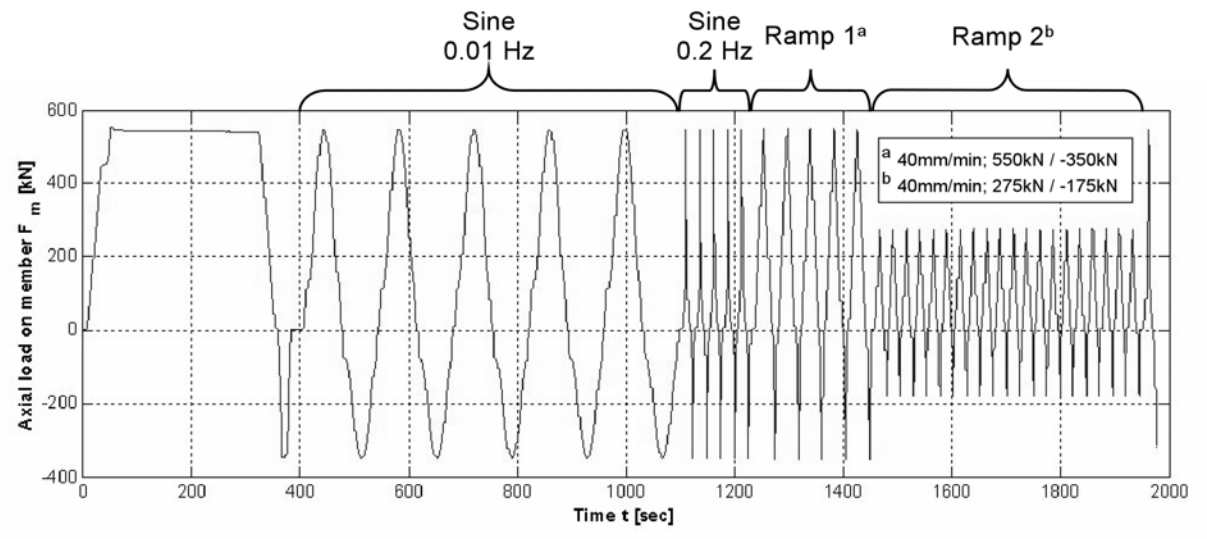

Figure 5.41 Anchorage component loading time history used to investigate the effect of the shape and rate of the crack cycles

As the cracks in the anchorage component opened, the fasteners underwent displacements. If the cracks opened 'too quickly' (Sine 0.2 Hz), the pressure on the hydraulic cylinders loading the fasteners dropped below the prescribed value (N_w = 16.2 kN) as the pressure regulator attempted to equalize the pressure (Figure 5.42). This pressure drop momentarily reduced the fastener loads during crack opening (here about 6% of N_w). The load increase above the applied value was a physical phenomena resulting from crack closure. The sharp drops in the fastener load at a displacement of about δ = 9 mm coincided with failure of other fasteners in the member.

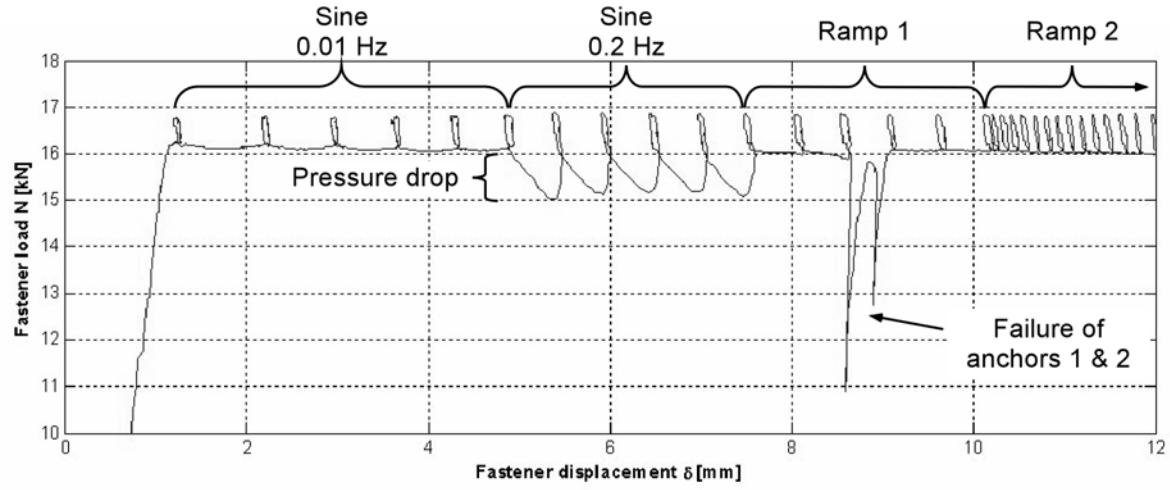

Figure 5.42 Detail of load-displacement curve for an undercut anchor M10 subjected to the crack cycling produced by the loading in Figure 5.41

The pressure drop due to crack opening is undesirable and can be reduced by:

- slowing the crack opening (compare Sine 0.2 Hz with Sine 0.01 Hz);
- reducing the crack opening width;
- using a faster pressure regulator for the fastener load cylinders.

Practical crack cycling rates for the seismic testing of fasteners appear to range between about 0.01 Hz (17 minutes for 10 cycles) and 0.2 Hz (50 seconds for 10 cycles). As shown in Figure 5.42, however, if crack cycling is performed too rapidly, a pressure drop on the fasteners could lead to inconsistent testing conditions, i.e. the anchor load at crack opening is artificially low. Therefore, the drop in the pressure during cycling must be limited.

Figure 5.43 shows fastener displacements plotted as a function of the number of crack cycles. The behavior of the fasteners indicates that neither the rate of the crack cycles - in the range investigated (Sine 0.01 Hz versus Sine 0.2 Hz) - nor the shape of the loading curve (Sine 0.2 Hz vs. Ramp 1) significantly affected the fastener displacement behavior during crack cycling. This can be seen in that the slope of the displacement curves remained approximately constant as the crack cycling was varied. This was true in spite of the 6% load drop that occurred for sinusoidal cycling at 0.2 Hz. A distinct change in the rate of the fastener displacement, however, can be observed when the crack cycling width was reduced (Ramp 2). The above conclusions are only strictly valid for the investigated fasteners and testing conditions.

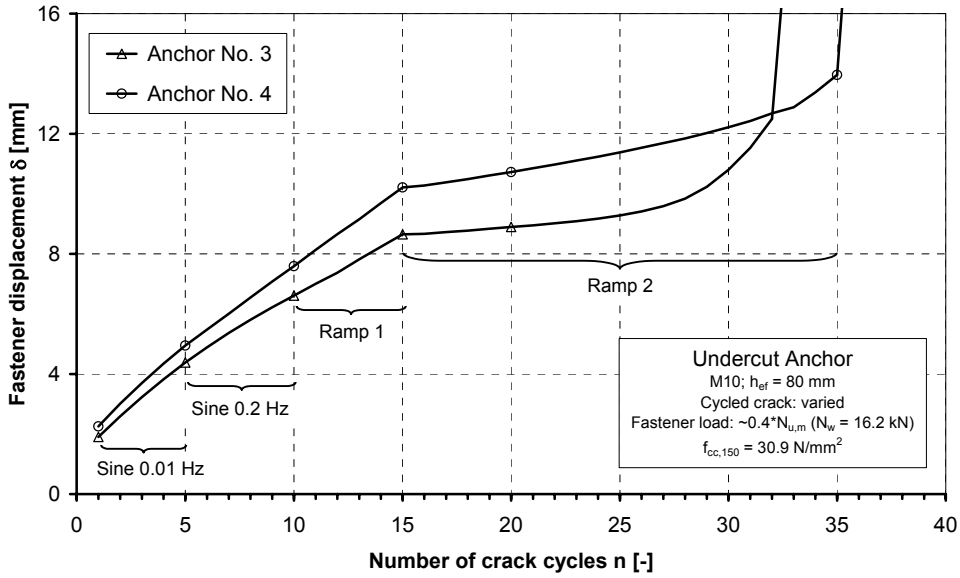

Figure 5.43 Fastener displacements as a function of the number of crack cycles for the member load history in Figure 5.41

5.3.3.5 Influence of crack closure

Applying compression force to the anchorage component during crack cycling negatively affects fastener performance. Figure 5.44 shows that when no compressive load was applied to the component that the relative fastener displacement during 10 crack cycles was about half of the value obtained when a compression load sufficient to cause full

crack closure was applied. Similar results were obtained for other fastener types. Large displacements reduce the residual bearing capacity of a fastener and can cause failure during crack cycling (see Section 5.3.3.1).

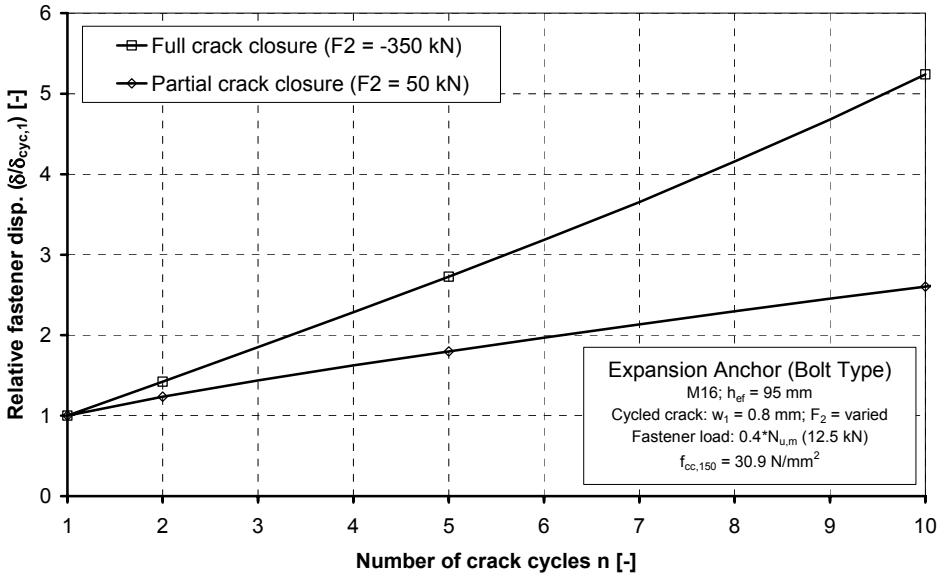

Figure 5.44 Relative fastener displacement as a function of the number of crack cycles for various compression loads on the anchorage component

The significant difference in the fastener displacement is a result of two factors:

(1) When insufficient or no compression load is applied to the anchorage component during crack cycling, the lower crack width w_2 grows rapidly, which results in a smaller crack width variation (Figure 5.45).

(2) The application of compression load crushes the concrete around the point of load transfer of the fasteners, which results in larger displacements during subsequent crack opening.

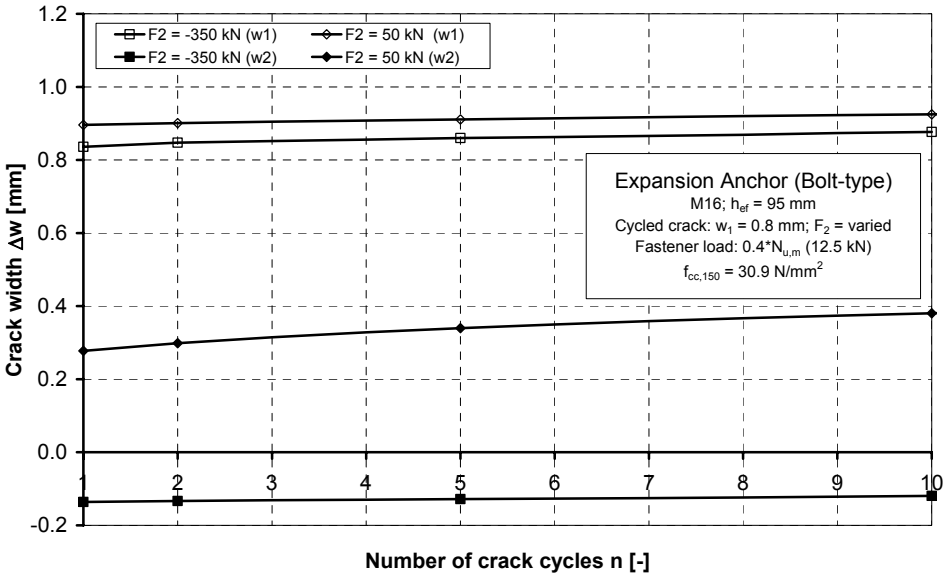

Figure 5.45 Average crack width as a function of the number of crack cycles for various compression load levels on the anchorage component

As discussed in Chapter 4, it must be assumed that full crack closure may occur in an anchorage component during an earthquake. The difficulty is that it is in general impossible to predict the compression load, thus complicating the establishment of compression load levels for fastener qualification tests.

It was hypothesized that compression loads applied to the anchorage component beyond those required to achieve crack closure around the loaded anchor would not affect fastener load-displacement behavior because the compression loads would be transferred through the surrounding anchorage material (Figure 5.46). Thus the required compressive load on the anchorage component for seismic fastener tests could be determined as that required to achieve and maintain crack closure during crack cycling.

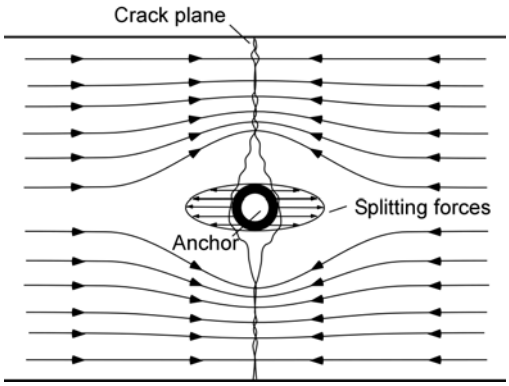

Figure 5.46 Representation of compressive load transfer around an anchor (plan view of member)

This hypothesis was investigated using headed studs located in anchorage components subjected to crack cycling with three different compressive load levels (F_2 = -50 kN, F_2 = -350 kN and F_2 = -500 kN). These load levels, which correspond to stresses in the anchorage component of about 2, 10 and 15 percent of concrete compressive strength ($f_{cc,150}$), were determined from the crack profile tests (see Figure 5.19). The compressive load F_2 = -50 kN closed the crack only to about Δw = 0.1 mm during the initial crack cycle. Both of the load levels F_2 = -350 kN and F_2 = -500 kN were sufficient for full crack closure during the initial crack cycle (Figure 5.47).

Figure 5.48 shows the relative fastener displacement for the various compressive load levels on the anchorage component as a function of the number of crack cycles. Each curve represents the average of three or more test replicates.

The results shown in Figure 5.48 support the hypothesis that compression loads beyond those required to achieve full crack closure do not affect the fastener displacement behavior during crack cycling. This can be seen because the rate of fastener displacement stopped increasing for compressive load greater than F_2 = -350 kN. For all three cases, the residual strengths obtained in pullout tests performed subsequent to the crack cycling were close to those obtained in comparable monotonic reference tests (Figure 5.49).

Based on the results, it is tentatively proposed that a compressive stress of $0.15 \cdot f_{cc,150}$ over the gross cross-section area of the anchorage component is sufficient to achieve crack closure for fastener testing. Further research is needed to verify this value.

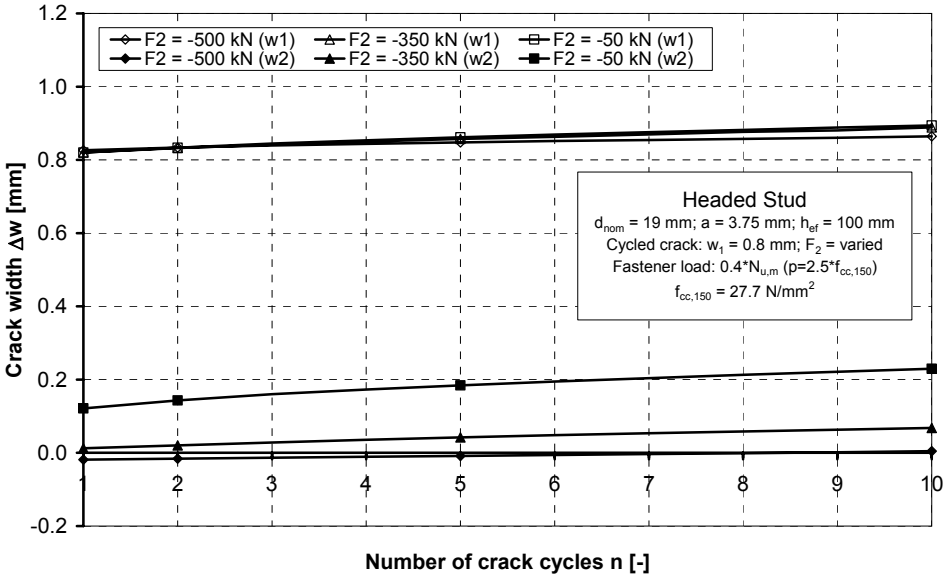

Figure 5.47 Crack width as a function of the number of crack cycles for various anchorage component compression loads

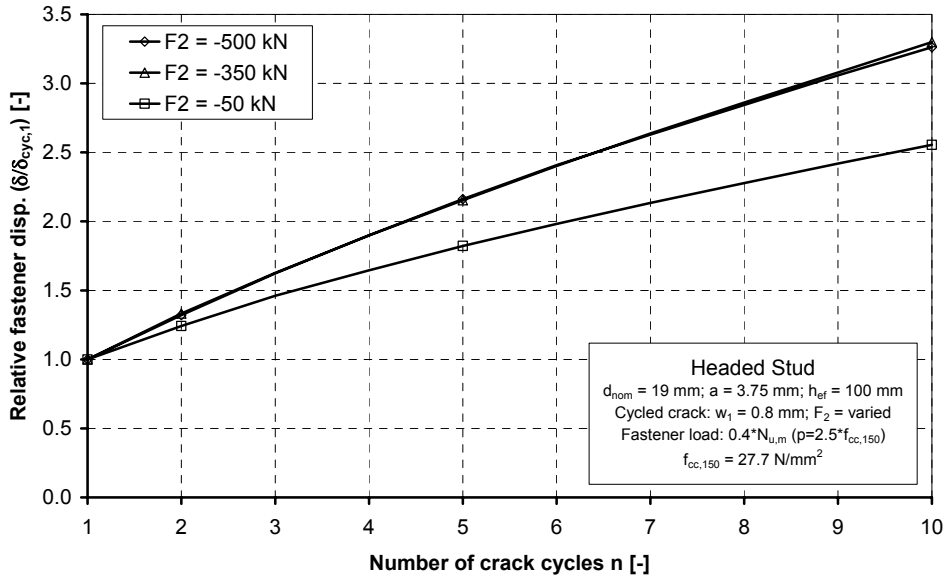

Figure 5.48 Relative fastener displacement as a function of the number of crack cycles for various anchorage component compression loads

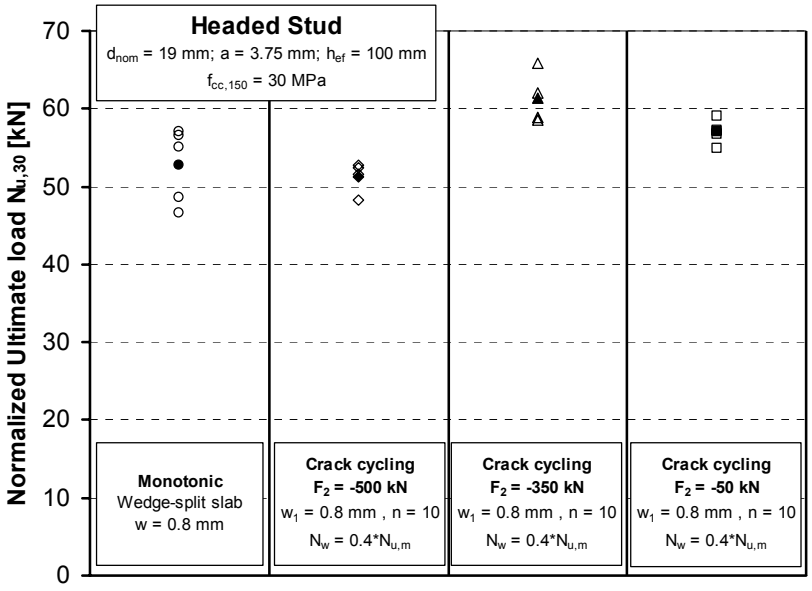

Figure 5.49 Residual loads for headed studs ($p = 2.5 \cdot f_{cc,150}$) tested in large cycled cracks with various compression loads on the anchorage component

5.3.3.6 Influence of crack opening width

Figure 5.50 shows the influence of the crack opening width in comparison to an applied compression load on the anchorage component on the fastener displacement behavior. All curves are for headed studs ($p = 2.5 \cdot f_{cc,150}$) and represent the average of three or more test replicates. Figure 5.50 shows that a compression load sufficient to cause full crack closure (F_2 = -350 kN) and a crack width difference of w_1-w_2 = 0.55 mm yields larger fastener displacements during crack cycling than a compression load F_2 = -50 kN and a crack width difference of w_1-w_2 = 0.70 mm. Thus it can be concluded that the additional crack with difference of w_1-w_2 = 0.15 mm was not sufficient to replicate the damage caused by the higher compression load. Presumably, if the crack width difference was larger the influence of the damage caused by the compression load could be replicated. Crack cycling widths of this magnitude, however, could not be achieved with the test setup used.

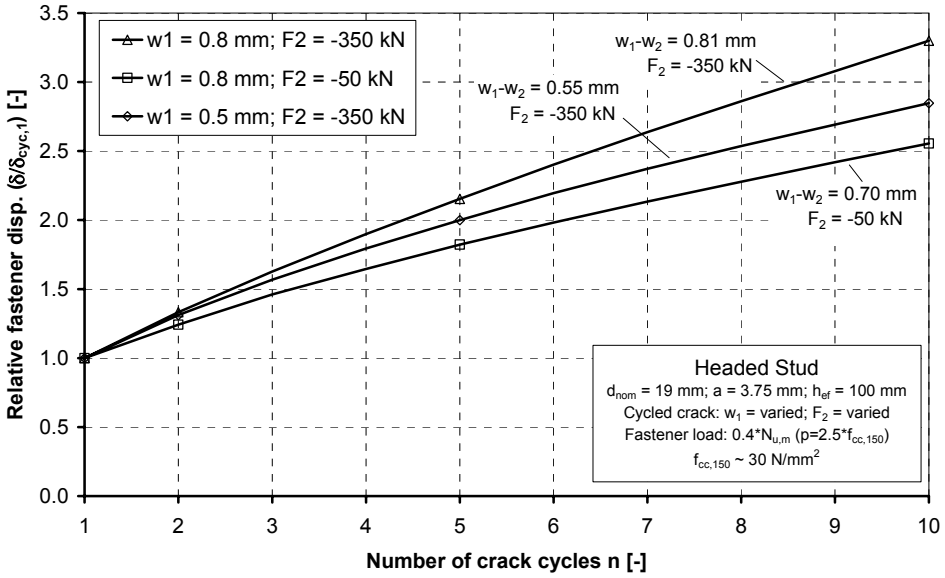

Figure 5.50 Relative fastener displacement as a function of the number of crack cycles for various crack widths (w_1) and anchorage component compression loads (F_2)

5.3.3.7 Influence of head bearing pressure

Figure 5.51 shows fastener displacements as a function of the number of crack cycles for headed studs subjected to large crack opening and closing cycles (w_1 = 0.8 mm; F_2 = -350 kN; n = 10), where the constant tension loads on the anchors were chosen to produce head bearing pressures ($p = N_w/A_h$) of $4.0 \cdot f_{cc,150}$ ($5.0 \cdot f_c$), $2.5 \cdot f_{cc,150}$ ($3.12 \cdot f_c$) or $1.0 \cdot f_{cc,150}$ ($1.3 \cdot f_c$). The bearing pressure of $2.5 \cdot f_{cc,150}$ roughly corresponds to the current allowable bearing pressure for headed studs in cracked concrete (*ACI 318 2005*) factored by 40% to represent the design load level for seismic applications ($0.4 \cdot (8 \cdot f_c) = 3.2 \cdot f_c \approx 2.5 \cdot f_{cc,150}$).

The degressive increase of displacements during crack cycling shown in Figure 5.51 for the head bearing pressures of $2.5 \cdot f_{cc,150}$ and $1.0 \cdot f_{cc,150}$ indicate that the existing limits for allowable bearing pressures for headed studs used for non-seismic applications are also suitable for crack cycling representative of seismic situations. Higher head bearing pressure ($4.0 \cdot f_{cc,150}$) led to progressively increasing displacements and a significant drop in the residual strength of the fastener (Figure 5.52).

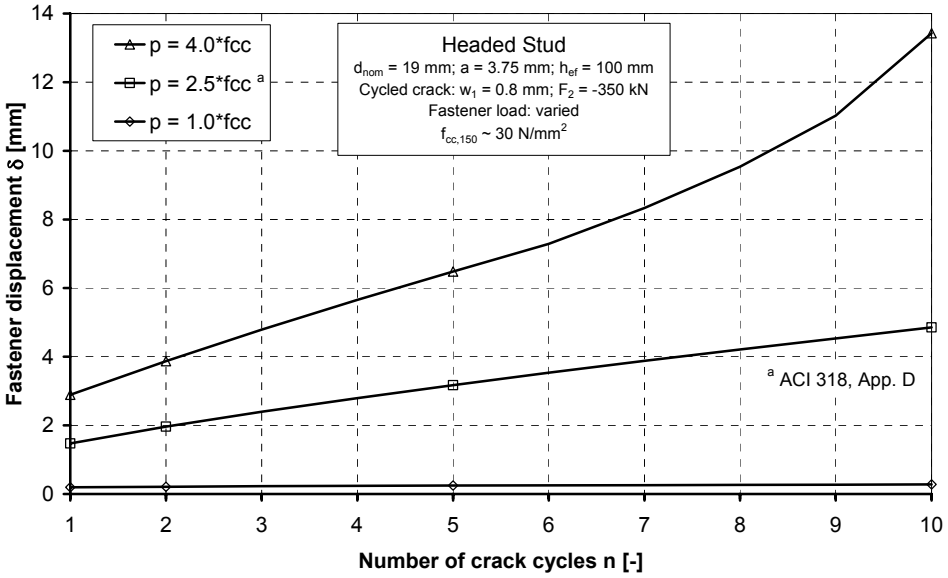

Figure 5.51 Fastener displacement as a function of the number of crack cycles for various head bearing pressures

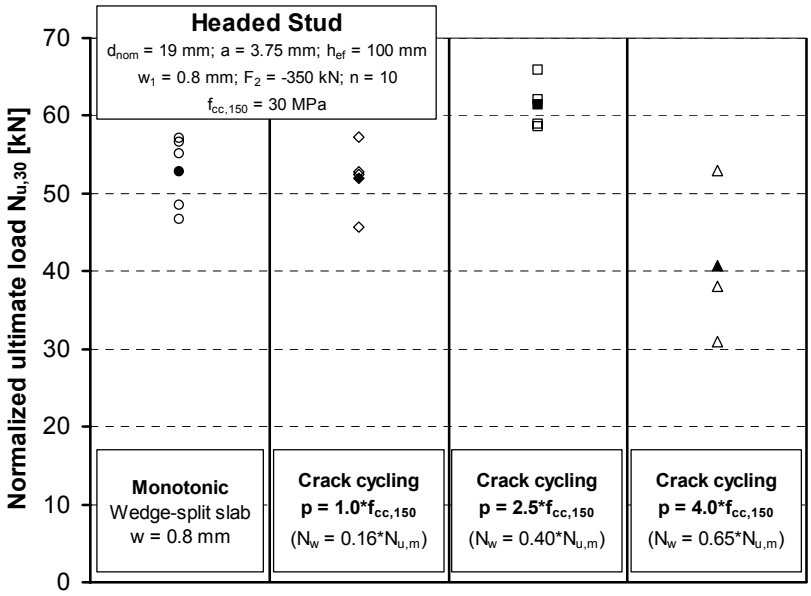

Figure 5.52 Residual load for headed studs tests in large cycled cracks with various head bearing pressures

5.4 Summary and consequences

The behavior of cast-in and post-installed fasteners during crack cycling representative of that which might occur outside of zones of plastic deformation in a reinforced concrete structure during an earthquake was investigated. A new test setup and anchorage component were developed for this purpose. The setup allowed cracks in the anchorage component to be pressed closed by an external compressive force.

Crack cycling tests were conducted to determine the performance of various fastener types when loaded by a constant tension load of $N_w = 0.4 \cdot N_{u,m}$ and subjected to 10 crack cycles between w_1 = 0.8 mm and w_2 = 0.0 mm. The investigated fasteners were headed studs (d_{nom} = 19 mm), bolt-type (M16) and sleeve-type (M12) torque-controlled

expansion anchors, undercut anchors (M10) and screw anchors (d_{nom} = 20 mm). The investigated headed studs, undercut anchors and sleeve-type expansion anchors failed by concrete cone breakout in pull-out tests performed in an open crack (Δw = 0.8 mm) subsequent to the crack cycling. The bolt-type expansion anchors failed by pull-through and the screw anchors failed by pull-out subsequent to the above-described crack cycling.

For anchors failing by concrete cone breakout:

(1) if the displacement during crack cycling is less than the displacement at ultimate load in comparable monotonic pull-out tests in a static crack, the crack cycling appears to have little influence on the residual strength;
(2) if the displacement during crack cycling is equal to or greater than the displacement at ultimate load in comparable monotonic pullout tests in a static crack, the residual strength is reduced as a function of the lost embedment depth according to $(h_{ef} - \delta)^{1.5}$;
(3) concrete cone failure during crack cycling can occur if the embedment depth is reduced sufficiently to cause failure at the applied fastener tension load;
(4) splitting of the member may occur for large fastener displacements and/or high compressive member loads before one of the above-stated failure cases occurs.

For anchors failing by pull-though:

(1) in the case of pull-through failure during crack cycling or in pullout tests performed subsequent to the crack cycling where the anchor expansion elements do not slip relative to the wall of the drilled hole, the load-displacement behavior is bounded by the monotonic envelope curve;
(2) this failure mode is typically associated with large fastener displacements;
(3) if the displacement during crack cycling is less than the displacement at ultimate load in comparable monotonic pullout tests in a static crack, the fastener behavior during subsequent pull-out becomes stiffer;
(4) if the displacement during crack cycling is equal to or greater than the displacement at ultimate load in comparable monotonic pull-out tests in a static crack, the residual strength is reduced following the descending branch of the monotonic curve and often exhibits a large amount of scatter.

For screw anchors failing by pull-out:

(1) if the screw anchors fail in pure pull-out failure in both monotonic and crack cycling tests, the load-displacement behavior is expected to be similar to that for pull-through failure, i.e. the load-displacement curve for the crack cycling test would be bounded by the monotonic load-displacement curve;
(2) the amount of fastener displacement that can occur during crack cycling is less than the anchor thread spacing.

For all of the above-mentioned failure modes, a linear or degressive increase of fastener displacement as a function of the number of crack cycles (linear-linear scale) appeared to be an indicator of suitable fastener performance. A progressive increase of displacement indicated the start of failure. The amount of fastener displacement during crack cycling is a function of several factors. The most important factors are the type of anchor and failure mode, the crack opening and closing widths (w_1, w_2), the number of crack cycles (n) and the fastener bearing pressure. Fastener displacement should be reported near the point of maximum crack opening (w_1) as opposed to after completion of a crack cycle. Further research is necessary to establish displacement assessment criteria for anchor prequalification that is less subjective than graphical intrepetation of displacement curves.

The residual strength of the investigated fasteners failing by concrete cone breakout (headed stud, undercut, expansion sleeve) and pull-out (screw anchor) was not significantly affected by the representative seismic crack cycling ($N_w = 0.4 \cdot N_{u,m}$; $w_1 = 0.8$ mm; $w_2 = 0.0$ mm; $n = 10$). The residual strength of the investigated fasteners failing by pull-through (expansion bolt) was reduced (> 20%) by the crack cycling. These results are only valid for the investigated testing conditions, products and anchor sizes.

The shape of the loading function applied to the anchorage component (sine or triangular) affects the duration and shape of the crack opening. The difference, however, did not significantly affect the displacement behavior of the investigated undercut anchors. Therefore, the easier to implement cycled ramp functions (triangular) are preferable for crack cycling tests where a compression load is applied to the anchorage component. Further testing is necessary to verify this for other fastener types and sizes.

Varying the crack cycling rates between 0.01 Hz (100 sec/cycle) and 0.2 Hz (5 sec/cycle) did not affect the displacement behavior of the investigated undercut anchors during crack cycling. High crack cycling rates (0.2 Hz), however, led to a drop in the anchor loads (approx. 5% of N_w) because the hydraulic loading cylinders had difficulty to equilibrate the oil pressure as the fasteners displaced rapidly. A drop of the fastener load of more than 5% over several cycles during crack opening should be restricted in qualification tests. A momentary drop in fastener load due to failure of another anchor in the member did not appear to affect the behavior of the remaining fasteners.

Compressive load on the anchorage component, as might occur during an earthquake, significantly increases fastener displacement during crack cycling. The influence of the compressive load stops increasing after the crack in the component has closed sufficiently around the fastener. When the crack has closed, the compressive forces are transferred through the surrounding concrete. Therefore, for seismic crack cycling qualification tests the compression load should be set sufficiently high to ensure closure of the cracks. It is proposed that a compressive stress of 15 percent of the concrete compressive strength ($0.15 \cdot f_{cc,150}$) over the gross cross-section area of the anchorage component is sufficient to achieve full crack closure ($w_2 = 0$ mm). Further testing is necessary, however, to verify this for other fastener types and sizes.

Extensive monitoring of crack widths showed that they varied significantly across the seismic anchorage component (±40% of the value at the anchor location). This variation had an approximately linear trend with local bulging at the fastener location. To obtain an average value it is essential to measure crack width symmetrically around the anchor. A minimum distance between the fastener and the crack width measurement device of $6 \cdot d_0$ (d_0 = diameter of drilled hole) is recommended to avoid the effects of the local bulging. Average crack width variation for cracks along the component during crack cycling was small (coefficient of variation about 10%).

The head bearing pressure of $8 \cdot f_c$ ($6.4 \cdot f_{cc,150}$) for headed bolts typically used for non-seismic applications appears to be a suitable limit for representative seismic crack cycling when the bolts are loaded in tension up to $0.4 \cdot N_{u,m}$. This tension load is representative of current design levels loads for seismic actions (ACI 318 2005).

The seismic crack cycling tests described in this chapter are relatively complicated compared to existing crack cycling tests in open cracks, i.e. tests without crack closure. It is foreseeable that a substitute test in open cracks that mimics the effect of full crack closure on fastener behavior will be required for qualification tests. Exploratory tests indicated that crack width differences (w_1-w_2) much larger than Δw = 0.8 mm would be required to mimic the effect of full crack closure with Δw = 0.8 mm. Further research is necessary on this issue.

6 Experimental Investigations with Cyclic Loading

6.1 Scope

A variety of experimental investigations were conducted to better understand the behavior of fasteners under cycled tension loads. Tests with cast-in headed bolts were performed since these anchors have performed well in past earthquakes (*Silva 2001*) and can serve as a reference for other types of fasteners. Tests with post-installed fasteners were performed to investigate the performance of various fastener load transfer mechanisms during tension cycling at near-ultimate load. The influence of load cycling frequency and load cycling pattern on fastener behavior as well as the definition of ductility for fasteners used in seismic applications are also discussed.

In this chapter, a summary of the test setups and procedures are presented along with detailed discussions of the key results. The complete test reports are available in *Hoehler (2004b, 2004c, 2004d, 2004e, 2004f, 2005a)*.

6.2 Cast-in headed bolts

6.2.1 Experimental setups and testing procedures

6.2.1.1 Investigated fasteners

Specially designed headed bolts were used (Figure 6.1). The design allowed various steel grades (10.9 and 8.8) and diameters of threaded rods (M20 and M16) to be used while maintaining a constant bearing area (A_h = 582 mm^2). The majority of the bolts tested used M20 grade 10.9 steel threaded rods, which could be loaded elastically to over 200 kN. The effective embedment depth in most tests was h_{ef} = 100 mm.

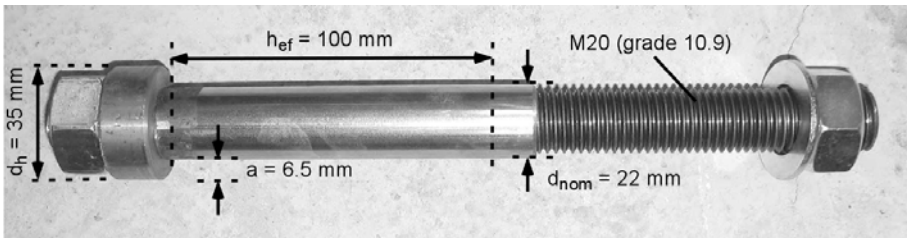

Figure 6.1 Special headed bolts used for tension load cycling tests

6.2.1.2 Anchorage components

Tests were performed in both normal strength (C20/25) and high strength (C45/55) unreinforced, uncracked concrete slabs (Figure 6.2a) and in normal strength wedge-split cracked concrete slabs (Figure 6.2b; for dimensions refer to Figure 5.1).

The anchorage components were produced according to the state of the art after *DIN 1045 (2001)* and *DIN 1048 (1991)*.

The average concrete cube compressive strength for the C20/25 slabs ranged between $f_{cc,150}$ = 27.0 N/mm^2 and $f_{cc,150}$ = 29.9 N/mm^2. The average concrete cube compressive strength for the C45/55 slab was $f_{cc,150}$ = 58.5 N/mm^2.

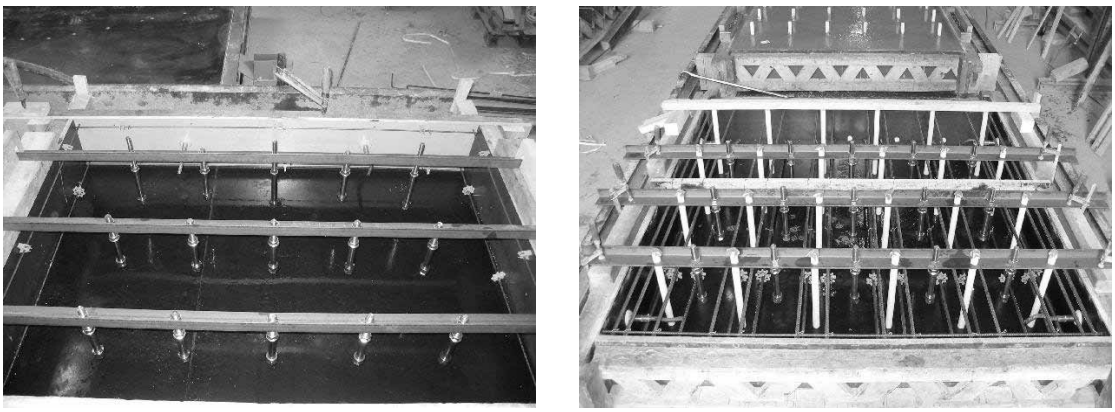

(a) *(b)*

Figure 6.2 Anchorage components for tension load cycling tests with headed bolts: (a) unreinforced slab; (b) reinforced wedge-split slab

6.2.1.3 Loading setups and testing procedures

The fasteners were loaded using a servo-hydraulic cylinder with a capacity of 250 kN. For the majority of the tests, a stiff steel plate was used in conjunction with the load cylinder support frame to prevent concrete cone breakout (close support; Figure 6.3). For a limited number of tests, the load cylinder support frame was supported such that concrete cone breakout could occur (wide support; Figure 6.4).

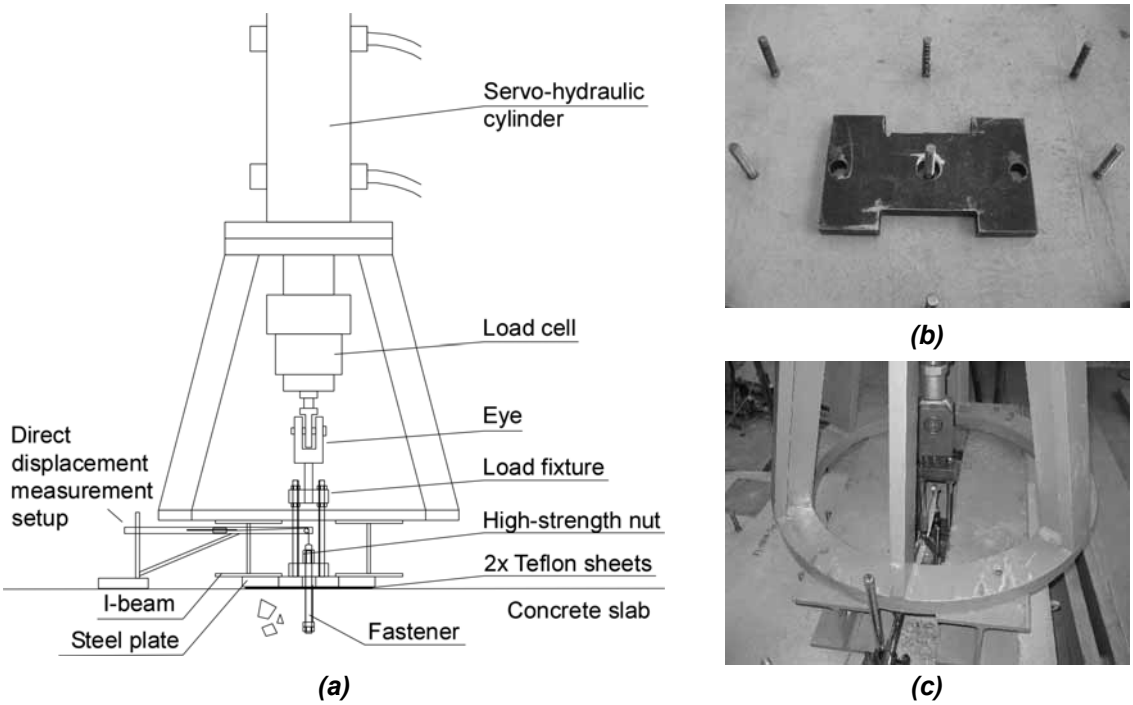

(a) *(b)* *(c)*

Figure 6.3 Test setup for tension load cycling tests with headed bolts (close support): (a) schematic; (b) detail of steel plate; (c) photograph of setup

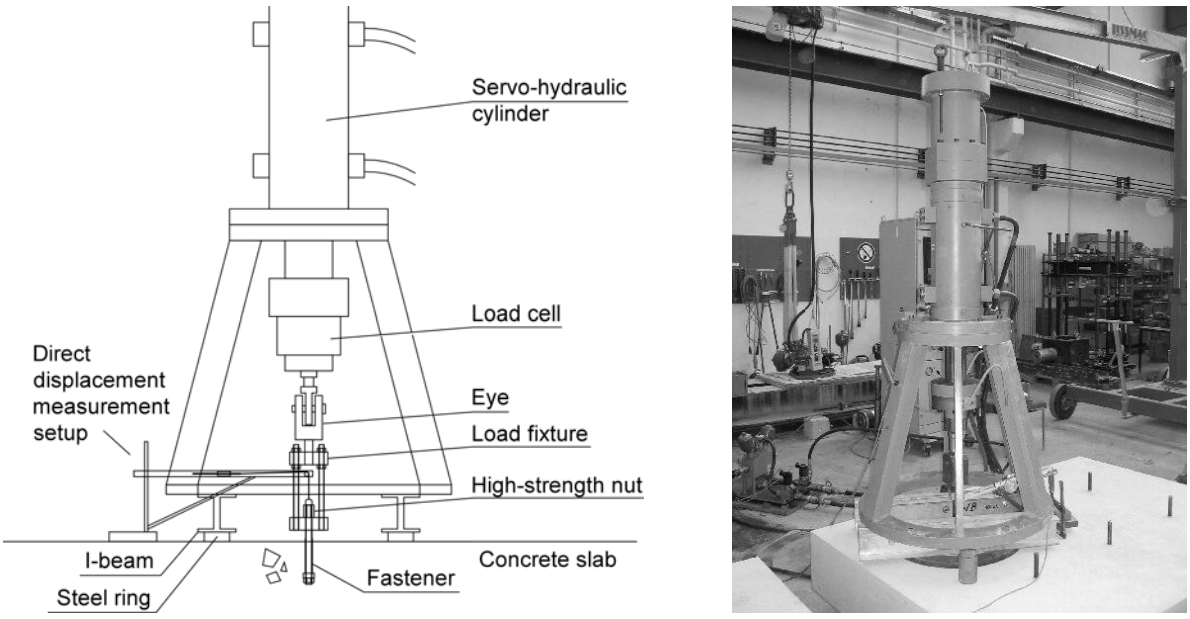

Figure 6.4 Test setup for tension load cycling tests with headed bolts (wide support): (a) schematic; (b) photograph

During testing it was observed that the steel ring used to transfer load to the concrete in the wide support setup (Figure 6.4) influenced the behavior of the fasteners in spite of the clear spacing of $5 \cdot h_{ef}$. The problem was eliminated by placing the ring on three steel blocks (Figure 6.5), which reduced hoop stresses in the concrete. Further details can be found in *Hoehler (2005a, 2006b)*.

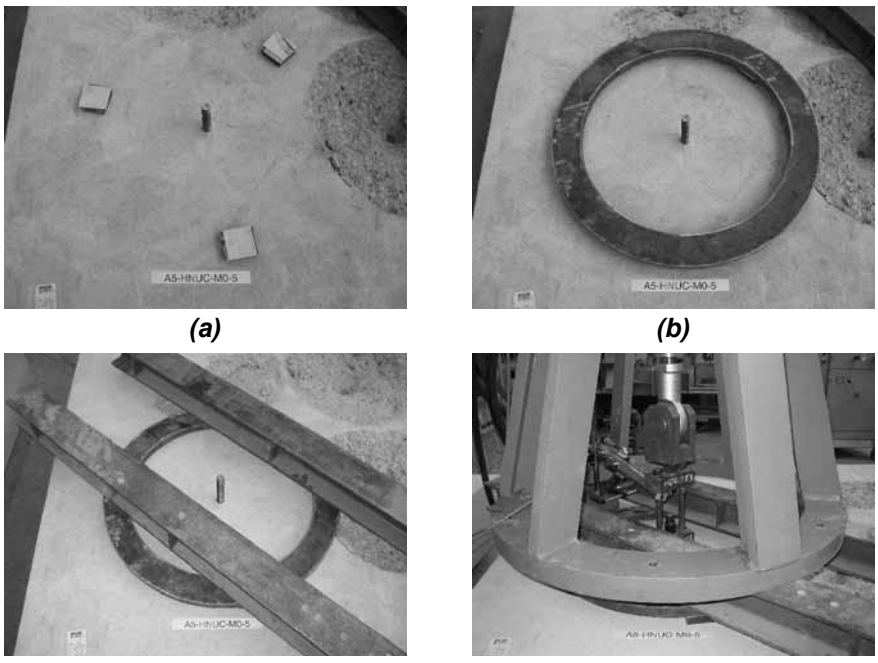

Figure 6.5 Test setup for tension load cycling tests with headed bolts (3-point wide support): (a) 3 steel blocks with Teflon; (b) steel ring placed on blocks; (c) I-beams placed on ring; (d) servo-hydraulic cylinder placed on I-beam and connected to anchor

Monotonic tension tests and pulsating tension load cycling tests were performed using both the close and wide support test setups. For the tests in cracked concrete, the cracks were opened by Δw = 0.8 mm after installation of the fasteners, but before loading.

In the monotonic tension tests, load was applied under control of the servo-hydraulic cylinder displacement (displacement-controlled test). Ultimate load was reached in approximately 1 to 3 minutes.

In the tension load cycling tests, the anchor was first loaded to a load level generating the desired maximum head bearing stress ($N_{max} = \sigma A_h$), where σ was equal to 4, 6, 8 or 12 times the concrete cube compressive strength ($f_{cc,150}$). The load was then decreased to $N_{mid} = (N_{max} - N_{min})/2 + N_{min}$ and cycled between N_{max} and N_{min} = 2 kN at a frequency of 0.5 Hz. The cycling was stopped after 30, 50 and 100 cycles to record displacements. If no failure occurred during cycling, the anchor was unloaded and re-loaded monotonically until the monotonic envelope curve was rejoined (close support) or failure occurred (wide support). The cyclic loading history is shown schematically in Figure 6.6.

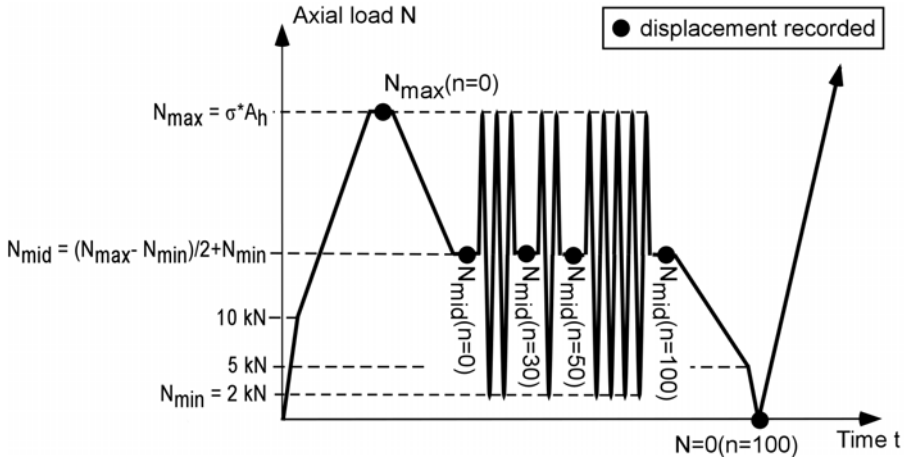

Figure 6.6 Load history for tension cycling tests

The tension load applied to the fastener N, the displacement of the servo-hydraulic cylinder δ_{cyl}, the fastener displacement δ and the crack opening width Δw (when applicable) were measured continually during the tests.

6.2.2 Results and discussion

6.2.2.1 Head slip during monotonic tension loading

Furche (1994) proposed the following equations to determine the head slip *s* of headed bolts during monotonic tension loading in uncracked and cracked concrete:

$$s = \frac{k_a \cdot k_A}{600} \left(\frac{\sigma}{f_{cc,200}} \right)^2 \quad \text{(uncracked)} \tag{6.1a}$$

$$s = \frac{k_a \cdot k_A}{300} \left(\frac{\sigma}{f_{cc,200}} \right)^2 \quad \text{(cracked)} \tag{6.1b}$$

where k_a is a factor that depends on the porosity of the concrete near the anchor head (k_a = 1.0 for shoulder width $a \geq 5$ mm), k_A is a factor that depends on the head bearing area A_h, σ is the bearing stress ($\sigma = N/A_h$) and $f_{cc,200}$ is the concrete cube compressive strength (200 mm side length). All units are in N and mm. The factor k_A can be calculated as:

$$k_A = \frac{\sqrt{{d_{nom}}^2 + m \cdot \left({d_h}^2 - {d_{nom}}^2 \right)}}{2} - \frac{d_h}{2} \tag{6.2}$$

where d_{nom} is the anchor shaft diameter, d_h is the anchor head diameter and m is a factor that may be taken as 9 for circular surfaces (*Furche 1994*). For the investigated headed bolts k_A = 24.8.

It was desired to verify whether Equations (6.1a,b) are applicable to headed anchors in high strength concrete (C45/55), as well as in normal strength concrete (C20/25), and to check if an improvement of the predicative capability could be achieved by replacing f_{cc} with $(f_{cc})^{0.5}$. The equations were normalized for a concrete compression strength determined for 150 mm cubes using the factor $f_{cc,200} = 0.95 \cdot f_{cc,150}$.

To achieve bearing pressures up to $12 \cdot f_{cc,150}$ without a very large embedment depth h_{ef}, the specially designed high strength (M20; grade 10.9) steel anchors (Figure 6.1) were used in conjunction with a close support setup (Figure 6.3). Loading was stopped before the anchor steel yielded.

For headed bolts loaded in tension where a full concrete cone is able to develop (wide support), the displacement measured at the top of the fastener δ is composed of the elongation of the anchor shaft δ_{st}, the displacement due to elastic and inelastic compression of the concrete above the head δ_{co} and displacement due to crack opening as the concrete cone forms δ_{cr} (Figure 6.7). The head slip s is equal to $\delta_{cr} + \delta_{co}$. Up to the ultimate load the displacement due to crack opening will be negligibly small.

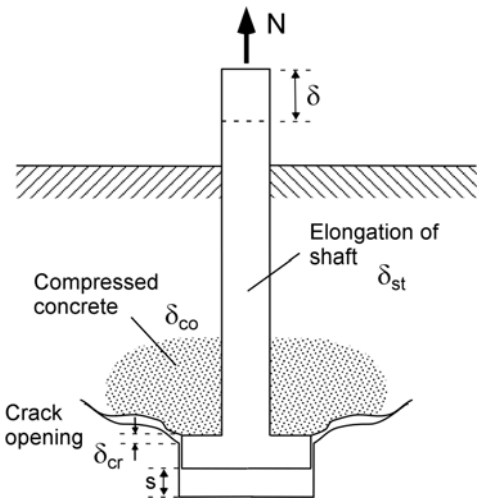

Figure 6.7 Schematic of displacement of a headed bolt loaded in tension with a wide support

For tests with a close support, the displacement due to crack opening is eliminated since the formation of a concrete cone is prevented. The anchor shaft behaved linear elastically throughout the loading. The elastic modulus was determined from experimental tests on the actual threaded rods (*Hoehler 2004b*). Thus, the head slip *s* for loading with close support was determined as:

$$s = \delta - \frac{N \cdot L}{E_s \cdot A_s} \tag{6.3}$$

where N was the applied tensile load, L was the loaded length of the anchor (170 mm) and A_s was the stressed area of the steel threaded rod (245 mm^2).

Figure 6.8 shows the load-slip curves for the headed bolts in uncracked C20/25 and C45/55 concrete. As expected, the C45/55 concrete produced stiffer load-slip response.

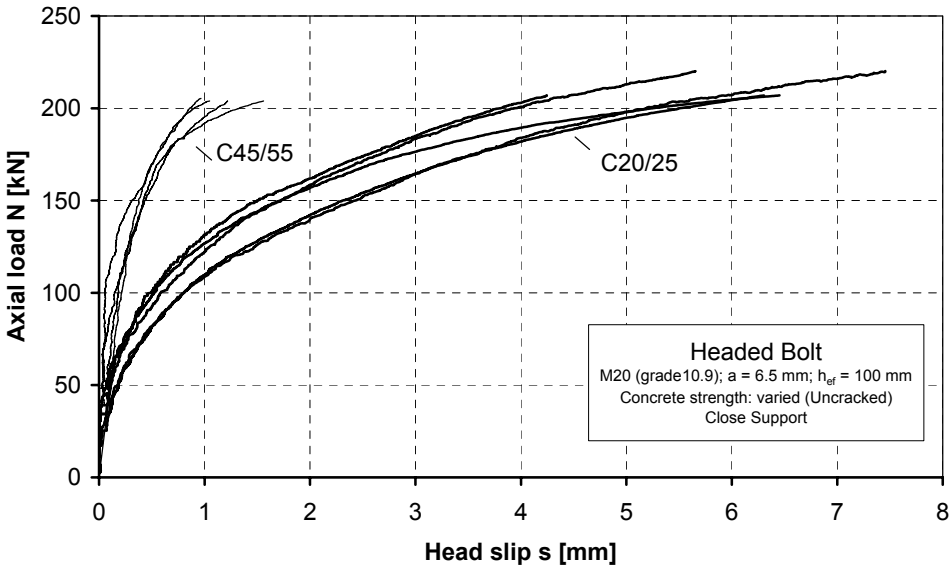

Figure 6.8 Load-slip curves for headed bolts in uncracked concrete

Figure 6.9 shows the bearing stresses ($\sigma = N/A_h$) divided by the concrete cube compressive strength ($f_{cc,150}$) as a function of the head slip calculated from the load-slip curves in Figure 6.8. Furche's equation for slip in uncracked concrete (Equation 6.1a) is shown for comparison. Figure 6.9 indicates that Equation (6.1a) predicts the slip behavior relatively well, however, the initial stiffness of the anchors is slightly higher and the curvatures slightly more nonlinear than predicted by the equation.

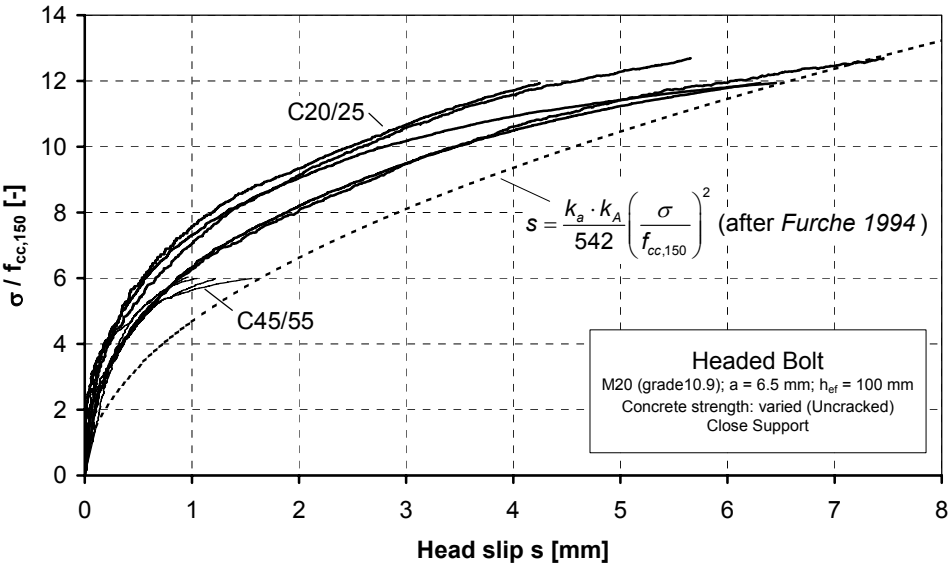

Figure 6.9 (σ / f_{cc}) versus slip curves for headed bolts in uncracked concrete

Figure 6.10 plots the data again as a function of the square root of the concrete cube compressive strength $(f_{cc,150})^{0.5}$. Based on the limited amount of data, it appears that the slip is better represented for both concrete strengths using a square root function of the concrete strength. This was to be expected as the elastic modulus of the concrete increases approximately as a square root function of the concrete compressive strength.

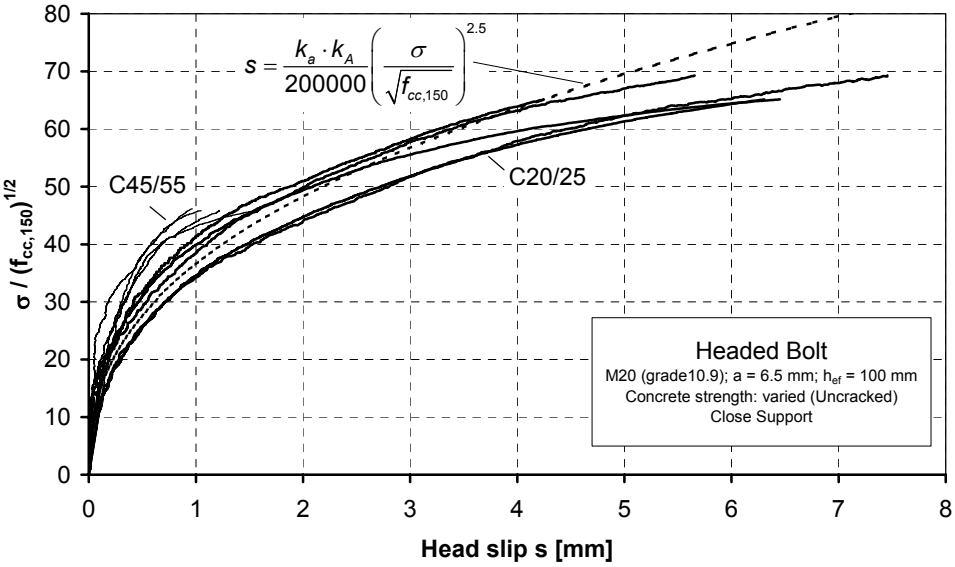

Figure 6.10 ($\sigma / f_{cc}^{0.5}$) versus slip curves for headed bolts in uncracked concrete

Equation (6.1a) was modified to use the square root of the concrete cube compressive strength. The selected denominator, as well as the exponent of 2.5, in Equation (6.4a) gave a good fit for the present experimental data, however, these values should be verified using a larger experimental database.

$$s = \frac{k_a \cdot k_A}{200000}\left(\frac{\sigma}{\sqrt{f_{cc,150}}}\right)^{2.5} \quad \text{(uncracked)} \tag{6.4a}$$

Tests in cracked concrete (Δw = 0.8 mm) were performed only in C20/25 concrete. The normalized head bearing pressure versus slip curves are shown in Figure 6.11. The value of the denominator was appropriately modified for cracked concrete.

$$s = \frac{k_a \cdot k_A}{70000}\left(\frac{\sigma}{\sqrt{f_{cc,150}}}\right)^{2.5} \quad \text{(cracked)} \tag{6.4b}$$

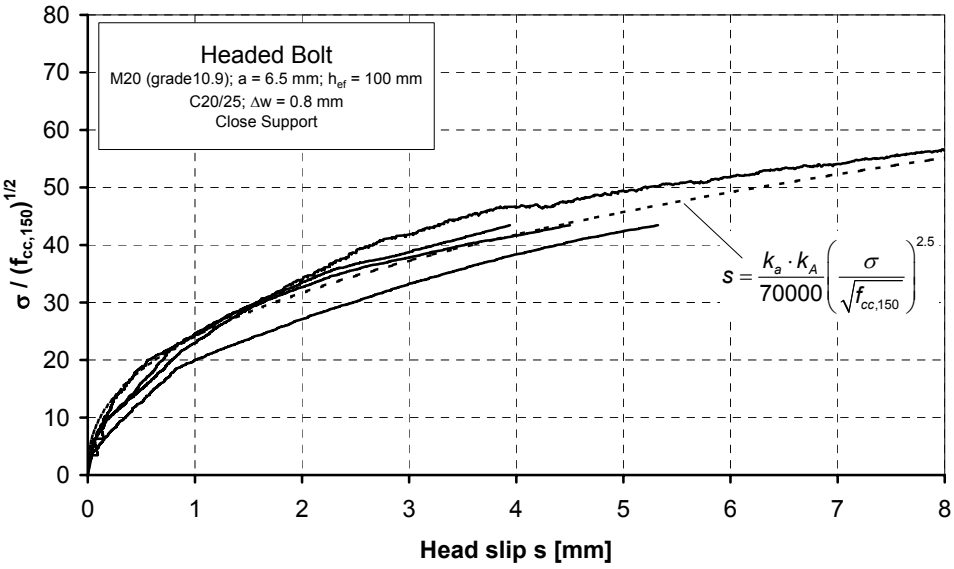

Figure 6.11 ($\sigma / f_{cc}^{0.5}$) versus slip curves for headed bolts in cracked (Δw = 0.8 mm) C20/25 concrete

6.2.2.2 Head slip during cyclic tension loading

The behavior of headed bolts during tension load cycling (<100 cycles) for bearing pressures of 4, 6, 8 and 12 times $f_{cc,150}$ was investigated. The influence of the bearing pressure, concrete strength, as well as the presence of line cracks (Δw = 0.8 mm) passing through the anchors on the cyclic slip behavior was studied. The tests were performed using the close support setup (Figure 6.3). Based on the results, an equation to predict head slip as a function of the number of tension load cycles is proposed.

Reference tests with monotonic load were first performed. The load-displacement curves for tests in C20/25 and C45/55 uncracked concrete and C20/25 cracked concrete (Δw = 0.8 mm) are shown in Figure 6.12 and Figure 6.13, respectively. The load-displacement curve for the anchor shaft (steel curve) is shown for comparison. Yielding

of the anchor steel occurred at about 220 kN. Loading was stopped before steel rupture could occur. Two curves are shown for each test series in concrete.

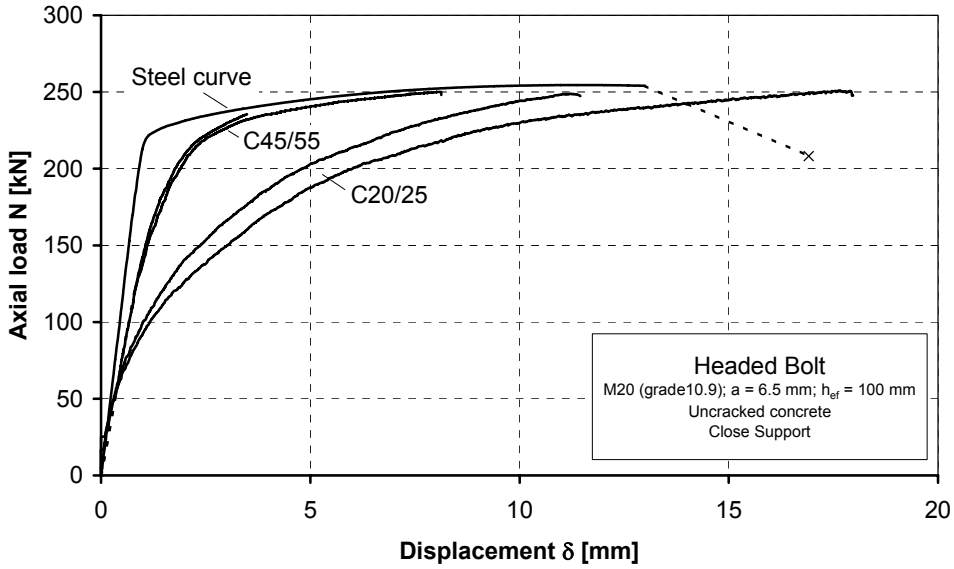

Figure 6.12 Load-displacement curves for the investigated headed bolts under monotonic loading with a close support in uncracked C20/25 and C45/45 concrete (steel curve shown for comparison)

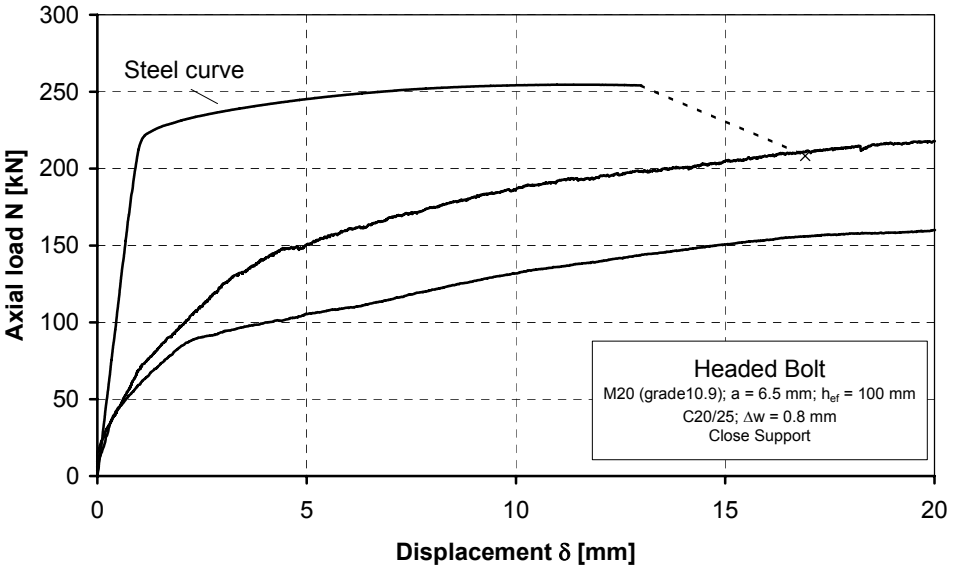

Figure 6.13 Load-displacement curves for the investigated headed bolts under monotonic loading with a close support in cracked (Δw = 0.8 mm) C20/25 concrete (steel curve shown for comparison)

Typical load-displacement curves obtained from the tension cycling tests are shown in Figure 6.14. For tests with high bearing pressure ($12 \cdot f_{cc,150}$) splitting of the anchorage component frequently occurred. Results where splitting was believed to have influenced the slip behavior were neglected when developing the cyclic slip equation.

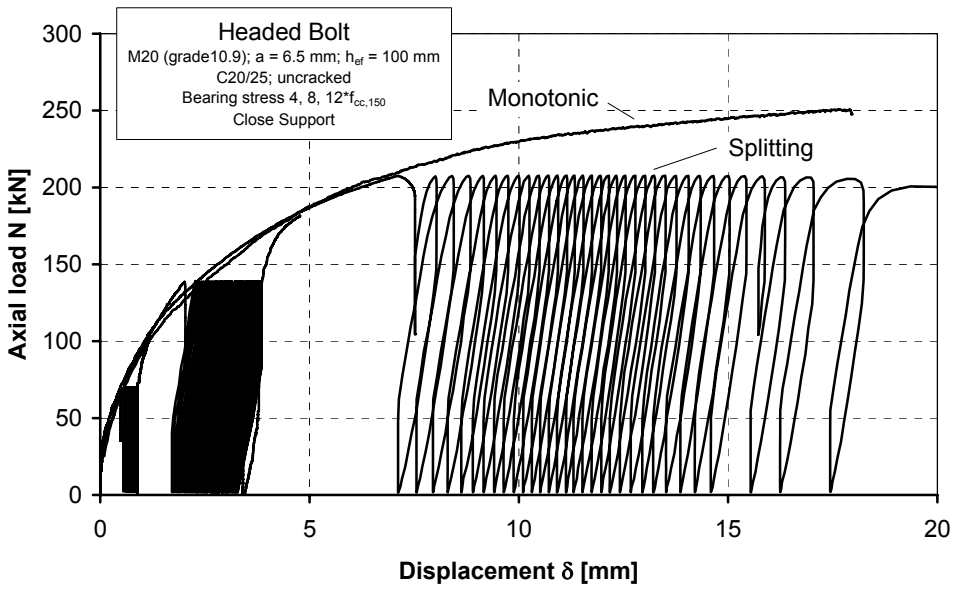

Figure 6.14 Typical load-displacement curves for the investigated headed bolts under tension load cycling with a close support in uncracked C20/25 concrete

Head slip of the anchor during load cycling (s_{cyc}) can be determined by subtracting the fastener displacement during a given cycle from the displacement at the start of cycling. By determining slip in this way, the elastic elongation of the anchor rod is neglected. A typical curve for head slip during cycling as a function of the number of load cycles is shown in Figure 6.15. The complete (full) measured curve is shown along with the curve connecting the slip values after 30, 50 and 100 load cycles. The figure shows that slip increases degressively with the number of load cycles.

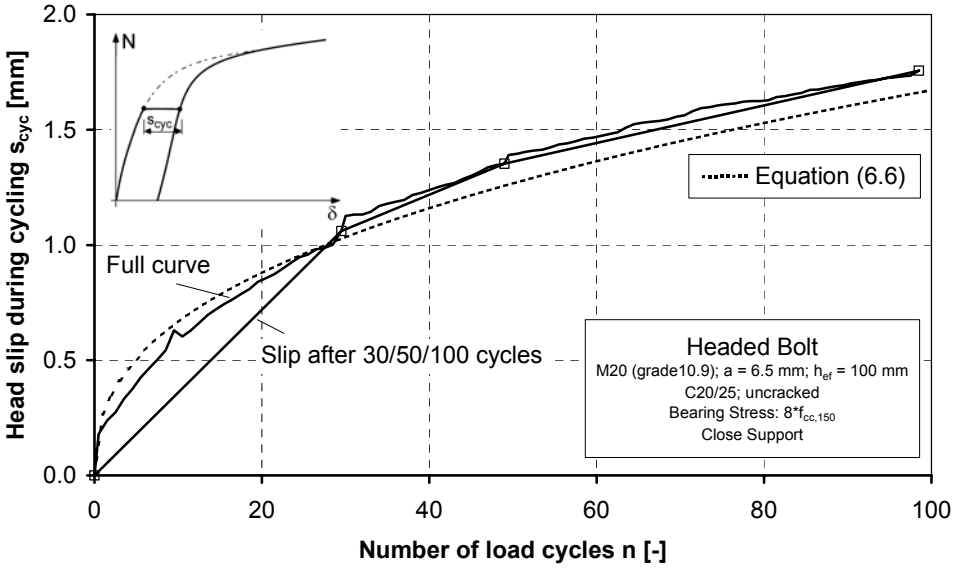

Figure 6.15 Typical head slip versus number of load cycles curve for the investigated headed bolts under tension load cycling

The slip behavior of headed bolts in concrete during tension load cycling is similar to creep behavior under constant load, however, displacement occurs at an accelerated rate during cycling. This behavior was observed by *Rehm and Eligehausen (1977)* for reinforcement lap splices in concrete and has been used in attempts to develop

accelerated creep tests for anchors (*Ehrenstein 1993*). Here, this observation is used to develop an equation to predict the slip of a headed bolt as a function of the number of load cycles for the case of low-cycle, high-magnitude tension load cycling.

Figure 6.16a shows load-displacement curves for the investigated headed bolts in the case where the axial tension load was increased up to a bearing stress of $8 \cdot f_{cc,150}$ and held constant for a duration of 500 seconds (creep loading). Displacement increased due to creep of the highly compressed concrete above the bearing area of the anchor (see Figure 6.7). Figure 6.16b shows load-displacement behavior in comparable tests in which the load was cycled 100 times between a bearing stress of $8 \cdot f_{cc,150}$ and approximately zero at a frequency of 0.5 Hz (cyclic loading). The duration of the cycling was about 200 seconds.

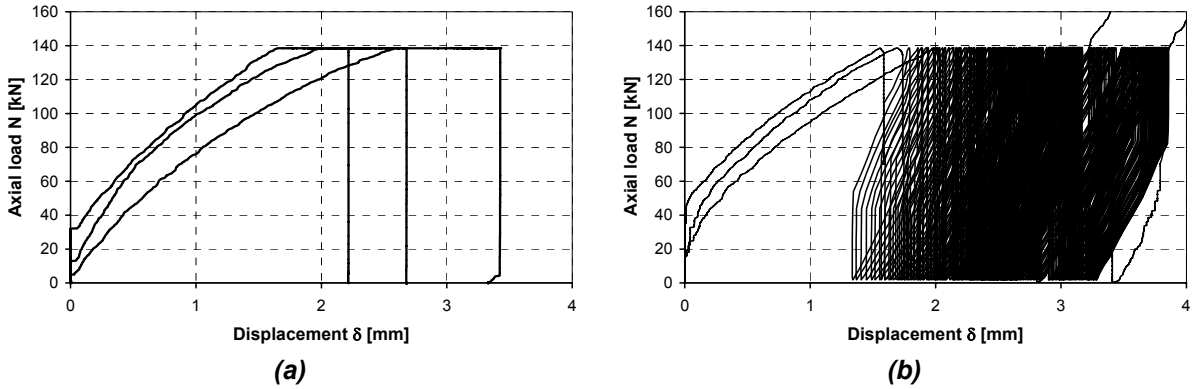

Figure 6.16 Load-displacement curves for investigated headed bolts at a (maximum) bearing stress of $8 \cdot f_{cc,150}$: (a) creep loading; (b) cyclic loading

In Figure 6.17, the slip of the anchors over the duration of the constant loading (creep loading) as well as the slip during cycling (cyclic loading) obtained from the load-displacement curves shown in Figure 6.16 are plotted as a function of time. The figure shows that cycling the load in tension between zero and the applied constant load used in the creep tests greatly accelerated the head slip rate, however, the shape of the curves is similar.

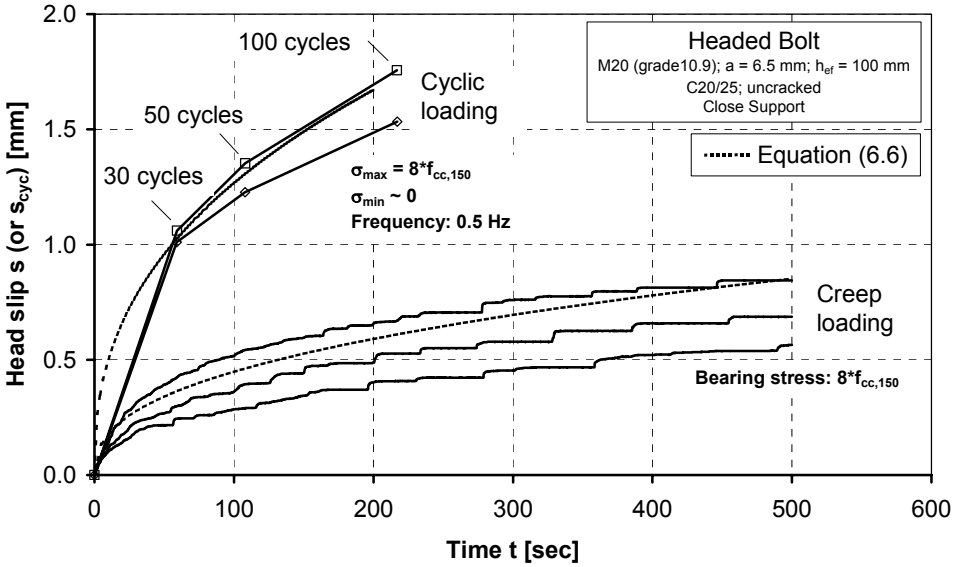

Figure 6.17 Head slip as a function of time for creep and tension load cycling tests with headed bolts in uncracked C20/25 concrete

It is postulated that as the magnitude of the load cycles decreases to zero, the head slip during tension load cycling must converge to the slip due to creep (Figure 6.18).

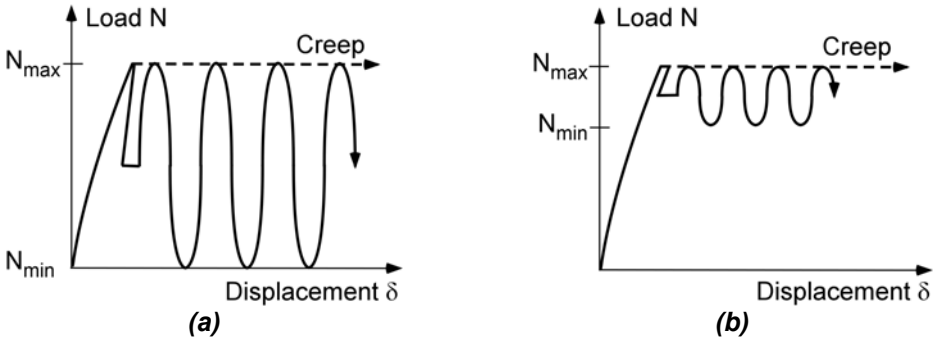

Figure 6.18 Schematic load-displacement curves for creep and cyclic loading; (a) large magnitude tension cycles; (b) small magnitude tension cycles

Deformation of concrete due to creep is frequently modeled by assuming a linear relation between the elastic strain caused by an instantaneous loading $\varepsilon_{el}(t_0)$ and the so-called creep coefficient $\phi(t,t_0)$ (*CEB 1993*). This is expressed:

$$\varepsilon_{cc}(t,t_0) = \varepsilon_{el}(t_0) \cdot \phi(t,t_0) \tag{6.5}$$

where ε_{cc} is the concrete creep strain, t_0 is the age of the concrete at the time of loading in days and t is the age of the concrete in days at the moment considered. The creep coefficient is a function of several material and environmental factors as well as time.

Since it was assumed that the cyclic slip behavior of headed bolts converges to the creep behavior for decreasing cycling amplitude, the proposed equation for head slip during tension load cycling is formulated similarly to Equation (6.5). The similarity is only notational, however, since the equations for creep are intended for uniaxial loading of

concrete up to levels of about 50 percent of the concrete compressive strength and in the case of headed bolts a multi-axial stress state exists with local stresses several times the concrete compressive strength. The proposed equation for head slip during tension load cycling (s_{cyc}) to a constant level can be written as:

$$s_{cyc}(n,f) = s_0 \cdot \Phi(n,f) \tag{6.6}$$

where s_0 is the head slip at the maximum bearing stress ($\sigma = N_{max}/A_h$), which can be calculated using Equation (6.4), n is the number of load cycles and f is the cycling frequency. The cycling coefficient $\Phi(n,f)$ is calculated as:

$$\Phi(n,f) = c_1 \cdot \left[\left(\frac{1}{f} + c_2 \cdot \frac{\Delta\sigma}{\sigma_{\max}} \right) \cdot n \right]^{\alpha} \tag{6.7}$$

where c_1, c_2 and α are constants determined from experimental tests, $\Delta\sigma = (\sigma_{max} - \sigma_{min})$ is the magnitude of the variation in the bearing stress during cycling, σ_{max} and σ_{min} are the maximum and minimum bearing stresses during cycling.

In Equation (6.7) when the magnitude of the variation in the bearing stress during cycling $\Delta\sigma$ goes to zero the cycling coefficient simplifies to:

$$\Phi(n,f) = c_1 \cdot \left(\frac{n}{f} \right)^{\alpha} = c_1 \cdot (t)^{\alpha} \tag{6.8}$$

Equation (6.8) has the same form as the creep coefficient for concrete given in *CEB (1993)*. The constant c_2 is used to weight the contribution to slip due to the load cycling. It was observed in the experiments that the rate of the cycling did not play as significant a role in determining the amount of slip as the number of cycles.

The constants c_1, c_2 and α were calibrated using the head slip data from the present experimental investigations. The values $c_1 = 0.045$, $c_2 = 25$ and $\alpha = 0.4$ were found to give good results when the static slip (s_0) is given in mm. These values should not be applied for general applications without verification using a larger experimental database.

The head slip during tension load cycling as a function of the number of load cycles, along with the values yielded by Equation (6.6) are shown in Figure 6.15 and Figure 6.19 to Figure 6.21. The dashed curves with the filled symbols are the mean values of the experimental tests.

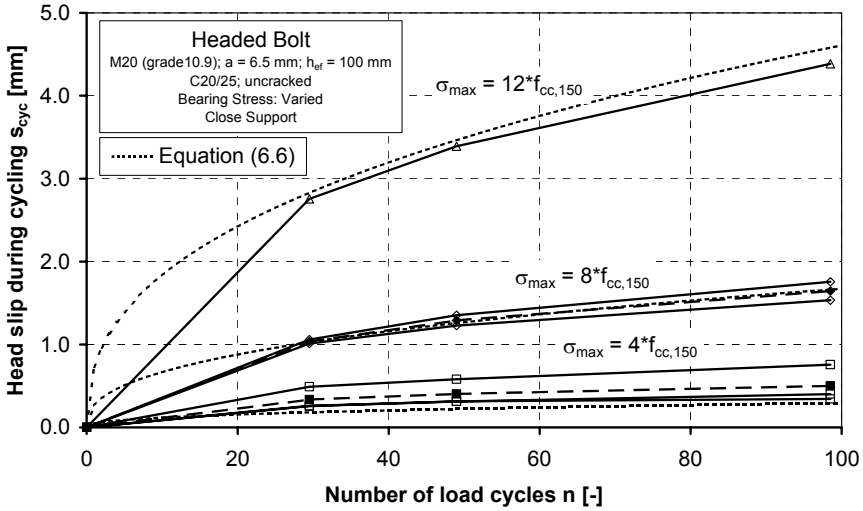

Figure 6.19 Head slip during tension load cycling as a function of the number of load cycles for headed bolts in uncracked C20/25 concrete

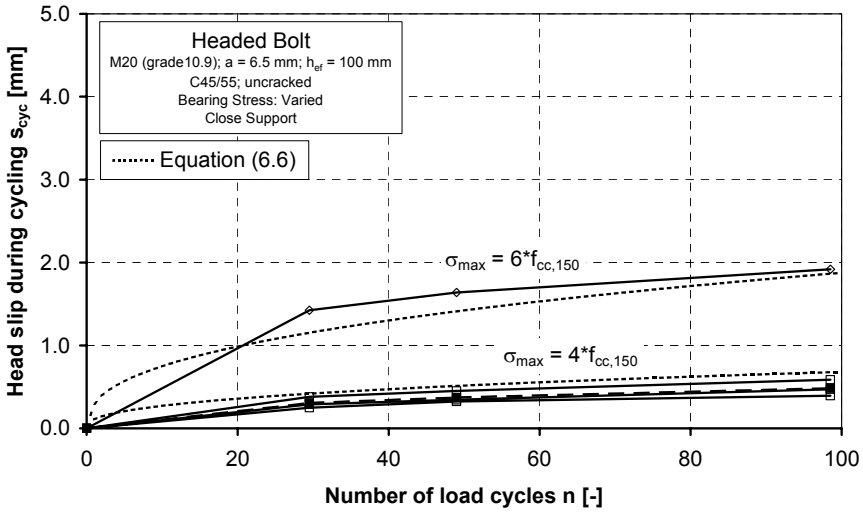

Figure 6.20 Head slip during tension load cycling as a function of the number of load cycles for headed bolts in uncracked C45/55 concrete

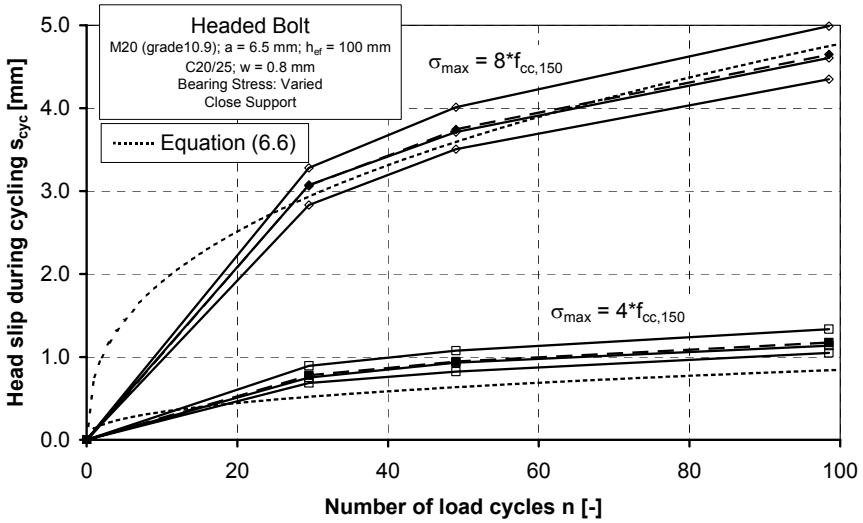

Figure 6.21 Head slip during tension load cycling as a function of the number of load cycles for headed bolts in cracked C20/25 concrete

6.2.2.3 Failure mechanisms for load cycling at near-ultimate levels

6.2.2.3.1 Concrete cone failure

For actual seismic fastening applications with headed anchors, the potential for concrete cone breakout usually exists. It is therefore desired to know how many load cycles of a given amplitude can be resisted without brittle concrete failure. Exploratory tests (*Hoehler 2005a*) with the investigated headed bolt (Figure 6.1) and the wide support setup (Figure 6.4) indicate that concrete cone breakout will occur during tension load cycling when the monotonic envelope curve is transected (Figure 6.22). If the fastener displacement during load cycling is less than that at ultimate load in a comparable monotonic test, the residual strength is not affected by the cycling (Figure 6.23).

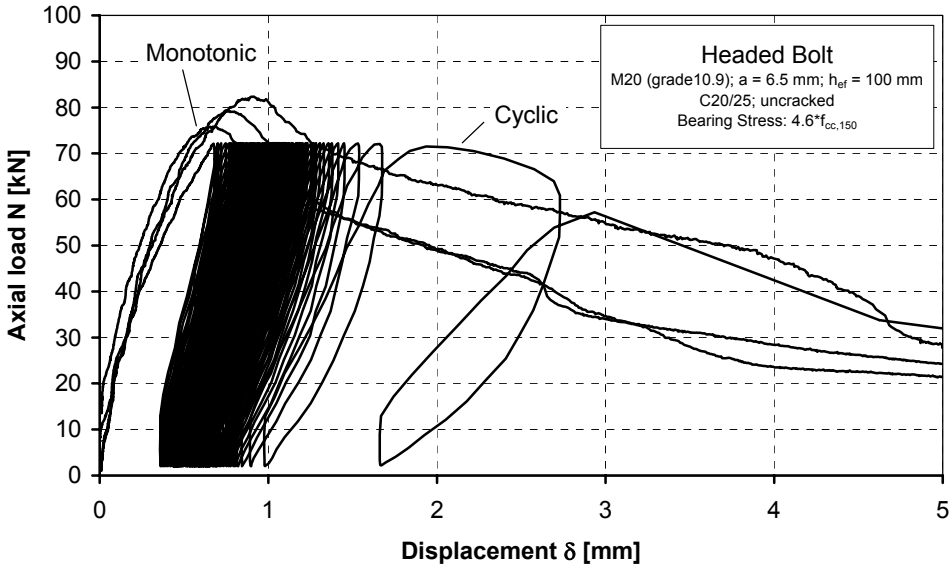

Figure 6.22 Load-displacement curves for headed bolts in uncracked C20/25 concrete (monotonic and cyclic loading with failure during cycling)

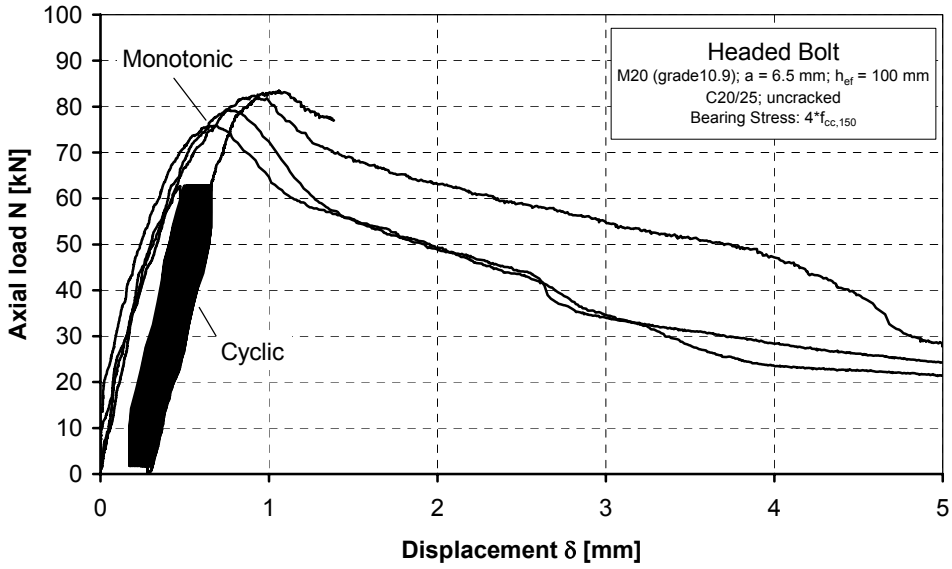

Figure 6.23 Load-displacement curves for headed bolts in uncracked C20/25 concrete (monotonic and cyclic loading with failure after cycling)

Since the shape of the descending branch of the monotonic load-displacement curve in the case of concrete breakout can vary depending on the loading rate and other factors, it is proposed that a reliable indicator for the initiation of failure during tension load cycling is the crossing of the displacement at ultimate load ($\delta_{u,m}$) in a corresponding monotonic test (Figure 6.24). A similar approach is used to design fastenings under creep loading.

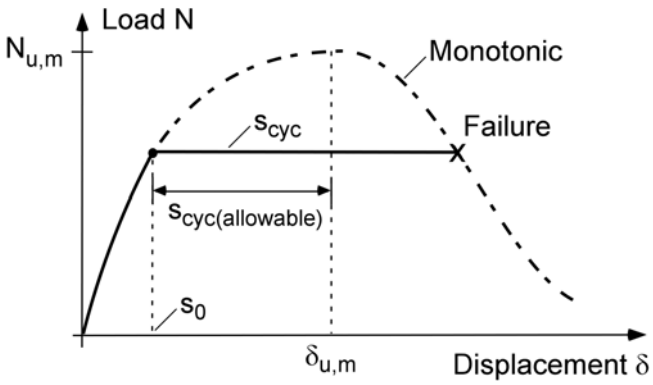

Figure 6.24 Schematic load-displacement curves for tension load cycling in the case of concrete breakout indicating the allowable displacement before failure

For a given anchor geometry and a known displacement at ultimate load from monotonic tests, it is possible to predict whether failure is likely to occur during *n* tension load cycles to a given load using the slip calculated with Equations (6.4) and (6.6). The required check is:

$$s_0 + s_{cyc} \leq \delta_{u,m} \tag{6.9}$$

6.2.2.3.2 Ductile steel failure

The fastener load-displacement curve in Figure 6.25 was generated using the special headed bolt (Figure 6.1) with a M16 grade 8.8 threaded rod. The constant strain length of the threaded rod was about 180 mm (11 times the rod diameter). One hundred tension load cycles were performed after yielding of the steel and the anchor still had significant reserve deformation capacity. Figure 6.25 is shown to contrast the case of ductile steel failure of typical post-installed fasteners as will be discussed in more detail in Section 6.3.2.1.2.

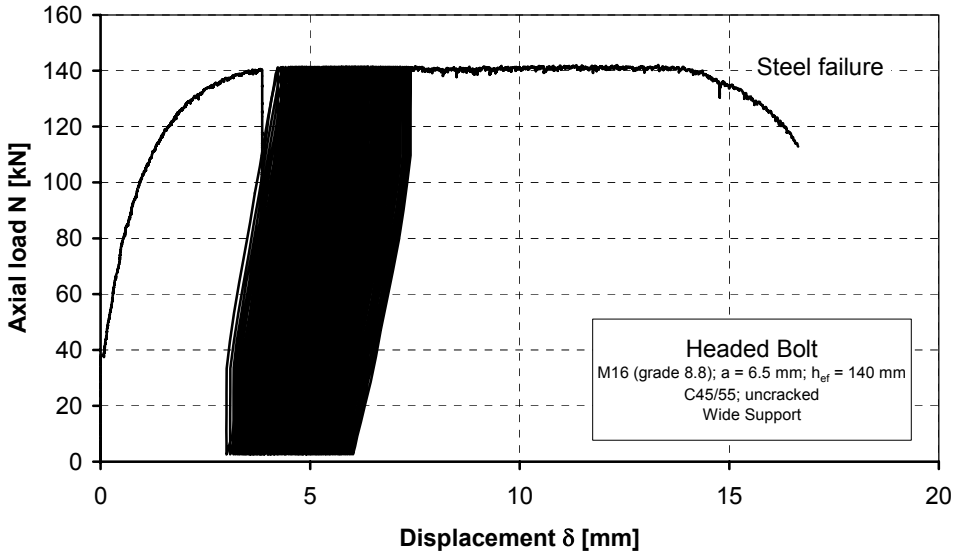

Figure 6.25 Load-displacement curve for tension cycling of a headed bolt with a constant strain length of 180 mm in uncracked C45/55 concrete in the case of steel failure

6.3 Post-installed fasteners

6.3.1 Experimental setups and testing procedures

6.3.1.1 Investigated fasteners

The relevant fastener parameters are summarized in Table 6.1. The fasteners were installed according to the manufacturer's recommendations, except where the effective embedment depth h_{ef} was modified to achieve a desired failure mode (see Table 6.1).

The modified sleeve-type expansion anchors were produced to ensure steel failure in tension. Further details are given in Section 6.3.2.1.2.

Table 6.1 Post-installed fasteners investigated in tension load cycling tests

Fastener Type	Size	Drill Hole Diameter d_0 [mm]	Effective Embedment h_{ef} [mm]	Illustration
Expansion anchor (bolt-type)	M16	16	95[a]	Figure 3.4
Expansion anchor (sleeve-type)	M12	18	80	Figure 3.4
Screw anchor	d_{nom} = 12 mm	10	64[b]	Figure 3.6
Modified expansion anchor (sleeve-type)	M12	18	80	Figure 6.35

[a] Actual h_{ef} = recommended h_{ef} + 10 mm.
[b] $h_{ef} = 0.85 \cdot h_{nom}$ (h_{nom} = 75 mm).

6.3.1.2 Anchorage components

All tests were performed in normal strength (C20/25) wedge-split cracked concrete slabs (see Figure 6.2b; without cast-in bolts).

The anchorage components were produced according to the state of the art after *DIN 1045 (2001)* and *DIN 1048 (1991)*.

The average concrete cube compressive strength ranged between $f_{cc,150}$ = 22.5 N/mm^2 and $f_{cc,150}$ = 31.5 N/mm^2.

6.3.1.3 Loading setups and testing procedures

The fasteners were loaded either monotonically or by cyclic tension loads using a servo-hydraulic cylinder with a capacity of 50 kN. The test setup is shown in Figure 6.26.

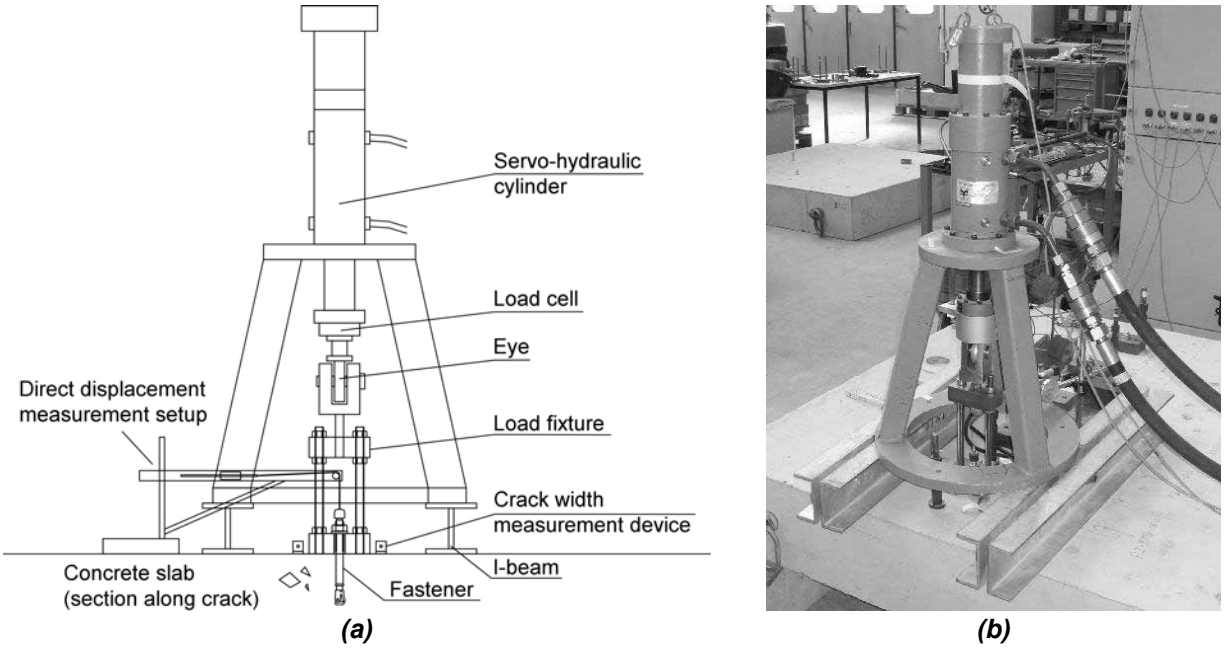

Figure 6.26 Test setup for tension load cycling tests with post-installed fasteners (wide support): (a) schematic; (b) photograph

All tests were performed on single anchors with large anchor spacing and edge distances. The I-beams supporting the load cylinder were located at a suitable distance from the fastener so that complete concrete cone breakout could occur (wide support). The cracks in the anchorage components were opened by Δw = 0.8 mm after installation of the fasteners, but before loading.

In the monotonic tension tests, load was applied under control of the servo-hydraulic cylinder displacement (displacement-controlled test). Ultimate load was reached in approximately 1 to 3 minutes.

In the tension load cycling tests, loading histories similar to that shown in Figure 6.6 were used. Exceptions are presented in the following sections where applicable.

The tension load applied to the fastener N, the displacement of the servo-hydraulic cylinder δ_{cyl}, the fastener displacement δ and the crack opening width Δw were measured continually during the tests.

6.3.2 Results and discussion

6.3.2.1 Failure mechanisms for load cycling at near-ultimate levels

The magnitude of the cyclic loads that might act on a fastener during an earthquake cannot be predicted with the same degree of accuracy as for the case of non-seismic conditions. Therefore, the probability that design load levels will be exceeded is higher than for non-seismic situations. The majority of available experimental studies on the tension load cycling behavior of fasteners conducted prior to the current investigation have focused exclusively on tension load cycling behavior at or below design load levels (< 60% of the mean ultimate capacity). The objective of the tension load cycling tests was to investigate the behavior of fasteners with various failure mechanisms (concrete cone, pull-through, pull-out, steel failure) when a low number of cycles (30 cycles) is performed at load levels of 50%, 90% and 100% of the mean ultimate monotonic capacity $N_{u,m}$. This was done to better understand the 'reserve capacity' of the various failure mechanisms in the case of tension load cycling beyond the intended design level (overload).

6.3.2.1.1 Concrete cone, pull-through and pull-out failure

The investigated unmodified fasteners were selected to produce distinctly different failure modes (Figure 6.27). All of the tested fasteners have a European approval for use in cracked concrete.

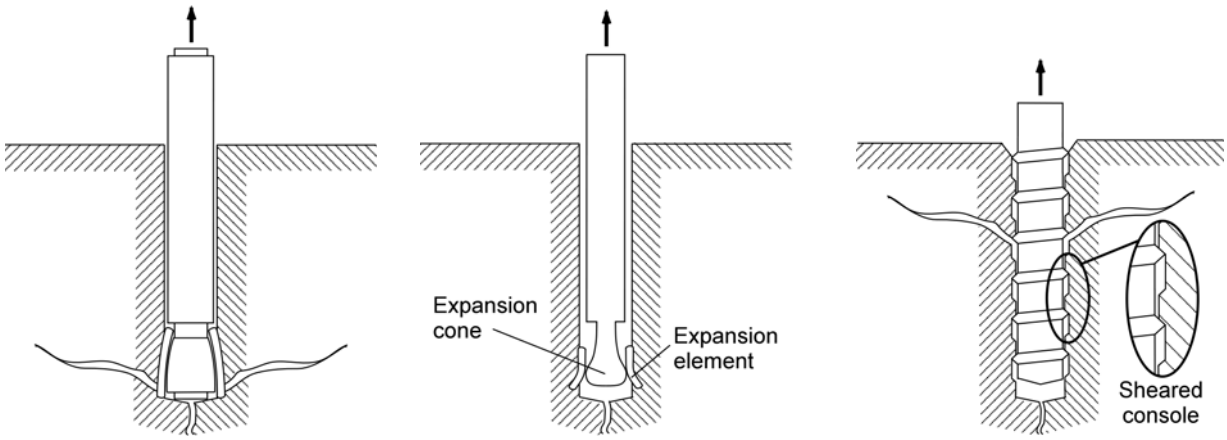

Figure 6.27 Failure modes: (a) sleeve-type expansion anchor (concrete cone); (b) bolt-type expansion anchor (pull-through); (c) screw anchor (pull-out / concrete cone)

Figure 6.28 to Figure 6.30 show typical load-displacement curves for the investigated unmodified fasteners in wide cracks (Δw = 0.8 mm) under tension load cycling. The fasteners were subjected to 30 load cycles at a frequency of 0.5 Hz between 2 kN and 50% or 90% of the mean ultimate reference tension capacity ($N_{u,m}$). If no failure occurred during cycling, the anchors were subsequently loaded to failure in tension to determine the residual strength.

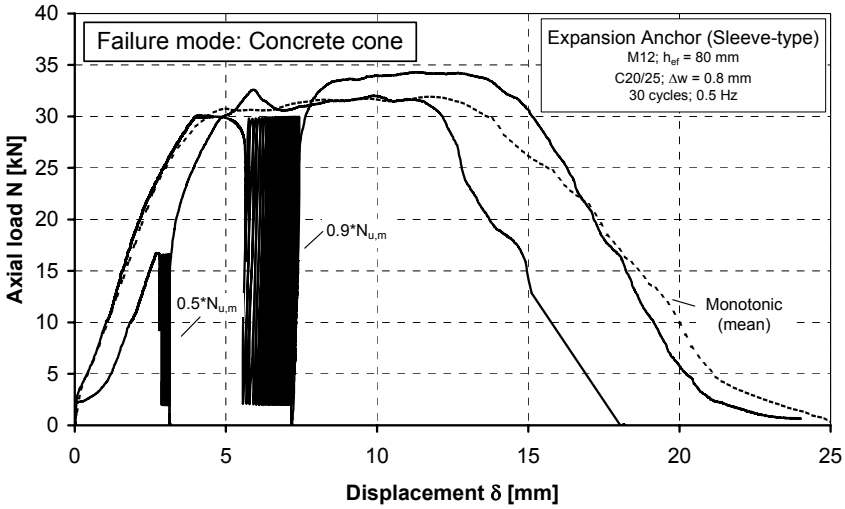

Figure 6.28 Typical load-displacement curves for the M12 expansion anchors (sleeve-type) in wide cracks (Δw = 0.8 mm) at two levels of tension load cycling

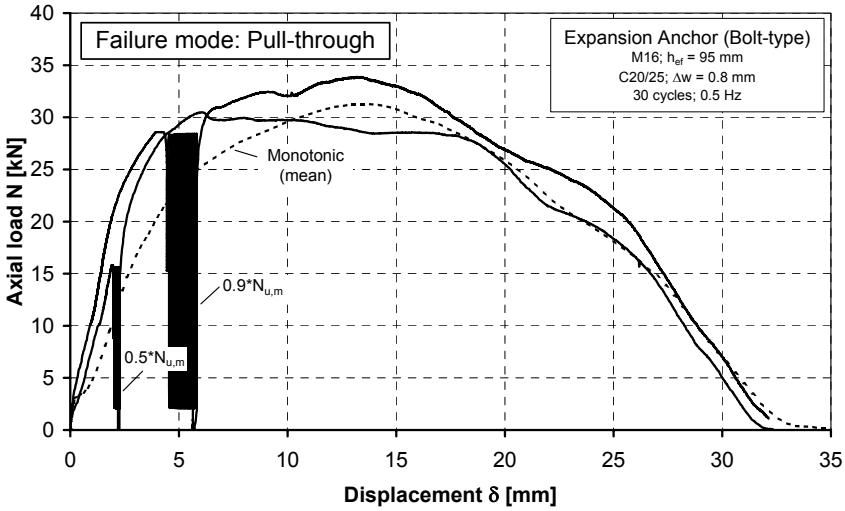

Figure 6.29 Typical load-displacement curves for the M16 expansion anchors (bolt-type) in wide cracks (Δw = 0.8 mm) at two levels of tension load cycling

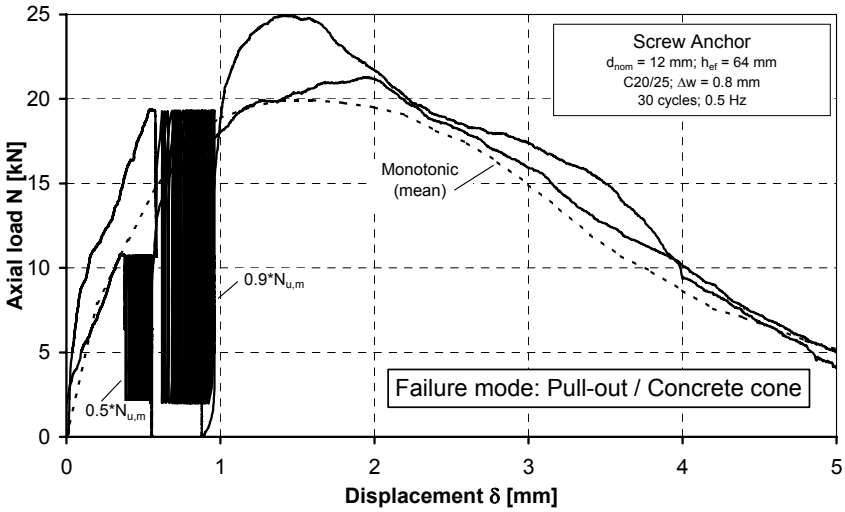

Figure 6.30 Typical load-displacement curves for the screw anchors (d_{nom} = 12 mm) in wide cracks (Δw = 0.8 mm) at two levels of tension load cycling

Figure 6.28 to Figure 6.30 indicate that the investigated fasteners could resist the prescribed load cycling at levels up to 90% of $N_{u,m}$ without difficulty. In fact, the strength subsequent to cycling was in several cases slightly greater compared to the mean monotonic reference strength (Figure 6.31). This is likely a result of compaction of the concrete around the point of load transfer during the load cycling.

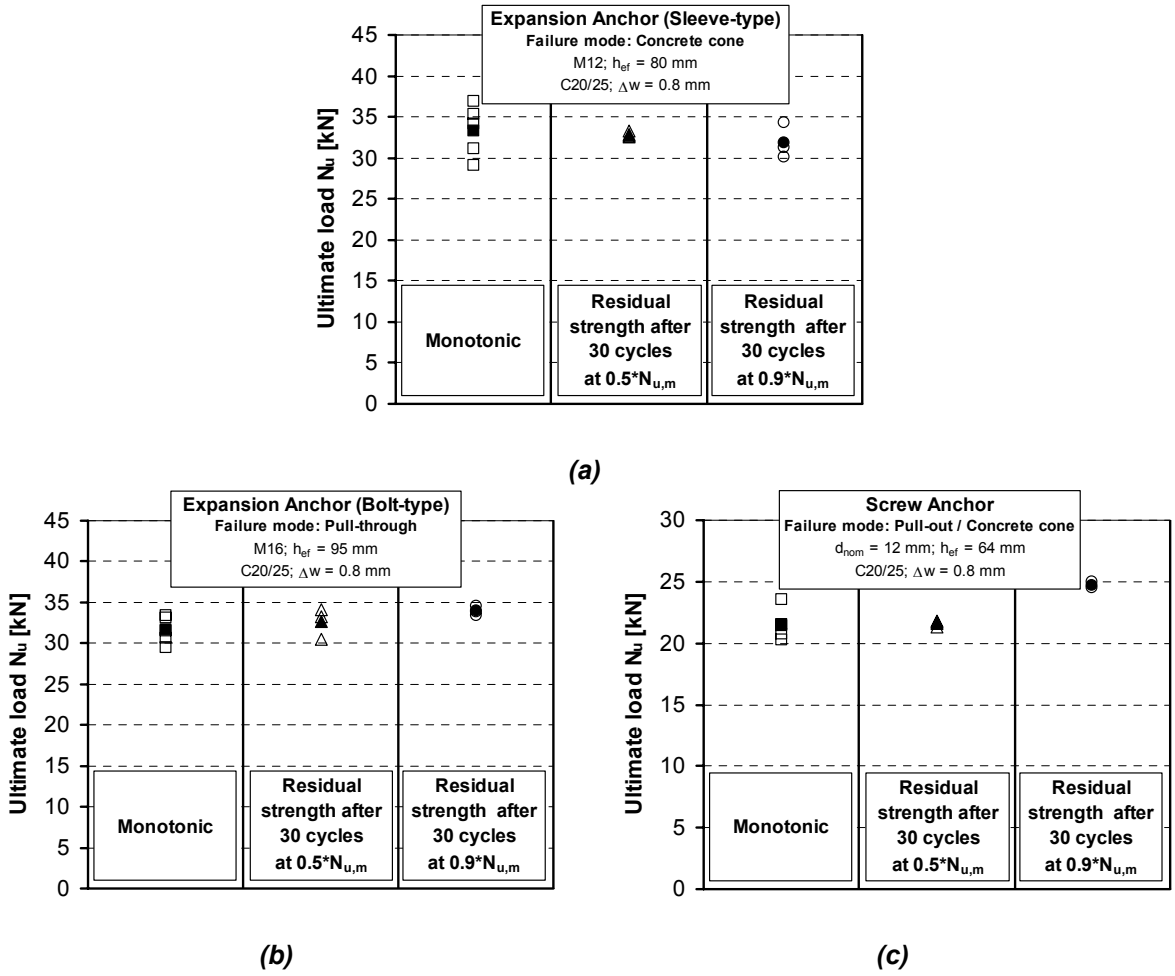

Figure 6.31 Ultimate loads for the investigated fasteners in wide crack widths (Δw = 0.8 mm) after various levels of tension load cycling (solid symbol = mean): (a) sleeve-type expansion anchor (concrete cone); (b) bolt-type expansion anchor (pull-through); (c) screw anchor (pull-out / concrete cone)

Load cycling at (near) 100% of the ultimate load was also performed. Typical load-displacement curves for the investigated unmodified fasteners are shown in Figure 6.32 to Figure 6.34. For all of the investigated fastener types it appeared that failure during tension load cycling occurred when the load-displacement curve transected the monotonic envelope. This was true in spite of the fact that each fastener failed by a different mode of failure. Furthermore, all of the investigated fasteners exhibited a capacity to resist several tension load cycles (> 5 cycles) at near-ultimate load levels.

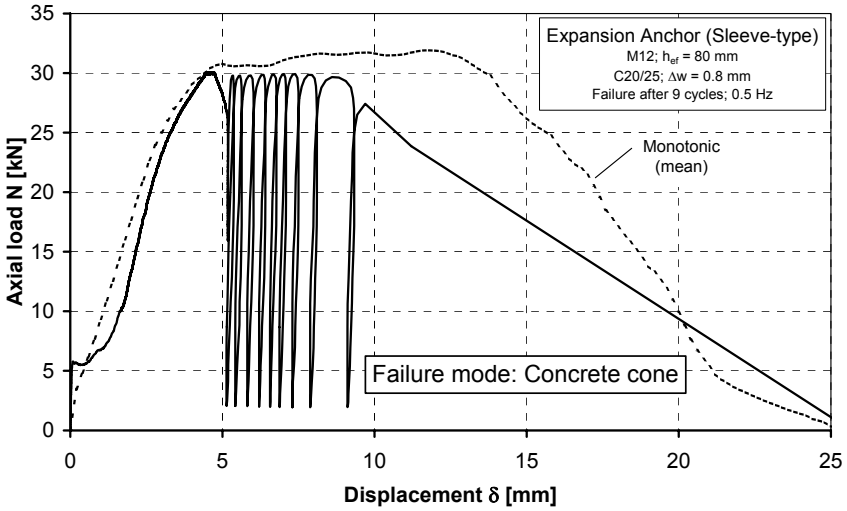

Figure 6.32 Load-displacement curve for the M12 expansion anchor (sleeve-type) in a wide crack (Δw = 0.8 mm) for tension cycling at 100% $N_{u,m}$ (monotonic curve shown for comparison)

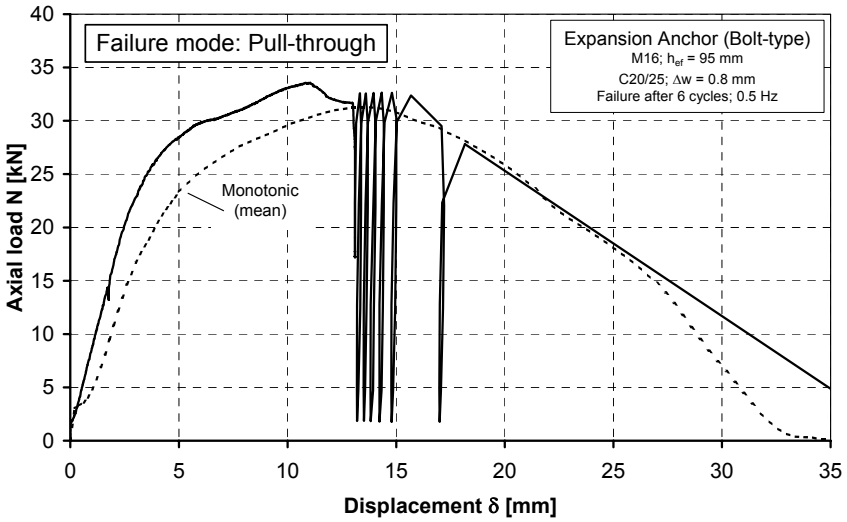

Figure 6.33 Load-displacement curve for the M16 expansion anchor (bolt-type) in a wide crack (Δw = 0.8 mm) for tension cycling just after ultimate load (monotonic curve shown for comparison)

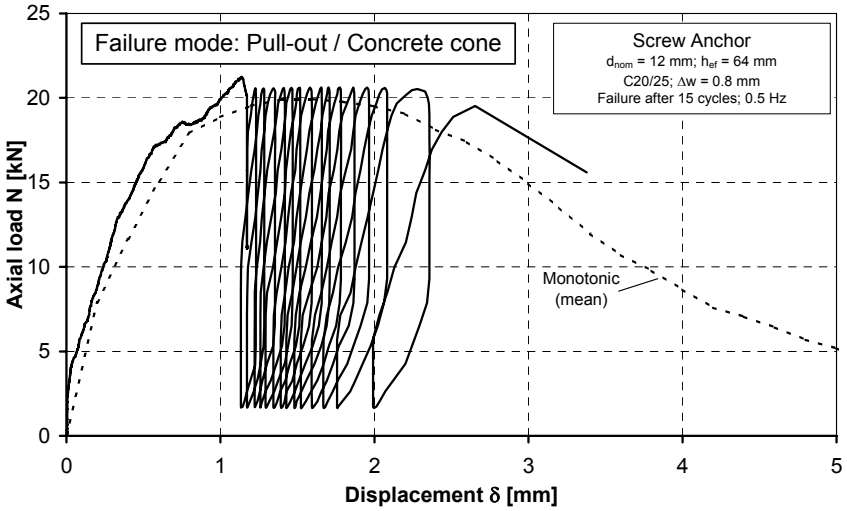

Figure 6.34 Load-displacement curve for the screw anchor (d_{nom} = 12 mm) in a wide crack (Δw = 0.8 mm) for tension cycling at 100% $N_{u,m}$ (monotonic curve shown for comparison)

In the case of concrete cone breakout, failure was initiated by repeated opening of the cracks that formed at the anchor head (Figure 6.27a). The observed load-displacement behavior (Figure 6.32) supports the conclusion that concrete cone breakout during tension load cycling will occur when the fastener displacement during load cycling exceeds the displacement at ultimate load ($\delta_{u,m}$) in a corresponding monotonic test (see Section 6.2.2.3.1). The predictive equations for anchor slip developed for headed bolts (Section 6.2.2.2) do not apply, however, to post-installed fasteners. The relatively long plateau for the investigated sleeve-type expansion anchors (Figure 6.32), which ultimately failed by concrete cone failure, indicates that the fastener expansion elements may have slipped or that the expansion cone was pulled into the expansion elements (follow-up expansion) at ultimate load prior to complete failure of the concrete cone. From the test results it was not possible to determine which of these two possibilities occurred. The relatively good cyclic performance at ultimate load in spite of the fact that concrete cone failure occurred, however, indicates that follow-up expansion, rather than slip, occurred. Nevertheless, concrete cone breakout is an undesirable failure mode as the high stress concentration at the crack tip during cycling will quickly lead to propagation of the crack and (fatigue) failure of the concrete.

In the case of pull-through failure (Figure 6.27b), failure during cycling occurred when the expansion cone slipped past the expansion elements and could no longer provide follow-up expansion. For the investigated bolt-type expansion anchors, which failed by pull-through, the behavior strongly depended on whether the cycling took place on the ascending or descending branch of the load-displacement curve. If load cycling took place on the ascending curve, the cycles were resisted without difficulty. If the cycling took place just after the peak load, failure occurred after fewer than 10 load cycles (Figure 6.33).

In the case of combined pull-out and concrete cone failure of the screw anchors (Figure 6.27c), failure occurred when the consoles between the screw threads were completely sheared off. Therefore, the amount of displacement that the anchor could undergo during cycling (Figure 6.34) before failing is a function of the thread spacing.

6.3.2.1.2 Ductile steel failure

Ductile steel failure is encouraged in seismic design standards based on three presumptions:

(1) steel failure is associated with larger deformations than other failure modes;
(2) material hysteresis can occur during cycling;
(3) load cycling behavior is predictable at high (near-ultimate) load levels.

Exploratory tests were performed using sleeve-type expansion anchors to see whether design for ductile steel failure according to the provisions in *ACI 318 Appendix D (2005)* and the *CEN TS (in preparation)* was possible and if the presumed behavior would indeed be observed.

In ACI 318, a ‘ductile steel element’ is simply defined as an element with a tensile test elongation of at least 14 percent and a reduction in area of at least 30 percent. Tensile

test elongation is typically determined after rupture by fitting the two broken pieces of a specimen (e.g. a bolt) closely together and comparing the initial and final lengths over a specified measurement length (*ASTM F606M 1998*), i.e. the plastic elongation is relevant. In the *CEN TS (in preparation)* the definition of ductility is similar, however, it is additionally stipulated that:

(1) the nominal ultimate steel strength should not exceed 800 MPa, the ratio of nominal steel yield strength to nominal ultimate strength should not exceed 0.8 and the tensile test elongation (measured over a length equal to 5 times the fastener diameter d) should be at least 12 percent;

(2) fasteners that incorporate a reduced section, e.g. threads, should satisfy the following conditions:
   a. for fasteners loaded in tension, the strength of the reduced section should either be greater than 1.1-times the yield strength of the unreduced section or the stressed length of the reduced section should be ≥ 5·d (d = fastener diameter outside the reduced section);
   b. for fasteners loaded in shear or which shall redistribute shear forces, the begin of the reduced section should either be ≥ 5·d below the concrete surface or in the case of threaded fasteners the threaded part should extend ≥ 2·d into the concrete;

(3) if a leveling layer is present between the fixture and the anchorage component, in the case of shear loading the mortar should have a compressive strength ≥ 30 N/mm^2 and a thickness ≤ d/2.

The additional requirements in the CEN Technical Specification are intended to ensure that the desired ductile behavior can be achieved.

According to ACI 318 Appendix D the seismic design resistance $R_{d,eq,ACI}$ shall be determined as:

$$R_{d,eq,ACI} = 0.75 \cdot \phi \cdot R_n \tag{6.10}$$

where ϕ is the reduction factor for a given failure mode and R_n is the governing nominal strength in tension or shear. To ensure that the design of a fastening is governed by the steel strength of the fastener, it must be shown that the design strength for steel failure is less than the design strength for all other appropriate failure modes. Considering the case of tension loading and assuming that only concrete breakout failure must be checked, i.e. splitting of the concrete and pull-out are assumed not to occur, it must be shown that:

$$N_{d,eq,ACI} \leq 0.75 \cdot \phi_s \cdot N_{sa} \leq 0.75 \cdot \phi_c \cdot N_{cb} \tag{6.11}$$

where N_{sa} is the nominal (characteristic) steel tensile strength and N_{cb} is the characteristic concrete breakout strength. Applying the required reduction factor ϕ_s = 0.75 for ductile steel failure in tension and ϕ_c = 0.65 for concrete breakout of a post-

installed fastener without supplementary reinforcement and low installation sensitivity, one obtains:

$$N_{sa} \leq 0.86 \cdot N_{cb} \tag{6.12}$$

Thus, the characteristic steel failure load must be below 86% of the characteristic concrete breakout load. The ratio between the failure loads in the *CEN TS (in preparation)* is more conservative.

Remaining by the case of tension, two possibilities exist to achieve the required ratio between the steel and concrete failure loads:

(1) increase the fastener embedment depth;
(2) reduce the fastener steel cross-section.

The investigated sleeve-type torque-controlled expansion anchors M12 (grade 8.8 steel) would require an effective embedment depth of about h_{ef} = 180 mm in normal strength (C20/25) cracked concrete to meet the ACI 318 requirements for steel failure in seismic design. This approach was not possible since the investigated fastener reaches its pull-out load limit long before the steel failure load. Therefore, the required ratio between the steel and concrete failure loads was achieved by reducing the steel cross-section of the anchor rod to a diameter of 5.5 mm over a length of about 40 mm (Figure 6.35). The reduced length of 40 mm (3.3·*d*) did not quite satisfy the CEN Technical Specification requirement of 5·*d* (60 mm). It should be noted that reducing the cross-section of a fastener is not allowed in practice and would not be practical for several reasons, e.g. failure could occur during torquing.

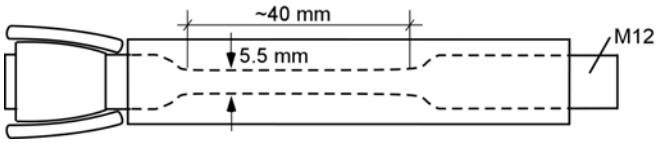

Figure 6.35 Sleeve-type torque-controlled expansion anchor with reduced cross-section

The monotonic load-displacement behavior of a modified and unmodified sleeve-type expansion anchor is shown in Figure 6.36. The figure demonstrates that the intended goal of achieving relatively large displacements is not met by the modified fastener. This is because the length over which plastic straining of the bolt occurred was not sufficient. The anchor rod elongated plastically about 3.5 mm before the steel ruptured (measured on failed specimen). This translates to about 9% plastic elongation measured over the length of the reduced section (40 mm). Had the modified anchor met the CEN Technical Specification requirement of an elongation of 12% over the length of the reduced section, the plastic elongation would have been 4.8 mm. To achieve the same displacement at peak load as for concrete cone failure (~12 mm), the length over which plastic strains occur must increase to about 15·d if a uniform strain of 5% in the steel is assumed.

Figure 6.36 also shows that the steel failure load exceeded the characteristic failure load allowed by the *ACI 318 Appendix D (2005)* requirements by about 25%. This is due to the fact that the mean ultimate steel strength is larger than the characteristic ultimate strength used for design and due to over-strength of the fastener steel. In light of this, it is questionable whether the 14% difference between characteristic steel and concrete failure loads required by ACI 318 is sufficient. This issue is discussed in Chapter 8.

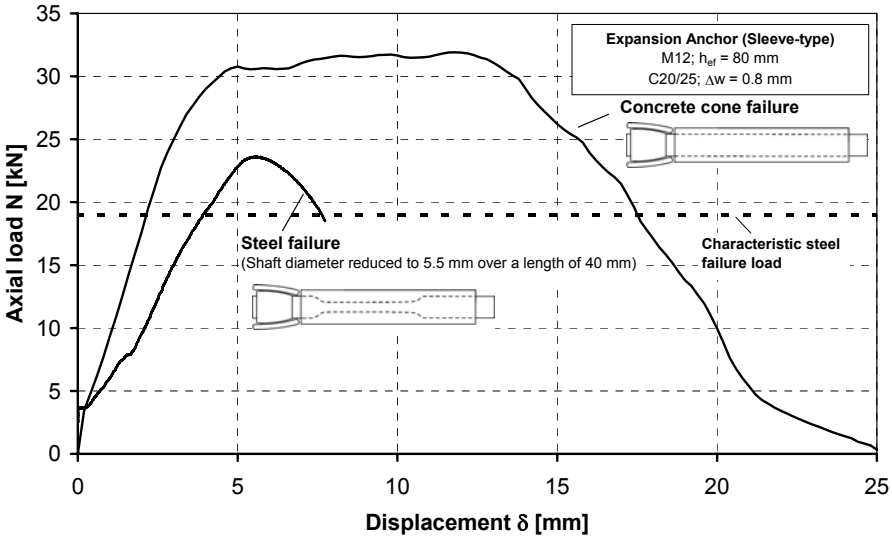

Figure 6.36 Load-displacement response of normal and modified M12 sleeve-type expansion anchors under monotonic loading

Tests in which the modified fasteners were subjected to 30 load cycles at 100% of the ultimate steel failure load were also performed. Figure 6.37 indicates that the cycles could be easily resisted by the fastener and residual deformation capacity was present. Furthermore, the ultimate load could be predicted with relatively high accuracy due to the low scatter of the failure strength of the steel. The figure demonstrates, however, that the hysteretic behavior in tension is nearly non-existent and thus little energy dissipation occurs.

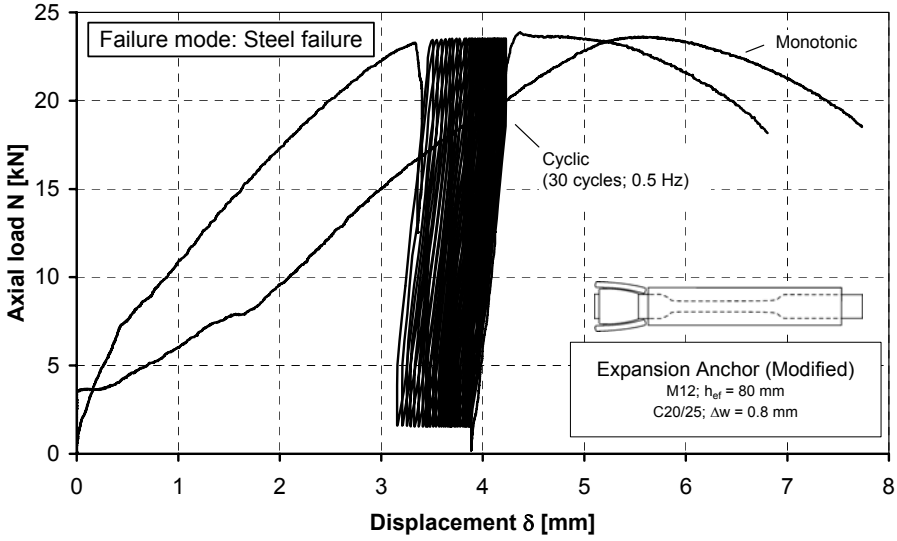

Figure 6.37 Load-displacement response of modified M12 sleeve-type expansion anchors under monotonic and cyclic loading at 100% $N_{u,m}$

6.3.2.2 Influence of load cycling frequency

Simulated seismic load cycling tests in fastener qualification guidelines (Chapter 3; Section 3.4.3) use load cycling frequencies between 0.1 Hz and 2 Hz. Load cycling frequencies ranging from 1 Hz to 10 Hz are believed to be representative of the energetic oscillations of nonstructural components and systems during an earthquake (Chapter 4; Section 4.3.2). It was desired to verify that increased cycling rate does not affect the response of fasteners.

Tension load cycling tests were performed using the investigated sleeve-type and bolt-type expansion anchors and screw anchors in wide static cracks (Δw = 0.8 mm). The tension load was first cycled 30 times between an upper limit of 90% of the mean ultimate load and a lower limit of 2 kN. Load cycling frequency of 0.5 Hz or 5 Hz was used. Subsequent to the load cycling, a quasi-static pull-out test was performed to determine the residual strength of the fastener.

The mean ultimate loads and the fastener displacements after 30 cycles are summarized in Table 6.2. Two series of (static) reference tests were performed for each fastener type to eliminate the influence of the concrete age and strength. In all tests, the sleeve-type expansion anchor failed by concrete breakout, the bolt-type expansion anchor failed by pull-through and the screw anchor failed in a combination of concrete cone failure and pull-out along at the lower portion of the screw.

Table 6.2 Fastener strength and displacement after 30 load cycles at 0.5 or 5 Hz

Fastener Type	Type of Loading	No. of Tests	Mean Ultimate Load $N_{u,m}$ [kN]	COV [%]	$\frac{N_{u,m}}{N_{u,m(static)}}$	Mean Disp. during 30 cycles δ_{30} [mm]	COV [%]	$\frac{\delta_{30}}{\delta_{30,0.5Hz}}$
Expansion Sleeve (M12)	Static	5	33.32	11.0	**1**	-	-	**-**
	Cycling 0.5 Hz	1	34.31[a]	-	**1.03**	1.75	-	**1**
	Static	3	29.75	2.6	**1**	-	-	**-**
	Cycling 5 Hz	2	32.10[a]	8.0	**1.08**	1.36	18.7	**0.78**
Expansion Bolt (M16)	Static	5	31.61	5.0	**1**	-	-	**-**
	Cycling 0.5 Hz	3	33.97[a]	1.8	**1.07**	1.43	11.1	**1**
	Static	5	28.46	6.1	**1**	-	-	**-**
	Cycling 5 Hz	2	28.86[a]	1.7	**1.01**	0.90	2.3	**0.63**
Screw Anchor (d_{nom} = 12 mm)	Static	5	21.50	6.0	**1**	-	-	**-**
	Cycling 0.5 Hz	2	24.74[a]	1.3	**1.15**	0.58	48.8	**1**
	Static	3	13.26	11.0	**1**	-	-	**-**
	Cycling 5 Hz	3	16.95[a]	8.6	**1.28**	0.33	22.1	**0.57**

[a] Residual strength after 30 tension load cycles.

It can be concluded from Table 6.2 that increasing the cycling frequency from 0.5 Hz to 5 Hz did not negatively affect the residual fastener strength regardless of the failure mode. Furthermore, the increased load cycling frequencies led to a decrease in the amount of slip during cycling for all of the investigated failure modes. The smaller

displacements at higher load cycling frequencies are believed to be a consequence of the shorter test duration and resulting smaller creep.

Reevaluation of the tests performed by *Eibl and Keintzel (1989a)* (Chapter 3, Section 3.3.1.1) generally support these conclusions (Table 6.3). Note that the results for cycling in a 1.1 mm crack are based on only two tests per series.

Table 6.3 Residual strength and fastener displacement after 10 load cycles at 1, 5 or 10 Hz (after Eibl and Keintzel 1989a)

Fastener Type	Crack Width [mm]	Type of Loading	No. of Tests	Mean Ultimate Load $N_{u,m}$ [kN]	COV [%]	$\frac{N_{u,m}}{N_{u,m(static)}}$	Mean Disp. after 10 cycles δ_{10} [mm]	COV [%]	$\frac{\delta_{10}}{\delta_{10,1Hz}}$
Undercut Anchor (M12)	0.7	Static	7	37.8	12.3	**1**	-	-	**-**
		Cycling 1 Hz	6	37.8[a]	7.2	**1.00**	4.28	51.3	**1**
		Cycling 5 Hz	6	36.2[b]	9.6	**0.96**	4.08	39.9	**0.95**
		Cycling 10 Hz	7	36.4[c]	12.2	**0.96**	2.91	35.5	**0.71**
	1.1	Static	2	28.7	19.2	**1**	-	-	**-**
		Cycling 1 Hz	2	29.1[a]	4.4	**1.01**	3.20	9.4	**1**
		Cycling 5 Hz	2	29.3[b]	5.3	**1.02**	3.95	16.1	**1.23**
		Cycling 10 Hz	2	30.4[c]	11.2	**1.06**	2.55	30.5	**0.80**

[a] Residual strength after 10 cycles.
[b] Residual strength after 50 cycles.
[c] Residual strength after 100 cycles.

6.3.2.3 Influence of load cycling pattern

Simulated seismic load cycling tests in existing fastener qualification guidelines (Chapter 3; Section 3.4.3) make use of three load cycling patterns:

(1) cycling at a constant load level followed by monotonic loading to failure (*DIBt 1998*);
(2) cycling at stepwise decreasing load levels followed by monotonic loading to failure (*ACI 355.2 2004*, *AC193 and AC308 2005*, *CSA-N287.2 2003*);
(3) cycling at stepwise increasing load levels up to failure (*SEAOSC 1997*).

Silva (2001) found that headed bolts and undercut anchors tested in tension and shear according to the DIBt, ACI 355.2 and SEAOSC methods yielded similar allowable design loads although the loading patterns and testing procedures are quite different. *Silva (2001)* remarks that the result is likely unique to undercut-type anchors that do not suffer dramatic capacity reductions in cracked concrete. *Silva (2001)* further argues that although all of the methods yield similar design loads, a stepwise increasing load (SEAOSC style test) is preferable because it provides additional information about the stiffness of the fastener throughout the entire loading range, whereas the 'pass/fail' style ACI 355.2 and DIBt tests provide only limited information about the cycling response at near-ultimate load levels.

The work performed by *Silva (2001)* is extended here to other fastener types suitable for use in cracked concrete for the case of tension load cycling. Since it has been shown

that small tension load cycles performed subsequent to larger load cycles do not have a significant influence on fastener behavior (Chapter 3; Section 3.3.1.4), in the present investigation only DIBt and SEAOSC style tests are investigated.

There were a few notable differences between the actual *SEAOSC (1997)* and *DIBt (1998)* tests and those performed in the present investigation. In the present investigation, all tests were performed in a crack width of Δw = 0.8 mm. In the DIBt style tests, 30 load cycles were performed between an upper load (N_{max}) of 90% of the mean ultimate reference tension capacity $N_{u,m}$ and a lower load (N_{min}) of 2 kN (Figure 6.38a). In the SEAOSC style tests, the load levels were selected such that 30 cycles were completed at the end of the load cycling at 90% $N_{u,m}$ (Figure 6.38b).

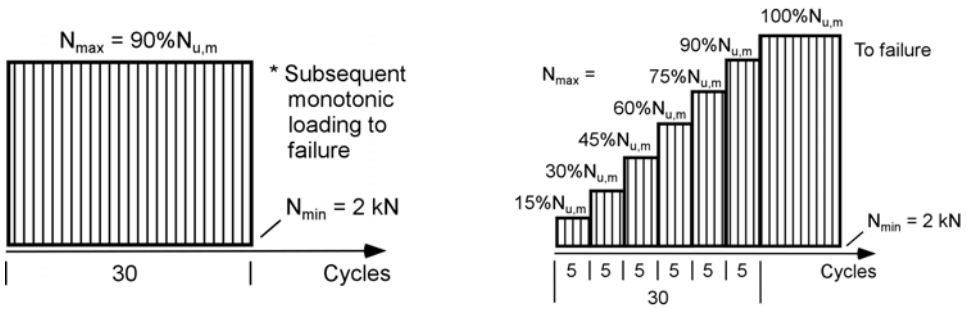

Figure 6.38 Tension load cycling: (a) DIBt style test; (b) SEAOSC style test

Typical load-displacement curves for the two loading histories are shown in Figure 6.39 for the investigated bolt-type expansion anchor.

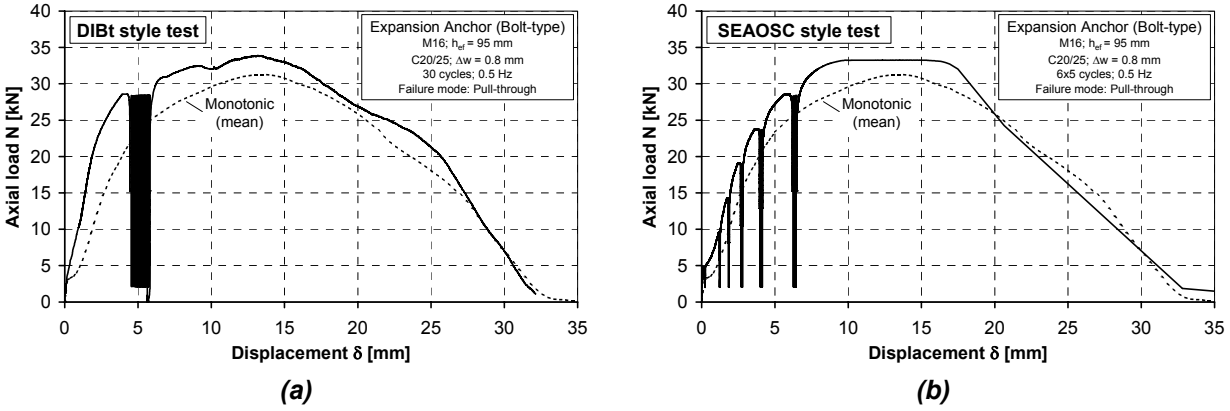

Figure 6.39 Comparison of typical load-displacement response for fasteners subjected to tension load cycling: (a) DIBt style test; (b) SEAOSC style test

The load-displacement curves for all of the investigated fasteners subjected to the SEAOSC style test are shown in Figure 6.40 to Figure 6.42. The failure modes for the fasteners were the same as discussed in Section 6.3.2.1.1. The figures show that for all of the fasteners the load-displacement curves during stepwise increasing load cycling with 5 cycles per step tended to follow the monotonic envelopes.

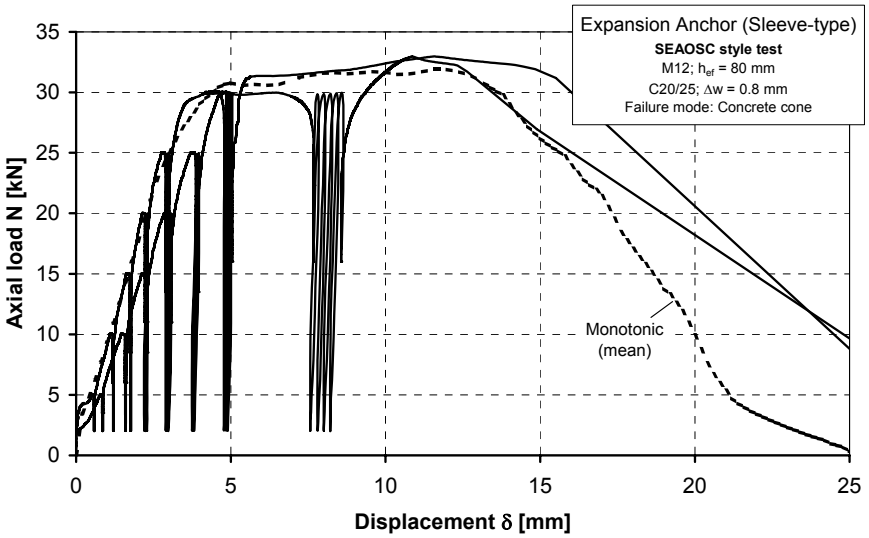

Figure 6.40 Load-displacement response for M12 expansion anchors (sleeve-type) subjected to SEAOSC style test tension load cycling

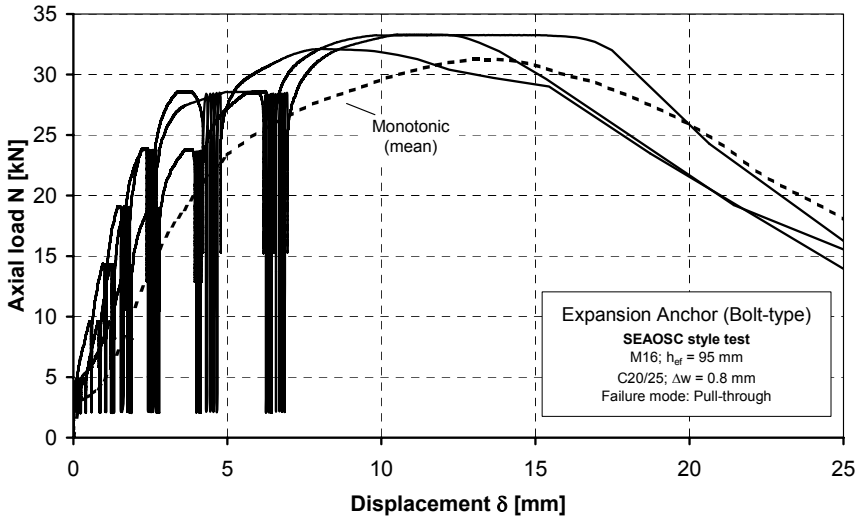

Figure 6.41 Load-displacement response for M16 expansion anchors (bolt-type) subjected to SEAOSC style test tension load cycling

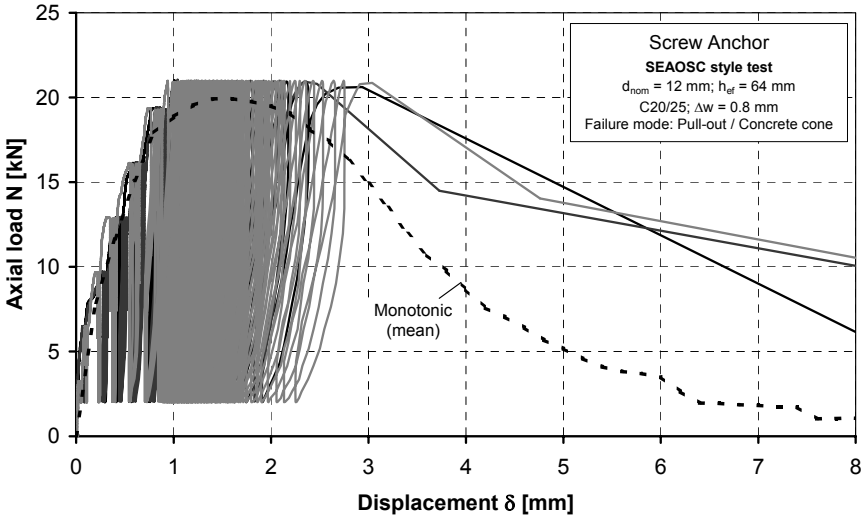

Figure 6.42 Load-displacement response for screw anchors (d_{nom} = 12 mm) subjected to SEAOSC style test tension load cycling

Table 6.4 shows fastener displacements recorded at $N_{mid} = (N_{max} - N_{min})/2 + N_{min}$ after 30 load cycles. The data show that the type of test (DIBt or SEAOSC style) had little influence on the fastener displacement after 30 load cycles in spite of the fact that in the SEAOSC style tests several of the cycles were performed at a low load level. Furthermore, the residual strength of the investigated fasteners was not affected by the manner of cycling (Table 6.5). The gaps in the data in the tables indicate that the tested fasteners were performing at their limit in the Δw = 0.8 mm cracks.

Table 6.4 Fastener displacement δ at N_{mid} after 30 tension load cycles in tests using the DIBt and SEAOSC style loading patterns

Fastener Type	DIBt style test					SEAOSC style test				
	Test No. 1	Test No. 2	Test No. 3	Mean	COV [%]	Test No. 1	Test No. 2	Test No. 3	Mean	COV [%]
Expansion anchor (sleeve-type)	7.39	-[a]	-[b]	**7.39**	-	-[b]	8.57	5.05	**6.81**	36.6
Expansion anchor (bolt-type)	6.05	5.40	5.83	**5.76**	5.8	6.95	6.51	4.79	**6.08**	18.8
Screw anchor	-[c]	1.77	0.96	**1.36**	41.8	0.92	0.95	0.88	**0.92**	4.0

[a] Failure occurred during cycling at 90% $N_{u,m}$ after 9 cycles.
[b] Large slip occurred at the start of loading that invalidated the results.
[c] Fastener failed before the start of load cycling.

Table 6.5 Ultimate fastener strength from monotonic reference tests (Static) and residual fastener strengths in tests using the DIBt and SEAOSC style loading patterns

Fastener Type	Static	DIBt style test					SEAOSC style test				
	Mean	Test No. 1	Test No. 2	Test No. 3	Mean	COV [%]	Test No. 1	Test No. 2	Test No. 3	Mean	COV [%]
Expansion anchor (sleeve-type)	**33.32**	34.31	-[a]	-[b]	**34.31**	-	-[b]	32.98	32.98	**32.98**	0.0
Expansion anchor (bolt-type)	**31.61**	34.61	33.41	33.88	**33.97**	1.8	33.33	33.27	32.12	**32.91**	2.1
Screw anchor	**21.50**	-[c]	24.51	24.96	**24.74**	1.3	21.02	21.05	21.00	**21.02**	0.1

[a] Failure occurred during cycling at 90% $N_{u,m}$ after 9 cycles.
[b] Large slip occurred at the start of loading that invalidated the results.
[c] Fastener failed before the start of load cycling.

6.4 Summary and consequences

Monotonic tension tests with headed bolts showed that a better correlation between the bearing pressure and the slip of an anchor can be achieved using a square root function of the concrete strength rather than a linear function as originally proposed by *Furche (1994)*. A modified form of Furche's equation is suggested (Equation (6.4)). The coefficients in Equation (6.4) should be checked using a larger experimental database before being applied for general applications.

Equation (6.6) is proposed to calculate the head slip of headed bolts during low-cycle tension load cycling. The equation is based on the assumption that load cycling results in an accelerated creep-like behavior of the fastener. The equation is calibrated using experimental results for tension load cycling at various head bearing pressures.

It is demonstrated that concrete cone breakout of headed bolts will occur during tension load cycling if the fastener displacement transects the descending branch of the

monotonic load-displacement curve. Since the descending branch of monotonic load-displacement curve exhibits a good deal of scatter, it is proposed that a reliable indicator for the initiation of failure during tension load cycling is the crossing of the displacement at ultimate load in a corresponding monotonic test. Using the results of monotonic tests and the anchor slip calculated with Equation (6.6), it possible to predict whether concrete cone breakout of a headed bolt will occur during a given number of tension load cycles to a prescribed load level.

Tension load cycling tests were performed with post-installed fasteners in seismic relevant crack widths (Δw = 0.8 mm). The investigated fasteners failing by concrete cone breakout (sleeve-type expansion anchor), pull-through (bolt-type expansion anchor) and pull-out (screw anchor) showed robust performance for tension load cycling at near-ultimate load levels. Although these results cannot be generalized to other proprietary fasteners of these types, they indicate that fastener failure modes other than steel failure may be suitable for seismic design in predominantly tensile loaded applications.

Requirements for ductile steel failure of a fastener must be coupled with a specific strain length to achieve large deformation capacity. In design guidelines, the specific strain length can either be specified directly, e.g. $\geq 5 \cdot d$ in the *CEN TS (in preparation)*, or indirectly through the required ratio between the steel and concrete failure loads, e.g. Equation (6.12) calculated from *ACI 318 Appendix D (2005)*. In either case, it must be ensured that yielding can occur uniformly along the fastener. Further research is necessary to establish the required strain length(s) for seismic applications.

It is noted that hysteresis during tension load cycling of the investigated post-installed fasteners was near to non-existent, even in the case of steel failure.

Tension load cycling frequencies between 0.1 and 2 Hz are used in existing simulated seismic load cycling qualification tests for fasteners. Cycling frequencies up to 10 Hz are relevant for seismic fastening applications. It was verified that increasing the tension load cycling frequency to 5 Hz did not negatively affect the residual strengths of the investigated fasteners. In fact, increasing the cycling frequency consistently reduced fastener displacement during cycling. These results were independent of the failure mode. The results support the continued use of the existing load cycling frequencies for seismic fastener qualification.

The investigated anchors yielded similar displacement behavior and residual strength when subjected to stepwise increasing tension load cycling to failure or cycling at a fraction of the ultimate load with subsequent monotonic loading to failure. As pointed out by *Silva (2001)*, stepwise increasing load cycling to failure is preferable for simulated seismic load tests for fasteners because it allows the calculation of stiffness throughout the entire fastener load cycling range. Additionally, stepwise increasing loading avoids the difficulty of having to specify a load level for cycling at a fraction of the ultimate strength. The stepwise increasing loading developed in Chapter 4 (Section 4.3.1) with approximately 35 cycles to ultimate load is recommended for seismic fastener qualification. Further testing for the case of shear is required to determine the influence of the loading pattern on low-cycle fatigue of the anchor steel.

7 Experimental Investigations with High Loading Rate

7.1 Scope

During an earthquake fasteners in a structure may be loaded to failure in less than 1/10th of a second (Chapter 4; Section 4.3.2). Previous studies indicate that the ultimate load-bearing capacity of fasteners typically increases with increasing load rate (Chapter 3; Section 3.3.2). None of these studies, however, provides a comprehensive description of the influence of load rate on fastener behavior for various modes of failure. Additionally, although the investigations by *Klingner et al. (1998)* and *Fujikake et al. (2003)* indicate that a change of failure mode can occur for some fastener types at high load rates, the consequences of this have not been investigated.

In this chapter, key results of new experimental tests with bonded anchors (epoxy and vinylester based mortars), bolt-type expansion anchors and bonded-expansion anchors in cracked concrete under high load rates are discussed. The presented results focus on load-bearing capacity reduction in the case of pull-through failure and the potential for a change of failure mode at high load rates. The complete test reports are available in *Hoehler (2004f, 2006b, 2006c)*. At the end of this chapter, a comprehensive summary of the influence of load rate for various failure modes is provided.

7.2 Experimental setups and testing procedures

7.2.1 Investigated fasteners

The relevant fastener parameters are summarized in Table 7.1. The threaded rods for the bonded anchors were made of grade 10.9 steel. The mean bond strengths of the tested epoxy and vinylester mortars (bonded anchors) for a M12 threaded rod in uncracked C20/25 dry concrete without the influence of edge distance and spacing measured in confined tests were about $\tau_{b,m}$ = 23 N/mm^2 and $\tau_{b,m}$ = 11 N/mm^2, respectively.

Table 7.1 Fasteners investigated at high load rates

Fastener Type	Size	Effective Embedment h_{ef} [mm]	Illustration
Bonded anchor (epoxy mortar)	M12	60[a]	Figure 3.7
(vinylester mortar)	M12	60[a]	Figure 3.7
Expansion anchor (bolt-type)	M16	95[b]	Figure 3.4
	M16	60[c]	Figure 3.4
Bonded-expansion anchor	M8	50	Figure 3.7
	M16	80[d]	Figure 3.7

[a] Actual h_{ef} = recommended h_{ef} - 50 mm.
[b] Actual h_{ef} = recommended h_{ef} + 10 mm.
[c] Actual h_{ef} = recommended h_{ef} - 25 mm.
[d] Actual h_{ef} = recommended h_{ef} - 45 mm.

The fasteners were installed according to the manufacturer's recommendations with the following exceptions:

(1) the drilled holes for all bonded and bonded-expansion anchors were 'optimally' cleaned using the following sequence: 2x compressed air burst + 2x mechanical brushing + 2x compressed air burst + 2x mechanical brushing + 2x compressed air burst;
(2) the effective embedment depths h_{ef} were modified to achieve the desired failure modes (see Table 7.1).

7.2.2 Anchorage components

All tests were performed in C20/25 wedge-split cracked concrete slabs (refer to Chapter 5; Figure 5.1). The slabs were produced according to the state of the art after *DIN 1045 (2001)* and *DIN 1048 (1991)*.

The average concrete cube compressive strength ranged between $f_{cc,150}$ = 24.3 N/mm^2 and $f_{cc,150}$ = 30.3 N/mm^2.

7.2.3 Loading setups and testing procedures

In the majority of the tests the fasteners were loaded using a servo-hydraulic cylinder with a capacity of 50 kN. In the tests with the M16 bonded-expansion anchor, a servo-hydraulic cylinder with a capacity of 250 kN was required. The test setup was the same as that shown in Figure 6.26.

All tests were performed on single anchors with large anchor spacing and edge distances. The I-beams supporting the load cylinder were located at a suitable distance from the fastener so that complete concrete cone breakout could occur (wide support). The cracks in the anchorage components were opened by Δw = 0.5 mm or 0.8 mm after installation of the fasteners, but before loading.

In the quasi-static monotonic tension tests, load was applied under control of the servo-hydraulic cylinder displacement (displacement-controlled test). Ultimate load was reached in approximately 1 to 4 minutes.

For the high-rate monotonic tension tests, the load rate was established by controlling the servo-hydraulic cylinder displacement. The cylinder was programmed to displace 40 mm at a rate between 1000 mm/min and 50000 mm/min. At these load rates the fasteners reached ultimate load in approximately 0.2 and 0.02 seconds, respectively. A displacement of 40 mm was large enough to cause failure of the investigated fasteners.

The tension load applied to the fastener N, the displacement of the servo-hydraulic cylinder δ_{cyl}, the fastener displacement δ and the crack opening width Δw were measured continually during the tests.

7.3 Results and discussion

7.3.1 Bonded anchors

The work by *Fujikake et al. (2003)* suggests that the concrete cone breakout load for fasteners increases more rapidly with loading rate than the bond failure load (Figure 7.1; equations given in Chapter 3; Section 3.3.2). It is therefore possible that a bonded anchor that uses close to its full bond strength to produced concrete cone failure at quasi-static load rate may fail by pull-out at higher load rates. This potential change of failure mode was investigated for both the epoxy and vinylester based mortars.

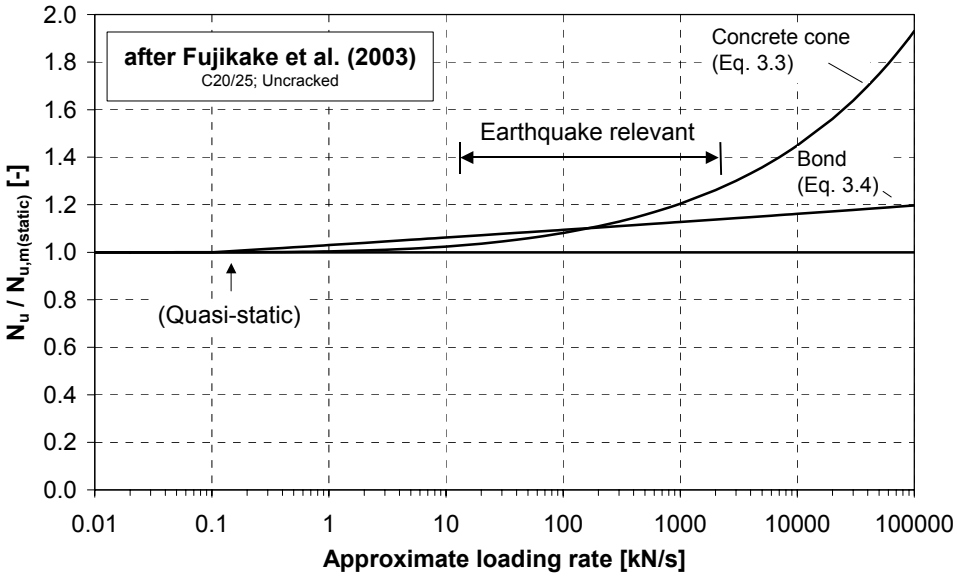

Figure 7.1 Increase of concrete cone breakout and bond failure loads for fasteners loaded at various tension rates

Figure 7.2a shows load-displacement curves for M12 bonded anchors with epoxy based mortar loaded to failure in C20/25 cracked concrete (Δw = 0.5 mm) at various tension load rates. Each curve is the average of three or more test replicates. The embedment depth h_{ef} = 60 mm (5·d) was selected such that the calculated bond failure load was marginally larger than the calculated concrete cone breakout failure load for quasi-static loading in cracked concrete. A significant increase of the failure load with load rate can be seen. In all cases concrete cone breakout occurred. No influence of the load rate on the shape or size of the concrete breakout body was observed (Figure 7.2b).

Figure 7.3a shows the response of similar tests with vinylester based mortar (middle load rate not tested). Once again the failure load increased with load rate, however, a shift of the failure mode from concrete cone breakout to pull-out at high load rate was observed (Figure 7.3b).

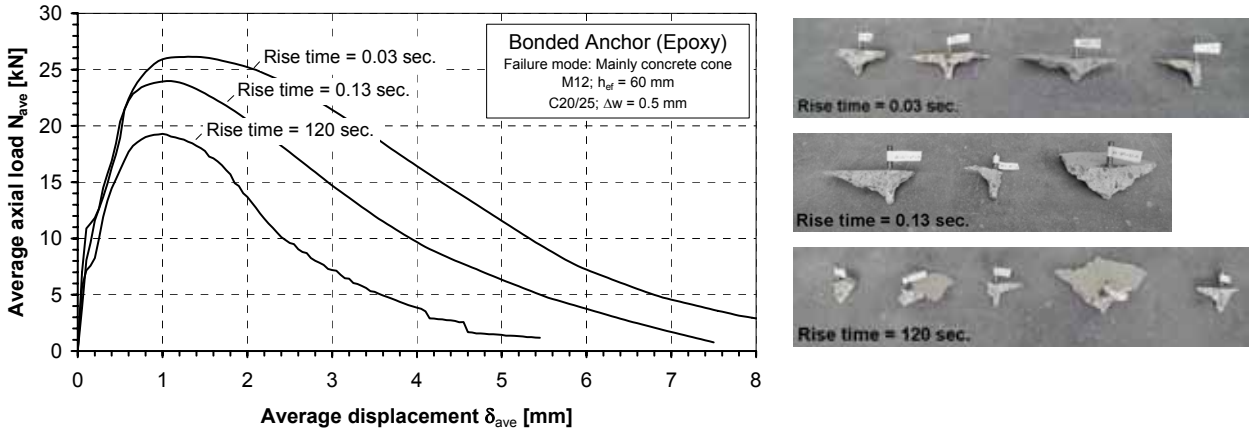

(a) *(b)*

Figure 7.2 Static and high-rate tension load tests with M12 bonded anchors (epoxy based mortar) in C20/25 cracked concrete (Δw = 0.5 mm): (a) average load-displacement; (b) photographs of failure bodies

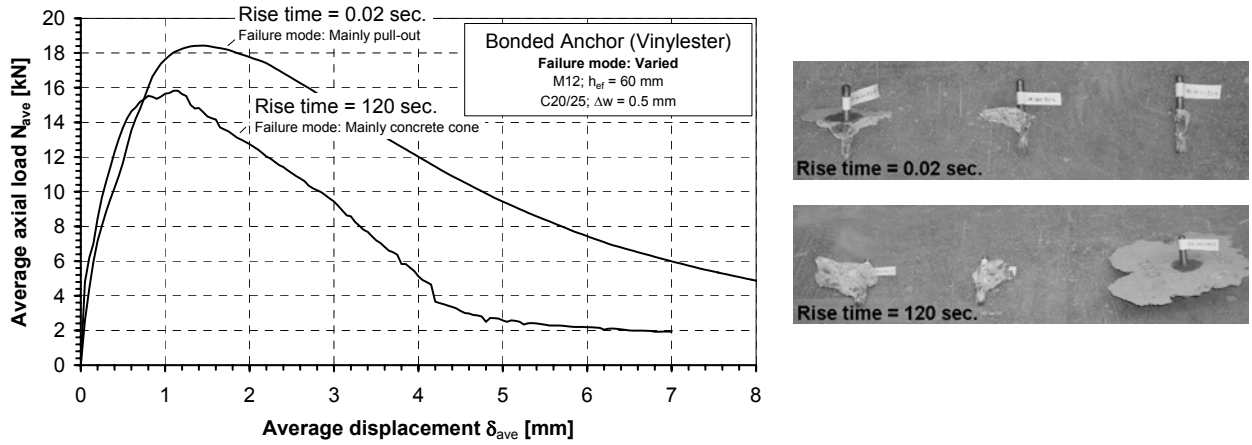

(a) *(b)*

Figure 7.3 Static and high-rate tension load tests with M12 bonded anchors (vinylester based mortar) in C20/25 cracked concrete (Δw = 0.5 mm): (a) average load-displacement; (b) photographs of failure bodies

Figure 7.4 plots the ultimate loads normalized by the mean quasi-static failure loads as a function of the applied load rate. The test results confirm the trend for the increase in concrete failure load suggested by *Fujikake et al. (2003)* as well as the trend for bond failure in the case of the investigated anchors with vinylester mortar. For higher load rates it is probable that the shift to pull-out failure with increasing load rate would become more pronounced. Regardless of the failure mode (concrete cone or bond failure) the ultimate loads at earthquake relevant loading rates are higher than those obtained under quasi-static load rates.

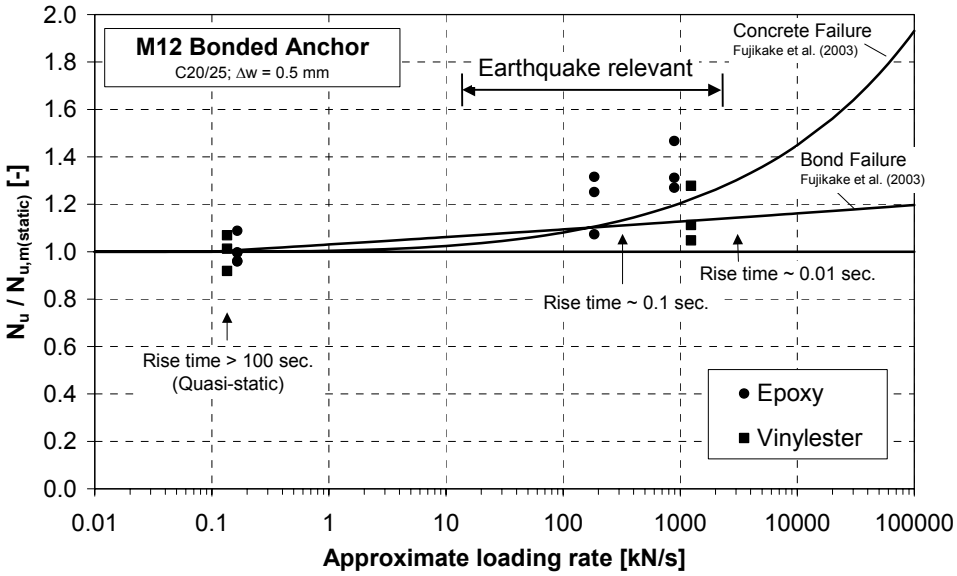

Figure 7.4 Influence of tension load rate on M12 bonded anchors in C20/25 cracked concrete (Δw = 0.5mm)

7.3.1.1 A remark on failure modes for bonded anchors in cracked concrete

The bonded anchors discussed in Section 7.3.1 performed surprisingly well in Δw = 0.5 mm cracks; particularly the anchors with epoxy based mortar. It is often assumed that standard bonded anchors are not well-suited for applications in cracked concrete because they lack follow-up expansion capacity (or an undercut) and lose approximately 50% of their bond area in a crack (*Eligehausen et al. 2006*). Moreover, for combined tension and shear loads, e.g. during an earthquake, a small shear load could easily destroy the adhesion on the side of the crack to which the anchor remains bonded (Figure 7.5).

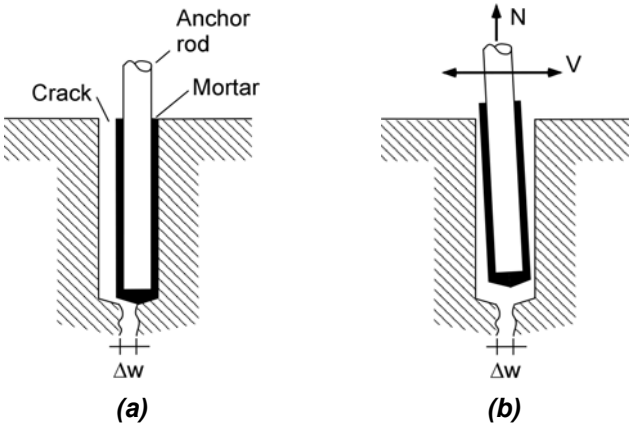

Figure 7.5 Presumed failure mode for bonded anchors in cracks: (a) anchor in crack without load; (b) failure under combined tension and shear load

Exploratory tests performed using threaded rods with epoxy based mortar were performed in which the anchor was installed in a closed hairline crack, after curing the mortar the crack was opened by Δw = 0.5 mm and several hammer blows in shear were delivered to the exposed portion of the threaded rod in shear to destroy all bond due to adhesion. Subsequent tension loading of the anchor to failure in the open crack resulted

in complete concrete cone breakout (Figure 7.6a). This was possible because mechanical interlock between the surface of the mortar and the concrete was sufficient to bridge the Δw = 0.5 mm crack (Figure 7.6b). Therefore, the presumed failure mode shown in Figure 7.5 was not valid.

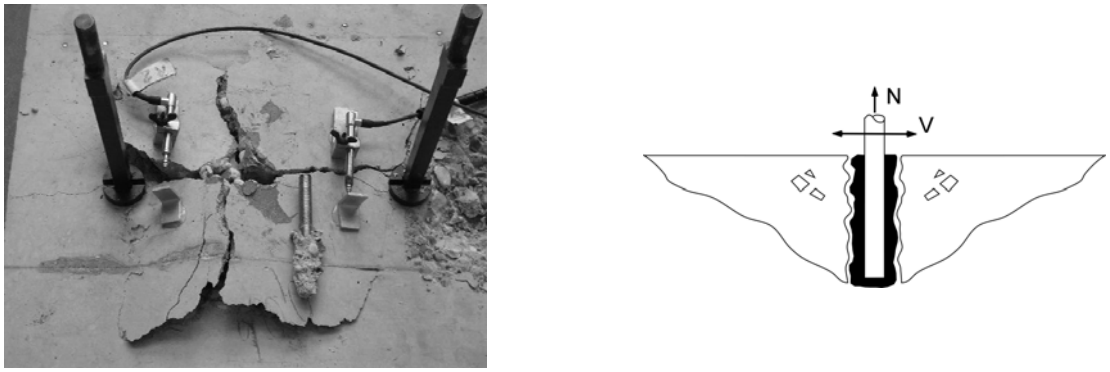

(a) *(b)*

Figure 7.6 Actual failure mode for a bonded anchor with epoxy based mortar in a Δw = 0.5mm crack: (a) photograph of concrete breakout; (b) schematic of failure body

Comparison of the anchor after failure with an anchor with vinylester based mortar, which failed by pull-out, illustrates an important difference between failure of bonded anchors with epoxy and vinylester based mortar (Figure 7.7). Although failure occurred between the mortar and the concrete in both cases, it appears that the epoxy was able to penetrate into the wall of the drilled hole, which strengthened the concrete in this interface zone and created an uneven surface. This uneven surface, which provides mechanical interlock, was not observed for the anchors with vinylester based mortar.

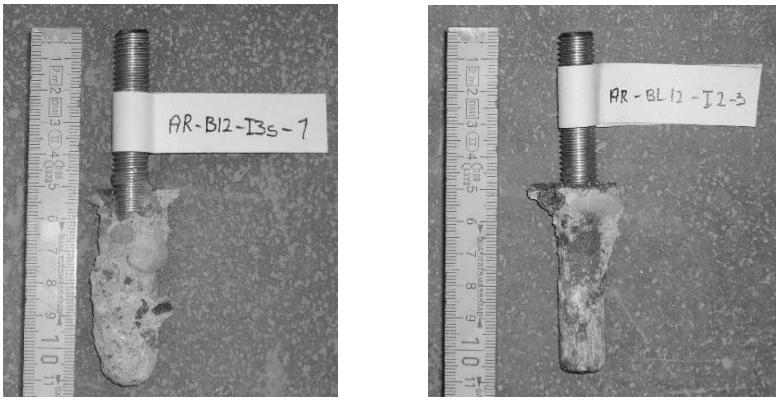

(a) *(b)*

Figure 7.7 Photographs of bonded anchors after failure illustrating the bond failure surface: (a) epoxy based mortar; (b) vinylester based mortar

7.3.2 Bolt-type expansion anchors

Two types of tests were performed at high load rate with bolt-type expansion anchors:

(1) tests in which pull-through was assured at all load rates;
(2) tests in which a change of failure mode from concrete cone breakout to pull-through was targeted.

Figure 7.8a shows average load-displacement curves of M16 bolt-type expansion anchors (h_{ef} = 95 mm) loaded to failure in tension at various rates in Δw = 0.8 mm cracks. Pull-through occurred at all load rates (Figure 7.8b). Each curve is the average of three or more test replicates. The figure shows that the failure load decreased slightly with increasing load rate. This can be attributed to the reduced coefficient of friction between the anchor expansion cone and the expansion elements at high load rates.

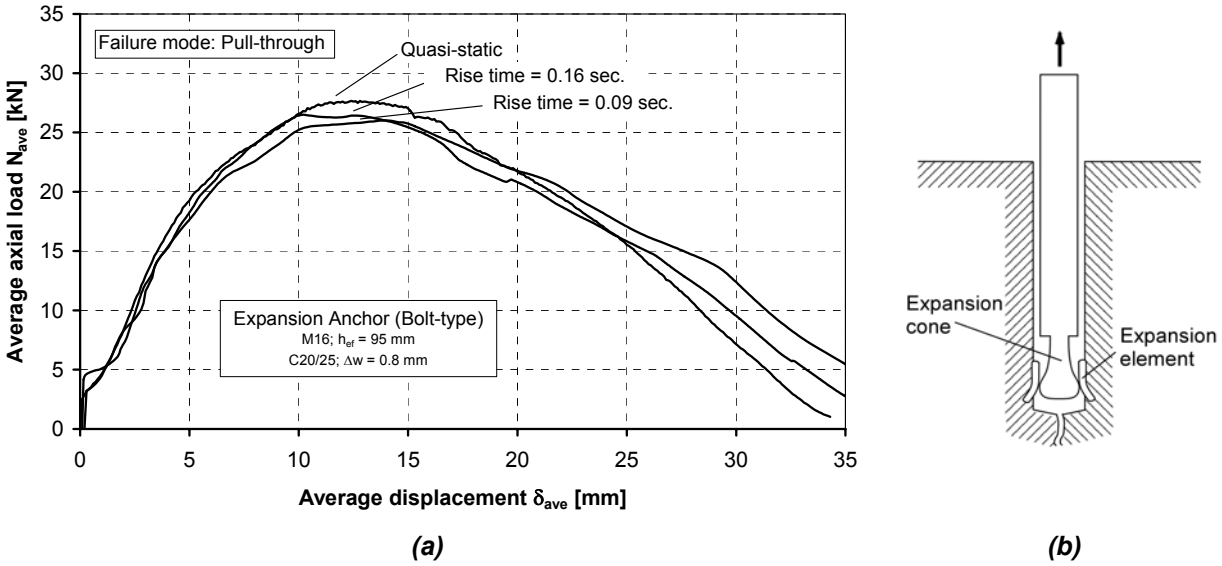

Figure 7.8 Static and high-rate tension load tests with M16 expansion bolts in C20/25 cracked concrete (Δw = 0.8 mm) in the case of pull-through: (a) average load-displacement; (b) sketch of failure mode

Similar to the case of bonded anchors (Section 7.3.1), an increasing concrete cone failure load and decreasing pull-through failure load indicates that a change of failure mode is possible for bolt-type expansion anchors loaded at high rates. Unlike the case of bonded anchors, however, the pull-through failure load at high rate could be lower than the concrete cone failure load under quasi-static loading. Attempts to demonstrate this behavior experimentally, however, were unsuccessful. The reason was that the decrease in pull-through failure load at earthquake relevant loading rates was relatively small (< 5%) compared to the scatter of the concrete failure load. To achieve a transition of failure mode at earthquake relevant loading rates it was necessary to anchor the fasteners at an embedment depth that was just at the transition point between concrete cone failure and pull-through failure (h_{ef} = 60 mm; Δw = 0.5 mm). This resulted in a mixed concrete cone and pull-through failure for both quasi-static and high-rate tension loading (Figure 7.9a). Although the fasteners tended more toward pull-through for high loading rates (Figure 7.9b) distinct failure modes were not achieved. As can be seen in Figure 7.9 the failure load increased with load rate in spite of the shift toward pull-through failure.

For even higher loading rate (rise time < 0.01 seconds) the failure load for pull-through should theoretically decrease further. These loading rates, however, are relevant for blast loading and not earthquake applications.

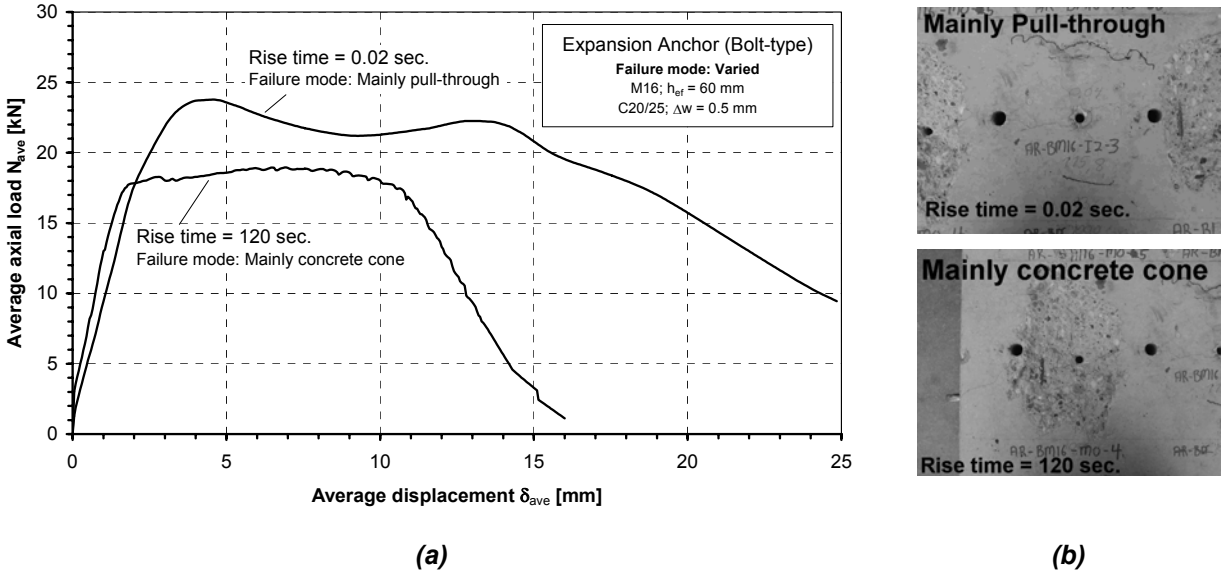

Figure 7.9 Static and high-rate tension load tests with M16 expansion bolts in C20/25 cracked concrete (Δw = 0.5 mm) in the case of a change of failure mode: (a) average load-displacement; (b) photographs of failure modes (top = mainly pull-through; bottom = mainly concrete cone)

7.3.3 Bonded-expansion anchors

Bonded-expansion anchors combine load-transfer mechanisms of bonded anchors and expansion anchors. Tests were performed to understand which failure modes dominate for these anchors at high (earthquake relevant) loading rates, i.e. does failure load decrease relative to quasi-static loading as with bolt-type expansion anchors or increase as with standard bonded anchors.

Small (M8) bonded-expansion anchors were installed at the manufacturer's recommended embedment depth h_{ef} = 50 mm and loaded in tension to failure at various rates. The tests were performed in Δw = 0.8 mm line cracks. The resulting load-displacement curves are shown in Figure 7.10a. Each curve is the average of three or more test replicates. A significant increase in the failure load with rate can be observed. The combination of small anchor dimensions and large crack width resulted in high local stresses at the anchor expansion cones. Failure occurred due to pull-out of the expansion cones through the mortar (Figure 7.10b). Thus the increase in failure load represents the increase in the shear strength of the mortar with loading rate.

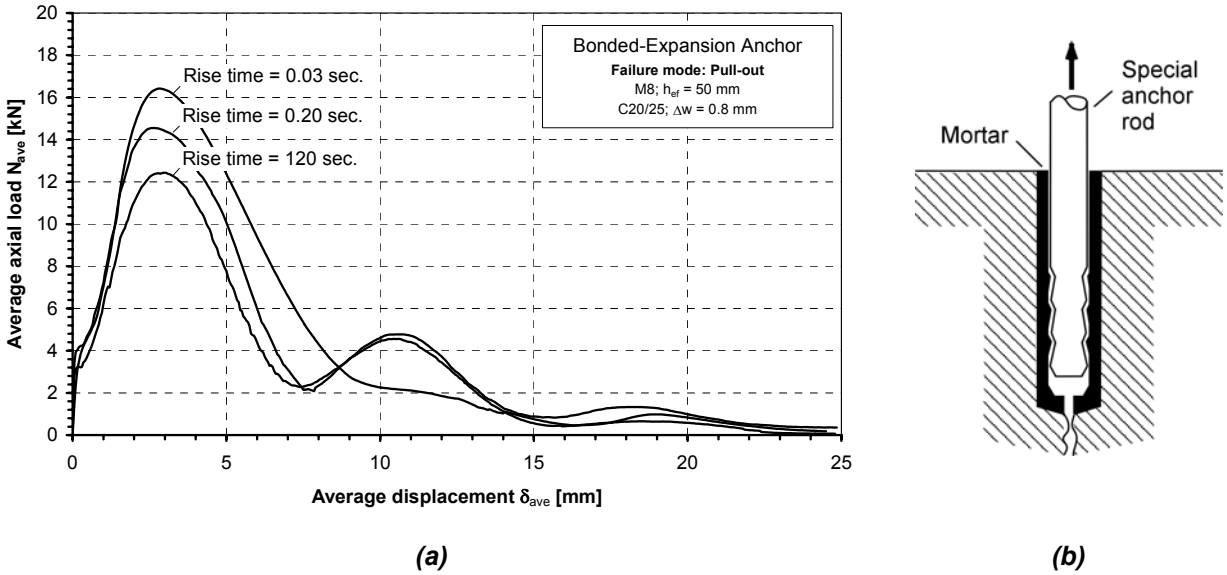

Figure 7.10 Static and high-rate tension load tests with M8 bonded-expansion anchors in C20/25 cracked concrete (Δw = 0.8 mm): (a) average load-displacement; (b) sketch of failure mode

Larger (M16) bonded-expansion anchor were installed at an embedment depth h_{ef} = 80 mm and tested under similar conditions. Under quasi-static load rate the anchor failed by concrete cone breakout. When the anchors were loaded to their ultimate capacity in 0.04 seconds, the lower portion of the anchor was pulled through the mortar (little damage to the mortar) and a concrete cone formed near the surface of the slab (Figure 7.11b). The resulting load-displacement curves are shown in Figure 7.11a. As with the investigated bolt-type expansion anchors (Section 7.3.2), the failure load increased with the loading rate in spite of the pull-through failure.

The influence of load rate on the failure load of the investigated bonded-expansion anchors is summarized in Figure 7.12.

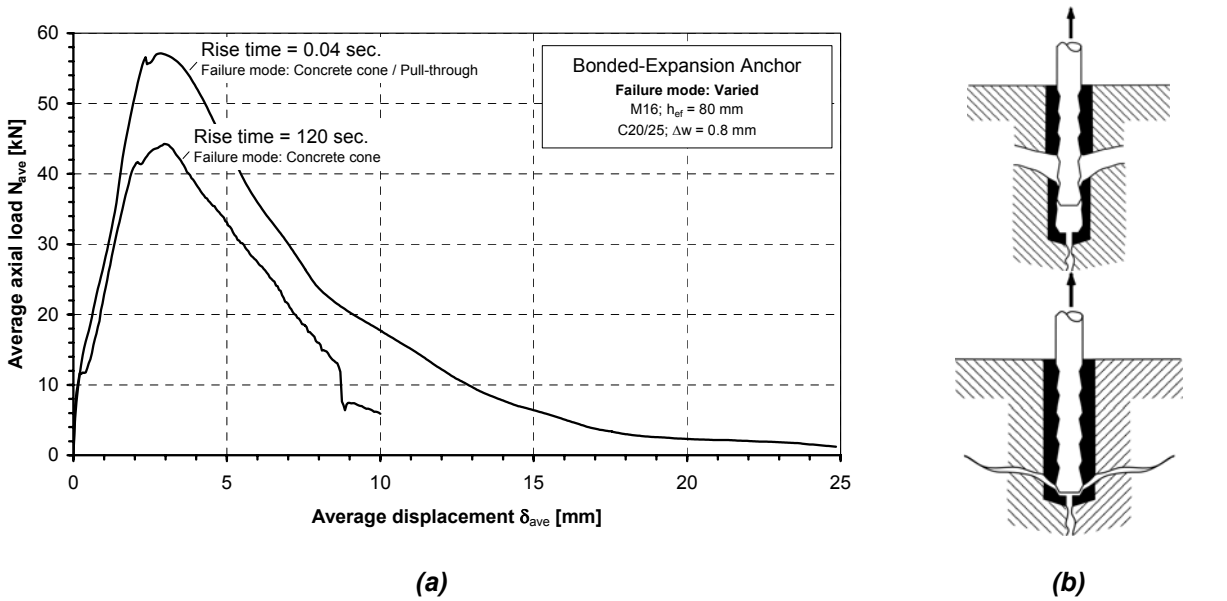

Figure 7.11 Static and high-rate tension load tests with M16 bonded-expansion anchors in C20/25 cracked concrete (Δw = 0.8 mm): (a) average load-displacement; (b) sketches of failure modes

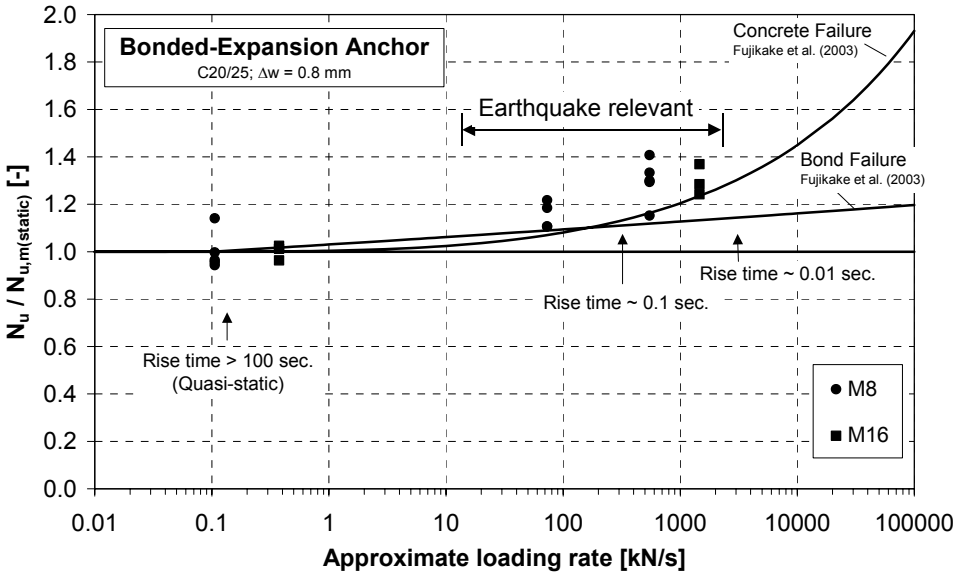

Figure 7.12 Influence of tension load rate on M8 and M16 bonded-expansion anchors in C20/25 cracked concrete (Δw = 0.8mm)

7.3.4 Influence of monotonic loading rate on ultimate strength

The following summary of the influence of load rate on the ultimate strength of various fastener failure modes includes data from the present investigations together with a re-analysis of data from other authors (Chapter 3; Section 3.3.2). The results are plotted as a function of the applied load rate, because this information could be determined from all of the available test data. Approximate values for the rise time to ultimate load are also provided.

7.3.4.1 High-rate tension loading

Steel failure

Although no test data was found for the specific case of steel failure of fasteners in tension at high loading rates, steel strength typically increases with increasing loading rate (see for example *CEB 1987*). Therefore, it can be inferred that steel failure at earthquake relevant loading rates will have an ultimate load capacity at least as large as that obtained for steel failure under quasi-static loading.

Concrete cone failure

If concrete cone failure occurs both under quasi-static and high-rate loading, the ultimate load capacity under high-rate loading will be at least as large as that under quasi-static loading. This appears to be true regardless of the fastener type or the condition of the concrete (cracked or uncracked). For earthquake relevant loading rates the available test data suggest that the increase in the concrete cone capacity for cast-in and post-installed fasteners will be less than 60% and on average around 20% (Figure 7.13). This increase in capacity is due to the increase in concrete tensile strength at high loading rates. In Figure 7.13 the equation suggested by *Fujikake et al. (2003)* for the increase in concrete cone resistance as well as the *CEB (1987)* equation for the increase in concrete tensile strength with loading rate are provided for comparison.

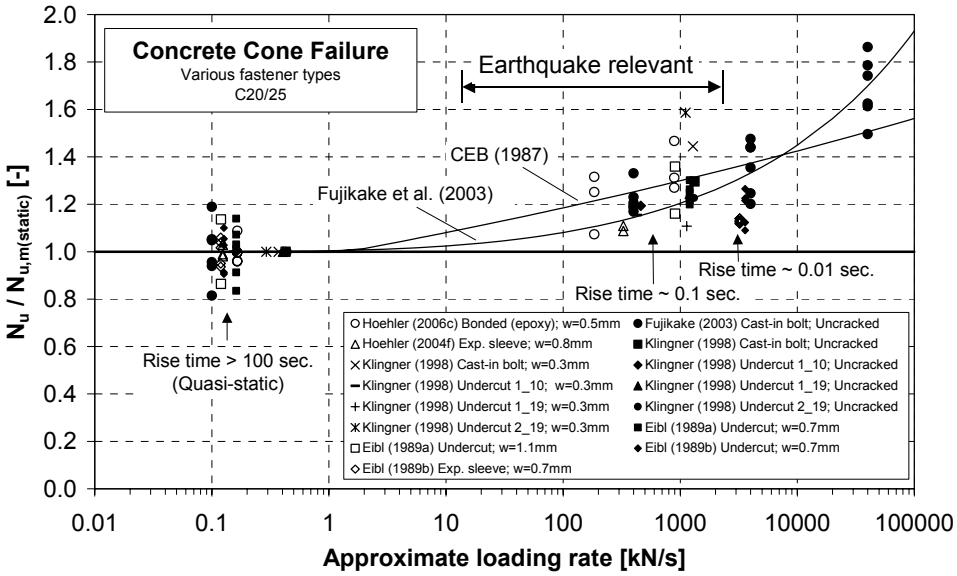

Figure 7.13 Influence of loading rate on the concrete cone failure load

Pull-through failure

The ultimate capacity of (mechanical) fasteners failing by pull-through decreases with increasing loading rate. The available data is limited, however, a decrease in capacity up to 20% for earthquake relevant loading rates has been observed (Figure 7.14). The decrease in ultimate load is a function of the counter-working effects of the increase in the elastic modulus of the concrete and the decrease of the coefficients of friction between the expansion cone and expansion elements at higher loading rate.

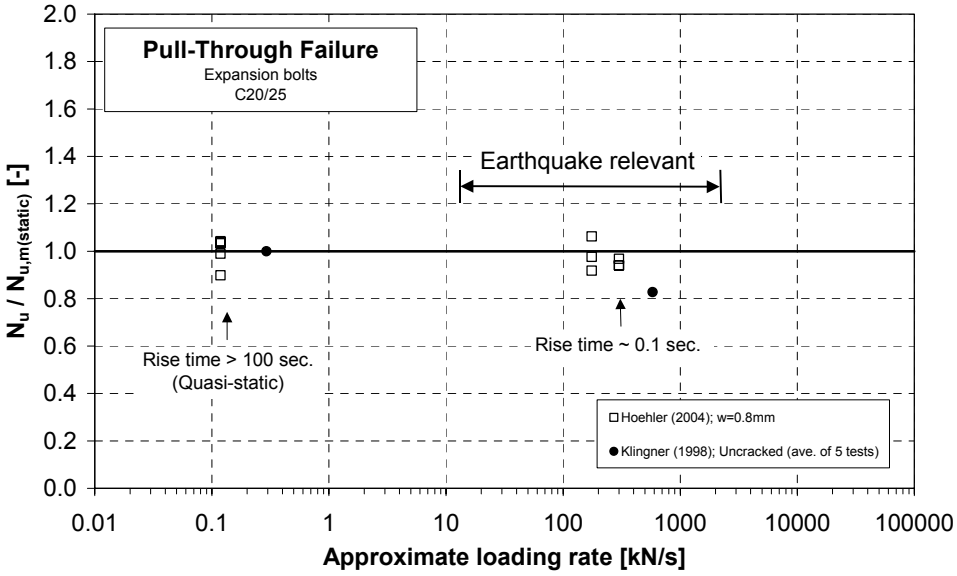

Figure 7.14 Influence of loading rate on the pull-through failure load

Pull-out failure

Pull-out failure is not an approved failure mode for mechanical fasteners. Therefore, the effect of loading rate was not investigated.

For bonded anchors, the bond strength increases with increasing loading rate (Figure 7.15) (*Fujikake et al. 2003*). Therefore, anchors failing by bond failure at earthquake relevant loading rates will have a load capacity at least as large as for bond failure under quasi-static loading. It is noted that in the test data presented in Figure 7.15 failure always occurred between the mortar and the wall of the drilled hole.

Bonded-expansion anchors that fail due to shearing of the mortar by the expansion cones, which is a type of pull-out failure, will have an increased load-bearing capacity at high load rates (refer to Figure 7.10).

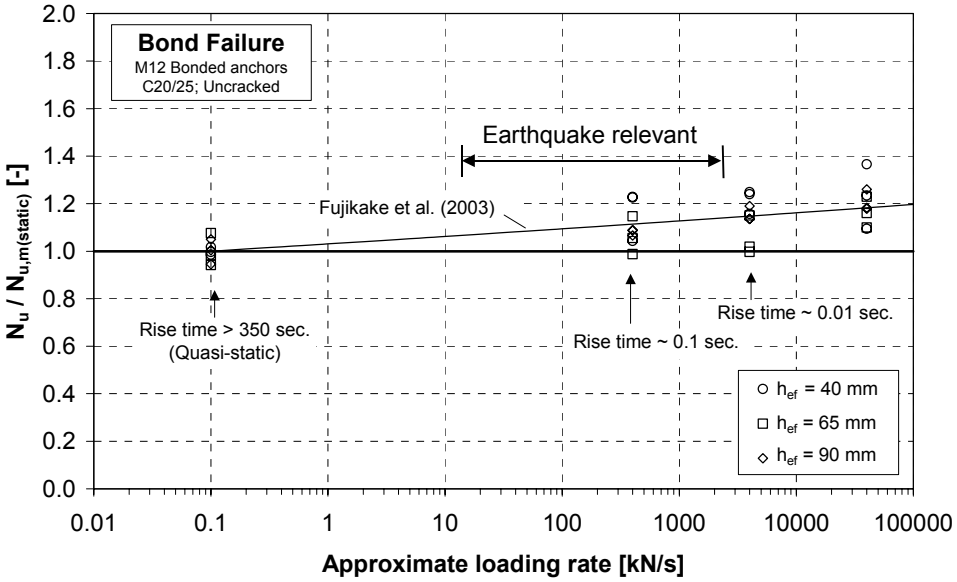

Figure 7.15 Influence of loading rate on the pull-out (bond) failure load (Fujikake et al. 2003)

Splitting and blow-out failure

The effect of loading rate on the concrete splitting and blow-out capacities for fasteners have to the knowledge of the author never been investigated. It is believed, however, that higher loading rates will lead to higher failure loads in these cases as a result of the increased concrete tensile strength at high loading rates.

Change of failure mode

Some fasteners that fail by steel or concrete cone breakout under tension loading at quasi-static loading rates may fail by pull-out or pull-through at higher loading rates.

In the case of standard bonded anchors that undergo a transition from concrete cone breakout to pull-out, the ultimate load capacity under high-rate loading will be at least as large as that under quasi-static loading.

In the case of sleeve-type or bolt-type expansion anchors that undergo a transition from concrete cone breakout to pull-through or pull-out, the ultimate load capacity under high-

rate loading might be less than under quasi-static loading. *Klingner et al. (1998)* observed a reduction of the failure load of 20% for bolt-type expansion anchors tested at high load rates (see Chapter 3; Section 3.3.2). The investigations performed within the scope of this dissertation (Section 7.3.1, 7.3.2 and 7.3.3) could not confirm this behavior. It should be noted, however, that the proper functioning of some expansion anchors can depend strongly on the relative values of friction between the anchor expansion cone and expansion elements (internal friction) and between the expansion elements and the wall of the drilled hole (external friction). For such anchors, if the external friction decreases more rapidly than the internal friction under high load rate, the anchor could fail to provide follow-up expansion, thereby changing the failure mode from pull-through to pull-out. This could negatively affect the anchor performance.

In general, for earthquake relevant loading rate the influence of a change of failure mode on the ultimate load-bearing capacity can be neglected. However, futher testing should be performed.

7.3.4.2 High-rate shear loading

Steel failure

Using the same reasoning as for steel failure in tension (Section 7.3.4.1), steel failure in shear at earthquake relevant loading rates will probably have an ultimate load capacity at least as large as that obtained for steel failure under quasi-static loading.

Concrete edge failure

If concrete edge failure occurs both under quasi-static and high-rate loading, the ultimate capacity under high-rate loading will be at least as large as that under quasi-static loading. As in the case of tension loading, the capacity increase is due to the increased concrete tensile strength at high loading rates. This has been confirmed by a limited number of experimental tests by *Klingner et al. (1998)* (see Chapter 3; Section 3.3.2).

Pry-out failure

The effect of loading rate on the pry-out capacity for fasteners has to the knowledge of the author never been investigated. It is believed that higher loading rates will lead to higher pry-out loads due to the increased concrete strength at high load rates.

Change of failure mode

Since pull-through, which can result in a reduced ultimate load at high load rates, is not common for fasteners loaded in shear, a change of failure mode can presumably be neglected for shear loading.

7.4 Summary and consequences

Load rates that occur as a result of earthquake loading do not negatively affect the ultimate load-bearing capacity of cast-in or post-installed fasteners if steel or concrete failure occurs. This is valid for tension and shear loading and is independent of the condition of the concrete (cracked or uncracked).

In the case of pull-through failure of mechanical fasteners, the load-bearing capacity is reduced at increased loading rates. In general, for earthquake relevant load rate the reduction is small.

Increased loading rate can lead to a change of failure mode for some fastener types and concrete conditions (cracked concrete). This particularly applies to anchors sensitive to the relative value of internal and external anchor friction. The potential for a reduction of the ultimate load-bearing capacity associated with change in failure mode appears to be small at earthquake relevant loading rates, however, further tests should be performed.

Pending the results of further testing of friction critical anchors under high load rate, it is believed that testing of post-installed fasteners to concrete at high load rates is not necessary for earthquake applications. For very high load rates, such as those associated with blast applications, monotonic tension tests at high rate in cracked concrete might be required if concrete or steel failure of the fastener cannot be guaranteed for all loading rates.

8 Probability of Brittle Failure During an Earthquake

In Chapter 6 (Section 6.3.2.1.2) ductile steel failure of fasteners is discussed. There it is demonstrated that a sufficient length over which the fastener can be strained in tension is necessary to achieve the large deformations that design codes intend for this failure mode. This required strain length can be imposed in design codes either by explicitly defining a required strain length, e.g. *CEN TS (in preparation)*, or implicitly through the prescribed margin of safety between steel failure and brittle failure modes, e.g. *ACI 318 Appendix D (2005)*. For the latter case, the required embedment depth increases with the margin of safety, which in turn increases the available strain length of the fastener.

In addition to the issue of ductility, the margin of safety between steel and concrete (brittle) failure determines the probability that the desired design goal, i.e. steel failure, is actually achieved. This issue is addressed in the following short study.

8.1 Formulation of the problem

The probability of brittle failure for various margins of safety between the mean (not characteristic) steel and concrete failure loads can be quantified using the method formulated by *Cornell (1967)*. The margin of safety M = C – S for steel failure (s) to occur prior to concrete failure (c) is determined using the mean value (μ) and standard deviation (σ) of the two failure modes. The relevant equations valid for independent and normally distributed variables c and s are given here:

$$\mu_m = \mu_c - \mu_s \tag{8.1}$$

$$\sigma_m = \sqrt{\sigma_c^{\,2} + \sigma_s^{\,2}} \tag{8.2}$$

$$\beta = \frac{\mu_m}{\sigma_m} \tag{8.3}$$

The probability of failure (p_f) can be obtained from the following equation using the safety index β:

$$p_f = \int_{-\infty}^{-\beta} \frac{1}{\sqrt{2\pi}} \cdot e^{-\frac{1}{2}x^2} dx \tag{8.4}$$

For the purpose of this study, it is assumed that the available analytic models can predict the mean failure loads for steel or concrete failure with 100 percent accuracy, i.e. model uncertainty is neglected, and that all variables are normally distributed. Thus, for the example case of tensile failure, the mean values of the normalized failure loads ($N_{actual} / N_{calculated}$) can be taken to be 1.0 for both steel and concrete failure. Therefore, if no margin of safety between concrete and steel failure is prescribed, then μ_m = 1.0 - 1.0 = 0, the safety index β = 0 and the probability of concrete failure is 50%, regardless of the amount of scatter of the values around the means. Since we want to ensure that steel failure does indeed occur prior to concrete failure, mean values of the

margin of safety (μ_m) greater than zero are required. This causes the mean values of the normalized failure loads for concrete and steel failure to move apart (Figure 8.1a). To determine the probability of concrete failure prior to steel failure, it is the ratio of the mean values μ_s / μ_c, and not the absolute magnitudes of μ_s and μ_c, that is important.

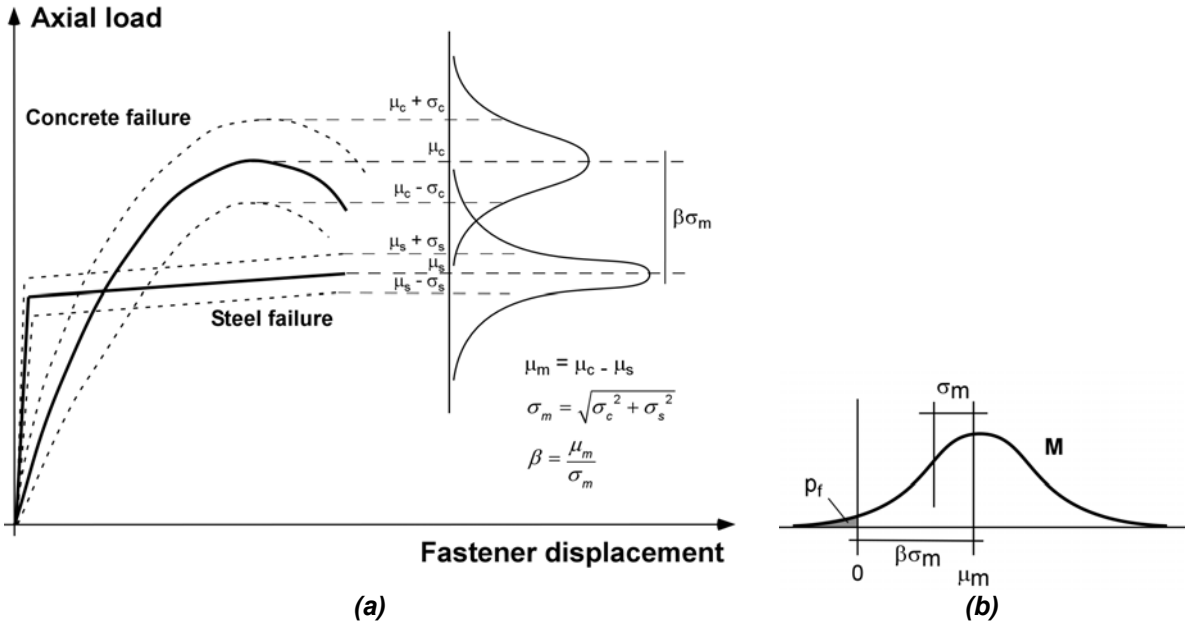

Figure 8.1 Schematic representation of the method used to determine the probability of brittle failure: (a) distributions of the normalized variables; (b) probability density function for the margin of safety

8.2 Numerical study

When the ratio μ_s / μ_c is not equal to one, the margin of safety μ_m is non-zero and the standard deviation (scatter) of the variables influences the probability of failure p_f (Figure 8.1b). The standard deviation is determined from the coefficient of variation (COV) as $\sigma = \text{COV} \cdot \mu$. The COV for fastener steel failure was taken as 5%. The COV for concrete failure was taken to be 15%. Ratios μ_s / μ_c of 0.70, 0.60, 0.50 and 0.40 were prescribed. The prescribed mean concrete strength was arbitrarily assumed to be μ_c = 1.0. Furthermore, the influence of steel over-strength ($\mu_{s,o}$) of 10%, which is rather low, and a reduction of the concrete failure load ($\mu_{c,u}$) of 15% on the probability of concrete failure was investigated. The reduction of 15% to the concrete failure load assumes that crack widths wider than those used during product qualification testing during an earthquake reduce the failure load by 25%. Simultaneously, in practice, concrete typically has an over-strength compared to the design value that increases the concrete failure load of the fastening. The increase was assumed to be 15% ((33 N/mm^2 / 25 N/mm^2)$^{0.5}$ = 1.15) for normal strength concrete. Taken together, these factors yield a reduction factor of approximately 15% (0.75·1.15 ~ 0.85). The results of the study are summarized in Table 8.1.

Table 8.1 Probability of concrete failure prior to steel failure as a function of the prescribed ratio of the mean failure loads

Prescribed Ratio of Mean Values	Coefficient of Variation		Modifications to the Mean Values		Actual Margin of Safety	Standard Deviation of Margin of Safety	Safety Index	Probability of Concrete Failure
			Steel Over-strength	Concrete Under-strength				
μ_s / μ_c	Steel	Concrete	$\mu_{s,o}$	$\mu_{c,u}$	μ_m	σ_m	β	p_f
0.70	5%	15%	-	-	0.30	0.154	1.95	0.025726
0.60					0.40	0.153	2.61	0.004463
0.50					0.50	0.152	3.29	0.000505
0.40					0.60	0.151	3.96	0.000037
0.70	5%	15%	1.10	-	0.23	0.155	1.49	0.068746
0.60					0.34	0.154	2.21	0.013424
0.50					0.45	0.153	2.95	0.001585
0.40					0.56	0.152	3.69	0.000110
0.70	5%	15%	1.10	0.85	0.08	0.133	0.60	0.274032
0.60					0.19	0.132	1.44	0.074558
0.50					0.30	0.130	2.30	0.010723
0.40					0.41	0.129	3.17	0.000765

Table 8.1 shows that the probability of concrete failure for a prescribed ratio between the mean steel and concrete failure loads of 0.70 in the absence of steel over-strength and with an unreduced characteristic concrete strength is about 2.6% (β = 1.95). If 10% steel over-strength is present simultaneously with a concrete 'under-strength' of 15%, the probability of concrete failure increases to 27%.

8.3 Application to seismic design guidelines

As shown in Chapter 6 (Section 6.3.2.1.2), the minimum ratio between the characteristic steel and concrete failure loads according to *ACI 318 Appendix D (2005)* is 0.86. This ratio can be converted to mean values using the relation that the characteristic value is (1 - 1.645·COV) times the mean value. The factor 1.645 is valid when an infinite number of tests are performed. For the assumed COVs the relations between the characteristic and mean values for steel and concrete failure are 0.92 and 0.75, respectively. Thus, the ratio between the mean steel and concrete failure loads according to *ACI 318 Appendix D (2005)* is:

$$0.92 \cdot N_{sa,m} \leq 0.86 \cdot \left(0.75 \cdot N_{cb,m}\right) \quad \Rightarrow \quad N_{sa,m} \leq 0.71 \cdot N_{cb,m} \tag{8.5}$$

where $N_{sa,m}$ is the mean steel tensile strength and $N_{cb,m}$ is the mean concrete breakout strength. Therefore, the mean steel failure load must be below 71% of the mean concrete breakout load and the probabilities of concrete failure in Table 8.1 for a ratio μ_s / μ_c of 0.70 apply. Expressed another way, the study shows that if 10% steel over-strength is present simultaneously with a concrete 'under-strength' of 15%, there is a 27 percent chance that the intended steel failure will not occur when using the *ACI 318 Appendix D (2005)* seismic provisions. This seems to be unacceptable.

It is important to note that the above given probabilities of failure denote the likelihood of concrete failure prior to steel failure. The absolute probability of failure may be significantly lower. The acceptable probability that concrete failure occur prior to steel failure depends on several parameters. Tentatively, $p_f = 10^{-2}$ (β = 2.3) is assumed. Further study is needed, however, to quantify the acceptable value for p_f.

To ensure the above assumed probability of steel failure prior to concrete failure within the context of *ACI 318 Appendix D (2005)*, Eq. (8.6) should be satisfied:

$$\phi_s \cdot N_{sa} \leq 0.70 \cdot \phi_c \cdot N_{cb} \tag{8.6}$$

where N_{sa} is the nominal (characteristic) steel tensile strength, N_{cb} is the characteristic concrete breakout strength and ϕ_s and ϕ_c are the design reduction factors for steel and concrete failure, respectively. Assuming 10% steel over-strength and 15% concrete under-strength this yields $N_{sa,m} \leq 0.50 \cdot N_{cb,m}$, resulting in $p_f = 0.01$ (see Table 8.1).

For other seismic design guides for fasteners, e.g. *CEN TS (in preparation)*, the ratio $N_{sa,m} \leq 0.50 \cdot N_{cb,m}$ should be ensured taking the relevant partial safety factors into account.

9 Recommendations for Testing and Assessment

Recommendations for the development of qualification tests and performance assessment criteria for fasteners used for seismic applications are presented in this chapter. The recommendations are formulated maintaining the framework of existing seismic qualification guidelines for fasteners (see Chapter 3; Section 3.4.3), which represents a reasonable simplification of the physical conditions to which fasteners may be subjected during an earthquake (refer to Chapter 4; Figure 4.35). The component tests of existing seismic qualification guidelines for fasteners are restated here:

(1) Reference tests to establish the tension and shear capacity in cracked concrete.
(2) Simulated seismic load cycling tests with pulsating tension and alternating shear.
(3) Simulated seismic crack cycling tests in which a sustained axial load is applied to the fastener while it is subjected to crack opening and closing cycles.

The presented recommendations differ from existing ones in the testing parameters and procedures, as well as the assessment criteria.

As was established in Chapter 7 (Section 7.3.4), the effects of dynamic loading rates relevant for earthquake applications can conservatively be neglected for fasteners failing by steel, concrete or bond failure. Additional testing is required with friction critical fasteners, e.g. torque and displacement controlled expansion anchors, to determine whether tests at dynamic load rates can be neglected altogether for the qualification of fasteners for earthquake applications.

It is assumed that all seismic tests are performed in normal strength concrete.

9.1 Reference tests

The purpose of the reference tests is to establish the behavior of the fastener under quasi-static tension and shear load (N and V) in representative seismic crack widths. The fastener should be installed in cracks opened by Δw = 0.8 mm prior to being loaded monotonically to failure. In addition to determining the behavior on the ascending branch of the load-displacement curve, the ultimate load N_u (or V_u) and the displacement at ultimate load δ_u, it is suggested that the displacement at 80% of N_u (or V_u) on the ascending (δ_{80a}) and descending (δ_{80d}) branches of the load-displacement curve be recorded (Figure 9.1). By comparing the relative displacements at 80% N_u (or V_u) on the ascending and descending branches ($\delta_{80d} / \delta_{80a}$), one gains additional information about the deformation capacity of a fastener. The development of quantitative assessment criteria based on the amount of absolute displacement at ultimate load δ_u and the relative displacement $\delta_{80d} / \delta_{80a}$ was not within the scope of this dissertation.

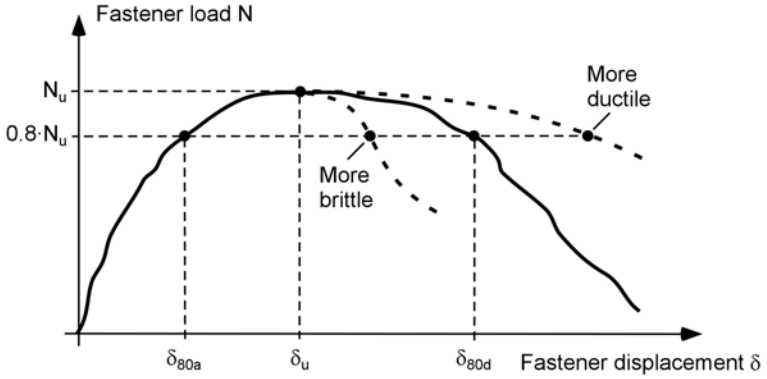

Figure 9.1 Schematic load-displacement curve for seismic reference test (tension)

9.2 Simulated seismic load cycling tests

Simulated seismic load cycling tests evaluate the response of the fastener to pulsating tension and alternating shear loading in representative seismic crack widths (Δw = 0.8 mm). The recommended test parameters and assessment criteria are summarized in Table 9.1.

Table 9.1 Test parameters and assessment criteria for simulated seismic load cycling tests

Load Cycling Amplitude	Load Type[a]	Crack Width [mm]	No. of Load Cycles[b]	Load Level Factors[c]	Assessment Criteria
Stepwise Increasing	PT	0.8	5/5/5/5/5/5/∞	$\frac{1}{7}$ / $\frac{2}{7}$ / $\frac{3}{7}$ / $\frac{4}{7}$ / $\frac{5}{7}$ / $\frac{6}{7}$ / $\frac{7}{7}$	$N_u \geq \frac{6}{7} \cdot N_{u,m}$[c,d]
	AS	0.8	5/5/5/5/5/5/∞	$\pm\frac{1}{7}$ / $\frac{2}{7}$ / $\frac{3}{7}$ / $\frac{4}{7}$ / $\frac{5}{7}$ / $\frac{6}{7}$ / $\frac{7}{7}$	Not available

[a] PT = Pulsating tension; AS = Alternating shear.
[b] ∞ = continue load cycling at the specified level until failure occurs.
[c] Factor(s) based on mean ultimate load ($N_{u,m}$, $V_{u,m}$) in reference tests in cracked concrete (Δw = 0.8 mm).
[d] The five load cycles at $\frac{6}{7} \cdot N_{u,m}$ must be completed without failure occurring.

9.2.1 Tension cycling

Install the fastener in a closed crack according to the relevant installation instructions. Open the crack by Δw = 0.8 mm. Subject the fastener to the sinusoidally varying loads specified in Figure 9.2a, using a loading frequency between 0.1 and 2 Hz (see comment in Section 9.2.3). The specified load values are fractions of the mean tension capacity (ultimate load) from the reference tests in cracked concrete (refer to Section 9.1). If possible, fastener load and displacement should be recorded continuously during the test to generate the envelope of the load cycling curve. The fastener should complete the five cycles at $6/7 \cdot N_{u,m}$ ($0.86 \cdot N_{u,m}$) without failing to be rated at the full capacity based on the reference tests.

9.2.2 Shear cycling

The testing procedure for shear load cycling is identical to that for tension cycling, however, the load history is given in Figure 9.2b. The shear load should be applied parallel to the crack direction. Experimental investigations using this loading history are needed to establish assessment criteria for the simulated seismic shear load cycling. The potential for low-cycle fatigue under shear load requires further study.

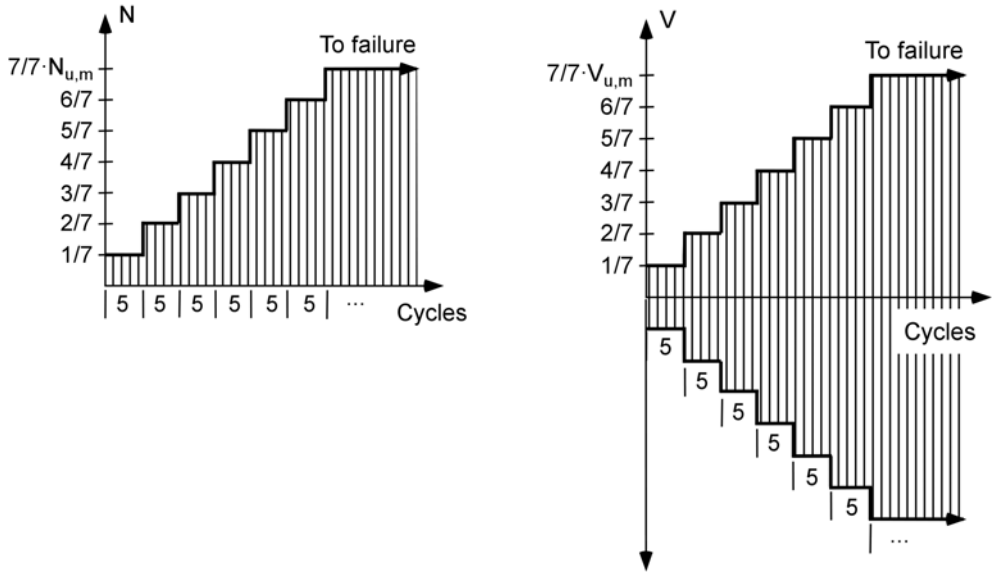

(a) *(b)*

Figure 9.2 Loading pattern for simulated seismic load tests: (a) tension cycling; (b) shear cycling

9.2.3 Comments on load cycling tests

The crack width of Δw = 0.8 mm is based on the results of numerical studies of cracks in reinforced concrete bending members when the tension reinforcement just reaches yield strain (see Chapter 4; Section 4.2). This crack width represents the maximum for which fasteners designed according to *ACI 318 (2005)* or the *CEN TS (in preparation)* need to be tested for typical earthquake situations.

The recommended stepwise-increasing loading patterns can be justified within the context of the cumulative damage studies discussed in Chapter 4 (Section 4.3). The fact that they are traceable to a theoretical framework makes them preferable to existing empirically determined seismic loading histories for fasteners. Moreover, because the load cycles increase up to failure, an arbitrarily defined constant load cycling level, or a stepwise-decreasing loading with arbitrarily cycling levels, is avoided. An additional advantage of stepwise-increasing loading is that the fastener stiffness during load cycling is defined for the entire ascending load branch.

The acceptance criteria of no failure up to $6/7 \cdot N_{u,m}$ ($0.86 \cdot N_{u,m}$) is based on current seismic qualification requirements (Section 3.4.3), which are around $0.80 \cdot N_{u,m}$. The test results presented in Chapter 6 indicate that typical anchors suitable for use in cracked concrete easily meet this requirement.

As demonstrated in Chapter 6 (Section 6.3.2.2), increasing the load cycling frequency typically reduces the fastener displacement during cycling. Therefore, restricting the load cycling frequency for both tension and shear to a single value, e.g. 1 Hz, would produce more consistent results. It must be established, however, whether this is tenable given the technical limitations of testing laboratories.

All tests performed to date (Chapter 3 and Chapter 6) indicate that tension load cycling of anchors, regardless of the cycling pattern, leads to ultimate loads equal to those

obtained in monotonic reference tests. Therefore it might be possible to eliminate the simulated seismic tension load cycling test arguing that it provides no additional information about anchor behavior. One must keep in mind, however, that new anchor types might not behave according to current experience. Elimination of load cycling tests will not be possible for simulated seismic shear load cycling since the low-cycle fatigue failure load will be decisive and must be established by testing.

9.3 Simulated seismic crack cycling test

Simulated seismic crack cycling tests evaluate the performance of the fastener in cycled crack widths representative of those that might occur outside of plastic hinges in reinforced concrete structures during an earthquake. The recommended test parameters and assessment criteria are summarized in Table 9.2. As in Section 9.2, the procedure is intentionally written in a language similar to existing crack cycling tests.

Table 9.2 Test parameters and assessment criteria for simulated seismic crack cycling tests

Crack Width w_1 [mm]	Crack Width w_2 [mm]	No. of Crack Cycles	Sustained Tension Load Level N_w	Assessment Criteria
0.8	0.0	10	$0.40 \cdot N_{u,m}$ [a]	$N_u \geq 0.9 \cdot N_{u,m}$ [a,b,c]

[a] Mean ultimate tension load ($N_{u,m}$) based on reference tests in cracked concrete (Δw = 0.8 mm).
[b] No failure allowed during crack cycling.
[c] Fastener displacement should increase linearly or degressively as a function of the number of crack cycles (linear-linear scale).

9.3.1 Crack cycling

Before installing the fastener, 10 crack opening and closing cycles should be performed to stabilize crack formation. Install the fastener according to the relevant installation instructions such that the axis of the anchor lies in the plane of the crack. Open the crack to a width of w_1 = 0.8 mm. Apply a sustained tensile load N_w equal to the design seismic tension load (~$0.4 \cdot N_{u,m}$) to the fastener. Close the crack completely (w_2 = 0.0 mm) by applying a compressive stress of $0.15 \cdot f_{cc,150}$ over the gross cross-section of the anchorage component. Unload the anchorage component and perform 10 additional crack opening and closing cycles between w_1 = 0.8 mm and w_2 = 0.0 mm. The crack cycling frequency should be a maximum of 0.2 Hz. As the crack width is varied cyclically, N_w must not drop below 95% of the initial prescribed value. Measure the fastener load-displacement relationship up to N_w. After this, measure the displacements of the fastener and the crack cycling width w_1 and w_2, either continuously or at least after 1, 2, 5 and 10 cycles of crack opening and closing. The fastener displacement should be reported at maximum crack opening w_1.

After completing the cycles of crack opening and closing, unload the fastener, measure the residual displacement, and perform a tension test to failure with an initial crack width of Δw = 0.8 mm. During the residual load test, monitor, but do not control, the crack width. The load history for the anchorage component and the fastener are depicted in Chapter 5 (Figure 5.7).

In each test, the fastener displacement should increase linearly or degressively when plotted as a function of the number of crack cycles (linear-linear scale). Additionally, the

mean residual capacity of the fastener should not be less than 90% of the mean capacity in the corresponding reference tests.

9.3.2 Comments on crack cycling test

The selected test parameters for the simulated seismic crack cycling test can be justified based on the discussion in Chapter 4. Further testing is necessary to verify that a compressive stress of $0.15 \cdot f_{cc,150}$ is always sufficient to achieve full crack closure during crack cycling (refer to Chapter 5).

The shape of the crack cycling function is intentionally not specified. Cycled ramp loading (triangular pulses) under control of the anchorage component displacement is likely the simplest implementation.

As illustrated by the test results in Chapter 5, the displacement of the fastener during the simulated seismic crack cycling test can vary significantly while the residual capacity remains unaffected. Additional research is necessary to establish the influence of these widely varying displacements on the load distribution and consequent ultimate load for groups of anchors. It might be necessary to place restrictions on the coefficient of variation of the fastener displacement during crack cycling in order to guarantee reliable design provisions. The experimental testing required to do this was beyond the scope of this dissertation.

The recommended assessment criteria of linearly or degressively increasing fastener displacements during crack cycling may be difficult to realize in qualification tests because graphical representations of the curve shape can be ambiguous. Absolute limits on the allowable fastener displacement during crack cycling, such as are used in serviceability crack cycling tests (Chapter 3, Section 3.4.3) provide quantities that are easier to evaluate. Absolute displacement limits might not be applicable for seismic applications, however, because as shown in Chapter 5 the displacement that an anchor can undergo during seismic crack cycling and still provide load-bearing capacity is strongly dependent on the mode of failure. Further investigation is required.

10 Summary and Open Questions

10.1 Summary

Despite significant advances in fastening technology over the past three decades, our understanding of fastener behavior during earthquakes is relatively poor. Today, Europe has no qualification testing guidelines and performance assessment criteria for fasteners used for general seismic applications. This undesirable situation will become increasingly problematic for designers and fastener manufacturers in the coming years as design standards that require the use of properly qualified fasteners for seismic applications become mandatory.

This dissertation first put into a cohesive framework existing literature related to the behavior and testing of fasteners under earthquake conditions. Normative standards for the design and testing of fasteners for seismic applications were reviewed and summarized.

The conditions to which fasteners are subjected during an earthquake were investigated. It was shown that fasteners used to connect structural and nonstructural elements to a reinforced concrete structure will be subjected to both crack cycling and load cycling at dynamic rates during an earthquake. Fasteners located outside of plastic hinges should be qualified for the maximum crack width that can occur when the reinforcement steel in the anchorage component just reaches the tension yield strain. Studies to establish this crack width were presented. Using structure cycle counting data, tension and shear load cycling time-histories, as well as crack cycling time-histories, were developed for fastener testing. Dynamic loading rates relevant for fasteners used to resist earthquake generated loads were established.

A test setup to investigate fastener performance in large cycled cracks where full crack closure occurs, i.e. as may happen in a reinforced concrete building during an earthquake, was developed. Tests performed with headed studs, expansion anchors, undercut anchors and screw anchors (sizes M10 to M20) showed that fasteners can resist repeated seismic crack cycles (w_1 = 0.8 mm; w_2 = 0.0 mm; n = 10; $N_w = 0.4 \cdot N_{u,m}$) in many cases without significant reduction of the residual strength. Moreover, the load-displacement response for various fastener failure modes during simulated seismic crack cycling was described in detail. It was shown that a linear or degressive increase of fastener displacement as a function of the number of crack cycles, when plotted on a linear-linear scale, is an indicator for suitable fastener performance. Of significant importance for testing, it was demonstrated that fastener displacement ceases to be influenced by a compression load on the anchorage component after the crack in which the anchor is situated has closed sufficiently. A limited number of tests suggest that a compressive stress of 15% of the concrete compressive strength applied over the gross cross-section of the anchorage component was adequate to achieve crack closure (w_2 = 0.0 mm) for the investigated fasteners and testing conditions.

Experimental investigations were conducted to understand the behavior of fasteners located in representative seismic crack widths under pulsating tension load.

Monotonic reference tests with headed bolts (M20) indicated that the slip behavior of these anchors can be better modeled by using a square root function of the concrete compression strength in the equations suggested by *Furche (1994)*. Tension load cycling tests with the same bolts produced an equation to predict head slip during tension load cycling. The equation assumes that the cyclic head slip behavior is an accelerated form of creep. Together with monotonic test data, the cyclic head slip equation can be used to predict whether concrete cone failure will occur for a headed bolt during tension load cycling.

Tension load cycling tests with post-installed fasteners were performed to investigate the performance of various fastener load transfer mechanisms during tension cycling at near-ultimate load. The influence of load cycling frequency and load cycling pattern on fastener behavior, as well as the definition of ductility for fasteners used in seismic applications were discussed. The key conclusions from these tests include the following:

- Fastener failure modes other than steel failure may be acceptable for predominantly tension loaded seismic fastening applications.
- Ductile steel failure of a fastener is meaningless if a sufficient uniform strain length is not present.
- The load capacity of fasteners is not sensitive to the tension load cycling pattern.

New experimental tests with bonded anchors, torque-controlled expansion bolts and bonded-expansion anchors were performed to supplement existing test data on the behavior of fasteners under high (earthquake relevant) load rates. Although under certain conditions some fasteners will exhibit a lower ultimate capacity at high load rate than at quasi-static load rate, the reduction is small and can be neglected for earthquake applications. The potential for a change of fastener failure mode at high load rate and the consequences were also investigated. Further research is required on the effect of loading rate on anchor load-bearing mechanisms that rely on friction to transfer load.

The interrelated nature of modern design and testing methods for fasteners led to a study of design provisions intended to avoid brittle fastener failure modes. It was found that in some instances the margin of safety in existing design guidelines is unconservative. Furthermore, the deformation capacity of anchors designed for ductile steel failure can be controlled over the margin of safety between steel failure and brittle failure in design guidelines.

Based on the literature reviews, theoretical studies and experimental investigations just discussed, recommendations were made to improve testing methods and assessment criteria for fasteners used for earthquake applications.

10.2 Open questions

This dissertation clarifies several fundamental issues related to the behavior and testing of fasteners for seismic applications. Nevertheless, the work reveals that many questions remain unanswered. The most critical open questions are:

(1) The simulated seismic crack cycling test with full crack closure, presented in Chapter 5, was only applied to a limited number of fastener types and sizes. Although the investigated fasteners exhibited surprisingly robust performance under the extreme conditions, further testing with smaller fasteners and a wider variety of fastener types and quality is necessary to generalize the conclusions. Furthermore, the suggested compression stress of 15% of the concrete component compressive strength to achieve full crack closure must be verified by additional tests.

(2) Because the suggested simulated seismic crack cycling test is relatively complicated, further research into the feasibility of a substitute test that mimics the effect of full crack closure on fastener behavior is recommended.

(3) The suggested stepwise-increasing alternating shear load cycling pattern for simulated seismic load cycling must be applied in experimental tests to evaluate its equivalence with existing cyclic shear tests for fasteners and to establish assessment criteria.

(4) The tension load cycling tests presented in Chapter 6 underscore that current seismic design requirements for ductile steel failure of fasteners do not ensure deformation capacity equivalent to the so-called ‘brittle’ failure modes. Quantitative values for the required deformation capacity of fasteners need to be established. It might prove sensible to create categories of required fastener deformation based on desired performance goals.

(5) Further tests on friction critical anchors, e.g. torque-controlled and displacement-controlled expansion anchors, should be performed to determine whether high load rate tests can be neglected in seismic qualification.

(6) Finally, experimental and theoretical investigations of groups of anchors under seismic conditions are necessary to determine load distribution to individual anchors during load or crack cycling and to determine whether the large scatter of displacements that occurs during seismic crack cycling can be tolerated by an anchor group designed using current provisions.

Zusammenfassung (German Summary)

Kapitel 1 – Problemstellung

Die überwiegende Mehrheit von Befestigungselementen, die sich heute auf dem Markt befinden, ist aufgrund fehlender Kenntnisse und Vorschriften unzureichend oder gar nicht für seismische Anwendungen geprüft. Diese Situation führt dazu, dass in vielen Erdbebenregionen häufig Befestigungsmittel verwendet werden, die für die Übertragung seismischer Lasten vermutlich nicht geeignet sind. Für die Öffentlichkeit besteht ein erhöhtes Sicherheitsrisiko, da im Erdbebenfall aufgrund fehlender Nachweise durch geeignete Zulassungsprüfungen ein Versagen solcher Befestigungen nicht auszuschließen ist.

Ziel dieser Arbeit ist es, das Tragverhalten von Befestigungselementen unter Erdbebenbelastung zu erforschen, und damit die Grundlage für ein realitätsnahes, seismisches Zulassungsverfahren zu legen.

Kapitel 2 – Kontext der Forschung

Ab 2007 werden europäische Bauvorschriften (Eurocode) in Kraft treten. Dadurch werden Befestigungsmittel mit einer Zulassung für seismische Anwendungen eine zunehmende Bedeutung einnehmen.

In Kapitel 2 sind Anwendungen für Befestigungselemente bei seismischen Verstärkungsmaßnahmen und bei Befestigungen von nichttragenden Bauteilen dargestellt. Zusätzlich werden Versagensbeispiele von Befestigungselementen bei Erdbeben dargestellt.

Kapitel 3 – Kenntnisstand

Kapitel 3 fasst die vorhandene Literatur zum Tragverhalten und Prüfen von Befestigungen unter Erdbebenbedingungen zusammen. Die Literaturanalyse erfolgt anhand der Auswirkung auf das Ankertragverhalten in drei Kategorien: Einfluss der Lastzyklen, Einfluss der Belastungsgeschwindigkeit und Einfluss von Rissbreitenänderungen. Wichtige Schlussfolgerungen sind:

- In gerissenem Beton sind im allgemeinen die Höchstlasten der Befestigungsmittel geringer und die zugehörigen Verschiebungen größer als in ungerissenem Beton.
- Zuglastzyklen bis zu einem Lastniveau von 80% der Höchstlast wirken sich für Befestigungen, die für gerissenen Beton zugelassen sind, in der Regel nicht negativ auf die Ankerresttagfähigkeit aus.
- Querlastzyklen können schon bei einer geringen Anzahl von Zyklen zu einem Ermüdungsbruch des Ankerstahls führen. Querlastzyklen mit wechselnden Lastrichtungen wirken sich ungünstiger aus als schwellende Querlastzyklen.
- Befestigungen mit einer geringen Verankerungstiefe tendieren unter Querlastzyklen mit wechselnder Lastrichtung zum Betonversagen.
- Die Annahme einer quadratischen Interaktion zwischen zyklischer Zug- und Querlast kann für einige Befestigungselemente auf der unsicheren Seite liegen.
- Zuglastzyklen mit absteigenden Amplituden haben nur einen geringen Einfluss auf die Verschiebungszunahme der Befestigungsmittel.

- Die Höhe der Belastungsgeschwindigkeit wirkt sich im Fall von Beton- oder Verbundversagen nicht ungünstig auf die Ankertragfähigkeit aus. Bei anderen Versagensarten sind reduzierte Höchstlasten im Vergleich zu statischen Versuchen bei geringer Belastungsgeschwindigkeit möglich. Allerdings liegt kein zusammenfassendes Ergebnis vor.
- Rissbreitenänderungen im Ankergrund haben einen signifikanten Einfluss auf das Tragverhalten eines Befestigungselementes.

Zusätzlich werden Vorschriften und Normen aus verschiedenen Ländern zur Bemessung und Zulassung von Befestigungselementen für seismische Anwendungen evaluiert und verglichen.

Kapitel 4 – Theoretische Grundlagen zur Bestimmung von Versuchsparametern
Während eines Erdbebens werden Befestigungen von tragenden und nichttragenden Bauteilen zyklischen Last- und Rissbreitenänderungen unterworfen. Die Amplitude dieser Last- und Rissbreitenänderungen und die Anzahl der Zyklen sind wichtige Parameter im Hinblick auf die Bedingungen für Zulassungsversuche.

Befestigungselemente, die außerhalb von plastischen Gelenken in einem Stahlbetongebäude montiert sind, können im Bereichen angeordnet werden, bei denen die maximale Rissbreite dadurch begrenzt ist, dass der Bewehrungsstahl im Ankergrund zu fließen beginnt. Diese Rissbreite wird anhand von theoretischen und numerischen Untersuchungen bei Δw = 0,8 mm festgelegt. Als Folge einer Momentenumkehr im Ankergrund können offene Risse zugedrückt werden (Δw = 0,0 mm). Numerische Studien, bei denen die Anzahl der Verformungszyklen in Stahlbetongebäuden während eines Erdbebens gezählt wurden, zeigen, dass zwischen 2 und 20 gleichmäßige, nicht elastische Verformungszyklen bei maximalen Verformungsamplituden die gleiche Schädigung wie die gesamte ungleichmäßige Verformungsgeschichte verursachen. Für simulierte seismische Rissversuche mit Befestigungselementen werden eine Anzahl von 10 extremen Rissbreitenänderungen (w_1 = 0,8 mm; w_2 = 0,0 mm) als realistisch erachtet.

Zyklische Zug- und Querlastgeschichten zur Prüfung von Befestigungselementen werden entwickelt, die auf kumulativen Schädigungsmethoden basieren. Es werden treppenförmig ansteigende Belastungen mit 30 Zyklen bis zu ca. 85% der Höchstlast und anschließende Zyklen bei 100% der Höchstlast vorgeschlagen.

Es wird weiterhin gezeigt, dass Belastungszeiten bis zur Höchstlast zwischen ca. 0,25 und 0,025 Sekunden für Befestigungselemente unter Erdbebenbelastungen repräsentativ sind.

Kapitel 5 – Experimentelle Untersuchungen in sich öffnenden und schließenden Rissen
Das Tragverhalten von einbetonierten und nachträglich montierten Befestigungen unter Risszyklen in Zonen außerhalb von plastischen Gelenken in Stahlbetongebäuden während eines Erdbebens wurde untersucht. Ein neuer Versuchsaufbau und die

dazugehörigen Prüfkörper wurden entwickelt. Die Besonderheit dieses Versuchsaufbau ist, dass die Risse überdrückt werden können.

Die untersuchten Befestigungselemente waren Kopfbolzen (d_{nom} = 19 mm), Spreizdübel des Bolzentyps (M16) und des Hülsentyps (M12), Hinterschnittdübel (M10) und Schraubanker (d_{nom} = 20 mm). Eine konstante Zuglast von $N_w = 0{,}4 \cdot N_{u,m}$ wurde auf den Anker aufgebracht und 10 Rissbreitenänderungen zwischen w_1 = 0,8 mm und w_2 = 0,0 mm wurden durchgeführt. Anschließend wurde ein Ausziehversuch durchgeführt um die Resttragfähigkeit zu bestimmen. Die Kopfbolzen, Hinterschnittdübel und Spreizdübel des Hülsentyps versagten durch Betonausbruch. Die Spreizdübel des Bolzentyps versagten durch Durchziehen. Die Schraubanker versagten durch Herausziehen.

Für Befestigungsmittel mit der Versagensart Betonausbruch gilt:

(1) Ist die Ankerverschiebung während der Risszyklen geringer als bei Höchstlast eines vergleichbaren monoton Versuchs in einem statischen Riss, haben die Risszyklen wenig Einfluss auf die Ankerresttragfähigkeit;
(2) Ist die Ankerverschiebung während der Risszyklen gleich oder größer als bei Höchstlast eines vergleichbaren monotonen Versuchs in einem statischen Riss, nimmt die Ankerresttragfähigkeit als Funktion der verlorenen Verankerungstiefe gemäß $(h_{ef} - \delta)^{1,5}$ ab;
(3) Betonausbruch während der Risszyklen kann auftreten, wenn die Verankerungstiefe zu stark reduziert wurde;
(4) Spalten des Betons tritt meist bei großen Ankerverschiebungen auf, bevor eine der oben beschriebenen Versagensarten eintritt.

Für Befestigungsmittel mit der Versagensart Durchziehen gilt:

(1) Beim Durchziehen des Dübels während der Risszyklen oder im anschließenden Ausziehversuch ist die Last-Verschiebungskurve von der umhüllenden monotonen Kurve begrenzt;
(2) Durchziehen ist mit großen Ankerverschiebungen verbunden;
(3) Ist die Ankerverschiebung während der Risszyklen geringer als bei Höchstlast eines vergleichbaren monotonen Versuchs in einem statischen Riss, wird das Tragverhalten beim anschließenden Ausziehversuch steifer;
(4) Ist die Ankerverschiebung während der Risszyklen gleich oder größer als bei Höchstlast eines vergleichbaren monoton Versuchs in einem statischen Riss, nimmt die Ankerresttragfähigkeit als Funktion des absteigenden Asts der monotonen Kurve ab und zeigt eine große Streuung.

Für Schraubanker, die durch Herausziehen versagen, gilt:

(1) Versagen Schraubanker durch Herausziehen in monotonen und simulierten seismischen Rissversuchen, ist das Last-Verschiebungsverhalten ähnlich wie beim Durchziehen, d. h. die Last-Verschiebungskurve während der Risszyklen ist von der umhüllenden monotonen Kurve begrenzt;

(2) Die maximal mögliche Ankerverschiebung während der Risszyklen ist etwas geringer als der Gewindeabstand der Schraube.

Für alle oben beschriebenen Versagensarten ist eine lineare oder degressiv steigende Ankerverschiebungszunahme als Funktion der Anzahl der Risszyklen (doppellinearere Darstellung) ein Zeichen für gutes Ankertragverhalten. Eine progressiv steigende Ankerverschiebungszunahme weist auf Beginn des Versagens hin.

Die Resttragfähigkeit der untersuchten Befestigungen, die durch Betonausbruch (Kopfbolzen, Hinterschnittdübel und Spreizdübel (Hülsentyp)) oder Herausziehen (Schraubanker) versagten, wurde nicht signifikant von den simulierten seismischen Risszyklen ($N_w = 0{,}4 \cdot N_{u,m}$; $w_1 = 0{,}8$ mm; $w_2 = 0{,}0$ mm; $n = 10$) beeinflusst. Die Resttragfähigkeit der untersuchten Befestigungen, die durch Durchziehen (Spreizdübel des Bolzentyps) versagten, wurde gegenüber den Referenzversuchen um mehr als 20% reduziert. Dieses Ergebnis gilt nur für die untersuchten Versuchsbedingungen, Produkte und Ankergrößen.

Die Form der Lastfunktion auf den Ankergrund (Sinus oder Dreieck) beeinflusst die Dauer der Rissöffnung. Allerdings hat dieser Unterschied keinen wesentlichen Einfluss auf das Verhalten des untersuchten Hinterschnittdübels. In Zulassungsversuchen ist die dreieckige Lastfunktion vorzuziehen, da sie einfacher zu steuern ist. Weitere Versuche sind nötig, um dieses Ergebnis für andere Produkte und Ankergrößen zu verifizieren.

Eine Steigerung der Frequenz der Risszyklen von 0,01 Hz (100 Sekunden/Zyklus) auf 0,2 Hz (5 Sekunden/Zyklus) hatte keinen Einfluss auf das Verschiebungsverhalten des untersuchten Hinterschnittdübels. Die hohe Risszyklenfrequenz (0,2 Hz) hat allerdings zu einer Senkung der Ankerlast während der Rissöffnungen geführt (ca. 5% von N_w). Ein Lastabfall von mehr als 5% über mehrere Risszyklen sollte in Zulassungsversuche vermieden werden.

Die Drucklast auf den Ankergrund, die während eines Erdbebens auftreten kann, führt zu einer signifikanten Steigerung der Ankerverschiebung. Der Einfluss der Drucklast verschwindet, nachdem der Riss sich ausreichend um den Dübel geschlossen hat. Wenn der Riss geschlossen ist, werden die Drucklasten durch von den umgebenden Ankergrund aufgenommen. Daher sollte in seismischen Rissversuchen die Drucklast auf den Ankergrund ausreichen um ein Schließen der Risse zu gewährleisten. Die Versuche zeigen, dass eine Druckspannung von $0{,}15 \cdot f_{cc}$ über den Bruttoquerschnitt des Prüfköpers ausreicht, um die Risse zu schließen. Weitere Versuche sind allerdings nötig.

Umfangreiche Überwachung der Rissbreiten zeigte eine signifikante Variation über den Prüfkörperquerschnitt (z. B. von links nach rechts). Die Variation war annähernd linear mit einer Aufwölbung um den Dübel. Es ist daher notwendig die Rissbreiten immer symmetrisch um den Dübel zu messen, so dass ein sinnvoller Mittelwert gebildet werden kann. Ein Mindestabstand zwischen den Dübeln und den Rissmesspunkten von $6 \cdot d_0$ (d_0 = Bohrlochdurchmesser) wird empfohlen, um den lokalen Einfluss der Rissbreitenzunahme zu minimieren. Die Variation der mittleren Rissbreite für Risse

entlang des Prüfkörpers war während der Risszyklen relativ klein (Variationskoeffizient < 10%).

Das Unterkopfpressungslimit von acht Mal der Zylinderdruckfestigkeit des Betons ($8 \cdot f_{cyl} = 6{,}4 \cdot f_{cc}$) für Befestigungen in nicht seismischen Anwendungen scheint auch für Anwendungen mit seismischen Risszyklen geeignet zu sein, solange die Ankerlast unter $0{,}4 \cdot N_u$ bleibt.

Die simulierten seismischen Rissversuche, die in diesem Kapitel beschrieben wurden, sind relativ kompliziert. Deshalb ist eine Ersatzprüfung für Zulassungen anzustreben. Tastversuche haben gezeigt, dass Rissbreitenunterschiede (w_1-w_2) deutlich größer als Δw = 0,8 mm notwendig wären um das Überdrücken eines Risses mit Δw = 0,8 mm nachzubilden.

Kapitel 6 – Experimentelle Untersuchungen mit zyklischen Lasten

Monotone Zugversuche mit Kopfbolzen haben gezeigt, dass eine bessere Korrelation zwischen Unterkopfpressung und Ankerschlupf erzielt werden kann, wenn man in der entsprechenden Gleichung von *Furche (1994)* die lineare Abhängigkeit von der Betondruckfestigkeit durch die Wurzel ersetzt. Eine entsprechend modifizierte Form der Gleichung von Furche wird vorgeschlagen.

Eine Gleichung zur Berechnung des Kopfschlupfs von Kopfbolzen unter zyklischer Zuglast wird entwickelt. Die Gleichung basiert auf der Annahme, dass der Ankerschlupf unter zyklischer Zuglast ein Zeitrafferverfahren für Kriechen ist. Die Gleichung wurde anhand von Versuchsergebnissen kalibriert.

Es hat sich gezeigt, dass Betonausbruch bei Kopfbolzen unter zyklischer Zuglast auftritt, wenn die Ankerverschiebung den absteigenden Ast der monotonen Last-Verschiebungskurve kreuzt. Da die Form des absteigenden Asts der monotonen Last-Verschiebungskurve in der Regel eine große Streuung aufweist, wird die Ankerverschiebung bei Höchstlast eines vergleichbaren monotonen Versuchs als ein zuverlässiger Grenzwert für die Ankerverschiebung unter zyklischer Zuglast vorgeschlagen. Mit diesem Kriterium und der Gleichung für Kopfschlupf unter zyklischer Zuglast ist eine Vorhersage des Versagensmodus für Kopfbolzen auf Basis von monotonen Versuchen möglich.

Nachträglich montierte Befestigungselemente werden in gerissenem Beton (Δw = 0,8 mm) unter zyklischer Zuglast geprüft. Die untersuchten Befestigungselemente, die durch Betonausbruch, Durchziehen und Herausziehen versagten, zeigten ein unerwartet robustes Verhalten unter versagensnaher zyklischer Zuglast. Obwohl die Ergebnisse nicht ohne weitere Untersuchungen für andere Dübelprodukte dieses Typs übernommen werden können, deuten sie darauf hin, dass auch andere Versagensarten als Stahlversagen für seismische Bemessung in vorwiegend zugbelasteten Anwendungen zugelassen werden könnten.

Anforderungen für duktiles Stahlversagen eines Befestigungselements müssen mit einer ausreichend Gleichmassdehnlänge gekoppelt werden um große Verformungen zu

erreichen. In Bemessungsnormen kann die Gleichmassdehnlänge explizit (wie z. B. ≥ 5·*d* in dem *CEN TS (in Vorbereitung)*) oder implizit über den Sicherheitsspielraum zwischen duktilem und sprödem Versagen (wie im *ACI 318 Appendix D (2005)*) festgelegt werden. Weitere Forschung ist dazu erforderlich.

Frequenzen zwischen 0,1 und 2 Hz werden für die Zuglastzyklen in bestehenden seismischen Zulassungen für Befestigungselemente verwendet. Frequenzen bis zu 10 Hz sind allerdings für seismische Anwendungen plausibel. Durch experimentelle Versuche wird bestätigt, dass Zuglastzyklenfrequenzen größer als 2 Hz keinen negativen Einfluss auf das Tragverhalten der untersuchten Befestigungselemente haben. Dieses Ergebnis war unabhängig von der Versagensart. Die Ergebnisse bestätigen die Verwendung des bisherigen Frequenzbereichs für Lastzyklen.

Die untersuchten Befestigungselemente hatten ein ähnliches Verschiebungsverhalten und eine ähnliche Tragfähigkeit unter treppenförmig ansteigenden Lastzyklen oder konstanten Lastzyklen mit einem anschließenden Ausziehversuch. *Silva (2001)* zeigte, dass treppenförmig ansteigende Lastzyklen für simulierte seismische Lastzyklenversuche vorzuziehen sind, da sie die Ankersteifigkeit über den gesamten Belastungsbereich bis zum Versagen verdeutlichen. Darüber hinaus vermeiden treppenförmig ansteigende Lastzyklen das Problem der Festlegung eines konstanten Lastzyklenniveaus.

Kapitel 7 – Experimentelle Untersuchungen mit hoher Belastungsgeschwindigkeit
Während eines Erdbebens können Befestigungselemente in Gebäuden bis zum Versagen in weniger als einem Zehntel einer Sekunde belastet werden.

In Kapitel 7 werden neue experimentelle Versuchsergebnisse für Verbundanker, Spreizanker und Spreizverbundanker unter hohen Zugbelastungsgeschwindigkeiten zusammen mit einer Neuauswertung von Versuchergebnissen aus der Literatur präsentiert.

Zusammenfassend kann gesagt werden, dass erdbebenrelevante Belastungsgeschwindigkeiten keine negative Auswirkung auf das Tragverhalten im Fall von Betonausbruch oder Stahlversagen haben. Diese Schlussfolgerung gilt sowohl für Zugbelastung als auch für Querbelastung und ist unabhängig vom Zustand des Betons (ungerissen oder gerissen).

Im Fall Durchziehen von mechanischen Befestigungselementen nimmt die Versagenslast mit der Belastungsgeschwindigkeit ab. Für erdbebenrelevante Belastungsgeschwindigkeiten ist aber die Abnahme in der Regel sehr klein.

Erhöhte Belastungsgeschwindigkeit kann für einige Befestigungstypen (z. B. Verbundanker, Spreizdübel) und Betonzustände (z. B. gerissener Beton) einen Wechsel des Versagensmodus verursachen. Die zu erwartende Abnahme der Versagenslast scheint bei erdbebenrelevanten Belastungsgeschwindigkeiten allerdings sehr klein.

Kapitel 8 – Wahrscheinlichkeit eines spröden Versagens während eines Erdbebens

Die meisten Bemessungsnormen für Befestigungselemente erlauben duktiles Versagen des Ankerstahls für seismische Anwendungen. Das Ankerstahlversagen vor einen anderen Versagensart (z. B. Betonausbruch oder Herausziehen) auftritt, wurde durch einen vorgeschriebenen Sicherheitsspielraum zwischen duktilen und spröden Versagensarten gewährleistet.

Numerische Untersuchungen zeigen, dass der Sicherheitsspielraum von nur 29 Prozent zwischen der mittleren Stahl- und Betonbruchlast, der sich aus den *ACI 318 (2005)* Bemessungsbeiwerten ergibt, nicht konservativ ist.

Im Falle einer 10prozentigen Stahlüberfestigkeit, die in die Praxis häufig vorkommt, zusammen mit einer Reduktion der Betonversagenslast von 15 Prozent, z. B. durch unerwartet breite Risse im Beton, ist ein Sicherheitsspielraum von mindestens 50 Prozent zwischen der mittleren Stahl- und Betonbruchlast nötig, um Stahlversagen mit ca. 99 Prozent Wahrscheinlichkeit zu gewährleisten.

Kapitel 9 – Empfehlungen für das Prüfen und die Beurteilung von Befestigungen

In Übereinstimmung mit bestehenden Zulassungsverfahren für Befestigungselemente für seismische Anwendungen werden drei Arten von Versuchen vorgeschlagen:

(1) Referenzversuche um die Ankertragfähigkeit unter Zug- und Querbelastung in gerissenem Beton zu ermitteln;
(2) Versuche mit Lastzyklen unter schwellender Zuglast und wechselnder Querlast in statischen Rissen;
(3) Versuche in sich öffnenden und schließenden Rissen, bei denen die Anker mit einer kontinuierlich wirkenden Axialzugkraft belastet und einer kleinen Anzahl von Rissbreitenwechseln mit großer Amplitude unterworfen werden.

Die Referenzversuche sollten in eine Rissbreite von $\Delta w = 0{,}8$ mm verschiebungsgesteuert durchgeführt werden. Die Ankerverschiebungen bei Höchstlast und bei 80% der Höchstlast im aufsteigenden und absteigenden Ast der Last-Verschiebungskurve, sind im Versuchsprotokoll festzuhalten. Anhand der Verschiebungswerte können zukünftige Verschiebungsannahmekriterien festgelegt werden.

Die Versuche mit Lastzyklen sollten mit treppenförmig ansteigenden Zug- und Querbelastungen mit einer Rissbreite von $\Delta w = 0{,}8$ mm durchgeführt werden. Belastungsgeschichten mit Inkrementen von einem Siebtel der mittleren Höchstlast aus den Referenzversuchen und fünf Zyklen per Inkrement werden basierend auf einer kumulativen Schädigungsmethode vorgeschlagen. Dabei ergeben sich ca. 35 Zyklen bis zum Versagen. In den Zugversuchen sollten die Anker fünf Lastzyklen bei $6/7 \cdot N_{u,m}$ (ca. $0{,}85 \cdot N_{u,m}$) überdauern, um mit der vollen Referenzelast bewertet zu werden. Beurteilungskriterien unter Schublastzyklen konnten im Rahmen dieser Arbeit nicht festgelegt werden. Die Versuchsparameter und Beurteilungskriterien sind in Tabelle Z.1 zusammengefasst.

Tabelle Z.1 Versuchsparameter und Beurteilungskriterien für Versuche mit Lastzyklen

Amplitude der Lastzyklen	Art der Belastung[a]	Riss-breite [mm]	Anzahl der Lastzyklen[b]	Lastniveau[c]	Beurteilungskriterien
treppenförmig ansteigend	PT	0,8	5/5/5/5/5/∞	$\frac{1}{7}$ / $\frac{2}{7}$ / $\frac{3}{7}$ / $\frac{4}{7}$ / $\frac{5}{7}$ / $\frac{6}{7}$ / $\frac{7}{7}$	$N_u \geq \frac{6}{7} \cdot N_{u,m}$[c,d]
	AS	0,8	5/5/5/5/5/∞	± $\frac{1}{7}$ / $\frac{2}{7}$ / $\frac{3}{7}$ / $\frac{4}{7}$ / $\frac{5}{7}$ / $\frac{6}{7}$ / $\frac{7}{7}$	nicht vorhanden

[a] PT = schwellende Zuglast; AS = wechselnde Querlast.
[b] ∞ = Lastzyklen weiterfahren bis zum Versagen.
[c] Faktoren basieren auf dem Mittelwert der Höchstlast ($N_{u,m}$, $V_{u,m}$) aus Referenzversuchen in gerissenem Beton (Δw = 0,8 mm).
[d] Das Befestigungselement muss die fünf Lastzyklen bei $\frac{6}{7} \cdot N_{u,m}$ überdauern.

In den Versuchen in sich öffnenden und schließenden Rissen sollen die Befestigungselemente mit einer kontinuierlich wirkenden Axialzugkraft N_w von 40% der mittleren Höchstlast aus den Referenzversuchen belastet und 10 Rissbreitenwechsel zwischen w_1 = 0,8 mm und w_2 = 0,0 mm unterworfen werden. Die Resttragfähigkeit wird in einem anschließenden Ausziehversuch mit eine Rissbreite von Δw = 0,8 mm ermittelt. Eine Drucklast von 15% der Betondruckfestigkeit ($0{,}15 \cdot f_{cc,150}$) über den Bruttoquerschnitt des Prüfkörpers solle das Schließen des Risses (w_2 = 0,0 mm) gewährleisten. Die Verschiebungszunahme während der Risszyklen sollte linear oder degressiv ansteigen und die Resttragfähigkeit sollte mindestens 90% der Höchstlast aus den Referenzversuche betragen. Die Versuchsparameter und Beurteilungskriterien sind in Tabelle Z.2 zusammengefasst.

Tabelle Z.2 Versuchsparameter und Beurteilungskriterien für Versuche in sich öffnenden und schließenden Rissen

Rissbreite w_1 [mm]	Rissbreite w_2 [mm]	Anzahl der Risszyklen	Kontinuierliche Zuglast N_w	Beurteilungskriterien
0,8	0,0	10	$0{,}40 \cdot N_{u,m}$[a]	$N_u \geq 0{,}9 \cdot N_{u,m}$[a,b,c]

[a] Mittelwert der Höchstlast ($N_{u,m}$) aus Referenzversuchen in gerissenem Beton (Δw = 0,8 mm).
[b] Das Befestigungselement darf nicht während der Risszyklen versagen.
[c] Die Ankerverschiebung muss linear order degressiv als Funktion der Anzahl der Risszyklen ansteigen (doppellineare Darstellung).

Monotone Versuche mit erhöhter Belastungsgeschwindigkeit werden aufgrund der in Kapitel 7 präsentierten Ergebnisse für seismische Anwendungen als nicht notwendig erachtet. Allerdings sind weitere Versuche mit reibungskritischen Dübeln unter hoher Belastungsgeschwindigkeit erforderlich.

Kapitel 10 – Zusammenfassung und offene Fragen

In der vorliegenden Dissertation wird das Verhalten von einbetonierten und nachträglich in Beton verankerten Befestigungssystemen unter Erdbebenbeanspruchung untersucht. Zusätzlich werden die Grundlagen für die Entwicklung von seismischen Zulassungsverfahren und Beurteilungskriterien für Befestigungselemente beschrieben.

Durch die vorliegende Arbeit konnten wesentliche Fragestellungen zum Tragverhalten und Prüfen von Befestigungselementen für seismische Anwendungen geklärt werden. Dennoch verbleiben einige offene Fragen:

- Die vorgeschlagenen seismischen Rissversuche sollten für weitere Ankertypen und Größen angewendet werden um allgemeine Schlussfolgerungen über die Eignung von Dübeln unter diese Bedingungen zu ziehen.
- Eine einfachere Ersatzprüfung für die seismischen Rissversuche wäre anzustreben.
- Beurteilungskriterien für zyklische Schublastversuche sind nötig.
- Eine neue Definition für die Duktilität von Befestigungssystemen ist notwendig. Zudem fehlen Beurteilungskriterien hinsichtlich der Ankerverschiebung.
- Weitere Versuche mit reibungskritischen Dübeln unter hoher Belastungsgeschwindigkeit sind erforderlich.
- Letztlich sind theoretische und experimentelle Untersuchungen über die Lastverteilung auf die Einzelnen Befestigungselemente innerhalb einer Ankergruppe unter Erdbebenbeanspruchung erforderlich.

Literature

AC01 (2005) International Code Council Evaluation Service, Inc. (ICC-ES) (2005). *AC01 – Acceptance criteria for expansion anchors in concrete and masonry elements*. ICC-ES, Whittier, California.

AC58 (2005) International Code Council Evaluation Service, Inc. (ICC-ES) (2005). *AC58 – Acceptance criteria for adhesive anchors in concrete and masonry elements*. ICC-ES, Whittier, California.

AC60 (2005) International Code Council Evaluation Service, Inc. (ICC-ES) (2005). *AC60 – Acceptance criteria for anchors in unreinforced masonry elements*. ICC-ES, Whittier, California.

AC106 (2005) International Code Council Evaluation Service, Inc. (ICC-ES) (2005). *AC106 – Acceptance criteria for predrilled fasteners (screw anchors) in concrete or masonry elements*. ICC-ES, Whittier, California.

AC156 (2004) International Code Council Evaluation Service, Inc. (ICC-ES) (2004). *AC156 – Acceptance criteria for seismic qualification by shake-table testing of nonstructural components and systems*. ICC-ES, Whittier, California.

AC193 (2005) International Code Council Evaluation Service, Inc. (ICC-ES) (2005). *AC193 – Acceptance criteria for mechanical anchors in concrete elements*. ICC-ES, Whittier, California.

AC308 (2005) International Code Council Evaluation Service, Inc. (ICC-ES) (2005). *AC308 – Acceptance criteria for post-installed adhesive anchors in concrete elements*. ICC-ES, Whittier, California.

ACI 318 (2005) American Concrete Institute (ACI) (2005). *Building code requirements for structural concrete (ACI 318-05) and commentary (ACI 318R-05)*. ACI, Farmington Hills, Michigan.

ACI 349 (1985) American Concrete Institute (ACI) (1985). *Code requirements for nuclear safety related concrete structures (ACI 349-85) and commentary (ACI 349R-85)*. ACI, Farmington Hills, Michigan.

ACI 349 (2001) American Concrete Institute (ACI) (2001). *Code requirements for nuclear safety related concrete structures (ACI 349-01) and commentary (ACI 349R-01)*. ACI, Farmington Hills, Michigan.

ACI 355.2 (2004) American Concrete Institute (ACI) (2004). *ACI 355.2-04: Qualification of post-installed mechanical anchors in concrete*, ACI, Farmington Hills, Michigan.

Akiyama et al. (1997) Akiyama, T., Hirosawa, M., Shimizu, Y. and Katagiri, T. (1997). “A study on shear strength of post-installed anchors.” *The papers to be related to design of anchors under seismic loading*, Universität Stuttgart.

Ammann (1983) Ammann, W. (1983). *Stahlbeton- und Spannbetontragwerke unter stossartiger Belastung (Reinforced concrete and prestressed concrete structures under impact loads)*. Report No. 142, Institut für Baustatik und Konstruktion, Eidgenössische Technische Hochschule Zürich. (in German)

Ammann (1991) Ammann, W. (1991). “Static and dynamic long-term behavior of anchors.” *Special Publication SP 130-8*, American Concrete Institute, Detroit, 205-220.

Ammann (1992) Ammann, W. (1992). "Fastening systems under seismic loading conditions." *Proceedings of the 10th World Conference on Earthquake Engineering*, Vol. 9, Madrid, Spain, 5247-5252.

ASTM 488 (1990) American Society for Testing and Materials (ASTM) (1990). *ANSI/ASTM 488 – Test method of strength of anchors in concrete and masonry elements*. ASTM, Pennsylvania.

ASTM F606M (1998) American Society for Testing and Materials (ASTM) (1998). *F606M Standard Test Methods for Determining the Mechanical Properties of Externally and Internally Threaded Fasteners, Washers, and Rivets [Metric]*. ASTM, Pennsylvania.

ATC-24 (1992) Applied Technology Council (ATC) (1992). *ATC-24 Guidelines for cyclic seismic testing of components of steel structures*. ATC, Redwood City, California.

ATC-29 (1990) Applied Technology Council (ATC) (1990). *Proceedings of ATC-29 seminar and workshop on seismic design and performance of equipment and nonstructural elements in buildings and industrial structures.* October 3-5, 1990, Irvine, California.

ATC-29-1 (1998) Applied Technology Council (ATC) (1998). *Proceedings of seminar on seismic design, retrofit, and performance of nonstructural components*. January 22-23, 1998, San Francisco, California.

ATC-40 (1996) Applied Technology Council (ATC) (1996). *ATC-40: Seismic evaluation and retrofit of concrete buildings*. ATC, Redwood City, California.

ATC-58 (2004) Applied Technology Council (ATC) (2004). *ATC-58 Project Task Report (Phase 2, Task 2.3) Engineering demand parameters for nonstructural components*. ATC, Redwood City, California.

Bachmann (1967) Bachmann, H. (1967). *Zur plastizitätstheoretischen Berechnung statisch unbestimmter Stahlbetonbalken (Plasticity theory calculations of statically indeterminate reinforced concrete beams)*. Dissertation, Institut für Baustatik, Eidgenössische Technische Hochschule (ETH), Zürich. (in German)

Bažant & Oh (1983) Bažant, Z. P. and Oh, B. H. (1983). "Spacing of cracks in reinforced concrete." *Journal of Structural Engineering, ASCE,* Vol. 109, No. 9, 2066-2085.

Broms (1965) Broms, B. B. (1965). "Crack width and crack spacing in reinforced concrete members." *Journal of the American Concrete Institute*, No. 10, Proceedings Vol. 62, 1237-1256.

Bursi (2005) Bursi, O. (Editor) (2005). *Seismic qualification of cast-in channels and shear connector devices between steel and concrete*. CASCADE Report No. 4, LNEC – Laboratório Nacional de Engenharia Civil.

Cannon (1981) Cannon, R. W. (1981). "Expansion anchor performance in cracked concrete." *ACI Journal*, Vol. 78, No. 6, 471-479.

CEB (1987) Comité Euro-International du Béton (CEB) (1987). *Concrete structures under impact and impulsive loading*. Bulletin No. 187, Thomas Telford Service Ltd., London.

CEB (1993) Comité Euro-International du Béton (CEB) (1993). *CEB-FIP Model Code 1990.* Bulletin No. 213/214, Thomas Telford Service Ltd., London.

CEB (1994) Comité Euro-International du Béton (CEB) (1994). *Fastenings to concrete and masonry structures: State of the art report*. Thomas Telford Service Ltd., London.

CEB (1997) Comité Euro-International du Béton (CEB) (1997). *Design of fastenings in concrete: Design guide*. Thomas Telford Service Ltd., London.

CEN TS (in preparation) European Committee for Standardization (CEN) (in preparation). *Design of fastenings for use in concrete*. Technical Specification, CEN, Brussels.

Chopra (1995) Chopra, A. (1995). *Dynamics of structures: Theory and applications to earthquake engineering*. Prentice Hall, N.J.

Coffin (1954) Coffin, L. F. Jr. (1954). "A study of the effect of cyclic thermal stresses in ductile metals." *Transactions of the ASME,* Vol. 76, 931-950.

Collins (1988) Collins, D. M. (1988). *Load-deflection behavior of cast-in-place and retrofit concrete anchors subjected to static, fatigue, and impact tensile loads*. PhD dissertation, The University of Texas at Austin.

Cook et al. (1998) Cook, R. A., Kunz, J., Fuchs, W. and Konz, R. C. (1998). "Behavior and design of single adhesive anchors under tensile load in uncracked concrete." *ACI Structural Journal*, Vol. 95, No. 1, 9-26.

Copley & Burdette (1985) Copley, J. D. and Burdette, E. G. (1985). "Behavior of steel-to-concrete anchorage in high moment regions." *ACI Journal*, *Proceedings,* Vol. 82, No. 2, 180-187.

Cornelissen & Reinhardt (1984) Cornelissen, H. A. W. and Reinhardt H. W. (1984). "Uniaxial tensile fatigue failure of concrete under constant-amplitude and programme loading." *Magazine of Concrete Research*, Vol. 36, No. 129, 216-226.

Cornell (1967) Cornell, A. C. (1967). *Bounds on the reliability of structural systems*. Proc. ASCE Journal of the Structural Division, Vol. 93.

CSA-N287.2 (2003) Canadian Standards Association (CSA) (reaffirmed 2003). *Material requirements for concrete containment structures for CANDU nuclear power plants*. CSA, Toronto, Canada.

CSA-N287.3 (1999) Canadian Standards Association (CSA) (reaffirmed 1999). *Design requirements for concrete containment structures for CANDU nuclear power plants*. CSA, Toronto, Canada.

CSA-N289.3 (2003) Canadian Standards Association (CSA) (reaffirmed 2003). *Design procedures for seismic qualification of CANDU nuclear power plants*. CSA, Toronto, Canada.

CSTB (2003) Centre Scientifique et Technique du Bâtiment (CSTB) (2003), "Seismic behavior of anchorages." *Presentation to fib SAG Fastenings*.

Czarnecki & Sliter (1988) Czarnecki, R. M. and Sliter, G. E. (1988). "Development of seismic anchorage guidelines for nuclear plant equipment." *Nuclear Engineering and Design*, Vol. 107, 1-2, 27-41.

DIBt (1998) Deutsches Institute für Bautechnik (DIBt) (1998). *Verwendung von Dübeln in Kernkraftwerken und kerntechnischen Anlagen, Leitfaden zur Beurteilung von Dübelbefestigungen bei der Erteilung von Zustimmungen im Einzelfall nach den Landesbauordnung der Bundesländer (Use of anchors in nuclear power plants and nuclear technology installations, guideline for evaluating fastenings for granting permission in individual cases according to the state structure regulations of the federal states of Germany)*. Deutsches Institute für Bautechnik, Berlin. (in German)

Dieterle & Optiz (1988) Dieterle, H. and Optiz, V. (1988). *Tragverhalten von nicht generell zugzonetauglichen Dübeln – Teil 1: Verhalten in Parallelrissen (Bearing behavior of anchors not suitable for use in cracked concrete. Part 1: Behavior in line cracks)*. Report No. 1/34-88/21, Institut für Werkstoffe im Bauwesen, Universität Stuttgart. (in German)

DIN 1045 (2001) Deutsches Institut für Normung (DIN) (2001). *Tragwerke aus Beton, Stahlbeton und Spannbeton: Teil 2 Festlegung, Eigenschaften, Herstellung und Konformität (Concrete, reinforced concrete and prestressed concrete structures: Part 2, regulation, properties, production and conformity)*. DIN, Berlin. (in German)

DIN 1048 (1991) Deutsches Institut für Normung (DIN) (1991). *Prüfverfahren für Beton (Test methods for concrete)*. DIN, Berlin. (in German)

Dutta & Mander (2001) Dutta, A. and Mander, J. B. (2001). "Energy based methodology for ductile design of concrete columns." *Journal of Structural Engineering*, Vol. 127, No. 12, 1374-1381.

EERI (1996) Earthquake Engineering Research Institute (EERI) (1996). *Post-earthquake investigation field guide: Learning from Earthquakes*. EERI, Oakland, California.

Ehrenstein (1993) Ehrenstein, G. W. (1993). *Hysteresis-Meßverfahren - das flexible Verfahren zur dynami-schen Werkstoff- und Bauprüfung nach R. Renz (Hysteretic measurement method - the flexible method for dynamic material and component testing from R. Renz)*. Lehrstuhl für Kunstofftechnik, Universität Erlangen-Nürnberg. (in German)

Eibl & Keintzel (1989a) Eibl, J. and Keintzel, E. (1989). *Zur Beanspruchung von Befestigungsmitteln bei dynamischen Lasten (On the dynamic loading of fastenings)*. Institut für Massivbau und Baustofftechnologie, Universität Karlsruhe. (in German)

Eibl & Keintzel (1989b) Eibl, J. and Keintzel, E. (1989). *Verhalten von Dübeln unter hoher Stoß- und Wechselbeanspruchung (Behavior of anchors under high speed impact and reversed cyclic loads)*. Institut für Massivbau und Baustofftechnologie, Universität Karlsruhe. (in German)

Eligehausen & Balogh (1995) Eligehausen, R. and Balogh, T. (1995). "Behavior of fasteners loaded in tension in cracked reinforced concrete." *ACI Structural Journal*, Vol. 92, No. 3, 365-379.

Eligehausen et al. (2006) Eligehausen, R., Mallée, R. and Silva, J. (2006). *Anchorage in Concrete Construction*. Wilhelm Ernst & Sohn, Berlin.

Eligehausen & Asmus (1991) Eligehausen, R. and Asmus, J. (1991). *Zuverlässigkeitsprüfungen an Dübeln in Linienrissen (Reliability tests on fasteners in line cracks)*. Report No. 1/49A - 91/1A, Institut für Werkstoffe im Bauwesen, Universität Stuttgart. (in German)

Endo & Shimizu (1985) Endo, T. and Shimizu, Y. (1985). "Behavior of expansion anchor bolts." *Memoirs of Faculty of Technology Tokyo Metropolitan University*, No. 35.

ETAG 001 (1997) European Organization of Technical Approvals (EOTA) (1997). *ETAG 001: Guideline for European technical approval of metal anchors for use in concrete, Parts 1 – 6*. EOTA, Brussels.

Eurocode 2 (2002) European Committee for Standardization (CEN) (2002). *Eurocode 2: Design of concrete structures: Part 1 General rules and rules for buildings*. prEN 1992-1-1.

Eurocode 8 (2003) European Committee for Standardization (CEN) (2003). *Eurocode 8: Design of structures for earthquake resistance Part 1: General rules, seismic actions and rules for buildings*. prEN 1998-1 : 2003, Stage 49, version: September, 2003.

FEMA 368 (2001) Building Seismic Safety Council (BSSC) (2001). *NEHRP recommended provisions for seismic regulations for new buildings and other structures, 2000 Edition*. Prepared for the Federal Emergency Management Agency (FEMA) by the BSSC, Washington, DC.

FEMA 412 (2002) Federal Emergence Management Agency (FEMA) (2002). *FEMA-412 Installing seismic restraints for mechanical equipment*. FEMA, Washington, DC.

Fuchs et al. (1995) Fuchs, W., Eligehausen, R. and Breen, J. E. (1995). "Concrete Capacity Design (CCD) approach for fastening to concrete." *ACI Structural Journal*, Vol. 92, No. 1, 73-94.

Fujikake et al. (2003) Fujikake, K., Nakayama, J., Sato, H., Mindess, S. and Ishibashi, T. (2003). "Chemically bonded anchors subjected to rapid pullout loading." *ACI Materials Journal*, Vol. 100, No. 3, 246-252.

Furche (1987) Furche, J. (1987). *Versuchseinrichtung zur Prüfung von in Rissen verankerten Dübeln und erste Versuche an Parallelrisskörpern (Test setup for the testing of fasteners in cracks and initial tests in parallel cracks)*. Institut für Werkstoffe im Bauwesen, Universität Stuttgart. (in German)

Furche (1988) Furche, J. (1988). *Versuche an Kopfbolzen mit unterschiedlichen Kopfformen bei Verankerungen in sich öffnenden und schließenden Rissen: Part 2 (Tests with headed bolts with various head shapes in opening and closing cracks: Part 2)*. Report No. 9/5 - 88/10 , Institut für Werkstoffe im Bauwesen, Universität Stuttgart. (in German)

Furche (1990) Furche, J. (1990). *Einfluß der Hinterschnittform auf das Last-Verschiebungsverhalten bei zentrischem Zug : Teil III: Verschiebungsverhalten von Verankerungen in sich öffnenden und schließenden Rissen (Influence of the undercut shape on the load-displacement behavior under centric tension load: Part 3: Displacement behavior in opening and closing cracks)*. Report No. 9/8 - 90/8, Institut für Werkstoffe im Bauwesen, Universität Stuttgart. (in German)

Furche (1994) Furche, J. (1994). *Zum Trag- und Verschiebungsverhalten von Kopfbolzen bei zentrischem Zug (Load-bearing and displacement behavior of headed bolts under centric tension load)*. PhD dissertation, Institut für Werkstoffe im Bauwesen, Universität Stuttgart. (in German)

Gergely & Lutz (1968) Gergely, P. and Lutz, L. A. (1968). "Maximum crack width in reinforced concrete flexural members." *Causes, Mechanisms and Control of Cracking in Concrete*, American Concrete Institute, SP-20, 87-117.

Guiriani & Grisanti (1986) Guiriani, E. and Grisanti, A. (1986). *Comportamente dei connettori a piolo delle travi miste in acciaio e calcestruzzo (Behavior of shear connectors in composite steel-concrete construction)*. Univ. Milano, 272-307.

Hallowell (1996) Hallowell, J. M. (1996). *Tensile and shear behavior of anchors in uncracked and cracked concrete under static and dynamic loading*. M.S. Thesis, The University of Texas at Austin.

Hancock & Bommer (2005) Hancock, J. and Bommer, J. J. (2005). "The effective number of cycles of earthquake ground motion." *Earthquake Engineering and Structural Dynamics*, Vol. 34, No. 6, 637-664.

Henzel & Stork (1990) Henzel, J., and Stork, J. (1990). "Anchors under predominantly static shear load with alternating direction." *Darmstadt Concrete: Annual Journal on Concrete and Concrete Structures*, Vol. 5, TH Darmstadt, 79-86.

Hilti (2003) Hilti (2003). *Guideline for earthquake resistant design of installations and non-structural elements*. Hilti, Schaan, Liechtenstein.

Hoehler (2004a) Hoehler, M. S. (2004). *Cracking in reinforced concrete structures under seismic excitations – Part I: Maximum crack widths under representative monotonic loading*. Institut für Werkstoffe im Bauwesen, Universität Stuttgart.

Hoehler (2004b) Hoehler, M. S. (2004). *Tension cycling of threaded rods at large inelastic deformations – Grades 4.6, 8.8, and 10.9: Series A1 – Test results*. Institut für Werkstoffe im Bauwesen, Universität Stuttgart.

Hoehler (2004c) Hoehler, M. S. (2004). *Tension cycling of fasteners at high load levels: Series A2 – Test results*. Institut für Werkstoffe im Bauwesen, Universität Stuttgart.

Hoehler (2004d) Hoehler, M. S. (2004). *Low-cycle tension load cycling of headed bolts under varying head pressures: Series A3 – Test report*. Institut für Werkstoffe im Bauwesen, Universität Stuttgart.

Hoehler (2004e) Hoehler, M. S. (2004). *Verification of the direct displacement measurement method*. Institut für Werkstoffe im Bauwesen, Universität Stuttgart.

Hoehler (2004f) Hoehler, M. S. (2004). *Tension cycling of fasteners at high load levels (Extension of Series A2 to high load rates): Series A4 – Test report*. Institut für Werkstoffe im Bauwesen, Universität Stuttgart.

Hoehler (2005a) Hoehler, M. S. (2005). *Tension load cycling of headed bolts in uncracked concrete: Series A5 – Test report*. Institut für Werkstoffe im Bauwesen, Universität Stuttgart.

Hoehler (2005b) Hoehler, M. S. (2005). *Seismic crack cycling test for fasteners: Series B1 – Feasibility study*. Institut für Werkstoffe im Bauwesen, Universität Stuttgart.

Hoehler (2006a) Hoehler, M. S. (2006). *Seismic crack cycling test for fasteners: Series B2 – Investigation of headed bolts, bolt anchors, sleeve anchors, screw anchors and undercut anchors*. Institut für Werkstoffe im Bauwesen, Universität Stuttgart.

Hoehler (2006b) Hoehler, M. S. (2006). *Fastener behavior under representative seismic tension loads: Summary report and discussion for test series A1 to A5*. Institut für Werkstoffe im Bauwesen, Universität Stuttgart.

Hoehler (2006c) Hoehler, M. S. (2006). *Influence of earthquake relevant tensile loading rates on fastener failure mode*. Institut für Werkstoffe im Bauwesen, Universität Stuttgart.

Hunziker (1983) Hunziker, P. (1983). „Prüfung and Zulassung von Dübeln für schocksicher Befestigungen" (Testing and prequalification of anchors for impact loading). *Verein Deutscher Ingenieure (VDI)*, Report No. 496 65-70. (in German)

Hunziker (1984) Hunziker, P. (1984). *Schockprüfung von Fischer-Zykonanker FZA (Impact testing of fischer Zykon anchor FZA)*, AC-Laboratorium Spiez, Report No. 150. (in German)

Hunziker (1987) Hunziker, P. (1987).*Schockprüfung von Fischer Hochleistungsankern FHA (Impact testing of fischer high-performance anchor FHA)*. AC-Laboratorium Spiez, Report No. 205. (in German)

IBC (2003) International Code Council (ICC) (2003). *International Building Code, 2003 Edition*. ICC, Whittier, California.

Jeong & Iwan (1988) Jeong, G. D. and Iwan, W. D. (1988). "The effect of earthquake duration on the damage of structures." *Earthquake Engineering and Structural Dynamics*, Vol. 16, No. 8, 1201-1211.

Klingner et al. (1982) Klingner, R.E., Mendonca, J.A. and Malik J.B. (1982). "Effect of reinforcing details on the shear resistance of anchor bolts under reversed cyclic loading." *ACI Journal*, Vol. 79, No. 1, 471-479.

Klingner et al. (1998) Klingner, R. E., Hallowell, J. M., Lotze, D., Park, H-G., Rodriguez, M. and Zhang, Y-G. (1998). *Anchor bolt behavior and strength during earthquakes*. U.S. Nuclear Regulatory Commission, NUREG/CR-5434.

Kraus (2003) Kraus, J. (2003). *Tragverhalten und Bemessung von Ankerschienen unter zentrischer Zugbelastung (Load-bearing behavior and design of anchor channels under tension load)*. PhD dissertation, Institut für Werkstoffe im Bauwesen, Universität Stuttgart. (in German)

Krausz & Krausz (1988) Krausz, A. S. and Krausz, K. (1988). *Fracture kinetics of crack growth*. Kluwer, Dordrecht, The Netherlands.

Krawinkler et al. (1983) Krawinkler, H., Zohrei, M., Lashkari-Irvani, B., Cofie, N. G. and Hadidi-Tamjed, H. (1983). *Recommendation for experimental studies on the seismic behavior of steel components and materials*. Report No. NSF/CEE-83220, Stanford University.

Kreller (1989) Kreller, H. (1989). *Zum nichtlinearen Trag- und Verformungsverhalten von Stahlbetonstabtragwerken unter Last- und Zwangeinwirkung (Nonlinear load-bearing and displacement behavior of reinforced concrete members under applied loads and displacements)*. PhD dissertation, Institut für Werkstoffe im Bauwesen, Universität Stuttgart. (in German)

Küenzlen & Sipple (2001) Küenzlen, J. and Sipple, T. M. (2001). "Behavior and design of fastenings with concrete screws." *Connections between Steel and Concrete*, RILEM Proceedings PRO 21, Vol. 2, 919-929.

Küenzlen (2005) Küenzlen, J. (2005). *Tragverhalten von Schraubendübeln unter statischer Zugbelastung (Load-bearing behavior of screw anchors under static tension load)*. PhD dissertation, Institut für Werkstoffe im Bauwesen, Universität Stuttgart. (in German)

Kunnath & Chai (2004) Kunnath, S. K. and Chai, Y. H. (2004). "Cumulative damage-based inelastic cyclic demand spectrum." *Earthquake Engineering and Structural Dynamics*, Vol. 33, No. 4, 499-520.

Leonhardt (1976) Leonhardt, F. (1976). *Vorlesungen über Massivbau. Teil 4: Nachweis der Gebrauchsfähigkeit (Lectures on large-scale construction. Part 4: Information on service conditions)*. Springer, Berlin. (in German)

Lieberum & Weigler (1984) Lieberum and Weigler (1984). *Belastungsprüfungen an Leibig-Einspannankern ultra-plus M16, verankert in kreuzartig gerissenen Betonprobkörpern bei stoßartiger und statischer Belastung (Testing of Leibig anchors Ultra-Plus M16 anchored in intersecting cracks under impact and static loads)*. Report of the Technische Hochschule Darmstadt, Institute für Massivbau. (in German)

Lindquist (1982) Lindquist, M. R. (1982). *Final repost USNRC anchor bolt study: Data survey and dynamic testing*. U.S. Nuclear Regulatory Commission, NUREG/CR-2999.

Lotze & Faoro (1988) Lotze, D. and Faoro, M. (1988). *Rißbreitenentwicklung und Dübelverschiebung bei veränderlichen Bauteilbelastung (Crack width development and fastener displacement under varying building component loads)*. Report No. 1/28-88/3, Institut für Werkstoffe im Bauwesen, Universität Stuttgart. (in German)

Lotze & Klingner (1997) Lotze, D. and Klingner, R. E. (1997). *Behavior of multiple-anchor connections to concrete from the perspective of plastic theory*. PMFSEL Report No. 96-4, The University of Texas at Austin.

Malhotra et al. (2003) Malhotra, P. K., Senseny, P. E., Braga, A. C. and Allard, R. L. (2003). "Testing of sprinkler-pipe seismic-brace components." *Earthquake Spectra*, Vol. 19, No. 1, 87-109.

Malhotra (2002) Malhotra, P. K. (2002). "Cyclic-demand spectrum." *Earthquake Engineering and Structural Dynamics*, Vol. 31, No. 7, 1441-1457.

Manson (1953) Manson, S. S. (1953). "Behavior of materials under conditions of thermal stress." *Heat Transfer Symposium*, Univ. of Michigan, 9-75.

Martin, Schießl & Schwarzkopf (1980) Martin, H., Schießl, P. and Schwarzkopf, M. (1980). *Ableitung eines allgemeingültigen Berechnungsverfahrens für Rissbreiten aus Lastbeanspruchung auf der Grundlage von theoretischen Erkenntnissen und Versuchsergebnissen (A general method for the calculation of crack widths under loading based on theoretical and experimental studies)*. Forschung Straßenbau und Straßenverkehrstechnik, 309, 33-66. (in German)

Meszaros & Eligehausen (1994) Meszaros, J. and Eligehausen, R. (1994). *Tragverhalten von nicht generell zugzonetauglichen Dübeln – Teil 5: Verhalten bei Belastung mit konstanter Axiallast und gleichzeitig wirkender Querkraft mit wechselndem Vorzeichen (Load-bearing behavior of anchors not suitable for use in cracked concrete. Part 5: Behavior under constant axial load and simultanious reversed cyclic shear load)*, Report No. 1/63-94/9, Institut für Werkstoffe im Bauwesen, Universität Stuttgart. (in German)

Meszaros (1999) Meszaros, J. (1999). *Tragverhalten von Verbundüblen im ungerissenen und gerissen Beton (Load-bearing behavior of bonded anchors in uncracked and cracked concrete)*. PhD dissertation, Institut für Werkstoffe im Bauwesen, Universität Stuttgart. (in German)

Miner (1945) Miner, M. A. (1945). "Cumulative damage in fatigue." *Journal of Applied Mechanics (ASME)*, Vol. 12, 159-164.

Oh & Kang (1987) Oh, B. H. and Kang, Y.-J. (1987). "New formulas for maximum crack width and crack spacing in reinforced concrete flexural members." *ACI Structural Journal*, Vol. 85, No. 2, 103-112.

Ohkubo (1996) Ohkubo, M. (1996). "Translation of the investigation report on the damage of fastenings systems due to the Kobe earthquake, 1995." Presented at the Meeting of CEB TG3/5 "Fastenings" on May 16/17, 1996 in Vienna, Austria.

Ohkubo (1997) Ohkubo, M. (1997). "Earthquake damage of fastenings systems due to the Kagoshimaken Hokuseibu earthquake, 1997." Presented at Meeting of CEB TG3/5 Fastenings on June 13-15, 1997 in Stockholm, Sweden.

Okada & Seki (1984) Okada, T. and Seki, M. (1984). "Nonlinear earthquake response of equipment system anchored on R/C building floor." *Proceedings of the 8th World Conference on Earthquake Engineering*, San Francisco, 1984, 1151-1158.

Ožbolt et al. (2006) Ožbolt, J., Rah, K. K. and Meštrović, D. (2006). "Influence of loading rate on concrete cone failure." *International Journal of Fracture*, 139(2) 239-252.

Ožbolt et al. (2001) Ožbolt, J., Li, Y.-J. and Kožar (2001). "Microplane model for concrete with relaxed kinematic constraint." *International Journal of Solids and Structures*, 38, 2683-2711.

Paulay & Priestley (1992) Paulay, T. and Priestley, M. J. N. (1992). *Seismic design of reinforced concrete and masonry buildings*. John Wiley, and Sons Inc.

Pregartner (2003) Pregartner, T. (2003). Tra*gverhalten von Kunststoffdübeln im ungerissenen und gerissenen Beton (Load-bearing behavior of plastic anchors in uncracked and cracked concrete)*. Dissertation, IWB, Universität Stuttgart. (in German)

Rabinowicz (1995) Rabinowicz, E. (1995). *Friction and wear of materials, 2nd edition*. John Wiley & Sons, Inc.

Rehm & Martin (1968) Rehm, G. and Martin, H. (1968). "Zur Frage der Rißbegrenzung im Stahlbetonbau" (The question of cracking limits in reinforced concrete structures). *Beton-und Sthalbetonbau*, Heft 8, 1-8. (in German)

Rehm & Eligehausen (1977) Rehm, G., and Eligehausen, R. (1977). "Übergreifungsstöße von Rippenstäben unter schwellender Belastungen" (Lap splices with ribbed bars under repeated loads). *Deutscher Ausschuss für Stahlbeton*, Heft 291, Berlin. (in German)

Rehm & Lehmann (1982) Rhem, G. and Lehmann, R. (1982). *Untersuchungen mit Metallspreizdübeln in der gerissenen Zugzone von Stahlbetonbauteilen (Investigations with metal expansion anchors in cracked reinforced conrete)*. FMPA, Universität Stuttgart.

Rehm et al. (1988) Rehm, G., Eligehausen, R. and Mallée, R. (1988). „Befestigungstechnik (Fastening technology)." *Betonkalender 1998, Teil II*, Ernst & Sohn, Berlin, 569-663. (in German)

Rieder (2002) Rieder, A. (2002). "Ductility – A basic requirement for seismic performance of fasteners." *4th International PhD Symposium in Civil Engineering*, September 19-21, 2002, Munich, 164-171.

Rieder (2004) Rieder, A. (2004). "Anchoring to concrete under seismic conditions." *5th International PhD Symposium in Civil Engineering*, June 16-19, 2004, Delft, 1489-1494.

Rieder (2005) Rieder, A. (2005). "Erdbebenverhalten von Betondübeln" (Earthquake behavior of concrete anchors). *45th DafStb Research Colloquium*, October 6-7, 2005, Vienna,181-184.

Rodriguez (1995) Rodriguez, M. (1995). *Behavior of anchors in uncracked concrete under static and dynamic loading*. M.S. Thesis, The Univ. of Texas at Austin.

SEAOSC (1997) Structural Engineers Association of Southern California (SEAOSC) (1997). *Standard method of cyclic load test for anchors in concrete or grouted masonry*. SEAOSC, Whittier, California.

Seghezzi (1985) Seghezzi, H. D. (1985). *Wechselbeziehungen zwischen Prüftechnik und Entwicklung von Befestigungselementen (Interations between testing technology and development of fastening elements)*. Lecture in Stuttgart on 15.01.1985.

Senkiw (1984) Senkiw, G. A. (1984). "Qualification tests for concrete anchors for CANDU nuclear power plants." *ACI Symposium on Anchorage to Concrete*, Phoenix, Arizona.

Silva (2001) Silva, J. F. (2001). "Test methods for seismic qualification of post-installed anchors." *International Symposium on Connections between Steel and Concrete*, RILEM Proceedings PRO 21, Vol. 1, 551-563.

Silva (2003) Silva, J. F. (2003). "U.S. codes and standards governing the design of anchors for seismic applications." *Conference Proceedings of the fib Symposium on Concrete Structures in Seismic Regions*, Athens, Greece, 2003.

Sippel et al. (2001) Sippel, T. M., Asmus, J. and Eligehausen, R. (2001). "Safety concepts for fastenings in nuclear power plants." *Connections between Steel and Concrete*, RILEM Proceedings PRO 21, Vol. 1., 564-575.

Tang & Deans (1983) Tang, J. H. K. and Deans, J. J. (1983). "Test criteria and method for seismic qualification of concrete expansion anchors." *Proceedings of the Fourth Canadian Conference on Earthquake Engineering,* University of British Columbia, Vancouver, Canada, 58-69.

UBC (1997) International Code Council (ICC) (1997). *Uniform Building Code, 1997 Edition*. ICC, Whittier, California.

UE Anchor Project (2001) UE Anchor Project (2001). *Anchorages in normal and high performance concretes subjected to medium and high strain rates*. Politecnico di Milano, University of Patras, Hilti Corporation, Densit, JRC-Ispra, Enel-hydro, Bekaert. Final Report, UE ANCHOR Project.

Usami et al. (1980) Usami, S., Abe, U. and Matsuzaki, Y. (1980). "Experimental study on the strength of headed anchor bolts under alternate shear load and combined load (shear and axial)." *Proceedings of the Annual Meeting of the Kantou Branch of the Architectural Institute of Japan*.

Usami et al. (1981) Usami, S., Abe, U. and Matsuzaki, Y. (1981). "Experimental study on the strength of bonded anchors under alternate shear load and combined load." *Proceedings of the Annual Meeting of the Kantou Branch of the Architectural Institute of Japan*.

Vintzeleou & Eligehausen (1991) Vintzeleou, E. and Eligehausen, R. (1991). "Behavior of fasteners under monotonic or cyclic displacements." *Anchors in Concrete – Design and Behavior, Special Publication SP 130*, American Concrete Institute, Detroit, 181-204.

XTRACT (2001) XTRACT (2001). *A fully interactive program for generating moment curvature and axial load moment interaction response for arbitrary cross sections*. Distributed by Imbsen and Associates, Inc., http://www.imbsen.com.

Zhang (1997) Zhang, Y. (1997). *Dynamic behavior of multiple-anchor connections in cracked concrete*, PhD dissertation, The University of Texas at Austin.

A Post-Earthquake Reconnaissance Form

Event name and date:_____
Name of observer:_____
Date of observation:_____
Address or location:_____

_____

_____

Structure owner / Manager / Engineer contact:_____

Primary Structure

Primary structure type: RC building / Masonry building / Steel frame building / Bridge / Other (specify):_____

Primary structure damage[1]: None / Slight / Moderate / Severe / Total / Collapse

Secondary Structure

Secondary structure type:

(Nonstructural) Awning / Ceiling / Electrical / Facade / Mechanical / Partition / Piping / Railing / Sign / Other (specify):_____

Estimated weight, height to center of gravity and base dimensions (if applicable):

(Structural) Steel braced frame / Infill wall / Other (specify):_____

Mounting location: Suspended from: Slab / Beam
Supported on: Slab / Beam / Foundation
Mounted on: Wall / Column / Other (specify):_____

Floor number of secondary structure (if applicable):_____

Was secondary structure 'operational' following the event: Yes / No / Unknown

If "No", was inoperability caused by anchorage failure: Yes / No / Unknown

Anchorage Material

Anchorage material: Concrete / Masonry

Type of masonry (if applicable): Solid / Perforated

Masonry material[2] (if applicable): Concrete / Lightweight concrete / Limestone / Clay / Other (specify):_____

Condition of anchorage material: Uncracked / Cracked

Degree of anchorage material damage[3]: Low / Medium / High

Fastening

(Provide a sketch on the following page)

Type of attachment[4]: Single anchors / Grouped anchors / Dowels

Total number of anchors (for entire secondary structure):_____

Number of anchors per group (if applicable):_____

Anchor type[5]: Cast-in: Headed anchor / Anchor channel / Shear lug

Post-installed: Torque-controlled expansion anchor (sleeve- or bolt-type) / Displacement-controlled expansion anchor / Undercut anchor / Bonded anchor / Plastic anchor / Ceiling hanger /

Other (specify):_____

Manufacture and model number (if available):_____

Anchor diameter (threaded section):_____

Anchor effective embedment depth[5] (if available):_____

Mounting[6]: Pre-positioned / In-place / Stand-off

Anchor spacing[7]:_____

Edge distances[7]:_____

Total number of anchors located in cracks:_____

Did anchor(s) fail: Yes / No

Failure Mode[8]	Number of anchors failed	Number of failed anchors located in cracks	Comments[9] Exp / Ins / Edge / DBM / Other (specify)
Steel Failure			
Pull-out			
Pull-through			
Concrete breakout			
Concrete edge breakout			

Was there deformation of the attachment around the anchor(s): Yes / No

Were hole diameters appropriate for anchor(s): Yes / No / Unknown

Was reinforcement installed around the anchor: Yes / No / Unknown

Describe placement, size, hooks, etc.:

Miscellaneous

Photos: Yes / No Roll(s) #: Frame(s) #:

!! Important - Sketch the secondary structure and the locations of all the anchors. Indicate any anchors that have failed, the locations of cracks and provide any crack widths that were measured.

Additional comments:

Glossary of Terms

(1) Categories of damage to the primary structure (after *EERI 1996*)

None	No damage.
Slight	Isolated nonstructural damage; repair cost less than 5 percent of the market value of the structure.
Moderate	Considerable nonstructural and slight structural damage; repair costs less than 25 percent of the market value.
Severe	Considerable structural and extensive nonstructural damage; repair costs less than 50 percent of the market value.
Total	More economical to demolish than repair.
Collapse	Structural collapse.

(2) Masonry material

The following guide to identify masonry materials is a suggestion and does not hold true in all cases.

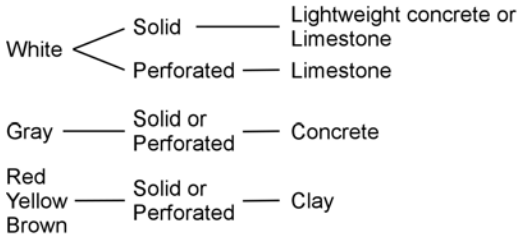

(3) Degree of damage to the anchorage material

Low	Small cracks (< 0.3 mm) in the anchorage material.
Medium	Obvious cracks (0.3 to 1.0 mm) in the anchorage material.
High	Large cracks (> 1.0 mm) in anchorage material, spalled concrete, obvious deformation of the anchorage material.

(4) Type of attachment

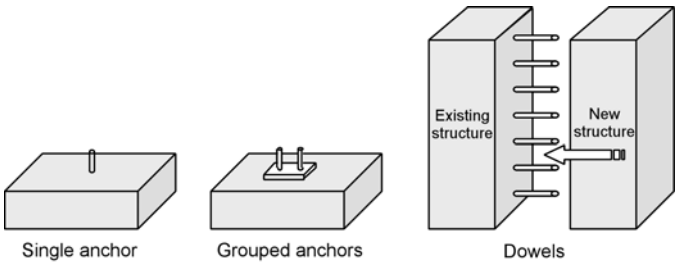

(5) Anchor types and effective embedment depths (after *CEB 1997*)

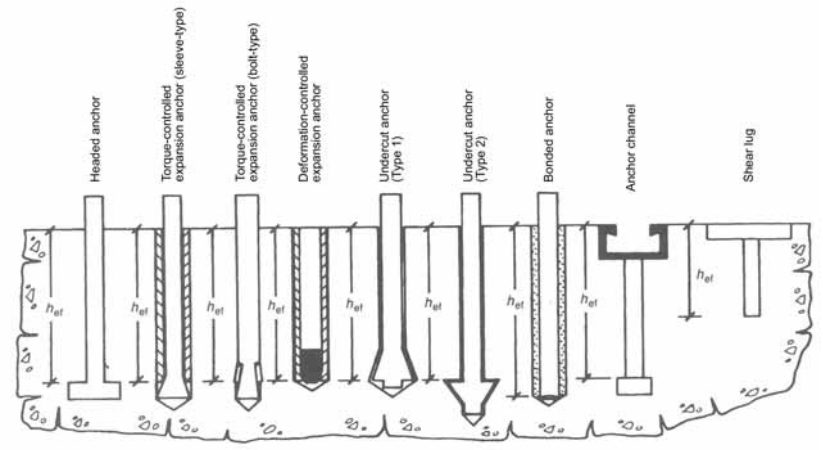

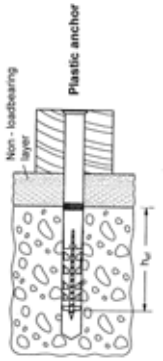

(6) Mounting (after *Eligehausen et al. 2006*)

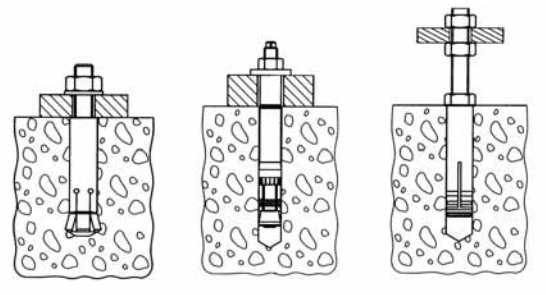

Pre-positioned In-place Stand-off

(7) Anchor spacing and edge distances (after *CEB 1997*)

Tension Loading

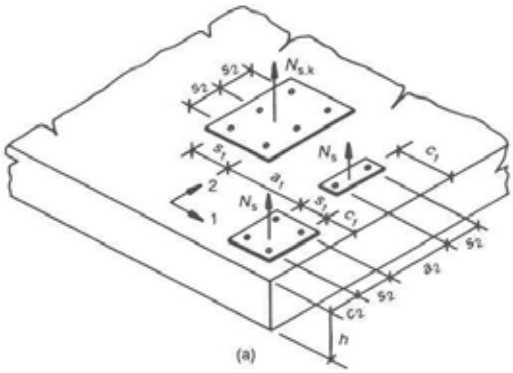

Shear Loading

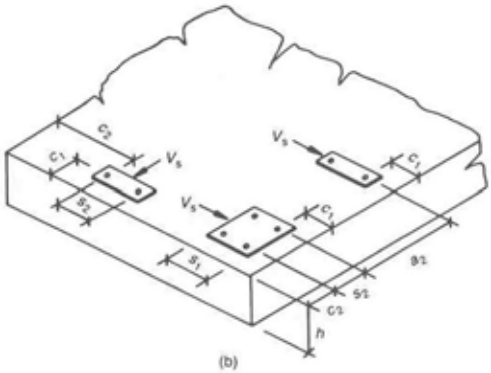

(8) Failure modes (after *ACI 355.2 2004*)

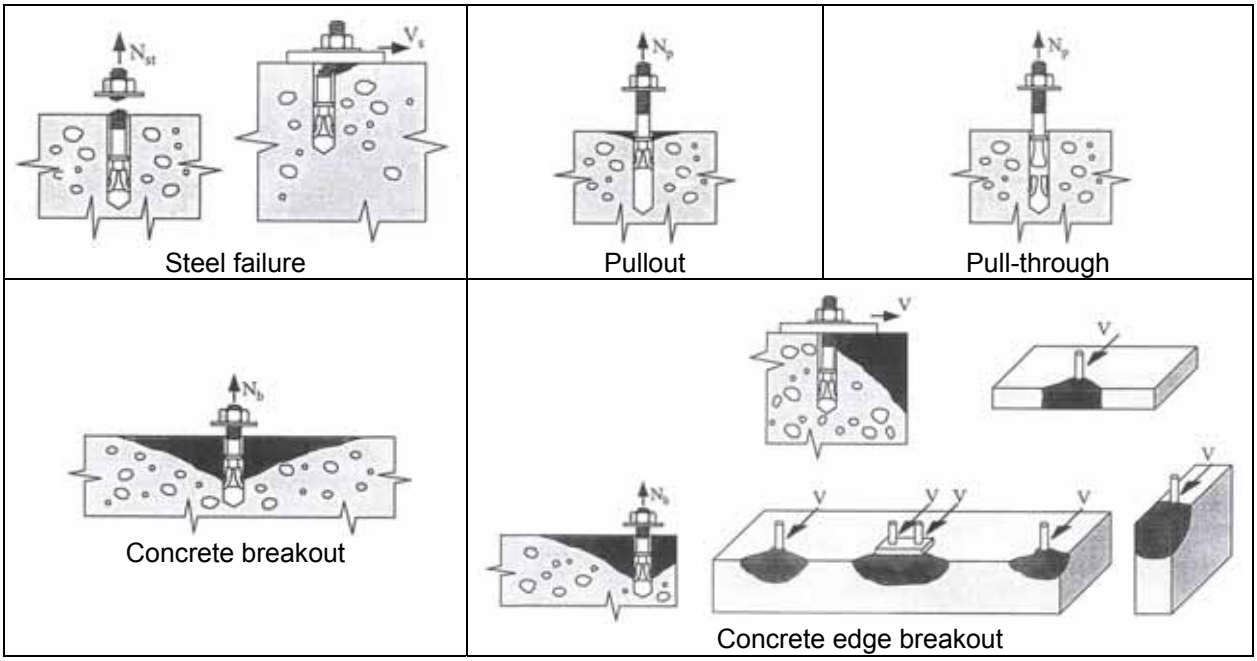

Steel failure | Pullout | Pull-through

Concrete breakout

Concrete edge breakout

(9) Comments on failure

Exp	Poor expansion
Ins	Improper installation
Edge	Insufficient edge distances
DBM	Extensive damage in base material

B Reviews of Normative Standards

B.1 Seismic design guidelines for fasteners

B.1.1 United States

B.1.1.1 ACI 318 Appendix D

Provisions for the design of fastenings for seismic applications are issued by the American Concrete Institute (ACI) in Appendix D of the ACI 318 building code (*ACI 318 2005*). The provisions apply to structures located in regions of moderate or high seismic risk, or for structures assigned to intermediate or high seismic performance or design categories. The Concrete Capacity Design (CCD) Method (*Fuchs et al. 1995*) is used for the determination of the anchor capacity. Specific references to anchor design for earthquake forces in *ACI 318 (2005)* can be summarized as follows:

(1) Section D.3.1 permits plastic analysis approaches for design when the nominal strength is controlled by ductile steel elements, provided that deformational compatibility is taken into account. A ductile steel element is defined as an element with a tensile test elongation of at least 14% and reduction in area of at least 30% (measured subsequent to steel rupture).

(2) Section D.3.3.2 requires that fasteners used for seismic applications have passed the Simulated Seismic Tests of ACI 355.2 (*ACI 355.2 2004*).

(3) Section D.3.3.1 states that the provisions in ACI 318 Appendix D do not apply to the design of anchors located in plastic hinge zones, because the seismic qualification procedures in ACI 355.2 do not simulate these conditions.

(4) Section D.3.3.3 requires that the design strength for seismic applications be reduced by an additional 25% over the nominal design strength. This is intended to provide additional conservatism (*ACI 318 2005*).

$$N_{eq}(seismic) \le 0.75 \cdot \phi \cdot N_n \quad \text{(B1a)}$$

$$V_{eq}(seismic) \le 0.75 \cdot \phi \cdot V_n \quad \text{(B1b)}$$

Two approaches are allowed for the design of the fastening.

(5) Section D.3.3.4 requires that the design be governed by the tensile or shear strength of a ductile steel element, i.e. steel failure of the anchor. For example, to prevent concrete failure the following conditions would need to be satisfied:

$$0.75 \cdot \phi_s \cdot N_{sa} \le 0.75 \cdot \phi_c \cdot N_{cb} \quad \Rightarrow \quad N_{sa} \le \frac{\phi_c}{\phi_s} \cdot N_{cb} \quad \text{(B2a)}$$

$$0.75 \cdot \phi_s \cdot V_{sa} \le 0.75 \cdot \phi_c \cdot V_{cb} \quad \Rightarrow \quad V_{sa} \le \frac{\phi_c}{\phi_s} \cdot V_{cb} \quad \text{(B2b)}$$

(6) Alternately, Section D.3.3.5 allows for design of the fasteners for a non-ductile failure mode if the attached component (or fixture) is designed to undergo

ductile yielding at a load level corresponding to anchor forces no greater than the design seismic fastener strength.

$$A_s \cdot f_{y,conn} \le 0.75 \cdot \phi \cdot N_n \quad \text{(B3a)}$$

$$A_s \cdot f_{y,conn} \le 0.75 \cdot \phi \cdot V_n \quad \text{(B3b)}$$

No distinction is made between the static and seismic loading case for the determination of material strength reduction factors or tension-shear load interaction.

B.1.1.2 ACI 349 Appendix B

Fastener design has been addressed in the Code Requirements for Nuclear Safety Related Structures since 1985 (*ACI 349 1985*). The provisions in ACI 349 Appendix B have been harmonized with those in ACI 318 Appendix D since the 2001 edition (*ACI 349 2001*) to the extent that both codes utilize the Concrete Capacity Design (CCD) Method for the determination of the anchor capacity. Specific references to anchor design for earthquake forces in *ACI 349 (2001)* can be summarized as follows:

(1) Section B.3.1 permits plastic analysis approaches for design when the nominal strength is controlled by ductile steel elements, provided that deformational compatibility is taken into account. A ductile steel element is defined as an element with a tensile test elongation of at least 14% and reduction in area of at least 30% (measured subsequent to steel rupture).

(2) Section B.3.3 requires post-installed anchors be tested to verify that they can sustain their design strength in cracked concrete under seismic loads.

Three approaches are allowed for the design of the fastening.

(3) Section B.3.6.1 requires that design be controlled by the strength of the embedment steel, i.e. ductile steel failure of the anchor. In tension, it is assumed that design is controlled by steel failure if the relevant concrete design capacities (concrete cone, blow-out and pull-out) multiplied by a factor of 0.85 exceed the nominal tensile strength of the steel. For ductile steel failure in shear, the relevant concrete design capacities (concrete edge breakout and pry-out) multiplied by a factor of 0.85 must exceed 65% of the nominal tensile strength of the steel, i.e. the nominal shear strength of the steel. For example, to prevent concrete failure the following conditions would need to be satisfied:

$$A_s \cdot f_u \le 0.85 \cdot N_{cb} \quad \Rightarrow \quad N_{sa} \le 0.85 \cdot N_{cb} \quad \text{(B4a)}$$

$$0.65 \cdot A_s \cdot f_u \le 0.85 \cdot V_{cb} \quad \Rightarrow \quad V_{sa} \le 0.85 \cdot V_{cb} \quad \text{(B4b)}$$

(4) As an alternate to Section B.3.6.1, Section B.3.6.2 allows for ductile design of the attached component or fixture if it is designed to yield at 75% of the anchor design strength. (Note that although the effect is the same as in ACI 318 Appendix D (point (6) above), the wording of the requirement is different.)

$$A_s \cdot f_{y,conn} \leq 0.75 \cdot \phi \cdot N_n \quad \text{(B5a)}$$

$$A_s \cdot f_{y,conn} \leq 0.75 \cdot \phi \cdot V_n \quad \text{(B5b)}$$

(5) Section B.3.6.3 allows for the non-ductile design of anchors (concrete cone, blow-out and pull-out in tension and concrete edge breakout and pry-out in shear) if the design strength is multiplied by a factor of 0.60.

$$N_{eq} \leq 0.60 \cdot \phi \cdot N_n \quad \text{(B6a)}$$

$$V_{eq} \leq 0.60 \cdot \phi \cdot V_n \quad \text{(B6b)}$$

B.1.1.3 International Building Code

The International Building Code (*IBC 2003*) issued by the International Conference of Building Officials (ICBO) is widely used for general structural design in the United States. The IBC provisions for anchorage that resist earthquake loads are derived from ACI 318 Appendix D (*ACI 318 2005*).

B.1.1.4 National Earthquake Hazard Reduction Program (NEHRP)

The following review is excerpted from *Silva (2003)* with minor modifications.

The seismic provisions for the model codes in the United States, including the IBC, are generally based on the NEHRP Recommended Provisions for Seismic Regulations prepared by the Building Seismic Safety Council for the Federal Emergency Management Agency (FEMA) of the U.S. Government. Specific references to anchor bolt design contained in the most current version of this document (*FEMA 368 2001*) are provided here**.**

Chapter 6 of the Provisions addresses design requirements for architectural, mechanical and electrical components. As a practical matter, many of the specific provisions relating to anchorage are contained in this section. For example:

(1) In Section 6.1, the explicit design of component anchorage for earthquake forces is required if the component is supported more than 4 feet (1.22 m) above the floor level and weighs more than 400 pounds (182 kg). It is also required for ceilings and piping weighing more than 20 pounds (9 kg) or 5 pounds per foot (7.5 kg/m).
(2) Section 6.1.6.1 requires an increase in the total lateral force to be applied to the anchorage in cases where "…shallow (low deformability)…" anchors are used. Low deformability is not defined.
(3) In Section 6.1.6.2, anchors are required to develop the lesser of a) the strength of the connected part, b) 1.3 times the calculated seismic force, or c) the maximum load that can be delivered to the anchor via the structure.
(4) Section 6.1.6.3 requires that load eccentricity and prying be taken into account in the design.
(5) Section 6.1.6.4 requires that the ability of the baseplate to adequately distribute load to a group of anchors be considered in the design, e.g. via a comparison of the relative stiffness of the anchors and the plate.

(6) Section 6.2.4.1 requires that bodies of connectors for exterior nonstructural wall elements (cladding) be provided with "…sufficient deformability and rotation capacity to preclude fracture of the concrete…" or other low deformation failure modes at or near welds.

In addition, the Provisions contain references to anchor design in concrete that are derived from ACI 318 Appendix D. The qualification of post-installed anchors for use in concrete is outlined to conform with the requirements of ACI 355.2.

B.1.1.5 Uniform Building Code

The following review is excerpted from *Silva (2003)* with minor modifications.

The Uniform Building Code (*UBC 1997*) is a model code that was used extensively in the earthquake prone regions of the United States prior to the introduction of the International Building Code (*IBC 2003*). The final edition of this code was issued in 1997. The UBC addresses the design of anchor bolts for seismic loading in a variety of ways: 1) through specific instructions for the design of cast-in fasteners in each material section, i.e. concrete, masonry or wood, 2) via special provisions in the seismic design section of the code (Chapter 16) and 3) by reference to evaluation reports for proprietary products, e.g. post-installed fasteners, issued by the International Code Council Evaluation Service, Inc. (ICC-ES).

In the U.S., the design of anchors has traditionally been performed on an allowable stress design basis, that is, through the use of a global factor of safety applied to a mean resistance value for comparison with unfactored loads. Accordingly, a table of permissible loads for cast-in anchors is provided in Table 19-D (for concrete) and in Tables 21-E-1, 21-E-2 and 21-F (for masonry) in the 1997 UBC. Specific references to anchor design for earthquake forces in the 1997 UBC include the following:

(1) Section 1632.1 mandates the explicit design of anchorages for elements of structures weighing more than 400 pounds (182 kg). The use of friction to resist lateral forces is not permitted.
(2) In Section 1632.2, the total design lateral force for anchorages is increased if the anchor has an embedment to diameter ratio less than 8.
(3) Section 1632.4 requires the relative motion of the points of attachment to be considered for equipment located in essential or hazardous buildings.
(4) In Footnote 16 of Table 16-O, expansion anchors are not permitted to resist tension loads caused by earthquake motion if "…operational vibrating loads are present."
(5) Section 1806.6 requires the use of steel anchor bolts with a minimum nominal diameter of 5/8 inch (16 mm) embedded at least 7 inches (178 mm) to secure wood-framed walls to reinforced concrete foundations in the highest seismic zone.
(6) In Section 1921.7.4, anchor bolts set in the top of a column must be enclosed by ties for all seismic zones.
(7) In Footnote 3 of Table 19-D, the allowable service loads for embedded bolts may be increased "… for duration of loads, such as wind or seismic forces."

(8) Footnote 4 of Table 19-D requires that an anchor bolt located in the top of a concrete column be provided with an additional 2 inches (51 mm) of embedment if the structure is located in a intermediate or high seismic zone.

While the UBC contains provisions in Sections 1923 and 2108.1.5 for the strength design of cast-in anchor bolts in concrete and masonry, respectively, no additional requirements or adjustments are made with respect to seismic loads in these sections.

B.1.2 Europe

B.1.2.1 CEN Technical Specification

The Technical Specification titled Design of Fastenings for Use in Concrete (*CEN TS in preparation*) which is scheduled to be issued by The European Committee for Standardization (CEN) in 2006, contains provisions for the seismic design of fastenings that are similar to those in ACI 318 (2005), albeit somewhat more detailed and conservative. The primary differences to ACI 318 Appendix D are that the partial safety factors are defined slightly differently and that design for non-ductile failure modes is allowed for the anchorage of non-structural elements using a large (2.5 times) increase factor for the design load. Specific references to anchor design for earthquake forces in the *CEN Technical Specification (in preparation)* can be summarized as follows:

(1) Fasteners used for seismic applications must be qualified for this use by a relevant testing standard issued by the European Organisation for Technical Approvals (EOTA) or by CEN.
(2) The concrete shall be assumed to be cracked in the region of the fastening when performing design.
(3) The provisions do not apply for design in plastic hinge zones.
(4) Displacement of the fastening should be accounted for when anchoring elements of great importance or of a particularly dangerous nature.
(5) Determination of distribution of forces to the individual fasteners of a group must take into account the stiffness of the fixture and its ability to redistribute loads to other anchors in the group beyond yield of the fixture. No guidance is provided for how to do this.
(6) Annular gaps between a fastener and its fixture are not allowed for seismic design situations.
(7) The design strength for seismic applications is taken as a fraction of the minimum design resistance as determined for the persistent and transient elastic design situation using characteristic seismic resistances for fasteners provided by an EOTA or CEN product qualification (α_{eq} = 0.75 (concrete failure), α_{eq} = 1.0 (steel failure)).

$$N_{eq} \le \alpha_{eq} \cdot N_n / \gamma_M \quad \text{(B7a)}$$

$$V_{eq} \le \alpha_{eq} \cdot V_n / \gamma_M \quad \text{(B7b)}$$

Three approaches are allowed for the design of the fastening.

(6) The fasteners shall be designed for ductile steel failure. (Note: ductile failure modes other than ductile steel failure may be allowed. However, ductility equivalent to that which occurs during ductile steel failure shall be shown by qualification tests.) To ensure ductile steel failure of a fastener, the seismic design resistance of the fasteners failing by concrete cone, splitting or pull-out under tension loading or pry-out or concrete edge failure under shear loading shall exceed the characteristic seismic resistance for steel failure provided in the relevant EOTA or CEN product qualification by a specified margin of safety. For example, to prevent concrete failure the following conditions would need to be satisfied (γ_{inst} = safety factor for installation sensitivity).

$$N_{sa} \le 0.6 \cdot \frac{1}{\gamma_{inst}} \cdot N_{cb} \tag{B8a}$$

$$V_{sa} \le 0.6 \cdot \frac{1}{\gamma_{inst}} \cdot V_{cb} \tag{B8b}$$

(8) The anchorage is designed for the minimum of the following:

- The force corresponding to yield of the fixture, or the element attached to the fixture, taking into account the steel over-strength.
- The maximum for that can be transferred to the connection by the attached component or structural system.

(9) Brittle failure of the fastening, i.e. concrete breakout, for non-structural attachments is allowed when the seismic design load is increased by an additional factor of 2.5.

$$2.5 \cdot N_{eq} \le \alpha_{eq} \cdot N_n / \gamma_M \quad \Rightarrow \quad N_{eq} \le (0.3 \text{ or } 0.4) \cdot \frac{1}{\gamma_M} \cdot N_n \tag{B9a}$$

$$2.5 \cdot V_{eq} \le \alpha_{eq} \cdot V_n / \gamma_M \quad \Rightarrow \quad V_{eq} \le (0.3 \text{ or } 0.4) \cdot \frac{1}{\gamma_M} \cdot V_n \tag{B9b}$$

B.1.3 Other countries

B.1.3.1 CANDU Nuclear Power Plants (Canada)

Design Requirements for Concrete Containment Structures for CANDU Nuclear Power Plants (*CSA-N287.3 1999*) contains seismic design provision for anchorages in nuclear power facilities in Canada issued by the Canadian Standards Association (CSA). A method for calculating the concrete breakout strengths based pyramids with a slope of 45° is provided. The requirements relevant for seismic design of anchorage systems can be summarized as follows:

(1) Section 13.4.1.1 requires that the deflection of embedded parts (fasteners) be within the acceptable limits of the attached equipment.
(2) Section 14.3.2 requires anchorage systems for structural elements to be designed such that ductile failure of the attached element occurs prior to

failure of the concrete and prior to the failure of the manufactured anchor elements in the case of embedded inserts and expansion anchors. Ductility is defined qualitatively as the ability "… to undergo substantial deformation while continuing to support the applied load."

(3) Section 14.2.3 and 14.3.4 mandates seismic qualification testing of the fastening elements according to Standard *CSA-N287.2 (2003)* under environmental conditions (temperatures) appropriate for the intended use.

An additional stipulation for seismic design given in the companion document Design Procedures for Seismic Qualification of Nuclear Power Plants (*CSA-N289.3 2003*) is that whenever possible more than one anchor per connection should be used. If only one fastener per connection can be accommodated, the capacity shall be 1.5 times the design load.

B.2 Seismic qualification methods and assessment criteria for fasteners

B.2.1 United States

B.2.1.1 ACI 355.2

ACI 355.2 (2004) prescribes testing programs and evaluation requirements for post-installed mechanical anchors for use in concrete under the design provisions of *ACI 318 (2005)*. The qualification of fasteners under ACI 355.2 involves four types of tests:

(1) identification tests to evaluate the anchor's compliance with critical characteristics;
(2) reference tests to establish the baseline capacity of the fastener in cracked and uncracked concrete;
(3) reliability tests to establish the ability of the fastener to perform under adverse conditions;
(4) service-condition tests to verify the capacity of the fastener in groups, in near-edge conditions and under simulated seismic loading in cracked concrete.

Fasteners approved for seismic applications must fulfill the requirements of all tests necessary for approval for use in cracked concrete in addition to passing the simulated seismic loading tests. With the exception of the crack cycling reliability tests, all of the assessment criteria in *ACI 355.2 (2004)* are strength-based, i.e. they do not assess the displacement behavior of the fastener.

The reference tests consist of monotonic tension tests on single anchors in low-strength (17 to 24 MPa) and high-strength (46 to 55 MPa) uncracked and cracked concrete (Δw = 0.3 mm). Fastener behavior under tensile load in 0.5 mm crack widths is verified during the reliability tests.

As part of the reliability test program, tests are performed in which a constant tension load of approximately 30% of the mean reference strength ($N_{u,m}$) in cracked concrete (Δw = 0.3 mm) is applied to the fastener while it is subjected to 1000 crack opening and

closing cycles between a crack opening width w_1 = 0.3 mm and an initial crack closing width w_2 = 0.1 mm (Figure B.1). The crack closing width is allowed to increase during the course of the crack cycling as long as the crack width difference remains greater than w_1 - w_2 = 0.1 mm. These crack cycling tests were developed to approximate crack cycling conditions in the anchorage material under service conditions over the life of the structure (*ACI 355.2 2004*) and not to represent seismic crack cycling conditions. In general, to be considered acceptable, the anchor displacement shall be less than 2.0 mm after the initial 20 cycles of crack opening and closing, and less than 3.0 mm after 1000 cycles. Furthermore, the mean residual strength obtained from a tension test performed in an open crack of width (Δw = 0.3 mm) after completion of the crack cycles must be greater than 90% of the corresponding mean reference strength.

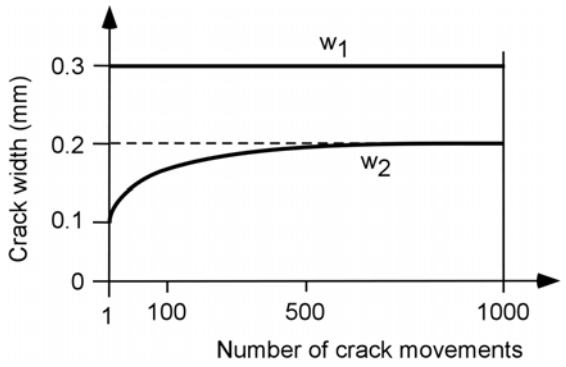

Figure B.1 Crack width requirements for crack cycling tests in ACI 355.2 (2004)

The simulated seismic tests subject fasteners situated in crack widths of 0.5 mm to stepwise decreasing, pulsating tension (Figure B.2a) or alternating shear (Figure B.2b) load cycles. The load steps are determined based on the mean ultimate strength from the reference tests in cracked concrete (Δw = 0.3 mm). The load cycling frequency is between 0.1 and 2 Hz. After completion of the load cycles, the fastener is loaded monotonically to failure using an initial crack width not less than the crack width at the end of the load cycling. Qualification of the fastener is based on the exclusion of failure during load cycling and attainment of a mean residual capacity after load cycling of at least 80% of the mean capacity from the corresponding static reference tests.

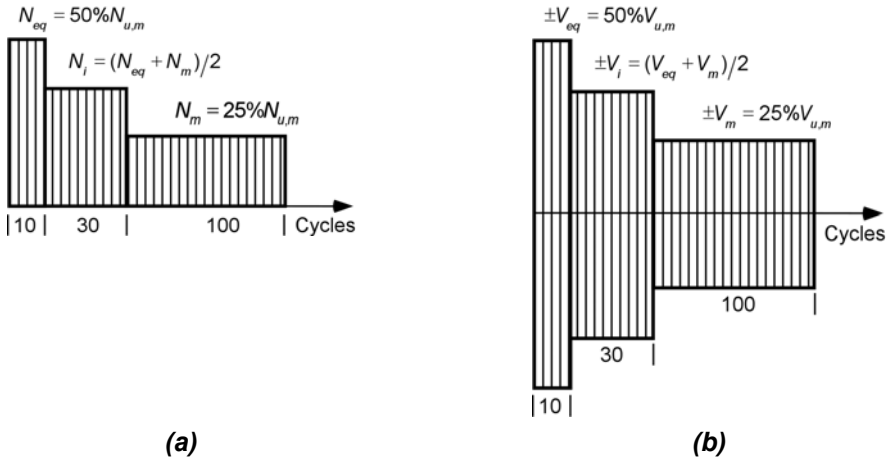

(a) ***(b)***

Figure B.2 Loading patterns for simulated seismic tests in ACI 355.2 (2004): (a) tension; (b) shear

B.2.1.2 ICC Evaluation Service reports

Evaluation reports issued by the International Code Council Evaluation Service Inc. (ICC-ES) verify performance features of building products, e.g. post-installed fasteners, for use under the design provisions of the ICC issued codes, e.g. *UBC (1997)* and *IBC (2003)*. Requirements for performing this verification are established by product specific acceptance criteria. Currently, there are six ICC-ES acceptance criteria that address the evaluation of post-installed fasteners for concrete and masonry, which are inserted into a pre-drilled hole (Table B.1).

Table B.1 ICC-ES acceptance criteria for post-installed anchors (after Silva 2003)

Document Title		Anchor Type	Base Materials	Design Basis [a,b,c,d]	Seismic	Cracked Concrete
AC01 (2005)	Expansion Anchors in Concrete and Masonry Elements	Mechanical	Concrete or new masonry	ASD $R_{u,m}/4 \geq WL$	Optional[e]	Not permitted
AC58 (2005)	Adhesive Anchors in Concrete and Masonry Elements	Bonded	Concrete or new masonry	ASD $R_{u,m}/4 \geq WL$	Optional[e]	Not permitted
AC60 (2005)	Anchors in Unreinforced Masonry Elements	Bonded	Existing unreinforced masonry	ASD[f] $R_{u,m}/5 \geq WL$	Mandatory	Not applicable
AC106 (2005)	Predrilled Fasteners (Screw Anchors) in Concrete and Masonry	Screw anchors	Concrete or new masonry	ASD $R_{u,m}/4 \geq WL$	Optional[e]	Not permitted
AC193 (2005)	Mechanical Expansion Anchors in Concrete Elements	Mechanical	Concrete	Strength design per ACI 318 Appendix D	Optional	Optional
AC308 (2005)	Adhesive Anchors in Concrete Elements	Bonded	Concrete	Strength design per ACI 318 Appendix D[g]	Optional	Optional

[a] Assumes on-site inspection of anchor installation.
[b] Allowable Stress Design (ASD).
[c] $R_{u,m}$ = mean ultimate test load.
[d] WL = working load or service load (unfactored).
[e] 1/3 increase in allowable loads permitted.
[f] Capacity limits defined in criteria may result in larger safety factors.
[g] Strength design amended for standard bonded anchors.

Each of these criteria contains specific requirements to qualify a product for use in seismic applications. With the exception of *AC60 (2005)*, which is intended to verify the static capacity of retrofit anchors in-situ, seismic qualification testing consists of pulsating tension and alternating shear loading nearly identical to that used in ACI 355.2 (see Section B.2.1.1). For historical reasons (*see Silva 2003*), however, only AC193 and AC308 require that the seismic tests be performed in cracked concrete (Δw = 0.5 mm). Furthermore, AC193 and AC308, which significantly reference to ACI 355.2, require crack movement tests similar to those discussed in Section B.2.1.1.

The ICC Evaluation Service adopted the *SEAOSC (1997)* method as an alternate means of qualification for seismic loading for mechanical and adhesive anchors in uncracked concrete in AC01 and AC58. A version of the SEAOSC methods for qualification in cracked concrete does not currently exist.

B.2.1.3 SEAOSC

The Structural Engineers Association of Southern California (SEAOSC) proposed a seismic test for fasteners based on the assumption that historical provisions for cast-in anchors in the Uniform Building Code (*UBC 1997*) had proven adequate in past earthquakes. Accordingly, the SEAOSC Standard Method of Cyclic Load Test for Anchors in Concrete or Grouted Masonry (*SEAOSC 1997*) requires side-by-side testing of post-installed anchors with code cast-in anchors (standard hex A307 bolts) of like diameter. It is not specified whether the tests are to be performed in uncracked or cracked concrete. The anchors are loaded cyclically in steps of five cycles each up to failure. The load steps are determined by first identifying (from static test data) the First Major Event (FME), which is the load level at which the load-displacement curve undergoes a significant change. The load steps are then established as 25% increments of the FME, i.e. 25%FME, 50%FME, 75%FME, 100%FME, 125%FME, etc. to failure (Figure B.3). The resulting load-displacement curves and ultimate loads of the post-installed and cast-in anchors are compared. Qualification of the post-installed anchor is based on performance equal to or exceeding that of the cast-in anchor.

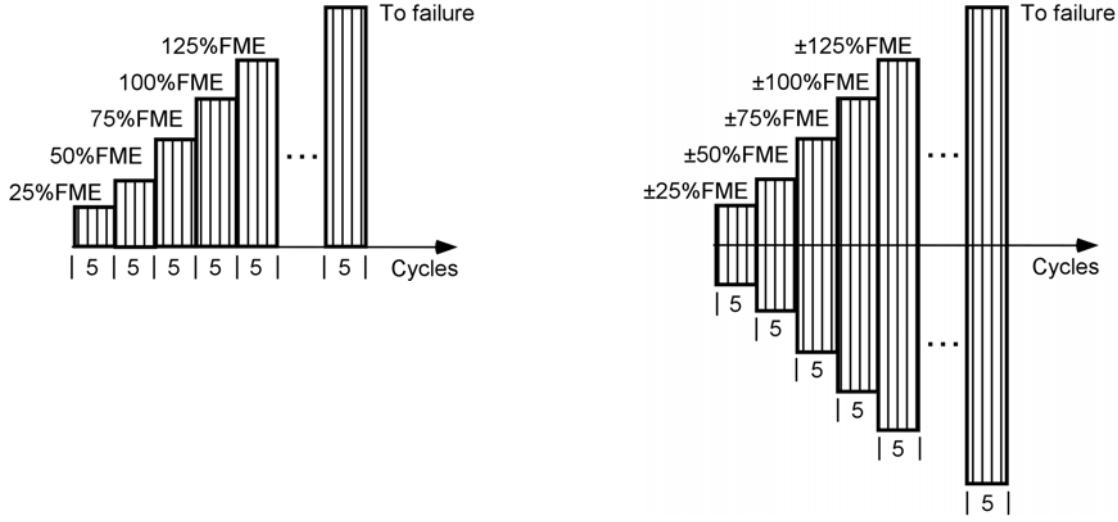

(a) *(b)*

Figure B.3 Loading patterns for simulated seismic tests in SEAOSC (1997): (a) tension; (b) shear

B.2.2 Europe

B.2.2.1 Deutsches Institut für Bautechnik (Germany)

In 1998, the *Deutsches Institut für Bautechnik* (DIBt) issued guidelines for the use and testing of fastenings in German nuclear facilities (*DIBt 1998*). The guidelines are applicable for anchors used to fasten safety relevant components in the case of extreme loading conditions such an earthquake, an explosion or an aircraft impact. In addition to the special testing requirements prescribed in the guideline, all fasteners for such applications are required to have a general approval for use in uncracked and cracked concrete, such as is issued by the European Organisation for Technical Approvals (*ETAG 001 1997*).

The tests required for approval of a fastener according to *DIBt (1998)* are summarized in Table B.2. All test are performed on single anchors without edge influences.

Table B.2 Summary of DIBt (1998) testing and assessment criteria for fasteners

Test No.	Description	Crack Width [mm]	No. of Load n or Crack n_w Cycles	Load Cycling or Sustained Load Level	Assessment Criteria
			Reference Tests		
1.1	Monotonic tension	1.0	-	-	Mean ref. strength $N_{u,m}$
1.2	Monotonic shear	1.0	-	-	Mean ref. strength $V_{u,m}$
1.3	Alternating shear	1.0	n = 15	$\pm V_{max} \sim 0.45 \cdot V_{u,m}$	$V_u \geq 0.9 \cdot V_{u,m}$ [a]
			Suitability Tests		
2.1	Monotonic tension	1.5	-	-	$N_u \geq 0.8 \cdot N_{u,m}$
2.2	Pulsating tension	1.5	n = 15	$N_{max} \sim 0.45 \cdot N_{u,m}$	$N_u \geq 0.7 \cdot N_{u,m}$ [a]
2.3	Crack movement	1.5 / 1.0	n_w = 10	$N_w \sim 0.45 \cdot N_{u,m}$	$N_u \geq 0.7 \cdot N_{u,m}$ [a]

[a] No failure during load or crack cycling.

The large crack opening widths are used to verify that fasteners located in plastic hinges, where reinforcement steel strain up to 0.005 has occurred, perform acceptably.

The monotonic references tests (Tests 1.1 and 1.2) are performed to establish the baseline performance of the fastener in wide cracks (Δw = 1.0 mm). The coefficient of variation (COV) of the mean ultimate load ($N_{u,m}$ or $V_{u,m}$) must be below 15% and the COV of the fastener displacement at $0.5 \cdot N_{u,m}$ must be less than 40%. The monotonic tension suitability test (Test 2.1) is intended to verify that the fastener continues to function in unanticipated wide crack widths (Δw = 1.5 mm). The failure load must be at least 80% of the mean reference capacity in a crack width of 1.0 mm.

The pulsating tension suitability test (Test 2.2) consists of 15 tension load cycles to approximately 45% of the mean ultimate reference load (Figure B.4a) followed by monotonic loading to failure in an open crack. The fastener is pushed back to its initial position during each unloading cycling. Qualification of the fastener is based on the exclusion of failure during load cycling and attainment of a mean residual capacity after load cycling of at least 70% of the mean capacity obtained in the reference tests. The alternating shear reference tests (Test 1.3) consist of 15 shear load cycles at approximately 45% of the mean ultimate reference load (Figure B.4b) followed by monotonic loading to failure in an open crack. Qualification of the fastener is based on the exclusion of failure during load cycling and attainment of a mean residual capacity after load cycling of at least 90% of the mean capacity obtained in the reference tests.

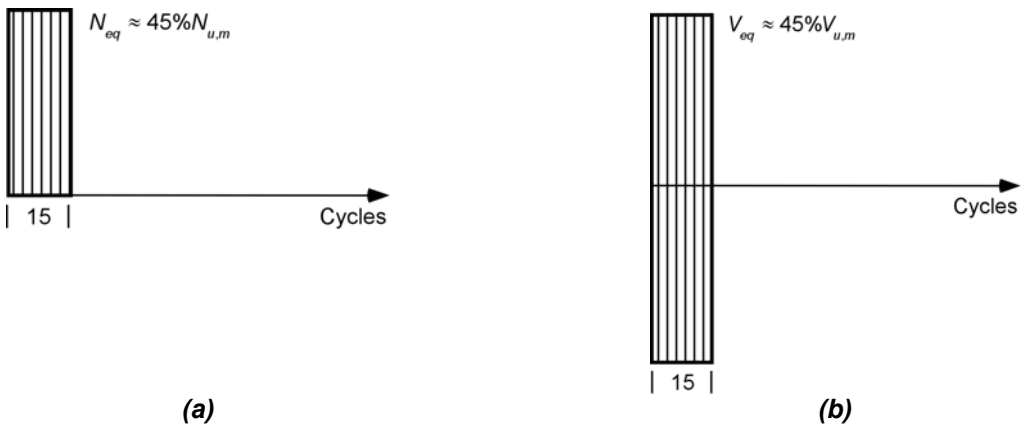

Figure B.4 Loading patterns for simulated seismic tests in DIBt (1998): (a) tension; (b) shear

In the crack movement suitability test (Test 2.3) a sustained axial load of approximately 45% $N_{u,m}$ is applied to the fastener as it is subjected to 10 crack opening and closing cycles between a crack opening width w_1 = 1.5 mm and an initial crack closing width w_2 = 1.0 mm. Qualification of the fastener is based on the exclusion of failure during crack cycling and attainment of a mean residual capacity after crack cycling of at least 70% of the mean capacity obtained in the reference tests.

B.2.3 Other countries

B.2.3.1 CANDU Nuclear Power Plants (Canada)

Seismic testing requirements for fastenings used in Canadian nuclear power plants are specified in *CSA-N287.2 (2003)*. It is stated in this document that *ANSI/ASTM Standard 488 (1990)* may be used as a guideline for preparing the test procedures and test equipment. All tests are performed in uncracked, unreinforced concrete (20 MPa).

Monotonic tension tests in which concrete cone failure occurs, e.g. by selecting a bolt strength large enough to prevent yielding of the steel, are to be performed to establish the concrete cone failure strength. Monotonic shear tests are to be performed using an anchor bolt material identical to that used in the actual application to establish the steel failure load in the case of shear.

Simulated seismic tests subject fasteners to stepwise decreasing, pulsating tension (Figure B.5a) or alternating shear (Figure B.5b) load cycles. The anchor bolt material must be identical to that used in the actual application. The load steps are determined based on the specified minimum yield strength of the fastener steel. The load cycling frequency is 5 Hz. After completion of the load cycles, the fastener is loaded monotonically to failure. Qualification of the fastener is based on the exclusion of failure during load cycling and attainment of the steel yield load after load cycling.

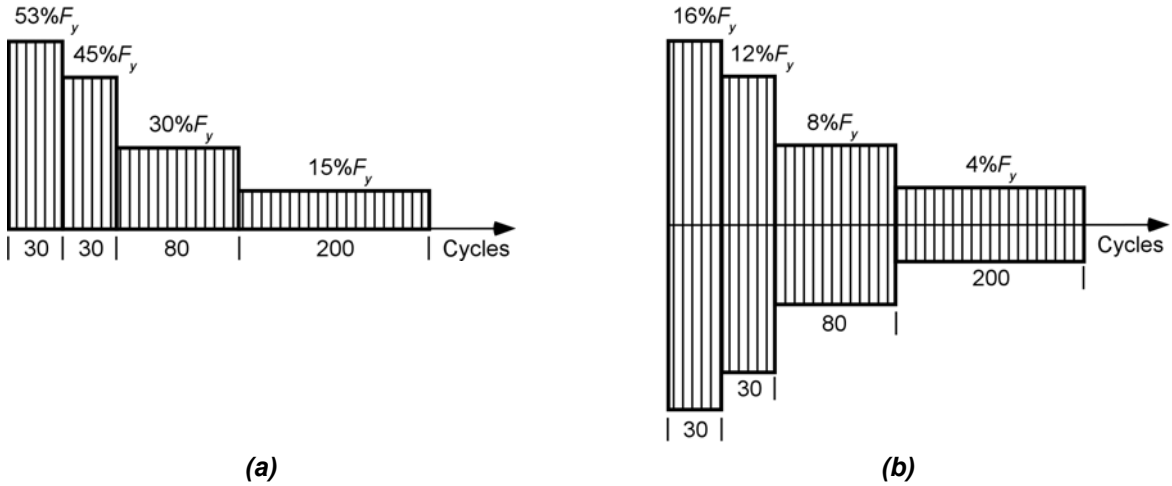

Figure B.5 Loading patterns for simulated seismic tests in CSA-N287.2 (2003): (a) tension; (b) shear (F_y = calculated fastener yield load)

C Empirical Crack Width Equations

The cross-section dimension notations shown in Figure C.1 are used in this appendix.

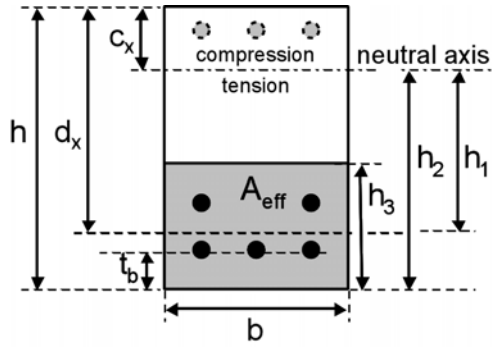

Figure C.1 Notations for the investigated empirical crack equations

<u>*Gergely/Lutz (1968)*</u>
Gergely and Lutz (1968) proposed empirical equations for the prediction of crack width in reinforced concrete flexural members based on an extensive statistical study of previous experimental investigations of crack width. When the coefficients for the equations were determined, all experimental results where yielding was believed to have occurred were discarded. Consequently, the equations are only valid for the prediction of crack width for steel strains up to yield. This conclusion also holds for the other investigated empirical equations.

The simplified equation for the prediction of the maximum crack width w_{max} at the extreme tension fiber of a member undergoing bending is given in Equation (C.1). All dimensions must be given in inches and stresses in ksi, which yields crack widths in thousandths of an inch.

$$w_{\max} = 0.076 \cdot B \cdot \sigma_s \cdot \sqrt[3]{t_b \cdot A} \qquad \text{(C.1)}$$

where,

B = $\dfrac{h_2}{h_1}$

σ_s = reinforcing steel stress

A = A_{eff} / m

A_{eff} = $2b\left(h - d_x\right)$

m = number of reinforcing bars in tension

Martin/Schießl/Schwarzkopf (1980)

Martin, Schießl and Schwarzkopf (1980) proposed empirical equations for the prediction of crack width and spacing. An average crack spacing s_{ave} multiplied by an average strain value is increased by a factor k_4 to obtain characteristic crack widths at the level of the longitudinal tension reinforcement. All dimensions must be given in mm and N. The characteristic crack width is given as:

$$w_k = k_4 \cdot s_{ave} \cdot \frac{\sigma_s}{E_s} \cdot \left(1 - k_5 \cdot k_6 \cdot \frac{\Delta\sigma_s}{\sigma_s}\right) \tag{C.2}$$

where,

k_4 = 1.7 (relation between characteristic and average crack width)

k_5 = 1.0 for short-term loading
0.5 for long-term or cyclic loading

k_6 = $\dfrac{1}{2 \cdot k_2}$

σ_s = steel stress

E_s = modulus of elasticity of the reinforcing steel

$\dfrac{\Delta\sigma_s}{\sigma_s}$ = for rectangular cross-sections:

$$\left((k_3)^2 \cdot \frac{f_{cb}}{(A_s / b \cdot h) \cdot \sigma_s} \right)^2 \leq 0.5$$

f_{cb} concrete tensile (bending) strength ($\sim 0.24 \cdot f_{cc}^{\,2/3}$)

A_s cross-sectional area of the longitudinal tension reinforcement

The equation for the average stabilized crack spacing is given as:

$$s_{ave} = 50 + \frac{1}{4} \cdot k_2 \cdot k_3 \cdot \frac{\phi}{\rho_{eff}} \tag{C.3}$$

where,

k_2 = 0.5 for ribbed bars
1.0 for smooth bars

k_3 = 0.5 for pure bending
1.0 for pure tension

ϕ = tension bar diameter

ρ_{eff} = $\dfrac{A_s}{b_{eff} \cdot h_{eff}}$

b_{eff} = $n_1 \cdot 15 \cdot \phi \leq b$

h_{eff} = $t_b + (n_L - 1) \cdot s_L + 8 \cdot \phi \leq \left\{ \dfrac{h - c_x}{2} \text{(bending) or } \dfrac{h}{2} (tension) \right\}$

n_1 = number of bars in outermost tension reinforcement layer

n_L = number of reinforcement layers

s_L = layer spacing

Oh/Kang (1987)

Oh and Kang (1987) proposed crack width and spacing equations for reinforced concrete flexural members based on the cracking theory advanced by *Bažant and Oh (1983)*. The maximum crack width w_{max} at the extreme tension face and average crack spacing s_{ave} can be determined using Equations (C.4) and (C.5), respectively.

$$w_{\max} = a_0 \cdot \left(\varepsilon_s - 0.0002\right) \cdot B \cdot \phi \tag{C.4}$$

where,

a_0 = $159 \cdot \left(\frac{t_b}{h_2}\right)^{4.5} + 2.83 \cdot \left(\frac{A_1}{A_{s1}}\right)^{1/3}$

B = $\frac{h_2}{h_1}$

A_1 = $A_{eff} / m = bh_3 / m$

h_3 = $h_2^{\,3} / \left(3h_1^{\,2}\right)$

ε_s = tension rebar strain

ϕ = tension rebar diameter

A_{s1} = area of a single rebar

m = number of reinforcing bars in tension

$$s_{ave} = \left(c_0 + \frac{0.236 \times 10^{-6}}{\varepsilon_s^2}\right) \cdot \phi \tag{C.5}$$

where,

c_0 = $25.7 \cdot \left(\frac{t_b}{h_2}\right)^{4.5} + 1.66 \cdot \left(\frac{A_1}{A_{s1}}\right)^{1/3}$

Eurocode 2 (2002)

Crack width in the *Eurocode 2 (2002)* is determined by multiplying the maximum (not average) stabilized crack spacing s_{max} by the difference between the mean steel strain and the mean concrete strain between cracks.

Characteristic crack widths are calculated from the relation:

$$w_k = s_{\max} \cdot \left(\varepsilon_{sm} - \varepsilon_{cm}\right) \tag{C.6}$$

where,

s_{max} = maximum crack spacing

ε_{sm} = mean strain in the reinforcement

ε_{cm} = mean strain in the concrete between cracks

The difference between the mean steel strain and the mean concrete strain between cracks $\varepsilon_{sm} - \varepsilon_{cm}$ may be calculated using Equation (C.7). All units are in mm and N.

$$\varepsilon_{sm} - \varepsilon_{cm} = \frac{\sigma_s - k_t \cdot \frac{f_{ct}}{\rho_{p,eff}} \cdot \left(1 + \alpha_e \cdot \rho_{p,eff}\right)}{E_s} \geq 0.6 \cdot \frac{\sigma_s}{E_s} \qquad \text{(C.7)}$$

where,

σ_s = stress in the tension reinforcement assuming a cracked section

k_t = 0.6 for short-term loading; 0.4 for long-term loading

f_{ct} = mean value of the tensile strength of the concrete

$\rho_{p,eff}$ = $\dfrac{A_s + \xi_1^2 A_p}{A_{eff}}$

A_s = area of the reinforcing steel within the area A_{eff}

A_p = the area of pre- or post-tensioned tendons within the area A_{eff}

ξ_1 = adjusted ratio of bond strength taking into account the parameters for prestressing and reinforcing steel

A_{eff} = area of concrete surrounding the tension reinforcement of depth h_3, where h_3 is the lesser of 2.5(h-d_x), (h-c_x)/3 or h/2

α_e = E_s / E_{cm}

E_s = modulus of elasticity of the reinforcing steel

E_{cm} = secant modulus of elasticity of concrete

In situations where bonded reinforcement is fixed at reasonably close centers within the tension zone (bar spacing ≤ 5(t_b + ϕ/2)), the maximum final crack spacing may be calculated from the following expression:

$$s_{\max} = 3.4 \cdot t_b + 0.425 \cdot k_1 \cdot k_2 \cdot \phi / \rho_{p,eff} \qquad \text{(C.8)}$$

where,

ϕ = tension reinforcement bar diameter. Where a mixture of bar diameters is used in a section, an average bar diameter should be used.

t_b = concrete cover to the reinforcement

k_1 = 0.8 for high-bond bars
1.6 for bars with an effectively plain surface (e.g. tendons)

k_2 = 0.5 for bending
1.0 for pure tension

Where the spacing of the bonded reinforcement exceeds 5(t_b + ϕ/2) or where there is no bonded reinforcement within the tension zone, an upper bound on the crack width may be found by assuming maximum crack spacing:

$$s_{\max} = 1.3\left(h - c_x\right) \qquad \text{(C.9)}$$

D Seismic Design Forces for Nonstructural Elements

The following equations for seismic design forces acting on nonstructural elements (components) are taken from the *CEN TS (in preparation)*. The equations represent a slight extension to those in the *Eurocode 8 (2003)* and are intended to work within the framework of the Eurocodes.

The horizontal effects of the seismic action may be determined by applying to the nonstructural element a horizontal force F_{ha} which is defined as follows:

$$F_{ha} = \left(S_a \cdot W_a \cdot \gamma_a\right) / q_a \tag{D.1}$$

where,

- F_{ha} horizontal seismic force, acting at the center of mass of the nonstructural element in the most unfavorable direction;
- W_a weight of the element;
- S_a horizontal seismic coefficient applicable to nonstructural elements, see Equation (D.2);
- γ_a importance factor of the element as determined by *Eurocode 8 (2003)*; it is either 1.0 or 1.5;
- q_a behavior factor of the element, see Table D.1.

The horizontal seismic coefficient S_a may be calculated using the following expression:

$$S_a = \alpha \cdot S \cdot \left[\left(1 + \frac{z}{H}\right) \cdot A_a - 0.5\right] \tag{D.2}$$

where,

$$A_a = \frac{3}{1 + \left(1 - \frac{T_a}{T_1}\right)^2} \tag{D.3}$$

- α ratio of the design ground acceleration on type A ground, a_g, to the acceleration of gravity g;
- S soil factor;
- z height of the nonstructural element above the level of application of the seismic action;
- H building height measured from the foundation or from the top of a rigid basement;
- A_a response amplification factor; if the values of T_a and/or T_1 are not known, the values in Table D.1 may be used;
- T_a fundamental vibration period of the nonstructural element;
- T_1 fundamental vibration period of the building in the relevant direction.

The value of the horizontal seismic coefficient S_a may not be taken less than $\alpha \cdot S$.

The vertical effects of the seismic action may be determined by applying to the nonstructural element a vertical force F_{va} which is defined as follows:

$$F_{va} = \left(S_{va} \cdot W_a \cdot \gamma_a\right) / q_a \qquad \text{(D.4)}$$

where,

F_{va} vertical seismic force, acting at the center of mass of the nonstructural element;

S_{va} vertical seismic coefficient applicable to nonstructural elements, see Equation (D.5).

All other terms in Equation (D.4) shall be defined as for Equation (D.1).

Note:
The vertical effects of the seismic action F_{va} for nonstructural elements may be neglected when the ratio of the vertical component of the design ground acceleration a_{vg} to the acceleration of gravity g is less than 1.0 and the gravity loads are transferred through direct bearing of the fixture on the structure (see Figure D.1).

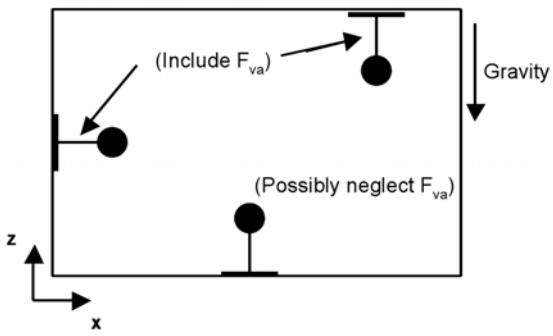

Figure D.1 Vertical effects of the seismic action

The vertical seismic coefficient S_{va} may be calculated as follows:

$$S_{va} = \alpha_v \cdot A_a \qquad \text{(D.5)}$$

where,

α_v ratio of the vertical design ground acceleration on type A ground, a_{vg}, to the acceleration of gravity g;

A_a response amplification factor, see Equation (D.3) or Table D.1.

Note:
For buildings with fewer than 10 stories, a factor of $A_a = 1.5$ may be slightly unconservative compared to the value yielded by Equation (D.3). A factor $A_a = 3.0$ is always conservative compared to using Equation (D.3)

Table D.1 Nonstructural element response amplification and behavior factors

Nonstructural Element	**A_a**	**q_a**
Architectural		
Exterior Wall Elements	1.5	2.0
Partitions	1.5	2.0
Interior Veneers	1.5	2.0
Ceilings	1.5	2.0
Parapets and Appendages	3.0	1.0
Canopies and Marquees	3.0	1.0
Chimneys and Masts[a]	3.0	1.0
Stairs	1.5	2.0
Mechanical Equipment		
Mechanical Equipment	1.5	2.0
Storage Vessels and Water Heaters[a]	3.0	1.0
High-Pressure Piping	3.0	2.0
Fire Suppression Piping	3.0	2.0
Fluid Piping (not Fire Suppression) for Hazardous Materials	3.0	1.0
Fluid Piping (not Fire Suppression) for Nonhazardous Materials	3.0	2.0
Ductwork	1.5	2.0
Electrical and Communications Equipment		
Electrical and Communications Equipment	1.5	2.0
Electrical and Communications Distribution Equipment	3.0	2.0
Light Fixtures	1.5	2.0
Furnishings and Interior Equipment		
Storage Racks	3.0	2.0
Bookcases	1.5	2.0
Computer Access Floors	1.5	2.0
Hazardous Materials Storage	3.0	1.0
Computer and Communications Racks	3.0	2.0
Elevators	1.5	2.0
Conveyors	3.0	2.0
Other Unspecified Equipment		
Other Rigid Components (fundamental period less than or equal to 0.06 sec)		
High deformability elements and attachments	1.5	2.0
Low deformability elements and attachments	1.5	1.0
Other Flexible Components (fundamental period greater than 0.06 sec)		
High deformability elements and attachments	3.0	2.0
Low deformability elements and attachments	3.0	1.0

[a] For chimneys, masts and tanks on legs acting as unbraced cantilevers along less than one half of their total height, or braced or guyed to the structure at or above their center of mass, A_a may be taken as 1.5 and q_a may be taken as 2.0.

E Experimental Data

Table E.1 Legend to abbreviations used in the tables of experimental data

Parameter	Abbreviation	Description
System	BA(E)	Bonded anchor (Epoxy based mortar)
	BA(V)	Bonded anchor (Vinylester based mortar)
	BE	Bonded-expansion anchor
	EB	Torque-controlled expansion anchor (bolt-type)
	ES	Torque-controlled expansion anchor (sleeve-type)
	HB	Headed bolt
	HS	Headed stud
	SA	Screw anchor
	UC	Undercut anchor
Fastener	D	Fastener diameter
	h_{ef}	Effective fastener embedment depth
	l_{uni}	Uniform strain length
Testing	$f_{cc,150}$	Concrete cube compressive strength (150x150x150mm)
	F_2	Compressive load on anchorage component
	n_F	Number of load cycles
	N_{max}	Maximum axial fastener load during load cycling or creep test
	N_{mid}	Middle axial fastener load during load cycling test
	N_{step}	Maximum axial fastener load at a given load cycling level
	N_u	Ultimate axial load
	N_w	Sustained axial fastener load
	n_w	Number of crack cycles
	t	Time
	w_1	Crack opening width
	w_2	Crack closing width
	Δw	Change in crack width, i.e. width by which crack is opened
Failure Mode	CC	Concrete cone failure
	CC(½)	Concrete cone failure (half cone)
	Po	Pull-out
	Pt	Pull-through
	S	Steel failure
	Sp	Splitting

Table E.2 Legend to references listed in the tables of experimental data

Reference	Title
/1/	Hoehler, M. S. (2006). Seismic crack cycling test for fasteners: Series B2 – Investigation of headed bolts, bolt anchors, sleeve anchors, screw anchors and undercut anchors. Institut für Werkstoffe im Bauwesen, Universität Stuttgart.
/2/	Hoehler, M. S. (2004). Tension cycling of threaded rods at large inelastic deformations – Grades 4.6, 8.8 and 10.9: Series A1 – Test results. Institut für Werkstoffe im Bauwesen, Universität Stuttgart.
/3/	Hoehler, M. S. (2004). Tension cycling of fasteners at high load levels: Series A2 – Test results. Institut für Werkstoffe im Bauwesen, Universität Stuttgart.
/4/	Hoehler, M. S. (2004). Low-cycle tension load cycling of headed bolts under varying head pressures: Series A3 – Test report. Institut für Werkstoffe im Bauwesen, Universität Stuttgart.
/5/	Hoehler, M. S. (2004). Tension cycling of fasteners at high load levels (Extension of Series A2 to high load rates): Series A4 – Test report. Institut für Werkstoffe im Bauwesen, Universität Stuttgart.
/6/	Hoehler, M. S. (2005). Tension load cycling of headed bolts in uncracked concrete: Series A5 – Test report. Institut für Werkstoffe im Bauwesen, Universität Stuttgart.
/7/	Hoehler, M. S. (2006). Influence of earthquake relevant tensile loading rates on fastener failure mode. Institut für Werkstoffe im Bauwesen, Universität Stuttgart.

E.1 Investigations with cycled cracks in the anchorage material

Table E.3 Experimental results of simulated seismic crack cycling tests in C20/25 concrete

Series	System	Size	h_{ef} [mm]	N_w [x N_u]	Crack Type	w_1 [mm]	w_2 [mm] - F_2 [kN]	n_w	Output					Mean	COV [%]	Ref.	Notes
									Failure mode								
									Ultimate load (N_u) [kN]								
									Displacement at N_u [mm]								
									Displacement during cycle 1 [mm]								
									Displacement during cycle n_w [mm]								
									Test Number								
									1	2	3	4	5				
B2.1	HS	Ø19	100	-	Static	0.8	-	-	CC 44.91 3.40 - -	CC 52.36 3.40 - -	CC 43.13 2.60 - -	CC 51.04 2.60 - -	CC 52.84 3.62 - -	- 48.86 3.12 - -	- 9.2 15.6 - -	/1/	a
B2.2	HS	Ø19	100	0.40	Cycled	0.8	F_2=-500	15	CC(½) 42.43 11.56 1.23 8.22	CC(½) 34.25 13.27 1.19 11.00	CC 40.63 12.08 0.99 8.48	CC 42.16 7.98 0.89 6.14	- - - - -	- 39.87 11.22 1.07 8.46	- 9.6 20.3 14.8 23.5	/1/	b
B2.3	HS	Ø19	100	0.40	Cycled	0.8	F_2=-500	10	CC 46.42 7.93 1.75 6.16	CC 50.53 8.62 1.74 5.77	CC 49.63 6.52 1.47 4.76	CC 50.82 10.33 1.73 5.13	- - - - -	- 49.35 8.35 1.67 5.46	- 4.1 19.0 8.2 11.5	/1/	-
B2.4	HS	Ø19	100	0.40	Cycled	0.8	F_2=-350	10	CC 59.61 8.04 1.64 5.63	CC 56.55 7.54 1.39 4.98	CC 56.28 7.63 1.43 4.97	CC 63.27 7.05 1.43 3.84	- - - - -	- 58.93 7.57 1.47 4.86	- 5.5 5.4 7.6 15.3	/1/	-
B2.5	HS	Ø19	100	0.40	Cycled	0.8	F_2=-50	10	CC 55.02 5.78 1.65 4.02	CC 56.81 7.76 1.61 4.27	CC 52.73 5.33 1.33 3.28	CC 54.46 3.69 0.96 2.62	- - - - -	- 54.76 5.64 1.39 3.55	- 3.1 29.7 23.0 21.1	/1/	-
B2.6	HS	Ø19	100	0.40	Cycled	0.5	F_2=-350	10	CC 60.01 4.41 0.73 2.28	CC 64.63 5.81 0.99 2.66	CC 58.30 4.04 0.51 1.81	CC 57.75 3.68 0.85 2.03	- - - - -	- 60.17 4.49 0.77 2.19	- 5.2 20.8 26.2 16.6	/1/	-
B2.7	HS	Ø19	100	0.16	Cycled	0.8	F_2=-350	10	CC 57.21 3.98 0.20 0.24	CC 52.33 4.04 0.13 0.18	CC 45.55 2.68 0.31 0.47	CC 52.73 3.38 0.15 0.22	- - - - -	- 51.96 3.52 0.20 0.28	- 9.3 18.0 40.8 47.7	/1/	-
B2.8	HS	Ø19	100	0.65	Cycled	0.8	F_2=-350	10	CC 52.92 10.00 2.49 9.18	CC 48.90* 6.09* - -	CC 30.86 16.40 2.59 14.03	CC 37.96 18.35 3.60 17.06	- - - - -	- 40.58 14.92 2.89 13.42	- 27.8 29.3 21.3 29.6	/1/	b,c
A2.1	EB	M16	95	-	Static	0.8	-	-	Pt 33.12 14.63 - -	Pt 31.47 11.78 - -	Pt 29.42 15.55 - -	Pt 30.64 14.87 - -	Pt 33.42 13.53 - -	- 31.61 14.07 - -	- 5.0 10.0 - -	/3/	a
B2.9	EB	M16	95	0.40	Cycled	0.8	F_2=-350	10	Pt 20.88 18.22 2.58 13.62	Pt 14.67 19.96 2.64 15.18	Pt 25.81 18.09 2.30 11.98	Pt 26.87 16.49 2.47 11.56	- - - - -	- 22.06 18.19 2.50 13.08	- 25.3 7.8 6.0 12.7	/1/	-
B2.10	EB	M16	95	0.40	Cycled	0.8	w_2=0.1	100	Pt 19.92 26.16 2.51 23.91	Pt 21.19 26.97 3.38 24.44	Pt 8.75 26.83 2.02 24.50	Pt 32.14 7.88* 0.35* 1.51*	- - - - -	- - 26.65 2.64 24.28	- - 1.6 26.1 1.3	/1/	d,e

* = not included in mean value.

a – Tests performed in wedge-split slabs.

b – Anchorage component split longitudinally during crack cycling.

c – Fastener 2 not loaded during crack cycling.

d – Fastener 4 not situated in crack along its entire axis.

e – Fasteners 1, 2 and 3 can be considered to have failed during the crack cycling (No. 1 = 58 cycles; No. 2 = 47 cycles; No. 3 = 40 cycles). However, because the displacement capacity of the loading cylinders (~ 25 mm) was slightly less than that required to pull the bolts completely through the sleeve (~ 30 mm) the fasteners stayed in place until the cycling ended. Fasteners 1 and 2 even exhibited significant residual strength during the pullout tests.

Table E.4 Experimental results of simulated seismic crack cycling tests in C20/25 concrete (continued)

Series	System	Size	h_{ef} [mm]	N_w [x N_u]	Crack Type	w_1 [mm]	w_2 [mm] - F_2 [kN]	n_w	Output Failure mode Ultimate load (N_u) [kN] Displacement at N_u [mm] Displacement during cycle 1 [mm] Displacement during cycle n_w [mm] Test Number 1	2	3	4	5	Mean	COV [%]	Ref.	Notes
A2.5	ES	M12	80	-	Static	0.8	-	-	CC 35.35 12.04 - -	CC 31.07 7.30 - -	CC 36.94 11.96 - -	CC 34.09 11.79 - -	CC 29.14 4.96 - -	- 33.32 9.61 - -	- 11.0 34.0 - -	/3/	a
B2.11	ES	M12	80	0.40	Cycled	0.8	F_2=-350	10	CC(½) 32.20 18.69 4.44 15.32	CC 22.88* 28.53* 5.61* 24.78*	CC 28.13 17.53 3.24 10.45	CC(½) 28.24 21.07 6.82 16.55	- - - - -	- 29.52 19.10 4.83 14.11	- 7.9 9.5 37.7 22.9	/1/	b
B2.12	SA	Ø20	76	-	Static	0.8	-	-	Po/CC 21.53 4.44 - -	Po/CC 19.37 1.45 - -	Po/CC 18.96 2.06 - -	Po/CC 21.27 2.26 - -	Po/CC 23.31 2.18 - -	- 20.89 2.48 - -	- 8.4 46.1 - -	/1/	a
B2.13	SA	Ø20	76	0.40	Cycled	0.8	F_2=-350	10	Po 20.54 6.55 1.05 5.06	Po 16.01 6.29 0.93 4.85	Po 21.44 6.79 0.81 3.70	Po 23.21 7.21 1.07 4.74	- - - - -	- 20.30 6.71 0.97 4.59	- 15.1 5.8 12.7 13.2	/1/	-
B2.14	UC	M10	80	-	Static	0.8	-	-	CC 37.57 3.37 - -	CC 39.92 3.21 - -	CC 35.23 2.43 - -	CC 45.73 6.46 - -	- - - - -	- 39.61 3.87 - -	- 11.4 45.9 - -	/1/	-
B2.15	UC	M10	80	0.40	Cycled	0.8	F_2=-350	10	CC(½) 38.32 9.77 1.46 6.94	CC 36.71 6.77 1.50 4.90	CC 36.60 4.43 1.00 3.19	CC 42.74 5.45 0.67 3.56	- - - - -	- 38.59 6.61 1.16 4.65	- 7.4 35.1 34.5 36.5	/1/	-
B2.16	UC	M10	80	Varied	Cycled	0.8 1.0	F_2=-350 F_2=-100	<50	CC 38.96 8.56 1.12 7.48	CC - - 1.16 20.57	CC 35.27 12.56 1.44 12.07	CC 37.07 15.41 1.55 14.92	- - - - -	- - - - -	- - - - -	/1/	c
B2.17	UC	M10	80	0.40	Cycled	Varied	Varied	Varied	CC - - - -	CC - - - -	CC - - - -	CC - - - -	- - - - -	- - - - -	- - - - -	/1/	c

* = not included in mean value.
a – Tests performed in wedge-split slabs.
b – Fastener 2 reached the maximum displacement capacity of the loading cylinder (~25 mm) after 8 cycles. This led to a drop in the axial fastener load, however, the fastener still had some residual load bearing capacity.
c – See reference for further details.

E.2 Investigations with cyclic loading

Table E.5 Experimental results of monotonic tension tests on threaded rods (l_{uni} = 170 mm)

Series	Bolt Steel Grade	Size	Output Ultimate load (N_u) [kN] Displacement at N_u [mm] Elastic modulus [MPa]				Mean	COV [%]	Ref.	Notes
			Test Number							
			1	2	3	4				
A1.1	4.6	M16	87.36 7.10 165061	85.60 6.01 167616	85.62 9.51 175780	86.90 10.10 164061	86.37 8.18 168130	1.0 23.8 3.2	/2/	-
A1.2	8.8	M16	- - 151441	142.61 6.84 143102	144.02 6.83 134789	- - -	143.32 6.84 143111	0.7 0.1 5.8	/2/	a
A1.3	10.9	M20	254.56 11.17 157223	253.82 11.64 151502	- - -	- - -	254.19 11.41 154363	0.2 2.9 2.6	/2/	-

a – Coupling nut stripped before ultimate load was reached in test 1.

Table E.6 Experimental results of tension load cycling tests with headed bolts with close support conditions (no yielding of the anchor; testing to failure was not intended)

Series	Bolt (Grade)	h_{ef} [mm]	Concrete	Δw [mm]	Load Type	Bearing Pressure During Cycling [x $f_{cc,150}$]	n_F	Output Displacement at N_{mid} (n_F=0) [mm] Displacement at N_{mid} (n_F=30) [mm] Displacement at N_{mid} (n_F=50) [mm] Displacement at N_{mid} (n_F=100) [mm]			Mean	COV [%]	Ref.	Notes
								Test Number						
								1	2	3				
A3.1	M20 (10.9)	100	C20/25	-	Cyclic	4	30/50/100	0.49 0.75 0.80 0.89	0.42 0.67 0.73 0.76	0.64 1.13 1.22 1.39	0.52 0.85 0.92 1.01	21.8 28.9 28.9 32.8	/4/	a
A3.2	M20 (10.9)	100	C20/25	-	Cyclic	8	30/50/100	1.74 2.61 - -	2.03 3.10 3.39 3.79	1.59 2.60 2.81 3.12	1.79 2.77 3.10 3.46	12.5 10.3 13.2 13.7	/4/	b
A3.3	M20 (10.9)	100	C20/25	-	Cyclic	12	30/50/100	5.51 8.27 8.90 9.90	- - - -	7.52 15.72* - -	6.52 8.27 8.90 9.90	21.8 - - -	/4/	c
A3.4	M20 (10.9)	100	C45/55	-	Cyclic	4	30/50/100	0.88 1.17 1.22 1.35	0.64 0.89 0.96 1.04	1.04 1.41 1.49 1.62	0.85 1.16 1.22 1.34	23.6 22.5 21.7 21.7	/4/	-
A3.5	M20 (10.9)	100	C45/55	-	Cyclic	6	30/50/100	2.53 7.40* 8.63* -	2.01 3.43 3.65 3.93	1.88 8.88* 12.34* 24.49*	2.14 3.43 3.65 3.93	16.1 - - -	/4/	d
A3.6	M20 (10.9)	100	C20/25	0.8	Cyclic	4	30/50/100	1.84 2.74 2.92 3.18	1.33 2.01 2.15 2.38	0.92 1.67 1.85 2.05	1.36 2.14 2.31 2.54	33.8 25.5 23.9 22.9	/4/	-
A3.7	M20 (10.9)	100	C20/25	0.8	Cyclic	8	30/50/100	6.17 9.24 9.88 10.77	4.71 7.54 8.22 9.06	5.33 8.61 9.34 10.32	5.40 8.46 9.15 10.05	13.6 10.2 9.3 8.8	/4/	-

* = not included in mean value.
a – Tests 1, 2 and 3 correspond to tests 2, 4 and 5, respectively, in the reference.
b – Test 1 terminated during cycling due to problems with servo-hydraulic control.
c – Tests 2 and 3 failed due to splitting of the anchorage component.
d – Tests 1 and 3 affected by splitting of the anchorage component.

Table E.7 Experimental results of tension creep tests with headed bolts with close support conditions (no yielding of the anchor; no failure)

Series	Bolt (Grade)	h_{ef} [mm]	Concrete	Δw [mm]	Load Type	Bearing Pressure During Creep [x $f_{cc,150}$]	n_F	Output	Test Number 1	2	3	Mean	COV [%]	Ref.	Notes
A3.8	M20 (10.9)	100	C20/25	-	Creep	8	-	Displacement at N_{max} (t=0) [mm]	2.58	1.66	1.99	2.08	22.4	/4/	a
								Displacement at N_{max} (t=59) [mm]	3.03	1.90	2.33	2.42	23.6		
								Displacement at N_{max} (t=108) [mm]	3.14	1.96	2.42	2.51	23.7		
								Displacement at N_{max} (t=217) [mm]	3.27	2.06	2.52	2.62	23.3		
								Displacement at N_{max} (t=500) [mm]	3.43	2.21	2.68	2.77	22.2		

a – The times t = 59, 108 and 217 seconds correspond to the duration of 30, 50 and 100 load cycles in Table E.6.

Table E.8 Experimental results of tension load cycling tests with headed bolts with wide support conditions (concrete cone failure)

Series	Bolt (Grade)	h_{ef} [mm]	Concrete	Δw [mm]	Load Type	Bearing Pressure During Cycling [x $f_{cc,150}$]	n_F	Output	Test Number 1	2	3	Mean	COV [%]	Ref.	Notes
A5.1	M20 (10.9)	100	C20/25	-	Mono	-	-	Ultimate load (N_u) [kN]	79.33	82.40	75.84	79.19	4.0	/6/	a
								Displacement at N_u [mm]	0.77	0.91	0.68	0.79	15.0		
								Displacement at N_{mid} (n_F=0) [mm]	-	-	-	-	-		
								Displacement at N_{mid} (n_F=30) [mm]	-	-	-	-	-		
								Displacement at N_{mid} (n_F=50) [mm]	-	-	-	-	-		
								Displacement at N_{mid} (n_F=100) [mm]	-	-	-	-	-		
A5.2	M20 (10.9)	100	C20/25	-	Cyclic	4 (0.79·N_u)	30/50/100	Ultimate load (N_u) [kN]	84.10	84.49	-	84.30	0.3	/6/	-
								Displacement at N_u [mm]	1.12	1.06	-	1.09	3.9		
								Displacement at N_{mid} (n_F=0) [mm]	0.42	0.37	-	0.39	10.6		
								Displacement at N_{mid} (n_F=30) [mm]	0.56	0.45	-	0.50	15.5		
								Displacement at N_{mid} (n_F=50) [mm]	0.58	0.48	-	0.53	13.7		
								Displacement at N_{mid} (n_F=100) [mm]	0.64	0.52	-	0.58	14.6		
A5.3	M20 (10.9)	100	C20/25	-	Cyclic	4.6 (0.90·N_u)	30/50/100	Ultimate load (N_u) [kN]	-	-	-	-	-	/6/	b
								Displacement at N_u [mm]	-	-	-	-	-		
								Displacement at N_{mid} (n_F=0) [mm]	0.487	0.561	0.57	0.54	8.2		
								Displacement at N_{mid} (n_F=30) [mm]	0.859	0.83	0.79	0.82	4.4		
								Displacement at N_{mid} (n_F=50) [mm]	-	0.98	0.87	0.92	8.7		
								Displacement at N_{mid} (n_F=100) [mm]	-	-	-	-	-		

a – Tests 1, 2 and 3 correspond to tests 5, 6 and 7, respectively, in the reference.
b – Tests 1, 2 and 3 failed after 34, 73 and 92 load cycles, respectively.

Table E.9 Experimental results of tension load cycling tests with headed bolts with ductile steel failure (l_{uni} = 180 mm)

Series	Bolt (Grade)	h_{ef} [mm]	Concrete	Δw [mm]	Load Type	Bearing Pressure During Cycling [x $f_{cc,150}$]	n_F	Output	Test Number 1	2	3	Mean	COV [%]	Ref.	Notes
A3.9	M16 (8.8)	140	C45/55	-	Cyclic	4	30/50/100	Displacement at N_{mid} (n_F=0) mm]	-	3.82	6.03	-	-	/4/	a,b
								Displacement at N_{mid} (n_F=30) [mm]	-	4.87	6.00	-	-		
								Displacement at N_{mid} (n_F=50) [mm]	-	4.85	6.14	-	-		
								Displacement at N_{mid} (n_F=100) [mm]	-	6.52	-	-	-		

a – Test terminated before load cycling due to problem with the setup.
b – In test 3, the steel ruptured during load cycle 95.

Table E.10 Experimental results of simulated seismic load cycling tests with post-installed fasteners in C20/25 cracked concrete (Δw = 0.8 mm) (constant load cycling at 0.5 Hz)

Series	System	Size	h_{ef} [mm]	Load Type	N_{max} [x N_u]	n_F	Output	Mean	COV [%]	Ref.	Notes
							Failure mode				
							Ultimate load (N_u) [kN]				
							Displacement at N_u [mm]				
							Displacement at N_{mid} (n_F=0) [mm]				
							Displacement at N_{mid} (n_F=30) [mm]				
							Test Number				
							1 2 3 4 5				
A2.1	EB	M16	95	Mono	-	-	Pt Pt Pt Pt Pt 33.12 31.47 29.42 30.64 33.42 14.63 11.78 15.55 14.87 13.53 - - - - - - - - - -	31.61 14.07 - -	5.0 10.0 - -	/3/	-
A2.2	EB	M16	95	Cyclic	0.5	30	Pt Pt Pt - - 30.49 34.11 33.20 - - 6.09 7.10 9.66 - - 1.98 1.41 1.32 - - 2.26 1.70 1.57 - -	- 32.60 7.62 1.57 1.84	- 5.8 24.2 22.7 19.8	/3/	-
A2.3	EB	M16	95	Cyclic	0.9	30	Pt Pt Pt - - 34.61 33.41 33.88 - - 8.78 8.52 13.15 - - 4.44 4.10 4.44 - - 6.05 5.40 5.83 - -	- 33.97 10.15 4.33 5.76	- 1.8 25.6 4.6 5.8	/3/	-
A2.4	EB	M16	95	Cyclic	1.0	30	Pt Pt Pt - - 29.35 33.58 31.06 - - 14.97 11.04 7.22 - - 13.15 13.11 13.13 - - 14.19 - - - -	- 31.33 11.08 13.13 14.19	- 6.8 35.0 0.2 -	/3/	a
A2.5	ES	M12	80	Mono	-	-	CC CC CC CC CC 35.35 31.07 36.94 34.09 29.14 12.04 7.30 11.96 11.79 4.96 - - - - - - - - - -	- 33.32 9.61 - -	- 11.0 34 - -	/3/	-
A2.6	ES	M12	80	Cyclic	0.5	30	CC CC CC - - 33.35 32.61 32.64 - - 12.20 5.92 11.30 - - 2.12 2.81 3.38 - - 2.43 3.13 3.76 - -	- 32.87 9.81 2.77 3.11	- 1.3 34.6 22.8 21.5	/3/	-
A2.7	ES	M12	80	Cyclic	0.9	30	CC CC CC - - 34.31 30.05* 31.28* - - 11.41 - 16.16* - - 5.64 5.179* 10.45* - - 7.39 - 14.75* - -	- 34.31 11.41 5.64 7.39	- - - - -	/3/	b,c
A2.8	ES	M12	80	Cyclic	1.0	30	CC CC CC - - 34.26 34.30 28.77 - - 5.82 14.18 7.43 - - - 8.98 - - - - 12.95 - - -	- 32.44 9.14 8.98 12.95	- 9.8 48.5 - -	/3/	d,e
A2.9	SA	Ø12	64	Mono	-	-	Po/CC Po/CC Po/CC Po/CC Po/CC 20.76 21.50 20.29 23.52 21.41 2.33 1.20 1.82 - 1.14 - - - - - - - - - -	- 21.50 1.65 - -	- 6.0 37.0 - -	/3/	f
A2.10	SA	Ø12	64	Cyclic	0.5	30	Po/CC Po/CC Po/CC - - 21.29 21.69 21.80 - - 1.94 1.14 1.47 - - 0.38 0.21 0.35 - - 0.56 0.35 0.49 - -	- 21.59 1.52 0.31 0.47	- 1.2 26.5 29.6 22.1	/3/	-
A2.11	SA	Ø12	64	Cyclic	0.9	30	Po/CC Po/CC Po/CC - - 19.03* 24.51 24.96 - - 1.35* 2.20 1.44 - - - 0.99 0.58 - - - 1.77 0.96 - -	- 24.74 1.48 0.79 1.36	- 1.3 21.0 36.5 41.8	/3/	g
A2.12	SA	Ø12	64	Cyclic	1.0	30	Po/CC Po/CC Po/CC - - 20.95 20.79 21.25 - - - - - - - 0.997 1.325 1.172 - - - - - - -	- 21.00 - 1.16 -	- 1.1 - 14.1 -	/3/	h

* = not included in mean value.
a – Tests 2 and 3 failed after 8 load cycles.
b – Test 2 failed after 12 load cycles.
c – Fastener in test 3 slipped during loading.
d – Tests 1 and 3 failed prior to the start of load cycling.
e – Fastener 2 withstood the load cycling without failing.
f – Displacement not recorded during test 4.
g – Test 1 failed prior to the start of load cycling.
h – Tests 1, 2 and 3 failed after 5, 7 and 16 load cycles, respectively.

Table E.11 Experimental results of simulated seismic load cycling tests with post-installed fasteners in C20/25 cracked concrete (Δw = 0.8 mm) (constant load cycling at 5 Hz)

Series	System	Size	h_{ef} [mm]	Load Type	N_{max} [x N_u]	n_F	Output	Mean	COV [%]	Ref.	Notes
							Failure mode				
							Ultimate load (N_u) [kN]				
							Displacement at N_u [mm]				
							Displacement at N_{mid} (n_F=0) [mm]				
							Displacement at N_{mid} (n_F=30) [mm]				
							Test Number				
							1 / 2 / 3 / 4 / 5				
A4.1	EB	M16	95	Mono	-	-	Pt / Pt / Pt / Pt / Pt	-	-		
							29.41 / 29.51 / 29.66 / 28.16 / 25.56	28.46	6.1		
							13.51 / 11.62 / 12.56 / 14.99 / 15.39	13.61	11.7	/5/	-
							- / - / - / - / -	-	-		
							- / - / - / - / -	-	-		
A4.2	EB	M16	95	Cyclic	0.9	30	Pt / Pt / Pt / - / -	-	-		
							28.51 / - / 29.20 / - / -	28.86	1.7		
							13.07 / - / 12.26 / - / -	12.67	4.5	/5/	a
							10.64 / 14.16 / 9.61 / - / -	11.47	20.8		
							11.53 / - / 10.53 / - / -	11.03	6.4		
A4.3	ES	M12	80	Mono	-	-	CC / CC / CC / - / -	-	-		
							29.44 / 30.62 / 29.18 / - / -	29.75	2.6		
							13.44 / 11.04 / 6.15 / - / -	10.21	36.4	/5/	-
							- / - / - / - / -	-	-		
							- / - / - / - / -	-	-		
A4.4	ES	M12	80	Cyclic	0.9	30	CC / CC / CC / CC / CC	-	-		
							26.73* / 30.29 / 24.14* / 31.79* / 33.90	32.10	8.0		
							15.99* / 11.32 / 10.60* / 12.75* / 14.21	12.77	16.0	/5/	b,c
							- / 7.26 / - / 5.85* / 4.97	6.12	26.5		
							- / 8.80 / - / 6.17* / 6.15	7.48	25.1		
A4.5	SA	Ø12	64	Mono	-	-	Po/CC / Po/CC / Po/CC / - / -	-	-		
							12.02 / 12.97 / 14.79 / - / -	13.26	11.0		
							1.81 / 1.70 / 1.26 / - / -	1.59	18.3	/5/	-
							- / - / - / - / -	-	-		
							- / - / - / - / -	-	-		
A4.6	SA	Ø12	64	Cyclic	0.9	30	Po/CC / Po/CC / Po/CC / - / -	-	-		
							18.15 / 15.34 / 17.37 / - / -	16.95	8.6		
							1.88 / 1.70 / 2.83 / - / -	2.14	28.4	/5/	-
							0.50 / 0.45 / 0.69 / - / -	0.55	23.2		
							0.79 / 0.73 / 1.10 / - / -	0.87	22.7		

* = not included in mean value.
a – Test 2 failed after 10 load cycles.
b – Tests 1 and 3 failed prior to the start of load cycling.
c – Test 4 underwent unusually little displacement during load cycling (cause unknown).

Table E.12 Experimental results of simulated seismic load cycling tests with post-installed fasteners in C20/25 cracked concrete (Δw = 0.8 mm) (stepwise increasing load cycling)

Series	System	Size	h_{ef} [mm]	Load Type	N_{step} [x N_u]	n_F	Output	Mean	COV [%]	Ref.	Notes
							Failure mode				
							Ultimate load (N_u) [kN]				
							Displacement at N_{mid} (n_F=0) [mm]				
							Displacement at N_{mid} (n_F=5) [mm]				
							Displacement at N_{mid} (n_F=10) [mm]				
							Displacement at N_{mid} (n_F=15) [mm]				
							Displacement at N_{mid} (n_F=20) [mm]				
							Displacement at N_{mid} (n_F=25) [mm]				
							Displacement at N_{mid} (n_F=30) [mm]				
							Test Number				
							1 / **2** / **3**				
A2.13	EB	M16	95	Cyclic	0.15 (per step)	5 (per step)	Pt / Pt / Pt	-	-	/3/	a
							33.33 / 33.27 / 32.12	32.91	2.1		
							0.127 / 0.222 / 0.383	0.24	53.0		
							0.128 / 0.249 / 0.409	0.26	53.8		
							0.602 / 1.268 / 0.889	0.92	36.3		
							1.073 / 1.893 / 1.336	1.43	29.2		
							1.649 / 2.789 / 1.834	2.09	29.3		
							2.694 / 4.161 / 2.580	3.15	28.0		
							6.950 / 6.506 / 4.787	6.08	18.8		
A2.14	ES	M12	80	Cyclic	0.15 (per step)	5 (per step)	- / CC / CC	-	-	/3/	a,b
							- / 32.98 / 32.98	32.98	0.0		
							- / 0.837 / 0.568	0.70	27.1		
							- / 0.869 / 0.590	0.73	27.0		
							- / 1.621 / 1.210	1.42	20.5		
							- / 2.304 / 1.779	2.04	18.2		
							- / 3.083 / 2.305	2.69	20.4		
							- / 3.957 / 3.005	3.48	19.3		
							- / 8.568 / 5.046	6.81	36.6		
A2.15	SA	Ø12	64	Cyclic	0.15 (per step)	5 (per step)	Po/CC / Po/CC / Po/CC	-	-	/3/	a
							21.02 / 21.05 / 21.00	21.02	0.1		
							0.020 / 0.009 / 0.045	0.02	74.8		
							0.020 / 0.019 / 0.056	0.03	66.6		
							0.094 / 0.088 / 0.114	0.10	13.8		
							0.315 / 0.323 / 0.239	0.29	15.9		
							0.476 / 0.522 / 0.414	0.47	11.5		
							0.670 / 0.698 / 0.645	0.67	4.0		
							0.919 / 0.953 / 0.880	0.92	4.0		

a – Load cycling level at 90% N_u when n_F = 30.
b – Coupling nut stripped during load cycling in test 1.

Table E.13 Experimental results of simulated seismic load cycling tests with post-installed fasteners in C20/25 cracked concrete (Δw = 0.8 mm) (cross-section reduced to ensure steel failure)

Series	System	Size	h_{ef} [mm]	Load Type	N_{max} [x N_u]	n_F	Output	Mean	COV [%]	Ref.	Notes
							Failure mode				
							Ultimate load (N_u) [kN]				
							Displacement at N_u [mm]				
							Displacement at N_{mid} (n_F=0) [mm]				
							Displacement at N_{mid} (n_F=30) [mm]				
							Test Number				
							1 / **2**				
A2.16	ES (modified) d=5.5mm l_{uni}=40mm	M12	80	Mono	-	-	S / -	-	-	/3/	-
							23.63 / -	23.63	-		
							5.58 / -	5.58	-		
							- / -	-	-		
							- / -	-	-		
A2.17	ES (modified) d=5.5mm l_{uni}=40mm	M12	80	Cyclic	1.0	30	S / -	-	-	/3/	-
							23.87 / -	23.87	-		
							4.36 / -	4.36	-		
							3.29 / -	3.29	-		
							4.13	4.13	-		
A4.7	ES (modified) d=5.5mm l_{uni}=105mm	M12	140	Mono	-	-	S / S	-	-	/5/	-
							22.38 / 22.63	22.51	0.8		
							7.47 / 9.46	8.47	16.6		
							- / -	-	-		
							- / -	-	-		
A4.8	ES (modified) d=5.5mm l_{uni}=105mm	M12	140	Cyclic	1.0	30	S / S	-	-	/5/	-
							21.31 / 20.19	20.75	3.8		
							8.50 / 7.91	8.21	5.1		
							6.63 / 7.19	6.91	5.7		
							7.14 / 7.56	7.35	4.0		

E.3 Investigations with high loading rate

Table E.14 Experimental results of high tension load rate tests with post-installed fasteners in C20/25 cracked concrete

Series	System	Size	h_{ef} [mm]	Δw [mm]	Cylinder Load Rate [mm/min]	Approx. Rise Time to N_u [sec]	Output: Failure mode / Ultimate load (N_u) [kN] / Displacement at N_u [mm] — Test Number 1	2	3	4	5	Mean	COV [%]	Ref.	Notes
A4.1	EB	M16	95	0.8	5	>120	Pt	Pt	Pt	Pt	Pt	-	-		
							29.41	29.51	29.66	28.16	25.56	28.46	6.1	/3/	-
							13.51	11.62	12.56	14.99	15.39	13.61	11.7		
A4.9	EB	M16	95	0.8	6000	0.15	Pt	Pt	Pt	-	-	-	-		
							30.23	27.77	26.13	-	-	28.04	7.4	/3/	-
							14.46	9.90	10.19	-	-	11.52	22.2		
A4.10	EB	M16	95	0.8	15000	0.10	Pt	Pt	Pt	-	-	-	-		
							26.76	27.55	26.76	-	-	27.02	1.7	/3/	-
							13.68	10.57	14.83	-	-	13.03	16.9		
AR.1	EB	M16	60	0.5	5	>120	CC	CC	CC	-	-	-	-		
							21.82	19.19	18.30	-	-	19.77	9.3	/5/	a
							9.80	2.70	5.48	-	-	5.99	59.7		
AR.2	EB	M16	60	0.5	50000	0.02	Pt	Pt	Pt	-	-	-	-		
							23.41	21.71	26.71	-	-	23.94	10.6	/5/	b
							4.60	3.86	4.03	-	-	4.16	9.3		
A4.3	ES	M12	80	0.8	5	>120	CC	CC	CC	-	-	-	-		
							29.44	30.62	29.18	-	-	29.75	2.6	/3/	-
							13.44	11.04	6.15	-	-	10.21	36.4		
A4.11	ES	M12	80	0.8	6000	0.15	CC	Pt	CC	-	-	-	-		
							32.98	35.27*	32.35	-	-	32.67	1.4	/3/	-
							11.31	19.12*	7.03	-	-	9.17	33.0		
AR.3	BA(E)	M12	60	0.5	1	>120	CC	CC	CC/Po	CC/Po	CC/Po	-	-		
							18.96	19.72	19.70	21.53	19.00	19.78	5.3	/7/	-
							0.88	0.81	1.38	1.27	0.98	1.06	23.4		
AR.4	BA(E)	M12	60	0.5	1000	0.13	CC/Po	CC/Po	CC/Po	-	-	-	-		
							26.02	24.75	21.23	-	-	24.00	10.3	/7/	c
							1.05	1.07	1.09	-	-	1.07	1.9		
AR.5	BA(E)	M12	60	0.5	15000	0.03	CC/Po	CC/Po	CC	-	-	-	-		
							25.11	25.95	29.02	-	-	26.69	7.7	/7/	-
							1.65	0.94	1.53	-	-	1.37	27.7		
AR.6	BA(V)	M12	60	0.5	1	>120	CC/Po	CC/Po	CC	-	-	-	-		
							16.38	17.30	14.86	-	-	16.18	7.6	/7/	-
							1.61	1.09	1.00	-	-	1.23	26.7		
AR.7	BA(V)	M12	60	0.5	50000	0.02	CC/Po	CC/Po	CC/Po	-	-	-	-		
							16.95	18.00	20.67	-	-	18.54	10.3	/7/	-
							1.32	1.10	1.47	-	-	1.30	14.4		
AR.8	BE	M8	50	0.8	3	>120	Pt	Pt	Pt	Pt	Pt	-	-		
							14.47	12.23	12.11	11.96	12.64	12.68	8.1	/7/	-
							2.87	2.44	3.22	3.30	2.97	2.96	11.5		
AR.9	BE	M8	50	0.8	1000	0.20	Pt	Pt	Pt	Pt	-	-	-		
							15.43	14.03	15.02	14.03	-	14.63	4.9	/7/	-
							2.88	2.75	2.35	2.77	-	2.69	8.6		
AR.10	BE	M8	50	0.8	15000	0.3	Pt	Pt	Pt	Pt	Pt	-	-		
							16.91	16.48	17.85	16.41	14.61	16.45	7.2	/7/	-
							3.28	2.82	2.83	2.74	2.96	2.93	7.3		
AR.11	BE	M16	80	0.8	3	>120	CC	CC	CC	-	-	-	-		
							43.38	46.15	45.55	-	-	45.03	3.2	/7/	-
							1.98	3.08	3.12	-	-	2.73	23.7		
AR.12	BE	M16	80	0.8	50000	0.04	CC/Pt	CC/Pt	CC/Pt	-	-	-	-		
							55.92	61.63	57.85	-	-	58.47	5.0	/7/	-
							2.34	2.74	2.87	-	-	2.65	10.4		

* = not included in mean value.
a – Tests 1, 2 and 3 correspond to tests 4, 5 and 6, respectively, in the reference.
b – Tests 1, 2 and 3 correspond to tests 3, 4 and 5, respectively, in the reference.
c – Tests 1, 2 and 3 correspond to tests 2, 3 and 4, respectively, in the reference.

Personal Data

Matthew Stanton Hoehler
Born on the 21st of August ,1976
in Tiburon, California, USA.
Married.

Education

1982 to 1990	St. Hilary School, Tiburon, California.
1990 to 1994	Redwood High School, Larkspur, California.
1994 to 1998	Princeton University, Princeton, New Jersey. Bachelor of Science in Engineering (B.S.E), Structural Engineering (with certificate in Geological Engineering).
1999 to 2000	University of California, Berkeley. Master of Science (M.Sc.), Structural Engineering, Mechanics and Materials.
2000 to 2006	*Universität Stuttgart*, Germany. *Doktor-Ingenieurs (Dr.-Ing.)*.

Experience

1992	Commercial halibut fishing, South Eastern Alaska (one season).
1997	Associated Western Universities Fellowship recipient. Summer internship at Lawrence Livermore National Laboratory.
1998 to 1999	Lawrence Livermore National Laboratory, Livermore, California. Engineer/Scientist, New Technologies Engineering Division.
2000 to 2005	*Universität Stuttgart*, Germany. Research Engineer, Institute of Construction Materials.
2004 to 2005	Teaching certification in higher education in the state of Baden-Württemberg, Germany.
2005 to 2006	Self-employed research consultant, Stuttgart, Germany.
since 2006	Hilti North America. Research Project Manager.